UNIVERSITY OF CALIFORNIA

Los Angeles

Aspects of magnetism: topology, transport, and quantum entanglement

A dissertation submitted in partial satisfaction

of the requirements for the degree

Doctor of Philosophy in Physics

by

Ji Zou

2022

ABSTRACT OF THE DISSERTATION

Aspects of magnetism: topology, transport, and quantum entanglement

by

Ji Zou
Doctor of Philosophy in Physics
University of California, Los Angeles, 2022
Professor Yaroslav Tserkovnyak, Chair

The general theme in this thesis is the exploration of topology, transport, and quantum entanglement in magnetic systems.

We first set up the stage in chapter 1 by introducing some notions that we use in later chapters. In chapters 2 and 3, we discuss the (hydro)dynamics of vortices and hedgehogs in two- and three-dimensional insulating magnets, respectively, in both classical and quantum regimes based on the topological conservation laws of vortices and hedgehogs, which follow from their topological nature instead of symmetries of the system Hamiltonian (thus are robust against impurities and anisotropies). To illustrate the applications in spintronics, we formulate an experimentally feasible energy-storage concept based on vorticity (hydro)dynamics within an easy-plane insulating magnet in chapter 2.

In chapter 4, we investigate entanglement between two arbitrary spins in a magnetic system in the presence of applied magnetic fields and axial anisotropies. We demonstrate that spins are generally entangled in thermodynamic equilibrium, indicating that the magnetic medium can serve as a resource to store and process quantum information in general. We, furthermore, show that the entanglement can jump discontinuously when varying the

magnetic field. This tunable entanglement can be potentially used as an efficient switch in quantum-information processing tasks.

Finally, in chapter 5, we present a study on the steady entanglement generation for two distant spin qubits interacting with a common magnetic medium. Our focus is a medium-induced effective coupling (between the two qubits) of dissipative nature. We explore the different dynamical regimes of the entanglement evolution in the presence of this dissipative coupling and demonstrate the advantage of its utilization as a route to generate steady entanglement and even Bell state, insensitive to the initial state. Our work points to a new direction of the application of spintronic schemes in future quantum information technology.

The dissertation of Ji Zou is approved.

Michael Gutperle

Stuart Brown

Rahul Roy

Yaroslav Tserkovnyak, Committee Chair

University of California, Los Angeles

2022

TABLE OF CONTENTS

LIST OF FIGURES

ACKNOWLEDGMENTS

First and foremost, I want to thank my advisor, Yaroslav Tserkovnyak, for being the most influential person in my graduate career. His optimism, genuine curiosity and passion for scientific research have influenced me in a profound way, and led to my own commitment to an academic career. I have learned a lot from his broad knowledge, original approach, and outlook on science through countless discussions with him and sitting in his class (PHY 241 and 242). Besides, the most valuable lesson that I learned from him is the way to address a new problem: a) always have a clear physical picture of what is happening in the system and of the calculation we are doing; b) try to predict what we may get based on physical argument before doing any calculation; c) try to summarize the story using simple and plain words without invoking any unnecessary jargon. This naturally leads me to the right/important questions and allows me to identify the essence of a complex problem when I try to do so. I also want to thank my other committee members: Rahul Roy, Stuart Brown, and Michael Gutperle for your support and giving constructive comments.

I am deeply grateful to our (previous) group members, Se Kwon Kim and Shu (Suzy) Zhang. Se Kwon has guided me through my first scientific projects. He is always so encouraging and supportive. Se Kwon is also a very nice friend to talk to. His insightful remarks on various physics and non-physics topics have shaped my opinions in an important way. Thank you, Se Kwon! I really enjoyed the discussions I had with Suzy in person and meetings via Skype/Zoom during Covid. She is modest, frank, and intelligent, and it has always been a delight to learn from, discuss and collaborate with her. I hope, in the near future, we can again discuss various problems in person! I also would like to thank other (previous) group members: Hector Ochoa, Mostafa Tanhayi Ahari, Benedetta Flebus, Ricardo Zarzuela, Chau Dao, Derek Reitz, and Dalton Jones for discussing various physical problems. I wish to thank my collaborator Jianwei (John) Miao for invaluable discussions and for inviting me to his group lunch and parties!

My graduate school experience would not be complete without my classmates: Dimitrios Kosmopoulos, Ziqi Pi, Andy Chan, Kevin Chen, Yujian Zhao, and many others whom I am unable to squeeze into these margins. You are the ones who brought joy to me and made my days memorable at UCLA. I miss the time we read A. Zee's QFT book together in the graduate student office in PAB. I will never be able to forget the badminton and various board games we played together. Thank you, Hongda, Jian, and Yushun, for being my close friends and for your tremendous amount of help in daily life. I miss a lot of the conversations we had when walking home from office almost every night. Thank you, Hongda, for taking me to the emergency room with just a call, in spite of other stuff you were busy with! I hope to visit you guys in the near future!

I would like to thank friends from my college, Xiaochuan Wu, Yichen Xu, and Haoxin Zhao, for hosting me when I was visiting KITP at Santa Barbara. Thank you, Xiaochuan, my college roommate, for always being so encouraging and supportive! Your enthusiasm for physics has been one of the driving forces for me.

I would also like to thank my Chinese friends (some are my neighbors at LA), Wenzhong Yan, Huan Wu, Hengjie Liu, Zhengyang Ming, Changjun Fan, Long Yang, Kai Huang, Jing Wang, Yingqing Lu, Yang Li, and Chen Jiang. I could hardly imagine Ph.D. life in a foreign country without their company over the past six years. Their everlasting love and friendship have always been dear to my heart.

Last, but by no means least, I would like to thank my sister, parents, and grandparents, whose continuing support, encouragement, and endless love have always guided me forward.

VITA

2011–2015 B.S. (Applied Physics)
University of Science and Technology, P.R.C.

2016–2017 M.S. (Physics)
University of California, Los Angeles, U.S.A.

2018 Ph.D. candidate in Physics
University of California, Los Angeles, U.S.A.

PUBLICATIONS

Ji Zou, Shu Zhang, Yaroslav Tserkovnyak, Bell-state generation for spin qubits via dissipative coupling, arXiv:2108.07365

Arjun Rana, Chen-Ting Liao, Ezio Iacocca, Ji Zou, Minh Pham, Emma-Elizabeth Cating Subramanian, Yuan Hung Lo, Sinéad A. Ryan, Xingyuan Lu, Charles S. Bevis, Robert M. Karl Jr, Andrew J. Glaid, Young-Sang Yu, Pratibha Mahale, David A. Shapiro, Sadegh Yazdi, Thomas E. Mallouk, Stanley J. Osher, Henry C. Kapteyn, Vincent H. Crespi, John V. Badding, Yaroslav Tserkovnyak, Margaret M. Murnane, Jianwei Miao, Direct observation of 3D topological spin textures and their interactions using soft x-ray vector ptychography, arXiv:2104.12933

Mostafa Tanhayi Ahari, Shu Zhang, Ji Zou, Yaroslav Tserkovnyak, Biasing topological charge injection in topological matter, *Phys. Rev. B* **104**, L201401 (2021)

Sayak Dasgupta, Ji Zou, Zeeman term for the Néel vector in a two sublattice antiferromagnet using Dzyaloshinsky-Moriya interaction and magnetic field,*Phys. Rev. B* **104**, 064415

(2021)

Yaroslav Tserkovnyak, Ji Zou, Se Kwon Kim, So Takei, Quantum hydrodynamics of spin winding, *Phys. Rev. B* **102**, 224433 (2020)

Ji Zou, Shu Zhang, Yaroslav Tserkovnyak, Topological transport of deconfined hedgehogs in magnets, *Phys. Rev. Lett.* **125**, 267201 (2020)

Dalton Jones, Ji Zou, Shu Zhang, Yaroslav Tserkovnyak, Energy storage in magnetic textures driven by vorticity flow, *Phys. Rev. B* **102**, 140411(R) (2020)

Ji Zou, Se Kwon Kim, Yaroslav Tserkovnyak, Tuning entanglement by squeezing magnons in anisotropic magnets, *Phys. Rev. B* **101**, 014416 (2020)

Yaroslav Tserkovnyak, Ji Zou, Quantum Hydrodynamics of Vorticity, *Phys. Rev. Research* **1**, 033071 (2019)

Ji Zou, Se Kwon Kim, Yaroslav Tserkovnyak, Topological Transport of Vorticity in Heisenberg Magnets, *Phys. Rev. B* **99**, 180402(R) (2019)

CHAPTER 1

Introduction

"*What we observe is not nature itself, but nature exposed to our method of questioning.*"

Werner Heisenberg

1.1 Motivation and outline

Magnetism, as one of the most common phenomena in nature and one of the oldest subjects of science, continues to actively contribute to the modern condensed matter physics. In particular, the merging of magnetism with topology has given rise to numerous vibrant new topics, such as skyrmions and topological insulators [1, 2, 3, 4, 5, 6, 7, 8]. These are not only fundamentally interesting, but also are promising for a transformative revolution of information technology using topological charges as robust information carriers. Spintronics [9, 10, 11, 12] has emerged as a field that aims to develop devices that transmit and process information utilizing spins. Many recent efforts have been made to understand the transport phenomenon of topological excitations in magnetic systems and to explore their potential applications in (quantum) spintronics [13, 14, 15, 16, 17, 18, 19, 20].

Another interesting direction is due to the marriage of condensed matter physics and quantum information science, which provides us with new insights into many-body phenomena and offers rich opportunities for creative research [21]. In return, condensed matter

systems render various platforms for realizing ideas in quantum information. Spin systems, due to their intrinsic quantum origin, are perfect platforms to explore quantum entanglement and potential utilities [22, 23]. There are many intriguing questions that one can ask: What is the entanglement dynamics within a generic magnetic medium? How can we explore the potential usefulness of magnetic systems for quantum computing?

These two topics are the main focus of this thesis. The main purpose of this chapter is to introduce the basic notions and set up the stage for our discussions of later chapters. In section 1.2, we introduce the basics of topology very briefly. We start with two simply but profound theorems—Poincaré-Hopf theorem and Gauss-Bonnet thorem, where the notion of winding number and skyrmion number is defined. We then introduce the general idea of homotopy group and some examples (including spin winding, magnetic skyrmions, hopfions, and 3D skyrmions in the Skyrme model) are discussed, where the notion of topological conservation laws are naturally introduced. In section 1.3, we recall all the basics of spin dynamics, including both ferromagnetic and antiferromagnetic case. We go through a thorough discussion of spin Berry phase in different representations. In the case of ferromagnet, we explore two examples—spin superfluid in an easy-plane ferromagnet and dynamics of skyrmions. For antiferromagnet, we derive the action for all dimensions and remarks are made for the topological term in one dimension. In section 1.4, we introduce various measures for quantum entanglement (for both pure states and mixed states). In section 1.5, we start with a general description of a non-unitary evolution. We then introduce the Lindblad master equation which is derived both formally from the Kraus operator sum representation of a quantum map, and from first principles. The theory of quantum trajectories is briefly discussed at the end, which provides another perspective for the Lindblad master equation.

Chapter 2 and 3 focus on the topological transport of vorticity [15] in 2D and magnetic hedgehogs [19] in 3D in both (semi)classical and quantum regimes. Identifying strategies to use magnetic insulators to achieve long-range signal transport is one key objective of spintronics studies. Insulating materials with dynamical spin degrees of freedom are good

platforms for spintronics applications. Since the signal transmission is based on pure spins without invoking any electric current, the process is immune to Joule heating and thus has high energy efficiency. Spin currents have been proposed to be promising data carriers in novel devices and computing architectures [9, 24, 25]. However, the spin flow decays exponentially beyond the associated spin-diffusion length [9] in that structural imperfections and anisotropies of materials are detrimental to its conservation law. We propose to utilize topological spin textures (vortex and hedgehogs) as spin signal carriers alternatively, which are shown to be topologically stable information carriers (in the presence of both quantum and thermal fluctuations). They are good candidates since their flows are conserved topologically, known as topological conservation laws, which are rooted in topology rather than symmetries of Hamiltonian, in contrast to Noether-conservation laws. As a result, the transport based on topological textures is robust against structural imperfections and anisotropies, and sustains long-distance spin transport, with broad applications such as energy storage, which is discussed in chapter 2 [18].

There has been much recent interest in coherently preparing and manipulating entanglement in various systems, stimulated by its importance in quantum information science. In chapter 4, we investigate the entanglement between two arbitrary spins in a magnetic system in the presence of applied magnetic fields and axial anisotropies [23]. Spins are shown to be generally entangled in thermodynamic equilibrium, forming a squeezed coherent state, which implies that the magnetic medium can serve as a resource to store and process quantum information. We furthermore show that the entanglement can jump discontinuously when decreasing the transverse magnetic field, which can potentially serve as a switch for quantum information processing tasks.

Chapter 5 focuses on the steady entanglement generation for two distant spin qubits interacting with a common bath (a magnetic system) [26]. Our particular focus is on the induced dissipative coupling between the spin qubits. In contrast to the conventional wisdom that dissipation is detrimental to quantum effects, we show that a sizable long-lifetime

entanglement can be established via a dissipative environment, in the absence of any coherent coupling. Moreover, we demonstrate that maximally-entangled two-qubit states can be achieved in this scheme when complemented by proper postselection. In this situation, there is a dynamical phase transition separated by an exceptional point. The resultant Bell state is robust against weak random perturbations and does not require the preparation of a particular initial state. This result may find applications in quantum information science, quantum spintronics, and for sensing of nonlocal quantum correlations.

1.2 Brief primer on topology

Topology is the study of continuous functions and continuous deformations of objects. It was developed in the twentieth century, while many other fields of mathematics, including calculus, had already been developed three hundred years ago. The origin of topology can most likely be traced to Euler's work in the eighteenth century, and that of Gauss and Riemann in the nineteenth century. As the development of this subject, many branches have emerged, such as general topology, algebraic topology, differential topology, and geometric topology [27]. In particular, algebraic topology is a field that uses tools from algebra (such as group) to study topological spaces. The basic goal is to find algebraic invariants that classify topological spaces up to homeomorphism ideally, though usually most classify up to homotopy equivalence. The most important of these invariants are homotopy groups, homology, and cohomology, which all play a significant role in modern condensed matter physics.

The purpose of this section is twofold. On the one hand, we hope to illustrate the beauty of topology with simplest examples (without invoking any fancy concepts), such as Poincaré-Hopf theorem and Gauss-Bonnet theorem, which have little prerequisites. On the other hand, from these examples, we would like to introduce concepts that we will use in the subsequent chapters, such as vortex number, skyrmion number, topological conservation

laws of topological defects.

1.2.1 Poincaré-Hopf theorem

For simplicity, we consider a two-dimensional orientable closed surface. We will introduce the Euler characteristic of a surface, the topological number associated with vortices of tangent vector fields living on the surface, and the Poincaré-Hopf theorem which relates these two [28]. This is also the first example that I start to really appreciate the beauty of topology. We will see how the global topology of a surface constraints the possible dynamics (the vector field) that can exist on the surface, and how the dynamics happening on the surface indicates its topology.

Any two-dimensional orientable closed surface can be partitioned into triangular pieces. The Euler characteristic is then defined to be $\chi = V - E + F$, where V, E, and F are respectively the numbers of vertices (corners), edges and faces. This is a topological invariant. For example, a tetrahedron and a cube, which can be deformed into each other smoothly, have the same Euler characteristic $\chi = 2$. In general, two-dimensional orientable closed surfaces can be classfied by the number of genus (g), having $\chi = 2(1 - g)$. Two familiar examples are the sphere ($g = 0$) and torus ($g = 1$), which have $\chi = 2$ and $\chi = 0$, respectively.

We now introduce tangent vector fields on a surface. Physically, one can imagine flows of water on the surface. In such a situation, we express a flow of water by vectors given at each point on the surface and indicating the velocity of the flow. The (tangent) vector field of most regions typically is smooth—both the direction and magnitude of the vector change continuously from point to point. There are also points where the water flow stops (the corresponding vector is a zero vector), which are called *critical points* or *vortices* of the vector field. In Fig. 1.1, we show how the flows of water create critical points and form vortices at the peak of a hill, at the low point of a valley, and at a saddle. One can associate

an integer number, known as winding number, to every vortex,

$$N_v = \frac{1}{2\pi} \oint_C d\mathbf{l}\, \hat{\mathbf{z}} \cdot \hat{\mathbf{n}} \times \partial_{\mathbf{l}} \hat{\mathbf{n}}, \tag{1.1}$$

where C is an infinitesimal loop enclosing an isolated vortex, parameterized by $\mathbf{l}$. $\hat{\mathbf{z}}$ is the normal vector perpendicular to the surface where the vortex locates, which also defines the counterclockwise direction of the loop C. $\hat{\mathbf{n}} = \mathbf{v}/|\mathbf{v}|$ is the directional unit vector of the vector field $\mathbf{v}(\mathbf{l})$ living on the loop C. To make it transparent, we set $\hat{\mathbf{z}} = (0, 0, 1), \hat{\mathbf{n}} = (\cos\varphi, \sin\varphi, 0)$, and we choose C to be a circle and parametrize it with the polar angle θ. Then Eq. (1.1) is simply reduced to $N_v = \oint_C d\theta\ \partial_\theta \varphi / 2\pi$. The physical meaning of this winding number is clear now—counting how many times the vector $\hat{\mathbf{n}}$ winds around the unit circle in parameter space $\varphi \in [0, 2\pi)$ when we move along the loop C counterclockwisely. In Fig. 1.1, vortices at the peak and valley have winding number $N_v = 1$ since $\Delta\varphi = 2\pi$ in both cases and, in contrast, the vortex at the saddle has winding number $N_v = -1$. We remark that here we only considered tangent vector fields ($\hat{\mathbf{z}}$ is always perpendicular to $\hat{\mathbf{n}}$). In general, the vector field can go out of plane, for example the magnetization field of an easy-plane ferromagnet. In this case, one needs to modify the definition of the vorticity, as we will discuss later.

At the end of the 19th century, Henri Poincaré showed that the Euler characteristic of a two-dimensional orientable closed surface S_g equals the sum of the winding numbers of all vortices of the vector fields living on the surface:

$$\chi(S_g) = \sum_i N_v(\text{vortex i}). \tag{1.2}$$

Heinz Hopf later generalized this theorem to general higher-dimensional smooth surfaces. We remark that the left-hand-side contains the information of global topology and the right-hand-side reflects the dynamics happening on the surface. Once the topology is given, possible dynamics is constrained. One well-known example is the hairy ball theorem, which simply states that there is no smooth tangent vector field on a sphere having no sources or sinks. In contrast, there is no problem to construct a smooth vector field on a torus as $\chi(\text{torus}) = 0$.

Once we know possible dynamics (possible vector field configuration), we can deduce the Euler characteristic. For example, we can easily obtain that $\chi(\text{surface of genus } g) = 2(1-g)$ by constructing a vector field created by a rainfall on the surface as shown in Fig. 1.1(d). This is, in spirit, similar to the Einstein field equation in general relativity [29]: $G_{\mu\nu} + \Lambda g_{\mu\nu} = \kappa T_{\mu\nu}$, where $G_{\mu\nu}, g_{\mu\nu}$ are the Einstein tensor and the metric tensor (reflecting the spacetime geometry), while $T_{\mu\nu}$ is the stress–energy tensor containing the information of the matter living within the spacetime (Λ, κ are cosmological constant and Einstein gravitational constant). What we can learn from this equation is that the matter field determines spacetime geometry and the sapcetime geometry also governs the motion of matter.

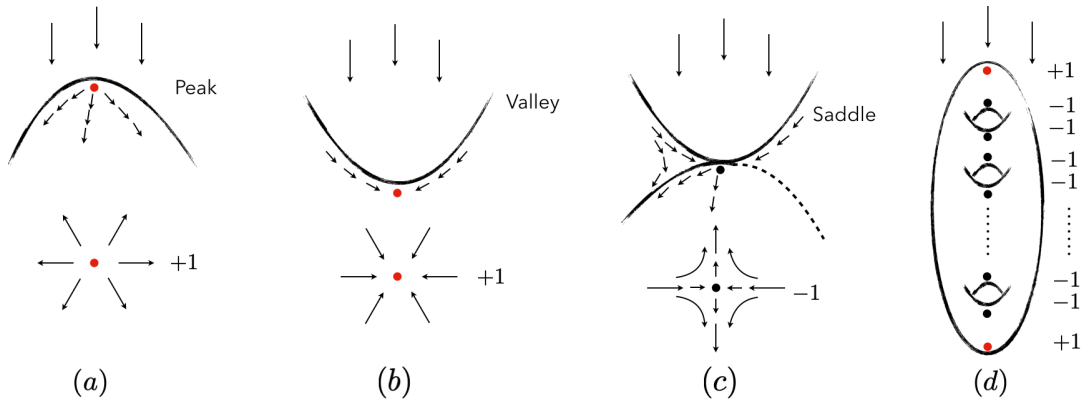

Figure 1.1: (a) A vortex is formed at the peak. (b) A vortex is form at the valley. (c) An anti-vortex is formed at the saddle point. (d) We can construct a tangent vector field on a closed surface with genus g by a rainfall. There are one peak, one valley, and $2g$ saddle points, giving us total vortex number: $2 - 2g$.

1.2.2 Gauss-Bonnet theorem

Gauss-Bonnet theorem describes a beautiful connection between curvature of a surface (from geometry) to its Euler characteristic (from topology) [28, 30, 31]. We again focus on two-dimensional orientable closed surfaces. In this case, it states that the intergral of the local

Gaussian curvature C_G over the closed surface S_g (with genus g) is dictated by its genus g:

$$\int_{S_g} dA\, C_G = 4\pi(1-g) = 2\pi\chi(S_g), \tag{1.3}$$

which is invariant under smooth distorions of the surface since the genus (Euler characteristic) is a topological invariant.

There are typically two ways to evaluate C_G. Let us consider a 2D surface embedded in 3D. For an arbitrary point on the surface, we choose the unit vector $\hat{\mathbf{z}}$ to be the local normal pointing in the outward direction (we have assumed the surface is orientable). Within the tangent plane at this point, we can define a right-handed Cartesian coordinate using orthogonal unit vectors lying in the plane, obeying $\hat{\mathbf{x}} \times \hat{\mathbf{y}} = \hat{\mathbf{z}}$. In the vicinity of the origin of this coordinate system, the surface is uniquely defined by its height relative to the plane, $z(x, y)$. By definition $z(0,0) = \partial_x z(0,0) = \partial_y z(0,0) = 0$. Therefore, we can approximate z locally from its second derivatives:

$$z(x,y) \approx \frac{1}{2}\begin{pmatrix} x & y \end{pmatrix} \begin{pmatrix} \partial_x^2 z & \partial_x\partial_y z \\ \partial_y\partial_x z & \partial_y^2 z \end{pmatrix} \begin{pmatrix} x \\ y \end{pmatrix}. \tag{1.4}$$

This Hessian matrix is evaluated at origin and is real and symmetric, which has two real eigenvalues and two corresponding eigendirections in the tangent plane. The magnitude of the eigenvalues is an inverse radius of curvature and the sign indicates whether the surface is curving toward or away from the positive $\hat{\mathbf{z}}$ direction. The Gaussian curvature C_G is given by the determinant of the Hessian matrix. One illustrating example is a sphere $x^2+y^2+(z+r)^2 = r^2$. Its Hessian matrix is the same for all points on the sphere $H = \mathrm{diag}(-1/r, -1/r)$. Thus we have $C_G = 1/r^2$. Integrating C_G over the sphere gives us 4π, which satisfies Eq. (1.3).

There is another more intuitive way to represent C_G, which is more often used by physicists. We can define $\hat{\mathbf{n}}(\mathbf{r})$ to be the unique unit vector pointing outward, normal to the surface at a point $\mathbf{r}$. Since $\hat{\mathbf{n}}$ lives in a 2-sphere S^2, this vector field $\hat{\mathbf{n}}(\mathbf{r})$ realizes a map from the given closed surface of interest to S^2. Then the local Gaussian curvature is given by

$$C_G(\mathbf{r}) = \hat{\mathbf{n}}(\mathbf{r}) \cdot \partial_x\hat{\mathbf{n}}(\mathbf{r}) \times \partial_y\hat{\mathbf{n}}(\mathbf{r}), \tag{1.5}$$

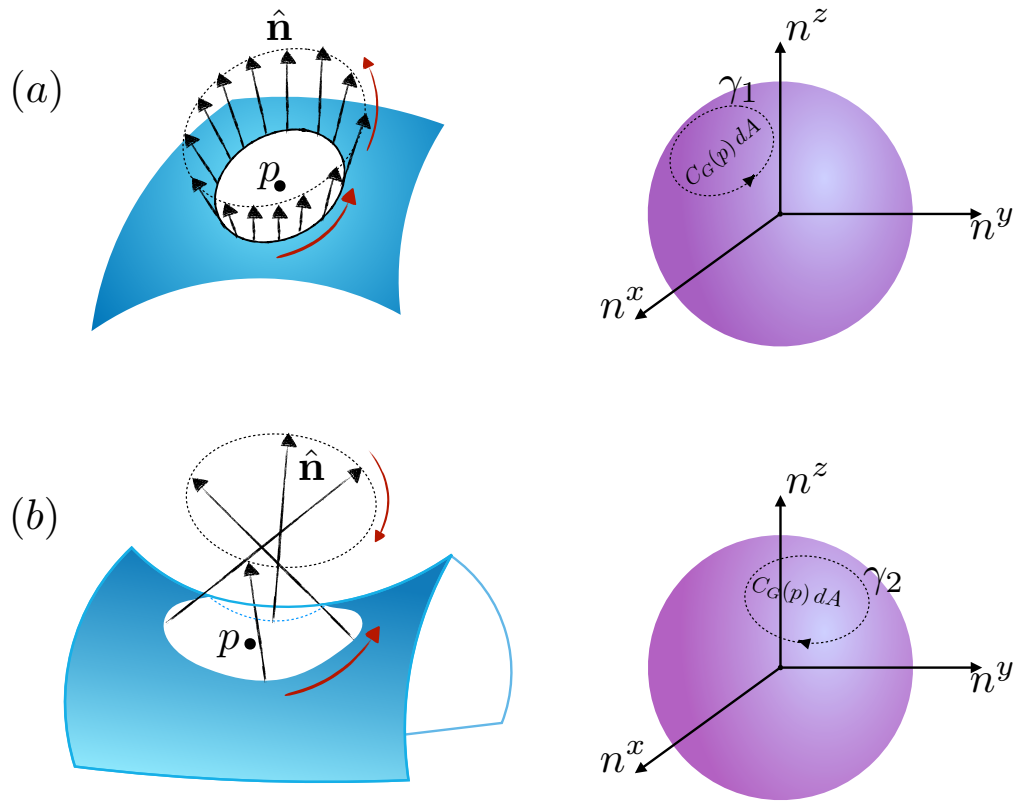

Figure 1.2: (a) To evaluate the curvature at point p, we draw a small circle around it with area dA. As we move counterclockwisely around the circle, (the tip of) unit normal vector $\hat{\mathbf{n}}$ also rotates counterclockwisely and traces out a small closed loop γ_1 on the unit sphere S^2. In this case, the local Gaussian curvature $\hat{\mathbf{n}}(p) \cdot \partial_x \hat{\mathbf{n}}(p) \times \partial_y \hat{\mathbf{n}}(p)\, dA$ is positive and the value is the solid angle or the area enclosed by the loop γ_1 on the unit sphere. (b) We repeat the same procedure. Now (the tip of) unit normal vector $\hat{\mathbf{n}}$ rotates clockwisely, tracing out a small closed loop γ_2 on the unit sphere S^2 (as we move around the circle enclosing the point p counterclockwisely). In this case, the curvature is negative and its value is given by the area enclosed by the loop γ_2 on the unit sphere.

where x, y are local Cartesian coordinate at $\mathbf{r}$. See Fig 1.2. The meaning of this expression is also clear by noting that

$$\hat{\mathbf{n}}(\mathbf{r}) \cdot \partial_x \hat{\mathbf{n}}(\mathbf{r}) \times \partial_y \hat{\mathbf{n}}(\mathbf{r}) \, dA = \sin\theta (\partial_x \theta \partial_y \phi - \partial_y \theta \partial_x \phi) \, dA, \tag{1.6}$$

is the solid angle subtended by the small loop on the unit sphere where $\hat{\mathbf{n}}$ lives, which is generated when moving around the boundary of a small area element dA on the surface of our interest (the tip of the surface normal arrow will trace out a small closed loop on the unit sphere), as we shown in Fig. 1.2. Therefore, the integration of the Gaussian curvature over a closed surface,

$$\frac{1}{4\pi} \int dA \; C_G = \frac{1}{4\pi} \int dA \; \hat{\mathbf{n}} \cdot \partial_x \hat{\mathbf{n}} \times \partial_y \hat{\mathbf{n}}, \tag{1.7}$$

simply counts how many times the normal vector field $\hat{\mathbf{n}}(\mathbf{r})$ of the closed surface wraps around the unit sphere. This is known as the skyrmion number, a natural generalization of the winding number we defined before.

1.2.3 Homotopy group and topological textures

Homotopy group [27], roughly speaking, is a method to extract information of a manifold of our interest by drawing circles and spheres (in general $n-$sphere) on it, which is just like how physicists obtain the information of a system by applying various external fields to it. Here we introduce the fundamental group or the first homotopy group. The generalization to higher homotopy group is straightforward.

We will assume the manifold M that we are interested in is arcwise connected (any $x_0, x_1 \in M$, there exists a continuous path α connecting these two points). This is typically the case in physics. The fundamental group of M is denoted as $\pi_1(M)$. Elements in this group are loops on the manifold M. All loops that can be continuously deformed into each other correspond to the same group element (these loops are said to be homotopic to each other). Therefore, loops that are not homotopic to each other form the fundamental group.

For example, for $M = S^1$, we can draw a loop L_1 winding around S^1 once or a loop L_2 winding twice. It is clear that one cannot continuously deform them into each other. Thus they are different group elements in $\pi_1(S^1)$. In fact, L_1 serves as the generator of this group. The composition of two such loops gives us L_2. In general, we obtain L_{n+m} when we composite L_n and L_m. Therefore, the fundamental group of S^1 is isomorphic to $(\mathbb{Z}, +)$, which is usually simply denoted as $\pi_1(S^1) = \mathbb{Z}$.

We now should make the above description more rigorous by introducing some mathematical definitions. First, what is a loop on a manifold M? A loop is a map $\alpha : S^1 \to M$. If we parametrize S^1 using $t \in [0, 1]$, then $\alpha(0) = \alpha(1)$. For this reason, the fundamental group $\pi_1(M)$ is said to be a classification of the map $S^1 \to M$ [Likewise, n-th homotopy group $\pi_n(M)$ is a classification of the map: $S^n \to M$]. Then, what is the operation of composition? Given two loops $\alpha, \beta : S^1 \to M$ with $\alpha(1) = \beta(0)$. The composition of α and β, denoted as $\alpha \circ \beta$, is a path in M defined by $\alpha \circ \beta(t) = \alpha(2t)$ for $0 \leq s \leq 1/2$ and $\alpha \circ \beta(t) = \beta(2t)$ for $1/2 \leq s \leq 1$. The inverse of a path is defined to be $\alpha^{-1}(t) = \alpha(1 - t)$. The most important question is probably what do we mean by continuous deformation of loops. Two loops L, L' can be deformed into each other continuously if there is a continuous function f from $[0, 1] \times [0, 1]$ to M that satisfies $f(x, 0) = L, f(x, 1) = L'$. With these definitions, one can show that loops form a group. We will introduce some examples of homotopy groups (which are often invoked in physics) and their applications.

The most often encountered homotopy group is $\pi_n(S^n) = \mathbb{Z}$, which is a generalization of the winding number that we discussed before. Here are some well-known examples.

Spin winding in one dimension. We consider a XY model in one dimension, as shown in Fig. 1.3(a). Each configuration is specified by an unit vector field $\mathbf{n}(x)$, which realizes a map from the base manifold $\mathbb{R}$ to the order parameter space S^1. If we consider the case that $\mathbf{n}(-\infty) = \mathbf{n}(+\infty)$ (so the base manifold can be effectively treated as a circle S^1), the spin textures $\mathbf{n}(x)$ can be classified according to $\pi_1(S^1) = \mathbb{Z}$. Every configuration can

be associated with an integer, which is often referred to as topological charge, defined by,

$$N = \frac{1}{2\pi} \int \epsilon_{\alpha_1 \alpha_2} n^{\alpha_1} \partial_x n^{\alpha_2} \, dx = \frac{1}{2\pi} \int \hat{\mathbf{z}} \cdot \mathbf{n} \times \partial_x \mathbf{n} \, dx, \tag{1.8}$$

where $\alpha_1, \alpha_2 \in \{x, y\}$ are different components of the order parameter field $\mathbf{n}$. If we parameterize $\mathbf{n}(x) = (\cos\phi(x), \sin\phi(x))$, we have $N = \int \partial_x \phi \, dx / 2\pi$. According to this definition, it is clear that the upper configuration in Fig. 1.3(a) has $N = -1$, while the lower has $N = 1$. In fact, the local spin winding is conserved. We define topological charge current as $j^\mu_W = \epsilon^{\mu\nu} \partial_\nu \phi / 2\pi$, where $\epsilon^{\mu\nu}$ is the antisymmetric tensor and $\mu, \nu \in \{t, x\}$. The two components respectively correspond to the density $\rho_W = \partial_x \phi / 2\pi$ and the flux $j_W = -\partial_t \phi / 2\pi$ of the spin winding. The conservation of this current $\partial_\mu j^\mu_W = 0$ follows directly from the antisymmetric symbol $\epsilon^{\mu\nu}$ and does not depend on the equation of motion. It is usually referred to as the topological conservation law since it does not follow from Noether's theorem but from topology [32].

We remark that this N can be also used to describe the vortex number for XY model in two dimensions. Now the contour in the integration is a loop circulating around the vortex (see Eq. (1.1)).

Magnetic Skyrmion in two dimensions. In 1975, Belavin and Polyakov wrote a paper titled "Metastable states of two-dimensional isotropic ferromagnets", where magnetic skyrmions are first discussed [33]. Here we describe what is a magnetic skyrmion and its topological nature. We consider a smooth unit vector field $\mathbf{n}(\mathbf{r})$, living on $\mathbf{r} = (x, y) \in \mathbb{R}^2$, where $\mathbf{n}$ is a three-dimensional unit vector those tip defines a point on S^2. One physical realization of such vector field would be the spin configuration of a ferromagnet in two dimensions. We now suppose that the $\mathbf{n}$ tends to the same unit vector at large distance in all directions, for example $\mathbf{n}(\infty) = +\hat{\mathbf{z}}$ as shown in Fig. 1.3(b). Then we can effectively treat the base manifold as S^2. Every configuration realizes a map $S^2 \to S^2$, which can be classified according to $\pi_2(S^2)$ and we define the toplogical charge to be

$$N = \frac{1}{4\pi} \int \epsilon_{\alpha_1 \alpha_2 \alpha_3} n^{\alpha_1} \partial_x n^{\alpha_2} \partial_y n^{\alpha_3} \, dxdy = \frac{1}{4\pi} \int \mathbf{n} \cdot \partial_x \mathbf{n} \times \partial_y \mathbf{n} \, dxdy. \tag{1.9}$$

One can check that this is a topological quantity by considering $\mathbf{n} \to \mathbf{n} + \delta\mathbf{n}$,

$$\delta N \propto \int_{S^2} \mathbf{n} \cdot \partial_i \delta\mathbf{n} \times \partial_j \mathbf{n}\, dx^i \wedge dx^j = \int_{S^2} d[\mathbf{n} \cdot \delta\mathbf{n} \times \partial_j \mathbf{n}\, dx^j] = 0, \tag{1.10}$$

where in the last step we used the Stokes' theorem and the fact that S^2 has no boundary [34]. The geometrical meaning of N is clear, reflecting the number of times that the field $\mathbf{n}(\mathbf{r})$ wraps around the unit sphere S^2. The upper configuration of Fig. 1.3(b) stands for a Skyrmion with $N = -1$. The spins at the center point along $-\hat{\mathbf{z}}$ and those at large distance point along $+\hat{\mathbf{z}}$. Spins in-between lie within xy plane, forming a vortex with charge $+1$. Other regimes are smoothly filled by spins. The lower configuration in Fig. 1.3(b) stands for a skyrmion with $N = 1$, where the in-between spins form an anti-vortex with $N = -1$. One specific configuration of a Skyrmion is $\mathbf{n}(x, y) = (2\lambda x, 2\lambda y, r^2 - \lambda^2)/(r^2 + \lambda^2)$, where λ is the size of the skyrmion and $r^2 = x^2 + y^2$, giving $N = -1$. To get a better intuition, we parametrize $\mathbf{r} = (r\cos\alpha, r\sin\alpha)$ and $\mathbf{n} = (\cos\phi\sin\theta, \sin\phi\sin\theta, \cos\theta)$, assuming $\theta(r, \alpha) = \theta(r)$ and $\phi(r, \alpha) = \phi(\alpha)$ (so the out-of-plane component of the spin is only determined by r and the in-plane components are fixed by α) [8]. In this situation, we can simplify the topological charge into the form:

$$N = \frac{n^z(r = 0) - n^z(r = \infty)}{2} \cdot \frac{\int_0^{2\pi} \partial_\alpha \phi\, d\alpha}{2\pi} = P \cdot W, \tag{1.11}$$

where $P = [n^z(r = 0) - n^z(r = \infty)]/2$ is the polarity and $W = \int \partial_\alpha \phi\, d\alpha/2\pi$ is the vortex number. As this formula suggests, we can produce skyrmions of higher topological number by employing structures with larger vorticities W. For example, we can set $\theta(r) = 2\arctan(\lambda/r)$ and $\phi = W\alpha$, where we obtain skyrmion number $N = -W$.

Analogous to the spin winding case, we can also construct a topologically conserved skyrmion current:

$$j^\mu = \frac{1}{4\pi} \epsilon^{\mu\nu\rho} \mathbf{n} \cdot (\partial_\nu \mathbf{n} \times \partial_\rho \mathbf{n}), \tag{1.12}$$

whose conservation law $\partial_\mu j^\mu = 0$ follows directly from the antisymmetric property of $\epsilon^{\mu\nu\rho}$ ($\mu, \nu, \rho \in \{t, x, y\}$). We should also point out that, similar to the spin winding case, the

topological number N can be also used to characterize the hedgehog number in three dimensions [19]. In this case, instead of integrating over the two-dimensional plane for skyrmion, we integrate over a closed surface in three dimensions enclosing the hedgehog.

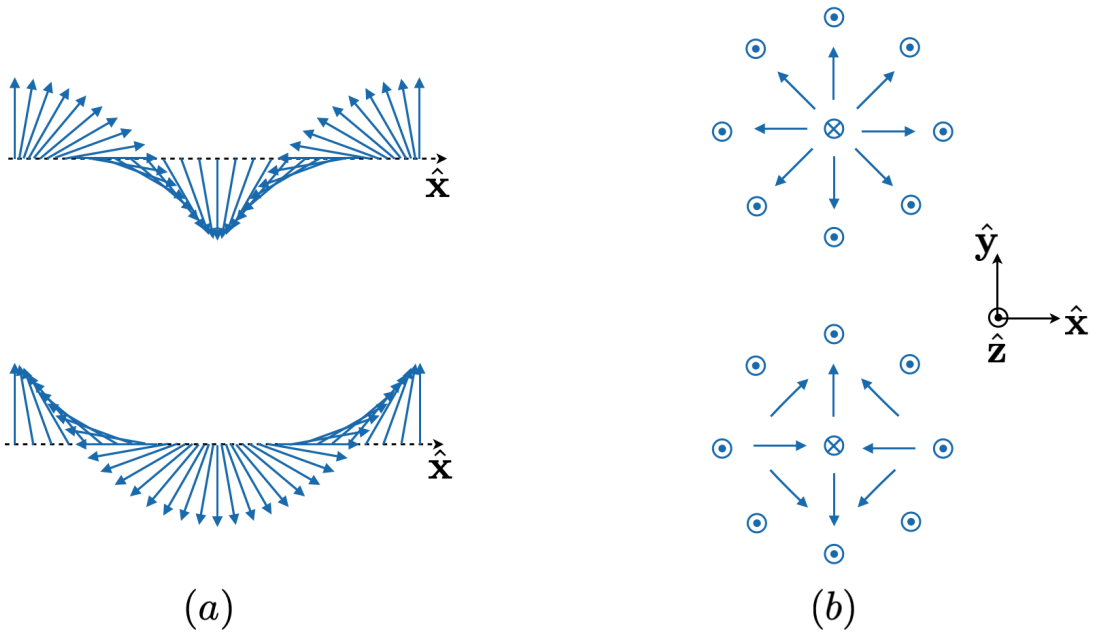

Figure 1.3: (a) The upper spin configuration has winding number -1. The spin angle increases by -2π as we move from left end to the right end. The lower spin texture has winding number $+1$, where the angle increases by $+2\pi$ as we move from the left to the right end. (b) The upper spin texture has skyrmion number -1. The polarity (the change of the spin z component from the center to infinity) is -1. The vortex number of the region in-between is 1. For the lower spin texture, the skyrmion number is $+1$, with polarity -1 and vortex number -1.

3D Skyrmion in the Skyrme Model. The Skyrme model was first proposed as a low energy description of QCD [35, 36]. The field $U(\mathbf{r})$ in this case is SU(2)-valued. Each field configuration $U(\mathbf{r})$ realizes a map from $\mathbf{r} \in \mathbb{R}^3$ to SU(2), which is a 3-sphere S^3. We again suppose the field configuration is the same at infinity such that we can effectively compactify the spatial $\mathbb{R}$ to S^3 by the addition of the point at infinity. In this case, the field configuration

is classified according to the homotopy group $\pi_3(S^3) = \mathbb{Z}$, where the topological charge is given by

$$B = -\frac{1}{24\pi^2}\int d^3\mathbf{r}\ \epsilon_{ijk}\,\mathrm{Tr}\big[(U^\dagger\partial_i U)(U^\dagger\partial_j U)(U^\dagger\partial_k U)\big]. \tag{1.13}$$

This generalized winding number is identified with the baryon number of QCD, hence the notation B. Let us now try to write the expression above into a more familiar form. We first note that group element in SU(2) can be written as $U = i\sum_{i=1}^{3} n_i\sigma_i + n_4$, with the constraint $\sum_{a=1}^{4} n_a^2 = 1$. Here, the three matrices $\boldsymbol{\sigma} = (\sigma_1, \sigma_2, \sigma_3)$ are the familiar Pauli matrices. One useful way to parametrize the four components of the unit vector $\mathbf{n}$ is $\mathbf{n} = (\mathbf{m}\sin\gamma, \cos\gamma)$ with $\mathbf{m}$ being a unit vector on S^2. In this case the matrix U can be written in the familiar form

$$U = \cos\gamma + i\sin\gamma\,\mathbf{m}\cdot\boldsymbol{\sigma} = e^{i\gamma\mathbf{m}\cdot\boldsymbol{\sigma}}. \tag{1.14}$$

Making use of the trace properties of Pauli matrices, such as $\mathrm{Tr}(\sigma_j\sigma_k\sigma_l) = 2i\epsilon_{jkl}$, the topological number can be cast into the form

$$B = \frac{1}{12\pi^2}\int d^3\mathbf{r}\ \epsilon_{ijk}\epsilon_{abcd}\,n_a\partial_i n_b\partial_j n_c\partial_k n_d, \tag{1.15}$$

which is a natural generalization of winding number and skyrmion number we discussed before. The topological nature of B can be also shown similar to what we did for skyrmion number. One should be able to write down the topological number associated with the n-th homotopy group of n-sphere $\pi_n(S^n) = \mathbb{Z}$:

$$\frac{1}{\mathrm{Vol}(S^n)}\frac{1}{n!}\int d^n\mathbf{r}\ \epsilon^{i_1 i_2\cdots i_n}\epsilon_{a_1 a_2\cdots a_{n+1}}n_{a_1}\partial_{i_1}n_{a_2}\partial_{i_2}n_{a_3}\cdots\partial_{i_n}n_{a_{n+1}} \in \mathbb{Z}, \tag{1.16}$$

where we have similarly compacted the $\mathbf{r} = (x^1, x^2, \cdots, x^n)$ into S^n, the n-sphere is $\sum_{a=1}^{n+1} n_a^2 = 1$, and $\mathrm{Vol}(S^n) = 2\pi^{(n+1)/2}/\Gamma(n/2+1/2)$ is the volume of the unit n-sphere. Here Γ is the gamma function. In general, we can define a topological current associated with this charge

$$j^\mu \propto \epsilon^{\mu\mu_1\mu_2\cdots\mu_n}\epsilon_{a_1 a_2\cdots a_{n+1}}n_{a_1}\partial_{i_1}n_{a_2}\partial_{i_2}n_{a_3}\cdots\partial_{i_n}n_{a_{n+1}}, \tag{1.17}$$

where $\mu \in \{t, x^1, \cdots, x^n\}$. Its conservation law also follows from the antisymmetric property of ϵ.

In order to develop some intuition, let us work out some examples. Inspired by the example of skyrmion that we looked into, we assume the "out-of-plane component" only depends on the radial distance r, $\gamma(\mathbf{r}) = \gamma(r)$, and the "in-plane components" $\mathbf{m}$ is independent of r. Similar to case of skyrmion where we can decompose the skyrmion number into the product of the polarity and vortex number, we expect that we can decompose B into the produce to the polarity (related to $\gamma(r)$) and the hedgehog number (related to $\mathbf{m}$) [8]. To this end, it is useful to parametrize the "in-plane components" $\mathbf{m} = (\cos\phi\sin\theta, \sin\phi\sin\theta, \cos\theta)$ and $\mathbf{r} = r(\cos\alpha\sin\beta, \sin\alpha\sin\beta, \cos\beta)$. We now can write the topological number to be

$$\begin{aligned} B =& \frac{1}{2\pi^2}\int \epsilon_{ijk}\sin\theta\sin^2\gamma\,\partial_i\phi\partial_j\theta\partial_k\gamma\; dr d\beta d\alpha \\ =& \frac{\gamma(0)-\gamma(\infty)}{\pi}\cdot\frac{1}{4\pi}\int \mathbf{m}\cdot\partial_\beta\mathbf{m}\times\partial_\alpha\mathbf{m}\; d\beta d\alpha \\ =& P\cdot H, \end{aligned} \tag{1.18}$$

where we have used the fact that we require $\sin[\gamma(0)] = \sin[\gamma(\infty)] = 0$ to ensure that the singularity of the hedgehog of $\mathbf{m}$ is invisible at origin and the field $\mathbf{n} = (\sin\gamma\,\mathbf{m}, \cos\gamma)$ has no variation at infinity. Here, we note that the polarity $P \equiv [\gamma(0) - \gamma(\infty)]/\pi$ is always integer-valued and also the hedgehog number $H \equiv \int \mathbf{m}\cdot\partial_\beta\mathbf{m}\times\partial_\alpha\mathbf{m}\, d\beta d\alpha/4\pi$. For example, one can set $\mathbf{m} = \mathbf{r}/r$ and $\gamma(r) = 2\arctan(\lambda/r)$, which will give us a 3D skyrmion with $B = 1$.

Magnetic Hopfion in three dimensions. Hopfions are first introduced in the contents of field theories [37, 38] and later are studied in various condensed matter systems, such as Bose-Einstein condensates, superconductors, and liquid crystals [39, 40, 41, 42]. It is relatively recent that hopfions are investigated theoretically [43, 44, 45, 46] and are directly observed in magnetic systems [47]. Let us consider a well-ordered magnet with order parameter field $\mathbf{n}(\mathbf{r}, t) \in S^2$. A hopfion is a nonlinear texture classified by the homotopy group $\pi_3(S^2) = \mathbb{Z}$ of the mapping $S^3 \to S^2$, where S^3 is the space manifold with infinity points being identified as one point and S^2 is the order parameter manifold. As a result, every hopfion texture can be associated with an integer, known as Hopf index which can be

expressed as [48]

$$\mathcal{Q}_H = -\int d^3\mathbf{r}\, \vec{\mathcal{B}} \cdot \vec{\mathcal{A}}, \tag{1.19}$$

where

$$\vec{\mathcal{B}}_i = \frac{1}{8\pi}\epsilon_{ijk}\mathbf{n} \cdot \partial_j \mathbf{n} \times \partial_k \mathbf{n} \tag{1.20}$$

and $\vec{\mathcal{A}}$ is the associated vector potential determined by $\nabla \times \vec{\mathcal{A}} = \vec{\mathcal{B}}$ (assuming the field configuration is smooth such that $\nabla \cdot \vec{\mathcal{B}} = 0$). One can intuitively visualize a hopfion as a twisted skyrmion tube with its two ends glued together.

We remark that the hopfion density cannot be written down locally in terms of the field variable $\mathbf{n}(\mathbf{r}, t)$. It is pointed out, in the study of fractional statistics of skyrmions [49, 50], that this nonlocality is not an essential feature of the hopfion density. $\vec{\mathcal{B}} \cdot \vec{\mathcal{A}}$ can be cast into a local form within the CP^1 representation $\mathbf{n} = \mathbf{z}^\dagger \hat{\boldsymbol{\sigma}} \mathbf{z}$, where $\mathbf{z} = (\chi_1 + i\chi_2, \chi_3 + i\chi_4)^T$ is a spinor with real parameters χ_a. The condition $|\mathbf{n}| = 1$ translates into $\mathbf{z}^\dagger \mathbf{z} = 1$ or $\chi_a \chi_a = 1$, taking values in S^3. Note that $\mathbf{n}$ remains unchanged under the transformation $\mathbf{z} \to e^{i\theta}\mathbf{z}$, indicating that the real spin dynamics happens within $S^3/S^1 = S^2$ instead of S^3. Note we can interpret $\mathbf{z}$ as the wavefunction of a spin-1/2 particle. One can parametrize

$$\mathbf{z} = e^{-i\psi/2}\left(e^{-i\phi/2}\cos\frac{\theta}{2}\,|\uparrow\rangle + e^{i\phi/2}\sin\frac{\theta}{2}\,|\downarrow\rangle\right) = e^{-i(\psi+\phi)/2}\begin{pmatrix}\cos\frac{\theta}{2}\\ e^{i\phi}\sin\frac{\theta}{2}\end{pmatrix}, \tag{1.21}$$

which gives us $\mathbf{n} = \mathbf{z}^\dagger \hat{\boldsymbol{\sigma}} \mathbf{z} = (\sin\theta\cos\phi, \sin\theta\sin\phi, \cos\theta)$. Therefore, the magnetic skyrmion with topological charge N that we discussed earlier, in this spinor representation, can be written as

$$\mathbf{z}(\mathbf{r}) = \begin{pmatrix}\cos\frac{\theta(r)}{2}\\ e^{iN\alpha}\sin\frac{\theta(r)}{2}\end{pmatrix}, \tag{1.22}$$

where $\mathbf{r} = r(\cos\alpha, \sin\alpha)$ and $\theta(r) = 2\arctan(\lambda/r)$.

In this spinor representation, we can write the hopfion density locally by noting that $\vec{\mathcal{A}} \equiv \vec{a}/2\pi$ with $a_i = -i\mathbf{z}^\dagger \partial_i \mathbf{z} = i(\partial_i \mathbf{z}^\dagger)\mathbf{z}$, which can be verified straightforwardly

$$\epsilon_{ijk}\partial_i \mathcal{A}_k = \frac{1}{8\pi}\epsilon_{ijk}\mathbf{n} \cdot \partial_j \mathbf{n} \times \partial_k \mathbf{n}. \tag{1.23}$$

In order to construct the configuration of a hopfion, it is useful to make connections to what we discussed in 3D skyrmions. We note that we can also parametrize $\mathbf{z}$:

$$\mathbf{z} = U(\gamma, \theta, \alpha)\mathbf{z}_0 = \begin{pmatrix} \cos\gamma + i\sin\gamma\cos\theta \\ ie^{i\phi}\sin\theta\sin\gamma \end{pmatrix}, \tag{1.24}$$

where $U = \cos\gamma + i\sin\gamma\mathbf{m}\cdot\boldsymbol{\sigma} \in SU(2)$ with $\mathbf{m} = (\cos\phi\sin\theta, \sin\phi\sin\theta, \cos\theta)$, and $\mathbf{z}_0 = \begin{pmatrix} 1 & 0 \end{pmatrix}^T$. Under this parametrization, the three-component unit vector field is

$$\mathbf{n} = \Big[2(m_x m_z \sin\gamma - m_y\cos\gamma)\sin\gamma, 2(m_x\cos\gamma + m_y m_z\sin\gamma)\sin\gamma, \cos^2\gamma + (m_z^2 - m_x^2 - m_y^2)\sin^2\gamma\Big], \tag{1.25}$$

which realizes a map from $S^3 \to S^2$, known as Hopf map, and one can calculate the gauge potential explicitly,

$$\vec{a} = -i\mathbf{z}^\dagger\nabla\mathbf{z} = \sin^2\theta\sin^2\gamma\nabla\phi + \cos\theta\nabla\gamma - \sin\gamma\cos\gamma\sin\theta\nabla\theta. \tag{1.26}$$

Then, we can express the hopfion charge

$$\begin{aligned} \mathcal{Q}_H &= -\frac{1}{4\pi^2}\int d^3\mathbf{r}\ \vec{a}\cdot\nabla\times\vec{a} \\ &= \frac{1}{2\pi^2}\int d^3\mathbf{r}\ \sin\theta\sin^2\gamma\nabla\phi\cdot\nabla\theta\times\nabla\gamma \\ &= -\frac{1}{24\pi^2}\int d^3\mathbf{r}\ \epsilon_{ijk}\,\mathrm{Tr}\big[(U^\dagger\partial_i U)(U^\dagger\partial_j U)(U^\dagger\partial_k U)\big] \in \mathbb{Z}, \end{aligned} \tag{1.27}$$

which is the same as the topological number that we encountered in the 3D skyrmion case (it is also straightforward to construct a topologically conserved hopfion current). This indicates that each topological 3D skyrmion configuration can induce a topological hopfion texture with the same topological number via the Hopf map Eq. (1.25). In other words, we can realize the map $S^3 \to S^2$ by introducing an intermediate step: $S^3 \to S^3 \to S^2$. We have explained the first map which gives us 3D skyrmion. The second part is given by Eq. (1.25). For example, one topological nontrivial 3D skyrmion texture is given by $\mathbf{m} = \mathbf{r}/r$ and $\gamma(r) = 2\arctan(\lambda/r)$, from which one can construct a hopfion configuration with $\mathcal{Q}_H = 1$ by substituting into Eq. (1.25).

1.3 Basic notions of spin dynamics

In this section, we will introduce some basic notions in spin-related physics. Starting from the path integral for a single spin, we construct the action for the ferromagnet. One of the most important feature is the naturally emergent spin Berry phase term, which distinguishes the spin dynamics from ordinary particle dynamics. We will discuss different representations of this term thoroughly, which are all commonly used when studying spin-related problems. Combined with a Rayleigh-Gilbert dissipation function, the Landau-Lifshitz-Gilbert equation is derived. Following this, the spin superfluid and its breakdown in the presence of damping and anisotropies are discussed, where topological hydrodynamics is then very briefly discussed. We then explore the dynamics of skyrmions, where special attentions are paid to the spin Berry phase effect and the generation of the mass term. We then switch to the antiferromagnetic case. We will derive the action in all spatial dimensions. There is a topological term in one dimension where some comments are made. Higher dimensional cases are also discussed.

1.3.1 Spin coherent path integral

Let us first consider the case of a single spin [51, 52, 53]. Consider a spin S degree of freedom whose Hilbert space is $(2S+1)-$dimension. Instead of choosing S^z eigenstates as our basis, we use an alternate scheme where an over-complete basis is used. The spin coherent state is

$$|\mathbf{n}\rangle \equiv |\theta, \phi\rangle = U[R(\mathbf{n})]\,|SS\rangle \tag{1.28}$$

where $|\mathbf{n}\rangle$ denotes the state obtained by rotating the normalized, fully polarized state $|SS\rangle$ by an angle θ around $y-$axis and then by ϕ around $z-$axis with a global phase using the unitary rotation operator $U[R(\mathbf{n})] = e^{-iS^z\phi}e^{-iS^y\theta}e^{-iS^z\chi}$ which is a $(2S+1)-$dimensional representation of the rotation. Given that $\langle SS|\,\mathbf{S}\,|SS\rangle = S\hat{\mathbf{z}}$, it is clear (by considering

$U^\dagger \mathbf{S} U$) that

$$\langle \mathbf{n}| \, \mathbf{S} \, |\mathbf{n}\rangle = S(\hat{\mathbf{z}} \sin\theta\cos\phi + \hat{\mathbf{y}} \sin\theta \sin\phi + \hat{\mathbf{z}} \cos\theta). \tag{1.29}$$

We can rewrite this coherent state in the $|S, M\rangle$ basis:

$$|\mathbf{n}\rangle = e^{-iS\chi} \sum_{M=-S}^{S} \begin{pmatrix} 2S \\ S+M \end{pmatrix}^{1/2} e^{-iM\phi} \Big(\cos\frac{\theta}{2}\Big)^{S+M} \Big(\sin\frac{\theta}{2}\Big)^{S-M} |S, M\rangle \, . \tag{1.30}$$

The Euler angle χ has to be fixed by the requirement that the coherent state be single valued upon $\phi \to \phi + 2\pi n, n = 0, \pm 1, \cdots$. Thus χ is only allowed to take the following values:

$$\chi = (2n+1)\phi, \quad n \in \mathbb{Z}. \tag{1.31}$$

Here, $n = 0$ and $n = -1$ correspond to the Dirac string lying along $\hat{\mathbf{z}}$ or $-\hat{\mathbf{z}}$. In following discussion, we use the north-pole gauge $\chi = -\phi$ (the Dirac string is along $-\hat{\mathbf{z}}$ direction).

The coherent state is one in which the spin operator has a nice expectation value: equal to a classical spin of length S pointing along the direction of $\mathbf{n} = (\sin\theta\cos\phi, \sin\theta\sin\phi, \cos\theta)$. But it is not an eigenvector of the spin operator. This is not expected anyway, since the three components of spin do not commute. Higher powers of spin operator do not have expectation values equal to the corresponding powers of the classical spin. For example, $\langle \Omega| \, S_x^2 \, |\Omega\rangle \neq S^2 \sin^2\theta\cos^2\phi$. However, the difference between this wrong answer and the right one is of order S. Generally, the n-th power of the spin operator will have an expectation value equal to the n-th power of the expectation value of that operator plus corrections that are of order S^{n-1}. If S is large, the corrections may be ignored. Another useful formula is

$$\langle \mathbf{n}_2 | \mathbf{n}_1 \rangle = \Big[\cos\frac{\theta_2}{2}\cos\frac{\theta_1}{2} + e^{i(\phi_1 - \phi_2)} \sin\frac{\theta_2}{2}\sin\frac{\theta_1}{2} \Big]^{2S}, \tag{1.32}$$

which is obviously true for $S = 1/2$ by noting that

$$|\mathbf{n}\rangle \equiv |\theta, \phi\rangle = \cos\frac{\theta}{2} \, |\uparrow\rangle + e^{i\phi} \sin\frac{\theta}{2} \, |\downarrow\rangle \, . \tag{1.33}$$

For a larger spin, one can imagine $2S$ spin-1/2 particles joining to form a spin-S state. There is only one direct product state with $S^z = S$, where all the spin-1/2 particles are pointing

up. Thus the normalized fully polarized state is

$$|SS\rangle = |\uparrow\rangle \otimes |\uparrow\rangle \otimes \cdots \otimes |\uparrow\rangle \,. \tag{1.34}$$

If we now rotate this state, it becomes a tensor product of rotated states and, when we form the inner product on the left-hand side of Eq. (1.32), we obtain the right-hand side. When those two states are close, we have

$$\langle \mathbf{n}_2 | \mathbf{n}_1 \rangle \approx 1 + iS\delta\phi(\cos\theta - 1). \tag{1.35}$$

If we choose the south-pole parametrization $\chi = \phi$, the overlap becomes $\langle \Omega_2 | \Omega_1 \rangle \approx 1 + iS\delta\phi(\cos\theta + 1)$. In general, it is $\langle \Omega_2 | \Omega_1 \rangle \approx 1 + iS\delta\phi(\cos\theta + 1 + 2n)$ under different gauge so that the value is invariant when $\delta\phi \in 2\pi\mathbb{Z}$. The resolution of the identity in terms of these state is $I = \int d\Omega \, |\mathbf{n}\rangle \langle \mathbf{n}| \,$, where $d\Omega = (2S+1)\sin\theta \, d\theta \, d\phi/4\pi$.

We now use the coherent states to derive the path integral for a spin. Let us proceed in the imaginary time τ (and with periodic boundary conditions), the path integral is simply the partition function $Z = \operatorname{tr} e^{-\beta H}$. Following the standard procedure, we split the imaginary-time interval into N steps with each of length δt. We are interested in the regime where $N \to \infty, \delta\tau \to 0$ while keeping $N\delta\tau = \beta$. We also assume $\tau_0 = 0, \tau_{N+1} = \beta$. We have

$$Z = \lim_{N\to\infty} \int d\Omega(\tau_0) \, \langle \mathbf{n}(\tau_{N+1}) | \left[e^{-\delta\tau \, H} \right]^N |\mathbf{n}(\tau_0)\rangle = \lim_{N\to\infty} \int \Pi_{j=0}^{N} d\Omega(\tau_j) \, \langle \mathbf{n}(\tau_{j+1}) | \, e^{-\delta\tau \, H} \, |\mathbf{n}(\tau_j)\rangle \,. \tag{1.36}$$

We now utilize the fact that

$$\frac{\langle \mathbf{n}(\tau_{j+1}) | \, H \, |\mathbf{n}(\tau_j)\rangle}{\langle \mathbf{n}(\tau_{j+1}) | \mathbf{n}(\tau_j)\rangle} = \langle \mathbf{n}(\tau_j) | \, H \, |\mathbf{n}(\tau_j)\rangle + \mathcal{O}(\delta\tau), \tag{1.37}$$

which implies

$$\langle \mathbf{n}(\tau_{j+1}) | \, e^{-\delta\tau \, H} \, |\mathbf{n}(\tau_j)\rangle = \exp\big\{ \delta\tau \big[\, \langle \dot{\mathbf{n}}(\tau_j) | \mathbf{n}(\tau_j)\rangle - \langle \mathbf{n}(\tau_j) | \, H \, |\mathbf{n}(\tau_j)\rangle \, \big] \big\}. \tag{1.38}$$

Therefore, we can write the partition function as $Z = \int \mathcal{D}\mathbf{n}(\tau) e^{-S_E[\mathbf{n}]}$, where $\mathcal{D}\mathbf{n}(\tau) = \Pi_{j=0}^{N} d\Omega(\tau_j)$ and

$$S_E[\mathbf{n}] = \int d\tau \, iS\dot{\phi}(1 - \cos\theta) + \int d\tau H[\mathbf{n}]. \tag{1.39}$$

We can switch to the real time formalism by identifying $\tau = it$. Then we have $Z = \int \mathcal{D}\mathbf{n}(t) e^{iS[\mathbf{n}(t)]}$, where

$$S[\mathbf{n}(t)] = -\int dt\ S\dot{\phi}(1-\cos\theta) - \int dt\ H[\mathbf{n}]. \tag{1.40}$$

We remark that the first term $S_B[\mathbf{n}(t)] = \int dt\, S\dot{\phi}(\cos\theta - 1)$ in the action is known as geometric phase (or Wess-Zumino or spin Berry phase term), which are of purely kinematic origin and exists even in the absence of a Hamiltonian. This term is also responsible for the distinct behavior of half-odd-integral and integer spins. The corresponding amplitude has the same form in both real and imaginary time, in contrast to the energetic part which is imaginary in real time but real in imaginary time. We will discuss this term and its effects in a more detail in the following subsections.

Path integral for many spins. We now generalize the one spin problem to a many spin system. For the purpose of illustration, we derive the continuum field theory to describe the quantum dynamics of a ferromagnet, starting from a microscopic Heisenberg spin Hamiltonian with local anisotropies:

$$H = -J\sum_{\langle i,j\rangle} \mathbf{S}_i \cdot \mathbf{S}_j + K\sum_{\langle i,j\rangle} S_i^z S_j^z, \tag{1.41}$$

where $\mathbf{S}_i$ denotes the spin operator at the lattice site i, $\langle \dots \rangle$ means summing over nearest neighbors, and $K > 0$ is the hard $\hat{z}$ axis anisotropy. For simplicity, we assume the spins form a simple hypercubic lattice with lattice constant a. Let us work in the real time. We simply sum over all site and making use of $\langle \mathbf{n}| \mathbf{S} |\mathbf{n}\rangle = S\mathbf{n}$, yielding

$$S[\mathbf{n}(\mathbf{r},t)] = \sum_{\mathbf{r}} S_B[\mathbf{n}(\mathbf{r},t)] - \int dt\ \sum_{\langle \mathbf{r},\mathbf{r}'\rangle} \Big[-JS^2 \mathbf{n}(\mathbf{r},t)\cdot\mathbf{n}(\mathbf{r}',t) + KS^2 n^z(\mathbf{r},t) n^z(\mathbf{r}',t)\Big], \tag{1.42}$$

where $\mathbf{r}, \mathbf{r}'$ are just lattice vectors. Making use of the constraint $\mathbf{n}^2 = 1$, we can have

$$-\mathbf{n}(\mathbf{r},t)\cdot\mathbf{n}(\mathbf{r}',t) = \frac{1}{2}\big[\mathbf{n}(\mathbf{r},t) - \mathbf{n}(\mathbf{r}',t)\big]^2 + \text{constant}. \tag{1.43}$$

Consider now the long-wavelength limit, in which $\mathbf{n}(\mathbf{r},t)$ is a smooth function of the spatial coordinates, Then we can write an effective contiuum action for the long-wavelength

fluctuations:

$$\begin{aligned} S[\mathbf{n}(\mathbf{r},t)] &= \int dtd^d\mathbf{r}\ \frac{S}{a^d}\dot{\phi}(\cos\theta-1) - \int dtd^d\mathbf{r}\ \frac{JS^2}{2a^{d-2}}(\nabla\mathbf{n})^2 - \int dtd^d\mathbf{r}\ \frac{zKS^2}{a^d}n_z^2+\cdots \\ &= \int dtd^d\mathbf{r}\ s\dot{\phi}(\cos\theta-1) - \int dtd^d\mathbf{r}\ \frac{\mathcal{A}}{2}(\nabla\mathbf{n})^2 - \int dtd^d\mathbf{r}\ \frac{\mathcal{K}}{2}n_z^2+\cdots, \end{aligned} \tag{1.44}$$

where $s \equiv S/a^d$ is the saturated spin density, $\mathcal{A} = JS^2/a^{d-2}$ is the stiffness of the field, and $\mathcal{K} = 2zKS^2/a^d$ is the easy-plane anisotropy that constrains the magnetic order to lie within xy plane in spin space (z is the number of nearest site, $z = 2d$ for hypercubic lattice).

Landau–Lifshitz–Gilbert equation. Let us denote the Hamiltonian as $H[\mathbf{n}]$ and thus the variation of action is

$$\delta S[\mathbf{n}] = \int dtd^d\mathbf{r}\ s(\mathbf{n}\times\partial_t\mathbf{n})\cdot\delta\mathbf{n} - \int dtd^d\mathbf{r}\ \frac{\delta H[\mathbf{n}]}{\delta\mathbf{n}}\cdot\delta\mathbf{n}, \tag{1.45}$$

which indicates $\delta_{\mathbf{n}}L - (d/dt)\delta_{\dot{\mathbf{n}}}L = s\mathbf{n}\times\partial_t\mathbf{n} - \delta_{\mathbf{n}}H$. The energy dissipation power can be taken into account by the Rayleigh dissipation function (having dimension of energy/time):

$$R[\mathbf{n}] = \frac{\alpha s}{2}\int d^2\mathbf{r}\ \dot{\mathbf{n}}^2, \tag{1.46}$$

where α is a dimensionless constant known as Gilbert damping factor. By implementing (recall L has dimension of energy):

$$\frac{\mathrm{d}}{\mathrm{d}t}\frac{\delta L}{\delta\dot{\mathbf{n}}} - \frac{\delta L}{\delta\mathbf{n}} + \frac{\delta R}{\delta\dot{\mathbf{n}}} = 0, \tag{1.47}$$

we have

$$(1+\alpha\mathbf{n}\times)\partial_t\mathbf{n} = \mathbf{n}\times\mathbf{h}, \quad \text{with} \quad \mathbf{h} \equiv -\frac{\delta H[\mathbf{n}]}{\delta s\mathbf{n}}, \tag{1.48}$$

which is known as the Landau–Lifshitz–Gilbert equation. One can also write it into an equivalent but a more suggestive form

$$(1+\alpha^2)\partial_t\mathbf{n} = \mathbf{n}\times\mathbf{h} + \alpha\mathbf{n}\times(\mathbf{h}\times\mathbf{n}). \tag{1.49}$$

It is clear from the right hand side that the precessional torque and the damping torque are perpendicular to each other. Meanwhile, they are both linear in the effective field.

1.3.2 Geometric phase in different representations

The geometrical phase distinguishes the spin dynamics from ordinary dynamics of particles that we often encounter. In different context, it may appears in different representations or forms [8, 54]. Therefore, it is useful to summarize all different representations that are often used when one studies spin-related problems. We will consider a single spin. First, in terms of angle variables θ, ϕ, we have (as we derived above):

$$S_B = S \int dt\ \dot{\phi}(\cos\theta - 1), \tag{1.50}$$

which we usually refer to as spin Berry phase. In spinor (CP^1) representation, it is given by

$$S_{CP^1} = 2iS \int dt\ \mathbf{z}^\dagger \partial_t \mathbf{z}. \tag{1.51}$$

We can also write the geometric phase into the Wess-Zumino form:

$$S_{WZ} = S \int dt \int_0^1 du\ \mathbf{n} \cdot \partial_t \mathbf{n} \times \partial_u \mathbf{n}. \tag{1.52}$$

One may also write it as a magnetic monopole action:

$$S_{MM} = \int dt\ \mathbf{A} \cdot \partial_t \mathbf{n}, \tag{1.53}$$

where $\nabla_{\mathbf{n}} \mathbf{A} = -S\mathbf{n}$. We now step through every representation one by one.

Spinor representation. As we have discussed previously, we introduce the new variable, $\mathbf{z} = [\cos(\theta/2),\ e^{i\phi}\sin(\theta/2)]^T$, and $\mathbf{z}^\dagger \boldsymbol{\sigma} \mathbf{z} = \mathbf{n}$. We note that $\mathbf{z}$ is simply a spin-1/2 coherent state. By noting that $-i\mathbf{z}^\dagger \partial_t \mathbf{z} = \dot{\phi}(1 - \cos\theta)/2$, we can write the geometric phase as

$$\exp\left\{ iS \int dt\ \dot{\phi}(\cos\theta - 1) \right\} = \exp\left\{ 2iS \int dt\ i\mathbf{z}^\dagger \partial_t \mathbf{z} \right\}. \tag{1.54}$$

To fully appreciate the beauty of this spinor representation (instead of just a rewriting of the phase in terms of new variable), we consider a spin texture living on some spacetime $\mathbf{n}(\mathbf{r}, t)$ and introduce a gauge field

$$a_\mu \equiv -i\mathbf{z}^\dagger \partial_\mu \mathbf{z} = \frac{1}{2}(1 - \cos\theta)\partial_\mu \phi, \tag{1.55}$$

where μ is spacetime index. We can further introduce the field tensor:

$$f_{\mu\nu} = \partial_\mu a_\nu - \partial_\nu a_\mu = \frac{1}{2}\mathbf{n}\cdot\partial_\mu\mathbf{n}\times\partial_\nu\mathbf{n}, \tag{1.56}$$

which can be verified by straightforward calculation and is known as the Mermin-Ho relation in the context of superfluid ^{3}He. As a result, we could introduce the emergent magnetic field and emergent electric field:

$$\epsilon_{\mu\nu\lambda}b_\lambda = \frac{1}{2}\mathbf{n}\cdot\partial_\mu\mathbf{n}\times\partial_\nu\mathbf{n}, \quad \text{and} \quad e_\mu = \frac{1}{2}\mathbf{n}\cdot\partial_t\mathbf{n}\times\partial_\mu\mathbf{n}, \tag{1.57}$$

which play a pivotal role in the dynamics of solitons (such as vortex, skyrmion, and hedgehog), and will also be experienced by electrons and magnons moving through a magnetic texture $\mathbf{n}(\mathbf{r},t)$.

Beside, the nonlinear $\sigma-$model $(\partial_\mu\mathbf{n})^2$ has an appealing form in the spinor representaion:

$$(\partial_\mu\mathbf{n})^2 = 4(D_\mu\mathbf{z})^\dagger D_\mu\mathbf{z}, \tag{1.58}$$

where $D_\mu = \partial_\mu - ia_\mu$. Another use of this representation is to construct configurations of hopfions which we have discussed before.

Wess-Zumino term. In order to elucidate the (skyrmionic) topological character of this term, it is illuminating to to write the phase term into a vectorial form:

$$S_{WZ} = 4\pi SW[\mathbf{n}] \quad \text{with} \quad W[\mathbf{n}] = \frac{1}{4\pi}\int dt\int_0^1 du\ \mathbf{n}\cdot\partial_t\mathbf{n}\times\partial_u\mathbf{n}, \tag{1.59}$$

where u is a dummy variable, such that $\mathbf{n}(t,u)$ satisfies $\mathbf{n}(t,0)=\hat{\mathbf{z}}$ and $\mathbf{n}(t,1)=\mathbf{n}(t)$. The geometric action written in a space with one extra dimension with the aid of a fictitious variable in this manner is commonly known as Wess-Zumino action in the literature.

There are several ways to justify this expression. For example, we can realize the boundary condition $\mathbf{n}(t,u)$ satisfies $\mathbf{n}(t,0)=\hat{\mathbf{z}}$ and $\mathbf{n}(t,1)=\mathbf{n}(t)$ by defining $\theta(t,u)=u\theta(t)$ and $\phi(t,u)=\phi(t)$ (so that one has $\theta(t,0)=0$ corresponding to the north pole and $\theta(t,1)=\theta(t)$ corresponding to the physical direction). Therefore, Eq. 1.56 indicates

$$\frac{1}{2}\mathbf{n}\cdot\partial_t\mathbf{n}\times\partial_u\mathbf{n} = \partial_t a_\nu - \partial_u a_t = -\partial_u a_t, \tag{1.60}$$

where we have used the fact that $a_u \propto \partial_u \phi = 0$. We also note that $a_t(t,0) = (1 - \cos 0)\partial_t\phi/2 = 0$ and $a_t(t, u = 1) \equiv a_t(t) = -i\mathbf{z}^\dagger \partial_t \mathbf{z}$. Integrating the Eq. (1.60) yields:

$$a_t(t) = -i\mathbf{z}^\dagger \partial_t \mathbf{z} = -\frac{1}{2}\int_0^1 du\ \mathbf{n} \cdot \partial_t \mathbf{n} \times \partial_u \mathbf{n}. \tag{1.61}$$

Therefore, we have

$$\exp\left\{2iS \int dt\ i\mathbf{z}^\dagger \partial_t \mathbf{z}\right\} = \exp\left\{iS \int dt \int_0^1 du\ \mathbf{n} \cdot \partial_t \mathbf{n} \times \partial_u \mathbf{n}\right\}. \tag{1.62}$$

We can also justify the form of the Wess-Zumino term by looking at the variation of this term. To this end, it is helpful to write the term as

$$S_{WZ} = -\frac{S}{2}\int dtdu\ \epsilon^{\mu\nu} \mathbf{n} \cdot \partial_\mu \mathbf{n} \times \partial_\nu \mathbf{n}, \tag{1.63}$$

where $\mu, \nu \in \{t, u\}$ and we use the convention: $\epsilon^{ut} = 1$. Then,

$$\begin{aligned}
\delta S_{WZ} =& -S \int dtdu\ \epsilon^{\mu\nu} \mathbf{n} \cdot \partial_\mu (\delta\mathbf{n} \times \partial_\nu \mathbf{n}) \\
=& -S \int dtdu\ \epsilon^{\mu\nu} \partial_\mu \big(\mathbf{n} \cdot \delta\mathbf{n} \times \partial_\nu \mathbf{n}\big) \\
=& -S \int dtdu\ \partial_u \big(\mathbf{n} \cdot \delta\mathbf{n} \times \partial_t \mathbf{n}\big) + S \int dtdu\ \partial_t \big(\mathbf{n} \cdot \delta\mathbf{n} \times \partial_u \mathbf{n}\big) \\
=& -S \int dt\ \mathbf{n} \cdot \delta\mathbf{n} \times \partial_t \mathbf{n} = -S \int dt\ (\partial_t \mathbf{n} \times \mathbf{n}) \cdot \delta\mathbf{n}
\end{aligned}, \tag{1.64}$$

where we have used the fact that $\delta\mathbf{n} \cdot \partial\mathbf{n} \times \partial\mathbf{n} = 0$, dropped a total time derivative term, and performed an integration by part for the variable u. If the Hamiltonian is $H[\mathbf{n}]$, then the equation of motion is given by $\partial_t \mathbf{n} = \mathbf{n} \times \mathbf{h}$, where $\mathbf{h} \equiv -\delta H/\delta \mathbf{n} S$ is the effective field.

Topological origin. To appreciate the topological aspect of the Wess-Zumino term, let us consider an action $e^{i2\pi g W[\mathbf{n}]}$ ($g = 2S$ in our case). To make sure the path integral to be well-defined, $e^{i2\pi g W[\mathbf{n}]}$ should not depend on unphysical configuration $\mathbf{n}(t, u)$ but only on the physical one $\mathbf{n}(t, u = 1)$. Let us explore the consequence of this constraint. We consider the physical trajectory of $\mathbf{n}$ is a loop $\mathbf{n}(t = 0) = \mathbf{n}(t = T)$. Then one extension of $\mathbf{n}(t, u)$ is a map from a disk $(t, u) \in \Sigma$ to $\mathbf{n} \in S^2$. We note that the boundary of Σ is given by $(t, u = 1)$.

Consider another extension $\tilde{\mathbf{n}}(t,\tilde{u})$ which is similarly a map from a disk $\tilde{\Sigma}$ to S^2. We require the difference between arbitrary extensions to be invisible to $e^{i2\pi gW[\mathbf{n}]}$. We have

$$\begin{aligned} W[\mathbf{n}]-W[\tilde{\mathbf{n}}] &= \frac{1}{4\pi}\int_{\Sigma} dtdu\ \mathbf{n}\cdot\partial_t\mathbf{n}\times\partial_u\mathbf{n} - \frac{1}{4\pi}\int_{\tilde{\Sigma}} dtdu\ \tilde{\mathbf{n}}\cdot\partial_t\tilde{\mathbf{n}}\times\partial_u\tilde{\mathbf{n}} \\ &= \frac{1}{4\pi}\int_{S^2=\Sigma-\tilde{\Sigma}} dtdu\ \mathbf{n}\cdot\partial_t\mathbf{n}\times\partial_u\mathbf{n}\in\mathbb{Z}, \end{aligned} \tag{1.65}$$

where we first note that $\Sigma-\tilde{\Sigma}$ forms a sphere and the result is integer-valued, which is just the wrapping number of the map $S^2\to S^2$.Therefore, we require the coefficient g to be integer-valued to make sure $e^{i2\pi gk}=1$. In our case, this translates into the constraint that the spin S must be an integer or a half integer, which is naturally satisfied.

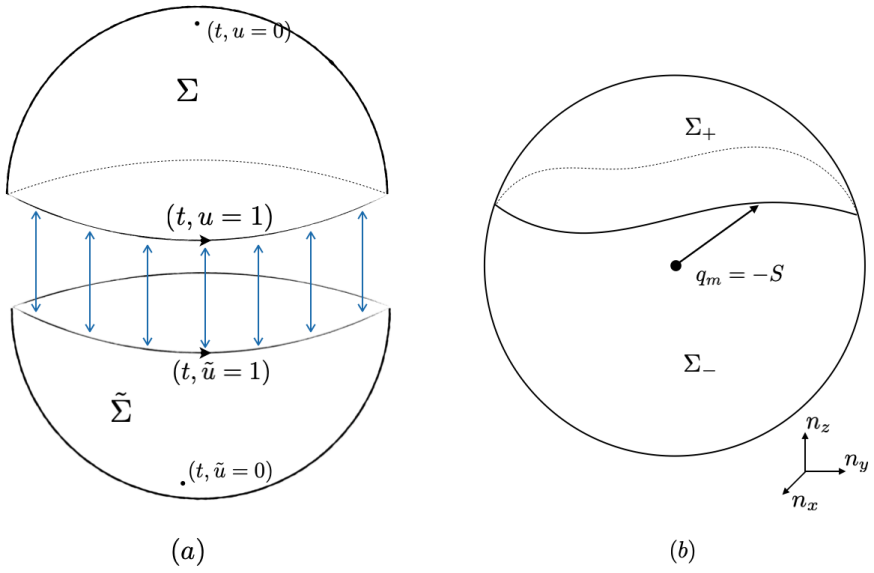

Figure 1.4: (a) Given a physical loop $\mathbf{n}(t)$, we consider two different extensions $\mathbf{n}(t,u),\mathbf{n}(t,\tilde{u})$. Their base manifolds are denoted as $\Sigma,\tilde{\Sigma}$, which have the same boundary since it is where the physical $\mathbf{n}$ field lives. After identifying their boundary, it is clear that $\Sigma-\tilde{\Sigma}$ forms a sphere (note that directions of both $\Sigma,\tilde{\Sigma}$ are defined according to the direction of the loop). (b) The dynamics of a spin is equivalent to a massless particle with charge $+1$ moving on a surface of a unit sphere whose center has a magnetic monopole $q_m=-S$. The spin Berry phase in this case corresponds to the Aharonov-Bohm phase picked up by the particle moving the magnetic field.

Wess-Zumino term as an emergent theory. It is always helpful and inspiring to see how the same structure emerges in different physical contexts. We have shown that the Wess-Zumino term arises naturally in the dynamics of a single spin [54]. Here we show that such a term can be also induced by interacting a spin with an electron. We couple a spinful fermion $\mathbf{c}_\alpha, \alpha = \uparrow, \downarrow$ to a single spin $\vec{S}$ in an SU(2) invariant way, $H = m(\mathbf{c}^\dagger \boldsymbol{\sigma} \mathbf{c}) \cdot \vec{S}$, where m is a coupling constant with dimension of energy. In the Euclidean path integral formalism, the partition function is

$$Z = \int \mathcal{D}\psi \mathcal{D}\bar{\psi} \mathcal{D}\mathbf{n}\; e^{-S_0[\mathbf{n}] - \int d\tau\, \bar{\psi}(\partial_\tau - m\mathbf{n}\cdot\boldsymbol{\sigma})\psi}, \tag{1.66}$$

where $\psi = (\psi_\uparrow, \psi_\downarrow)$ is a two-component Grassmann spinor, $\mathbf{n}^2 = 1$, and $S_0[\mathbf{n}] = 4\pi S W[\mathbf{n}]$. We are interested in the action of $\mathbf{n}$ induced by the interaction with the fermion. To this end, we integrate out $\psi, \bar{\psi}$, which yields $Z = \int \mathcal{D}\mathbf{n} e^{-S_0[\mathbf{n}] - S_1[\mathbf{n}]}$, with

$$S_1[\mathbf{n}] = -\ln \int \mathcal{D}\psi \mathcal{D}\bar{\psi} e^{-\int d\tau\, \bar{\psi} D \psi} = -\ln \det D, \tag{1.67}$$

where we defined an operator $D = \partial_\tau - m\mathbf{n}\cdot\boldsymbol{\sigma}$. The variation of $S_2[\mathbf{n}]$ with respect to $\mathbf{n}$ is

$$\delta S_1[\mathbf{n}] = -\delta \,\mathrm{tr} \ln D = -\,\mathrm{tr}\left[\delta D D^\dagger (D D^\dagger)^{-1}\right], \tag{1.68}$$

where $\delta D = -m\delta\mathbf{n}\cdot\boldsymbol{\sigma}$, $D^\dagger = -\partial_\tau - m\mathbf{n}\cdot\boldsymbol{\sigma}$, and $DD^\dagger = -\partial_\tau^2 + m^2 - m\dot{\mathbf{n}}\cdot\boldsymbol{\sigma}$. Expanding the denominator in $\dot{\mathbf{n}}/m$ and perform the trace, we get

$$\delta S_1 = \int d\tau\, \Big[-\frac{m}{2|m|} \delta\mathbf{n}\cdot\mathbf{n}\times\dot{\mathbf{n}} + \frac{1}{4m}\delta\dot{\mathbf{n}}\cdot\dot{\mathbf{n}}\Big], \tag{1.69}$$

where we have dropped higher order in the expansion. Therefore, we conclude that

$$S_1 = -2\pi\,\mathrm{sign}(m)\, W[\mathbf{n}] + \int dt\, \frac{\dot{\mathbf{n}}^2}{8m}. \tag{1.70}$$

As we can see that, by integrating out the fermion, we produce a Wess-Zumino term which shifts the spin in $S_0[\mathbf{n}]$: $S \to S - \mathrm{sign}(m)/2$, which is what we expect since $S \otimes 1/2 = (S - 1/2) \oplus (S + 1/2)$ (depending on the coupling is antiferromagnetic or ferromagnetic).

Magnetic monopole action. It is inspiring to make the analogy between the spin dynamics and the charged particle dynamics in magnetic field. As we will see, the geometric phase can be regarded as the Aharonov-Bohm (AB) phase experienced by a massless particle (with charge +1) moving on a surface of a unit sphere whose center has a magnetic monopole $q_m = -S$. If this statement is true, we expect the Lagrangian to have the form $L = \mathbf{A} \cdot \dot{\mathbf{n}} = (\mathbf{A} \cdot \hat{\theta})\dot{\theta} + (\mathbf{A} \cdot \hat{\phi})\dot{\phi} \sin\theta$, where we have used the fact that $\dot{\mathbf{n}} = \dot{\theta}\hat{\theta} + \sin\theta\dot{\phi}\hat{\phi}$. When we try to match it with $L = S\dot{\phi}(\cos\theta - 1)$, we have $\mathbf{A} \cdot \hat{\theta} = 0$ and $\sin\theta \mathbf{A} \cdot \hat{\phi} = S(\cos\theta - 1)$. Thus the vector potential is

$$\mathbf{A} = S\frac{\cos\theta - 1}{\sin\theta}\hat{\phi}, \tag{1.71}$$

which corresponds to a magnetic field

$$\nabla_{\mathbf{n}} \times \mathbf{A} = -S\mathbf{n}, \tag{1.72}$$

generated by a magnetic monopole $q_m = -S$ at the center of sphere $|\mathbf{n}| = 1$. Indeed, the statement is correct. We remark that the gauge potential $\mathbf{A}$ is not globally well-defined. In the expression above, the Dirac string extends along $-\hat{\mathbf{z}}$ direction. One can write down a general vector potential with Dirac string along $\mathbf{n}_0$:

$$\mathbf{A} = -S\frac{\mathbf{n}_0 \times \mathbf{n}}{1 - \mathbf{n}_0 \cdot \mathbf{n}}. \tag{1.73}$$

We should note that there are choices (Σ_+ or Σ_- in Fig. 1.4) when one calculates the flux through a loop $\mathbf{n}(t = 0) = \mathbf{n}(t = T)$. To have a self-consistent theory, we require:

$$e^{-iS\vec{\Sigma}_+ \cdot \mathbf{n}} = e^{-iS\vec{\Sigma}_- \cdot \mathbf{n}}, \tag{1.74}$$

where $-S\mathbf{n}$ is the magnetic field, $\vec{\Sigma}_+, \vec{\Sigma}_-$ are the surface areas with sign. Since $\vec{\Sigma}_+ \cdot \mathbf{n} - \vec{\Sigma}_- \cdot \mathbf{n} = 4\pi$, we again arrive at the constraint that $e^{i4\pi S} = 1$, which indicates that the spin S should be integer- or half integer-valued.

1.3.3 From spin superfluid to topological hydrodynamics

Spin superfluid. As an example to utilize the result that we derived above, we explore the phenomenon of spin superfluidity [55, 14] in a two dimensional easy-plane ferromagnets (with order parameter field $\mathbf{n}$, assuming the system is ordered $|\mathbf{n}| = 1$) with Lagrangian density:

$$L[\mathbf{n}] = \int d^2\mathbf{r} \, \Big[s\dot{\phi}(\cos\theta - 1) - \frac{\mathcal{A}}{2}(\nabla \mathbf{n})^2 - \frac{\mathcal{K}}{2} n_z^2 \Big], \tag{1.75}$$

where $\mathbf{n} = (\cos\phi \sin\theta, \sin\phi\sin\theta, \cos\theta) = (\sqrt{1-n_z^2}\cos\phi, \sqrt{1-n_z^2}\sin\phi, n_z)$, $s = S/a^2$ is the saturated spin density, $\mathcal{A} = JS^2$ is the stiffness of the field, and $\mathcal{K} = KS^2/a^2$ is the easy-plane anisotropy that constrains the magnetic order to lie within the plane of the film. These three parameters of the model can be combined to define characteristic scales of energy $\mathcal{A}$, length $\xi = \sqrt{\mathcal{A}/\mathcal{K}}$ and time, or equivalently, velocity ($c = \mathcal{A}/s\xi = \sqrt{\mathcal{A}\mathcal{K}}/s$). Expressing the Lagrangian in terms of variables n_z, ϕ, we have

$$\mathcal{L}[\mathbf{n}] = s\dot{\phi}(n_z - 1) - \frac{\mathcal{A}}{2}\Big[(1-n_z^2)(\nabla\phi)^2 + \frac{(\nabla n_z)^2}{1-n_z^2}\Big] - \frac{\mathcal{K}}{2} n_z^2. \tag{1.76}$$

The energy dissipation power can be taken into account by the Rayleigh dissipation function (having dimension of energy/time):

$$R[\mathbf{n}] = \frac{\alpha s}{2}\int d^2\mathbf{r} \, \dot{\mathbf{n}}^2 = \frac{\alpha s}{2}\int d^2\mathbf{r} \, \Big[(1-n_z^2)(\dot{\phi})^2 + \frac{(\dot{n}_z)^2}{1-n_z^2}\Big] \tag{1.77}$$

where α is a dimensionless constant known as Gilbert damping factor. By implementing

$$\frac{\mathrm{d}}{\mathrm{d}t}\frac{\delta L}{\delta \dot{q}_i} - \frac{\delta L}{\delta q_i} + \frac{\delta R}{\delta \dot{q}_i} = 0, \tag{1.78}$$

we have the equation of motions (which are the Landau–Lifshitz–Gilbert equations):

$$\begin{aligned} &s\sqrt{1-n_z^2}\dot{\phi} - s\alpha\frac{\dot{n}_z}{\sqrt{1-n_z^2}} = -\mathcal{A}n_z\sqrt{1-n_z^2}(\nabla\phi)^2 - \mathcal{A}\nabla\Big(\frac{\nabla n_z}{\sqrt{1-n_z^2}}\Big) + \mathcal{K}\sqrt{1-n_z^2}n_z, \\ &s\dot{n}_z - \mathcal{A}\nabla\big[(1-n_z^2)\nabla\phi\big] + \alpha s(1-n_z^2)\dot{\phi} = 0. \end{aligned} \tag{1.79}$$

In terms of θ, ϕ, we have

$$\begin{aligned} s\sin\theta\dot{\phi} + s\alpha\dot{\theta} &= \mathcal{A}\nabla^2\theta - \frac{\mathcal{A}}{2}\sin 2\theta\,(\nabla\phi)^2 + \frac{\mathcal{K}}{2}\sin 2\theta \\ s\sin\theta\,\dot{\theta} + \mathcal{A}\nabla\big[\sin^2\theta\nabla\phi\big] &- \alpha s\sin^2\theta\,\dot{\phi} = 0. \end{aligned} \tag{1.80}$$

The $z-$spin current following from the U(1) symmetry of our system is $\vec{j}_z = -\mathcal{A}(1-n_z^2)\nabla\phi$, by invoking the Noether's theorem. Spin superfluidity is often consider in the regime where $n_z \ll 1$ such that we can neglect the possible phase slips, which is accomplished by a local tilt of of the spin out of the easy plane. Besides this assumption, we focus on the long wavelength, low frequency, small damping regime, working with a much simpler Hamiltonian in the Lagrangian and a Rayleigh dissipation function,

$$H = \int d^2\mathbf{r}\,\Big[\frac{\mathcal{A}}{2}(\nabla\phi)^2 + \frac{\mathcal{K}}{2}n_z^2\Big], \quad R = \frac{\alpha s}{2}\int d^2\mathbf{r}\,(\partial_t\phi)^2. \tag{1.81}$$

The z-spin current now is $\vec{j}_z = -\mathcal{A}\nabla\phi$ and the equation of motions derived above are reduced to:

$$\dot{\phi} = \frac{\rho_z}{\chi} \qquad \text{and} \qquad \dot{\rho}_z - \mathcal{A}\nabla^2\phi = -\alpha s\dot{\phi}, \tag{1.82}$$

where we have identified $\rho_z \equiv sn_z$ as the z-spin density and $\chi \equiv s^2/\mathcal{K}$ as the local spin susceptibility. The first equation can be interpreted as the Josephson relation for the phase ϕ, while the second equation can be understood as the continuity equation (in the absence of damping):

$$\partial_t\rho_z + \nabla\cdot\vec{j}_z = 0, \qquad \text{where } \vec{j}_z = -\mathcal{A}\nabla\phi. \tag{1.83}$$

The underlying conservation law is dictated by the symmetry under uniform rotations within the easy plane. Combined with $\dot{\phi} = \rho_z/\chi$, we obtain the wave equation for the angular dynamics $(\partial_t^2 - c^2\nabla^2)\phi = 0$, with the sound velocity $c = \sqrt{\mathcal{A}/\chi} = \sqrt{\mathcal{A}\mathcal{K}}/s$. The linearly dispersing elementary excitations are akin to the first sound in a neutral superfluid. If we inject a spin current at one end of the system with proper boundary condition, we would generate a uniform spiraling flow (spin superflow).

Breakdown of spin superfluid. Our discussion above sets the stage for a superfluid-like treatment of easy-plane spin dynamics. However, there are at least two ways in which

it will differ from the genuine superfluidity—the damping and anisotropies in practice. In contrast to the genuine superfluidity, which is rooted in the fundamental gauge symmetry of the underlying condensate, the spin superfluid is constructed in terms of an approximate (structural) U(1) symmetry. In practice, one can break this symmetry microscopically, while preserving it on average, which introduces the Rayleigh-Gilbert damping. It spoils the continuity equation:

$$\partial_t \rho_z + \nabla \cdot \vec{j}_z = -\alpha s \dot{\phi} = -\frac{\rho_z}{\tau}, \tag{1.84}$$

where $\tau \equiv \chi/\alpha s = s/\alpha \mathcal{K}$ is understood as the spin relaxation time.

In the presence of anisotropies, the U(1) symmetry is broken macroscopically. For the sake of concreteness, we introduce an easy-axis anisotropy within the easy plane: $H \to H - \int d^2\mathbf{r}\, \mathcal{K} \cos^2\phi$. Combined with the Gilbert damping, the wave equation that we derived above becomes the damped sine-Gordon equation:

$$(\partial_t^2 + \tau^{-1}\partial_t - c^2\nabla^2)\phi + \frac{\sin 2\phi}{\xi^2/c^2} = 0, \tag{1.85}$$

where $\xi = \sqrt{\mathcal{A}/\mathcal{K}}$ is a natural length scale. The physical consequences of this equation are discussed in detail in Ref. [55]. One may not expect a hydrodynamics description in the presence of the damping and anisotropies since they would compromise the conservation law. However, it turns out such a description is possible in terms of a robust topological conservation law.

Topological hydrodynamics. To this end, we need to switch from the hydrodynamics of spin density $\rho_z \propto \partial_t \phi$, which is no longer conserved, to the (dual) hydrodynamics of the spin winding $\rho_W \equiv \partial_x \phi/2\pi$, which is conserved, as long as the large-angle out-of-plane excursions of the order parameter are penalized by a strong easy-plane anisotropy and can be neglected [56, 57, 58]. The flux is $j_W = -\partial_t \phi/2\pi$. We can write the spin winding current into a compact form: $j_W^\mu = \epsilon^{\mu\nu}\partial_\nu \phi/2\pi$, whose conservation law follows direction from the antisymmetric symbol $\epsilon^{\mu\nu}$ and does not depend no the equation of motion. Thus it is referred to as the topological conservation law, as we discussed in subsection 1.2.3.

We remark that this conservation law does not depend on the symmetry properties of the Hamiltonian (thus robust against damping and anisotropies). One can construct a transport theory based on this conservation law (we will do it for the conservation laws of vortices and magnetic hedgehogs in later chapters). If we are in a regime where the underlying lattice structure is unimportant and the umklapp scattering process can be neglected, we have another conservation law—total momentum is conserved due to the homogeneity of space. This conservation law, combined with our topological conservation law, would yield a sound mode, as one may expect.

Analogy between spin superfluid and sound wave. We close this subsection by drawing the analogy between the spin superfluid and the sound wave of a one-dimensional lattice model. It is always helpful to put similar concepts together, which may allow us to gain insights into both problems, since often some hidden aspects of one system manifest in another system. We start with the Hamiltonian

$$H = \sum_i \frac{p_i^2}{2m} + \sum_i \frac{m\omega^2}{2}(x_i - x_{i-1})^2 = \int dr \left[\frac{p(r)^2}{2m} + \frac{m\omega^2}{2}(x')^2\right], \tag{1.86}$$

where we have set the lattice distance to be $a = 1$. Then we have the correspondence below:

spin superfluid	sound wave
ρ_z	$p(r)$
ϕ	$x(r)$
χ	m
$\mathcal{A}$	$m\omega^2$
$\{\phi(x), \rho_z(y)\} = \delta(x-y)$	$\{x(r), p(r')\} = \delta(r-r')$
$\chi\dot{\phi} = \rho_z$	$m\dot{x} = p$
$\mathcal{R} = \int dx \frac{\alpha s \dot{\phi}^2}{2}$	$\mathcal{R} = \int dr \frac{\kappa \dot{x}^2}{2}$
$j_z = -A\partial_x \varphi$	$j_p = -m\omega^2 x'$
$\partial_t \rho_z + \partial_x j_z = -\rho_s/\tau$	$\partial_t p + \partial j_p = -\kappa\dot{x} = -\kappa p/m$

First, we note that the local Josephson relation that we have mentioned above is just

$m\dot{x} = p \leftrightarrow \chi\dot{\phi} = \rho_z$. For the dissipation, we assume that the dissipation force for every atom is $F_i = -\kappa\dot{x}_i$ ($\kappa > 0$). Then the Rayleigh dissipation function is given by

$$\mathcal{R} = \int dr\ \frac{\kappa\dot{x}^2}{2}, \tag{1.87}$$

which gives us the equation of motion: $m\ddot{x} - m\omega^2 x'' = -\kappa\dot{x}$. We note the last dissipation term breaks the time reversal symmetry explicitly. Let us rewrite the equation as

$$\partial_t p + \partial j_p = -\kappa\dot{x} = -\kappa p/m \tag{1.88}$$

where $j_p = -m\omega^2 x'$ can be regarded as momentum flux. This is analogous to $\partial_t\rho_z + \partial_x j_z = -\rho_s/\tau$ in the case of spin superfluid. We should remark that one crucial difference between spin superfluid and sound wave is that the dynamical variable of the former is compact (S^1) whereas the latter is noncompact ($\mathbb{R}$). As a result, we can have spin winding textures in the spin system, while there is no counterpart in the model of vibration.

1.3.4 Skyrmion dynamics

In this subsection, we explore the dynamics of skyrmion to illustrate the effects of the spin Berry phase. We employ the collective coordinate approach by treating the skyrmion as a point-particle moving in a ferromagnetic background [8]. We consider a two-dimensional ferromagnet with action:

$$S = s\int dtd^2\mathbf{r}\ \dot{\phi}(\cos\theta - 1) - \int dtd^2\mathbf{r}\ H[\mathbf{n}]. \tag{1.89}$$

By taking the collective coordinate approach, the field configuration is given by $\mathbf{n}(\mathbf{r}, t) = \mathbf{n}_0(\mathbf{r} - \mathbf{R}(t))$, where $\mathbf{n}_0$ is a skyrmion texture and $\mathbf{R} = (X, Y)$ is the position of this skyrmion. Then the variation in the spin configuration $\delta\mathbf{n}$ can be regarded as a consequence of the displacement of the skyrmion position $\mathbf{R} \to \mathbf{R} + \delta\mathbf{R}$, which implies:

$$\delta\mathbf{n} = -(\partial_x\mathbf{n}\,\delta X + \partial_y\mathbf{n}\,\delta Y). \tag{1.90}$$

Therefore, we have

$$\begin{aligned}\delta S &= s\int dtd^2\mathbf{r}\ (\mathbf{n}\times\partial_t\mathbf{n})\cdot\delta\mathbf{n} - \int dtd^2\mathbf{r}\ \delta_{\mathbf{n}}H[\mathbf{n}]\cdot\delta\mathbf{n}\\ &= s\int dtd^2\mathbf{r}\ \left[\mathbf{n}_0\times(\dot{X}\partial_x\mathbf{n}_0+\dot{Y}\partial_y\mathbf{n}_0)\right]\cdot(\partial_x\mathbf{n}_0\,\delta X+\partial_y\mathbf{n}_0\,\delta Y)\\ &\quad+\int dtd^2\mathbf{r}\ \delta_{\mathbf{n}_0}H\cdot(\partial_x\mathbf{n}_0\,\delta X+\partial_y\mathbf{n}_0\,\delta Y)\\ &= 4\pi sQ_s\int dt(\dot{X}\delta Y-\dot{Y}\delta X)+\int dt\ \left[F_x(\mathbf{R})\delta X+F_y(\mathbf{R})\delta Y)\right],\end{aligned} \tag{1.91}$$

where $Q_s=\int d^2\mathbf{r}\,\mathbf{n}_0\cdot\partial_x\mathbf{n}_0\times\partial_y\mathbf{n}_0/4\pi$ is the skyrmion number associated with the configuration $\mathbf{n}_0$, $F_x=\int d^2\mathbf{r}\,\delta_{\mathbf{n}_0}H\cdot\partial_x\mathbf{n}_0$ is the force acting on the skyrmion in the x direction (similarly for the y component). Or equivalently, one can obtain the force by noting that the potential energy for the skyrmion is given by $V(\mathbf{R})=\int d^2\mathbf{r}\,H[\mathbf{n}_0]$. We remark that, if H only depends on the field configuration, $V(\mathbf{R})$ should have no position dependence. The reason is also clear—we must have the same energy no matter we place the skymrion since the system is completely homogeneous. To introduce the $\mathbf{R}$ dependence, there are two ways. One is to consider finite-size system where the translational symmetry breaks down naturally. Otherwise, we need to explicitly break the symmetry by introducing position dependence in the Hamiltonian $H[\mathbf{n},\mathbf{r}]$. From our discussion, we can write down the action for the skyrmion motion:

$$S[\mathbf{R}(t)]=-2\pi sQ_s\int dt\ (X\dot{Y}-Y\dot{X})-\int dt\ V(\mathbf{R}). \tag{1.92}$$

It is useful to draw the analogy with the action for a charged particle in magnetic field:

$$S[\mathbf{r}(t)]=\int dt\ \left[\frac{1}{2}m\dot{\mathbf{v}}+q\mathbf{v}\cdot\mathbf{A}-V(\mathbf{r})\right]. \tag{1.93}$$

Therefore, we can think of our system as a massless ($m=0$) particle with charge one ($q=1$) moving in a magnetic field [$B=\hat{z}\cdot(\nabla\times\mathbf{A})=-4\pi sQ_s$ where $\mathbf{A}=2\pi sQ_s(Y,-X)$] and in an external potential V. Here we regard Q_s as the magnetic field instead of the charge q, since it corresponds to the magnetic field in the dual theory. The equation of motion $m\ddot{\mathbf{r}}=q\mathbf{v}\times\mathbf{B}-\nabla V$ becomes

$$0=\dot{\mathbf{R}}\times(B\hat{z})-\nabla V(\mathbf{R}), \tag{1.94}$$

which gives us the drift motion: $B\dot{\mathbf{R}} = \hat{z} \times \nabla V$.

Discussion about the mass term. We remark that we have zero mass because of the absence of $\dot{\mathbf{n}}^2$ in the spin action and the fact that we treat the skyrmion as a rigid particle. We only captured the two zero modes and other relatively high energy modes (deformation modes of skyrmion) are simply dropped in our treatment. However, those deformation modes are typically coupled with the zero modes. When we integrate out the high energy modes to produce an effective action for the skyrmion in terms of its position, one can generate a finite mass. It is always inspiring to use some simple example to illustrate the idea. Let us consider an Euclidean-time action [59],

$$S[Q,q] = \int dt \, \Big[S_q + \frac{1}{2}(\dot{Q}^2 + \Omega^2 Q^2) + A(Q,q) \Big], \tag{1.95}$$

where q is a zero mode (or a slow mode in general) and Q is a faster mode. This indicates that the mode of q is much more important than Q as it can be activated via very low energy perturbation. To excite Q, we need much larger energy. $A(Q,q)$ describes the coupling between these two modes. Physically, we wish to integrate out Q since it is hard to detect (difficult to couple with low energy probe).

The partition function is given by $Z = \int [dQdq] e^{-S[Q,q]} \equiv \int dq e^{-S_{\rm eff}[q]}$, where the effective action (theory) for q is defined by

$$e^{-S_{\rm eff}[q]} = e^{-S_q} \int dQ \; e^{-S_Q} e^{-\int dt \, A(Q,q)} = e^{-S_q} \langle e^{-\int dt A(Q,q)} \rangle_Q. \tag{1.96}$$

Therefore we only need to evaluate an average $\langle \rangle_Q$, which may need diagrammatic tools to achieve that. For simplicity, we here choose $A(Q,q) = gQC(q)$ and as a result the average can be carried out exactly by invoking the identity: $\int dx e^{-\frac{1}{2}x\cdot G^{-1}\cdot x + x\cdot J} = \mathcal{N} e^{\frac{1}{2}J\cdot G\cdot J}$, where $\mathcal{N}$ is an unimportant constant factor. In our case,

$$(-\partial_t^2 + \Omega^2) G(t) = \delta(t), \;\; J(t) = gC(q), \tag{1.97}$$

where we have used the time translation invariant $G(t,s) = G(t-s)$. We can solve it in the

Fourier space

$$G(\omega) = \frac{1}{\omega^2 + \Omega^2} \longrightarrow G(t) = \int \frac{d\omega}{2\pi} e^{-i\omega t} \frac{1}{\omega^2 + \Omega^2}. \tag{1.98}$$

Therefore, we have the effective action

$$S_{\text{eff}} = S_q + \frac{g^2}{2} \int dt ds \;\; C(q(s)) G(s,t) C(q(t)). \tag{1.99}$$

This implies that, physically, the fast mode Q mediates a nonlocal interaction between slow mode in time domain, which is intuitively clear. To proceed, we need to put more physics into the problem, let us assume, we are only interested in physics that has time scale much larger than $1/\Omega$,

$$G(t) = \frac{\delta(t)}{\Omega^2} + \frac{\partial_t^2 \delta(t)}{\Omega^4} + \mathcal{O}\left(\frac{1}{\Omega^6}\right). \tag{1.100}$$

This gives us $L_{\text{eff}} = L_q + V_{\text{eff}}(q)$, with

$$V_{\text{eff}}(q) = \frac{g^2}{2\Omega^2} C(q)^2 + \frac{g^2}{2\Omega^4} C(q)^2 \partial_t^2 C(q)^2 + \mathcal{O}\left(\frac{\omega^4}{\Omega^6}\right). \tag{1.101}$$

By solving this simply model, one can see that, by integrating out high-energy modes, a mass term would generate naturally for low-energy modes. For example, when one studies the dynamics of a superfluid [60], the zero mode is associated with the angle θ along the bottom of the Mexican hat and the hard mode is the density fluctuation $\delta\rho$. The coupling between them is $\propto \dot{\theta}\delta\rho$. Therefore, to the lowest order in our result above, we generate a term $\propto \dot{\theta}^2$.

Friction force. It is relatively easily to include the effect of dissipation. Considering the Rayleigh dissipation function and using $\mathbf{n}(\mathbf{r}, t) = \mathbf{n}_0(\mathbf{r} - \mathbf{R}(t))$, we have

$$R = \frac{\alpha s}{2} \int d^2\mathbf{r} \; \partial_i \mathbf{n}_0 \cdot \partial_j \mathbf{n}_0 \; \dot{\mathbf{R}}_i \dot{\mathbf{R}}_j \equiv \frac{1}{2} D_{ij} \dot{\mathbf{R}}_i \dot{\mathbf{R}}_j. \tag{1.102}$$

$D_{ij} = \alpha s \int d^2\mathbf{r} \; \partial_i \mathbf{n}_0 \cdot \partial_j \mathbf{n}_0$ is the dissipation tensor which is symmetric, giving rise to a friction force $-\partial R / \partial \dot{\mathbf{R}}_i = -D_{ij} \dot{\mathbf{R}}_j$.

1.3.5 Antiferromagnets and topological terms

Our discussion so far mainly focuses on the ferromagnet. For antiferromagnets, each magnetic unit cell comprises two or more magnetization fields $\mathbf{n}_i$ which are constrained by the exchange interaction to follow $\sum_i \mathbf{n}_i = 0$. To make this explicit, we convert the nearest neighbour exchange into:

$$H = J \sum_{\langle i,j \rangle} \mathbf{S}_i \cdot \mathbf{S}_j = \frac{JS^2}{2} \sum_{\alpha} \left(\sum_i \mathbf{n}_i \right)_{\alpha}^2 - \frac{N}{2} \sum_{\alpha} S^2. \tag{1.103}$$

Here $\sum_i \mathbf{n}_i$ is a sum over all the spins that constitute the antiferromagnetic unit cell—if there are N sublattices, the sum is over N spins. The other sum α is over the lattice, broken down into the magnetic unit cell clusters. The second term is dropped as it is constant and does not enter equations of motion.

In general, to get to the continuum model, we express the vector fields $\mathbf{n}_i$ in terms of the appropriate normal modes of the systems, dictated by the point group symmetry of the order, and expand the exchange interaction (and the other energies) in them. The particular construction of the field theory depends on the specific lattice geometry. However, generically they all stem from labeling the sublattice magnetizations as individual fields and then putting them together by expressing the respective magnetization fields in terms of the normal modes. These are of two kinds—soft modes which do not break the constraint $\sum_i \mathbf{n}_i = 0$, and hard modes which do, inducing a net magnetization per unit cell.

In this subsection, we will focus on antiferromagnets on bipartite lattices such as the hypercubic lattice for the sake of simplicity [52, 54]. A continuum theory of a collinear antiferromagnet with two sublattices operates with two slowly varying (in space) fields $\mathbf{n}_1(\mathbf{r})$ and $\mathbf{n}_2(\mathbf{r})$. $\mathbf{n}_1$, $\mathbf{n}_2$ are unit vector fields. In a state of equilibrium, $\mathbf{n}_1(\mathbf{r}) = -\mathbf{n}_2(\mathbf{r})$. More generally, the two sublattice fields are expressed in terms of dominant staggered magnetization $\mathbf{m} = (\mathbf{n}_2 - \mathbf{n}_1)/2$ and small uniform magnetization $a\mathbf{l} = (\mathbf{n}_1 + \mathbf{n}_2)/2$ (the corresponding rescaling by the lattice constant a is made). Or equivalently $\mathbf{n}_j = (-1)^j \mathbf{m} + a\mathbf{l}$. We note

that the constraint $\mathbf{n}_j^2 = 1$ translates into

$$\mathbf{n}_j^2 = \mathbf{m}^2 + 2(-1)^j a\mathbf{m}\cdot\mathbf{l} + a^2\mathbf{l}^2 = 1. \tag{1.104}$$

We can solve this condition to the order of a^2 by two conditions:

$$\mathbf{m}^2 = 1, \qquad \text{and} \qquad \mathbf{m}\cdot\mathbf{l} = 0. \tag{1.105}$$

Effective action for antiferromagnets in d dimensions. We consider a following Hamiltonian:

$$H = J\sum_{\langle j,k\rangle}\mathbf{S}_j\cdot\mathbf{S}_k - \sum_j \mathbf{h}\cdot\mathbf{S}_j. \tag{1.106}$$

The corresponding spin path integral in real time is given by

$$S[\mathbf{n}] = \sum_j S_B[\mathbf{n}_j(t)] - JS^2\int dt\ \sum_{\langle j,k\rangle}\mathbf{n}_j\cdot\mathbf{n}_k + S\int dt\ \sum_j \mathbf{h}\cdot\mathbf{n}_j. \tag{1.107}$$

We first deal with the energy part which is less tricky. We note that

$$\mathbf{n}_j\cdot\mathbf{n}_{j+a} = \frac{1}{2}[\mathbf{n}(j)+\mathbf{n}(j+a)]^2 = \frac{a^2}{2}\left[2\mathbf{l}_j - (-1)^j\partial_x\mathbf{m}_j\right]^2 = \frac{a^2}{2}\left[(\partial_x\mathbf{m}_j)^2 + 4\mathbf{l}_j^2 - 4(-1)^j\partial_x\mathbf{m}_j\cdot\mathbf{l}_j\right], \tag{1.108}$$

where we considered a pair of spins in x direction and we have dropped constants. We also have

$$\mathbf{h}\cdot\mathbf{n}_j = (-1)^j\mathbf{h}\cdot\mathbf{m}_j + a\mathbf{h}\cdot\mathbf{l}_j. \tag{1.109}$$

Then the energy part is

$$\begin{aligned} H[\mathbf{n}] &= JS^2\sum_j\frac{a^2}{2}\left[(\nabla\mathbf{m})^2 + 4d\mathbf{l}^2\right] - Sa\sum_j\mathbf{h}\cdot\mathbf{l}_j \\ &= \frac{\mathcal{A}}{2}\int d^d\mathbf{r}\ \left[(\nabla\mathbf{m})^2 + 4d\,\mathbf{l}^2\right] - \frac{S}{a^{d-1}}\int d^d\mathbf{r}\ \mathbf{h}\cdot\mathbf{l}, \end{aligned} \tag{1.110}$$

where we have dropped all oscillating terms in the sum $\sum_j$ and $\mathcal{A} = JS^2/a^{d-2}$ is the stiffness of the staggered field $\mathbf{m}$ (similar to the ferromagnetic case). Let us now simplify the geometric

phase:

$$\begin{aligned}\sum_j S_B[\mathbf{n}_j] &= \sum_j (-1)^j S_B[\mathbf{m}_j + (-1)^j a\mathbf{l}_j] \\ &\approx \sum_j (-1)^j S_B[\mathbf{m}_j] + Sa\sum_j \int dt\ (\mathbf{m}_j \times \partial_t \mathbf{m}_j)\cdot \mathbf{l}_j. \\ &= \sum_j (-1)^j S_B[\mathbf{m}_j] + \frac{S}{a^{d-1}}\int dt d^d\mathbf{r}\ \mathbf{l}\cdot(\mathbf{m}\times\partial_t\mathbf{m})\end{aligned} \tag{1.111}$$

We now deal with the first term:

$$\begin{aligned}\sum_{j_1,j_2,\cdots,j_d} (-1)^{j_1+\cdots+j_d} S_B[\mathbf{m}(j_1,\cdots)] &= \sum_{j_2,\cdots}(-1)^{j_2+\cdots+j_d}\Big[\sum_{j_1}(-1)^{j_1}S_B[\mathbf{m}(j_1)]\Big] \\ &= \sum_{j_2,\cdots}(-1)^{j_2+\cdots+j_d}\Big[\sum_{r=1}^{N_x/2} S_B[\mathbf{m}(2r)] - S_B[\mathbf{m}(2r-1)]\Big] \\ &= \sum_{j_2,\cdots}(-1)^{j_2+\cdots+j_d}\sum_{r=1}^{N_x/2}\int dt\ Sa\partial_x\mathbf{m}(2r)\cdot\mathbf{m}(2r)\times\partial_t\mathbf{m}(2r) \\ &= S\sum_{j_2,\cdots}(-1)^{j_2+\cdots+j_d}\int \frac{dxdt}{2}\partial_x\mathbf{m}\cdot\mathbf{m}\times\partial_t\mathbf{m}\end{aligned} \tag{1.112}$$

where we have suppressed the labels $j_2,\cdots,j_d$ in $\mathbf{m}$ and summed over j_1 along the x direction (assuming there are even number of sites N_x). We note that, in the last step when we convert the sum $\sum_r$ to an integral, we have used $\sum_r \to \int dx/2a$. One notice that this term is inconsequential in two or higher dimensions due to the summation over $j_2,\cdots,j_d$. It is only present in the one-dimensional antiferromagnetic system. Therefore, we can write down the continuum description for the antiferromagnetic system. In the 1D case, we have (let us drop the external magnetic field for simplicity),

$$S_{d=1}[\mathbf{l},\mathbf{m}] = 2\pi S Q_s - \frac{\mathcal{A}}{2}\int dtdx\ (\partial_x\mathbf{m})^2 + \int dtdx\ \big[S\mathbf{l}\cdot(\mathbf{m}\times\partial_t\mathbf{m}) - 2\mathcal{A}\mathbf{l}^2\big], \tag{1.113}$$

where $Q_s = \int dtdx\mathbf{m}\cdot(\partial_t\mathbf{m}\times\partial_x\mathbf{m})/4\pi$ is the skyrmion number. We can integrate out the fast mode $\mathbf{l}$ and generate an effective action for the slow mode $\mathbf{m}$:

$$S_{d=1}[\mathbf{m}] = 2\pi S Q_s + \int dtdx\ \Big[\frac{S^2}{8\mathcal{A}}(\partial_t\mathbf{m})^2 - \frac{\mathcal{A}}{2}(\partial_x\mathbf{m})^2\Big], \tag{1.114}$$

where a mass term is generated in this process (consistent with what we discussed in the skyrmion mass section). Equivalently, one can write down the Lagrangian density into the form:

$$\mathcal{L}_{d=1}(\mathbf{m}) = \frac{1}{2g}\Big[\frac{1}{v_s}(\partial_t \mathbf{m})^2 - v_s(\partial_x \mathbf{m})^2\Big] + \frac{\theta}{8\pi}\epsilon_{\mu\nu}\mathbf{m}\cdot\partial_\mu\mathbf{m}\times\partial_\nu\mathbf{m}, \tag{1.115}$$

where $g \equiv 2/S$ is the coupling constant, $v_s = 2\mathcal{A}/S = 2aJS$ is the spin-wave velocity, and $\theta = 2\pi S$ ($\mu, \nu \in \{t, x\}$ and we use the convention $\epsilon_{t,u} = 1$).

In two dimensions or higher, the action reads:

$$S_{d\geq 2}[\mathbf{l}, \mathbf{m}] = -\frac{\mathcal{A}}{2}\int dt d^d\mathbf{r}\ (\nabla\mathbf{m})^2 + \frac{S}{a^{d-1}}\int dt d^d\mathbf{r}\ \mathbf{l}\cdot\mathbf{m}\times\partial_t\mathbf{m} - 2\mathcal{A}d\int dt d^d\mathbf{r}\ \mathbf{l}^2. \tag{1.116}$$

Similarly, we can integrate out the fast mode $\mathbf{l}$ which will generate a mass term for the slow mode $\mathbf{m}$:

$$S_{d\geq 2} = \frac{1}{2g}\int dt \frac{d^d\mathbf{r}}{a^{d-1}}\Big[\frac{1}{v_s}(\partial_t\mathbf{m})^2 - v_s(\nabla\mathbf{m})^2\Big], \tag{1.117}$$

where the coupling is $g = 2\sqrt{d}/S$ and the spin-wave velocity is $v_s = 2JSa\sqrt{d}$. The ordered ground state $\mathbf{m}_0(\theta, \phi)$ spontaneously breaks the $SO(3)$ symmetry of the system up to $SO(2)$. Hence in this case, there are two Goldstone modes, residing in the coset space $S^2 = SO(3)/SO(2)$, one for each continuous degree of freedom, dispersing linearly according to $\omega = v_s k$. They classically correspond to the opposite circular polarizations of the small-angle oscillations of $\delta\mathbf{m} \perp \mathbf{m}_0$. One can also discuss the dynamics of solitons in antiferromagnets based on collective coordinate approach, similar to what we discussed in the skyrmion dynamics section.

In terms of applications, antiferromagnets hold a promise for a faster spintronics platform. The spin wave dynamics of an antiferromagnetic system is controlled by an energy scale $\propto J$. For ferromagnets the same scale is $\propto \sqrt{KJ}$ where K is a local anisotropy. In most materials $J \gg K$. The energy scale for the antiferromagnet translates to a frequency scale of a few THz. Antiferromagnets offer another significant advantage over ferromagnetic devices. Since the net magnetic moment largely cancels over a unit cell, they do not produce stray fields. This is particularly important in device design, where we would like our individual memory

components to be isolated from one another. However, these advantages also present a significant handicap–of coupling antiferromagnetic solitons to external probes. The absence of a local spin density implies a minor response to spin currents. The response to external magnetic fields is also tuned down by a factor of the exchange strength. Therefore, one main topic in spintronics is to explore how to effective control and manipulate antiferromagnetic solitons. For example, one can achieve the goal by transferring linear momentum, exploiting the inertial dynamics of the solitons. This can be achieved, for instance, by using magnons to scatter from the domain walls. Other methods involve creating a local Berry phase which can then be coupled to an external spin current field [61].

Remarks on the topological term in 1D. The contribution from the geometric phase term in the partition function is simple:

$$e^{2\pi i S Q_s} = \begin{cases} +1, & \text{if } S \in \mathbb{Z} \\ (-1)^{Q_s}, & \text{if } \ S \in \mathbb{Z} + \frac{1}{2}, \end{cases} \tag{1.118}$$

which implies that, for integer S, the contribution is a factor of unity and thus the full field theoretic action is a nonlinear sigma model. In contrast, for half integer S, space-time configurations with even and odd skyrmion number Q_s destructively interfere with each other. First, we conclude that antiferromagnetic Heisenberg chains generically fall into two classes: integer spin and half integer spin. The field theory for the former is simply that of the classical O(3) model in two (space-time) dimensions. The Hohenberg-Mermin Wagner theorem precludes any spontaneous breaking of the continuous O(3) symmetry in $d = 1$ at any finite value of $\mathcal{A}$. The system is gapped, and correlation functions decay exponentially, up to power law corrections $\langle \mathbf{S}_0 \cdot \mathbf{S}_j \rangle \sim (-1)^j |j|^{-1/2} e^{-|j|/\xi}$, where ξ is the correlation length.

In the second class, we have a new topological term, known as θ-term. While there is no exact solution to this field theory yet, we nonetheless conclude that all half integer antiferromagnetic chains behave equivalently, since they all map onto the same model. From Bethe's Ansatz, we know that the $S = 1/2$ Heisenberg antiferromagnetic chain possesses a disordered ground state with gapless excitations and power law correlations $\langle \mathbf{S}_0 \cdot \mathbf{S}_j \rangle \sim$

$(-1)^j/|j|$ (up to logarithmic corrections). We conclude that the same is also true for $S = 3/2, 5/2, \cdots$ spin chains [62, 63, 64].

Remarks on the geometric phase in higher dimensions. From the derivation above, one can see that the topological terms cancel out when we sum over the Berry phase term along other directions $(j_2, \cdots, j_d)$. The conclusion is that there are no interesting topological terms in the field theory in more than one space dimension, as long as the field $\mathbf{m}(\mathbf{r}, t)$ is a smooth function of space and time. When the smoothness constraint is relaxed, however, the geometric phase term can play an important role. For a two-dimensional antiferromagnet, there exist topology-changing instanton for which $\Delta Q_s = \pm 1$. Such field configurations are called 'hedgehogs', because the direction of the field $\mathbf{n}(t, x, y)$ points radially outward from the center of the hedgehog. For quantum disordered two-dimensional antiferromagnets (i.e. small $\mathcal{A}$), Haldane argued that geometrical phase considerations associated with the presence of hedgehogs would distinguish not only between integer and half-odd integer S on the square lattice, but between even and odd integer S as well [65].

1.4 Quantum entanglement

Quantum mechanics is full of counterintuitive concepts. The idea of entanglement [66, 67]—when two or more particles instantaneously exhibit dependent characteristics when measured, no matter how far apart they are—is one of them. It is a measure of how much quantum information is stored in a quantum state and is one of the most fundamental properties that distinguish a quantum phenomenon from its classical counterpart. In this section, we will introduce some measures that are often used to quantify the quantum entanglement.

1.4.1 Entanglement monotone: requirements of entanglement measures

In this subsection, we assert some general statements which should be valid for all good entanglement measures [67, 68, 69, 70].

1. *Nullification.* If a state ρ is separable, it contains no entanglement $E(\rho) = 0$. For a general state, we have $E(\rho) \geq 0$. Here, a state ρ of two parties A, B is said to be separable, if it can be written in the form of

$$\rho = \sum_i p_i \; \rho_A^i \otimes \rho_B^i, \tag{1.119}$$

where p_i is a probability distribution, satisfying $\sum_i p_i = 1$. In the case of a pure state, considering a bipartite system with Hilbert space equal to the direct product $\mathcal{H} = \mathcal{H}_A \otimes \mathcal{H}_B$. A pure state $|\chi\rangle$ living in $\mathcal{H}$ is separable if it can be written as a product state, i.e. there exist $|\psi\rangle_A \in \mathcal{H}_A$ and $|\phi\rangle_B \in \mathcal{H}_B$ such that $|\chi\rangle = |\psi\rangle_A \otimes |\phi\rangle_B$. Otherwise, $|\chi\rangle$ is an entangled state. We remark that, for a mixed state ρ, we do not necessarily require the converse [namely, if $E(\rho) = 0$, then ρ is separable].

2. *Local invariance.* The entanglement $E(\rho)$ should be invariant under any unitary transformation $U_A \otimes U_B$ where $U_{A/B}$ acts on $\mathcal{H}_{A/B}$. Therefore, we require

$$E(\rho) = E(U_A \otimes U_B \, \rho \, U_A^\dagger \otimes U_B^\dagger). \tag{1.120}$$

This simply means a change of basis should not alter the amount of information stored in the state ρ.

3. *LOCC monotonicity.* The entanglement $E(\rho)$ should not increase on average under local quantum operations and classical communications (LOCC),

$$E(\hat{O}_{\mathrm{LOCC}}(\rho)) \leq E(\rho). \tag{1.121}$$

This requirement is also quite natural since LOCC, which can also generate classical correlations, does not increase quantum correlations within the system. This can be regarded as the definition of classical correlations in the context of quantum information. One example of LOCC is to prepare a state $\rho = (|00\rangle \langle 00| + |11\rangle \langle 11|)/2$ from the product state $|00\rangle$. Alice throws an unbiased coin (that shows heads or tails each with 1/2 probability) and flips her qubit if the coin shows "tails", otherwise it is left

unchanged. She then sends the result of the coin-flip (classical information) to Bob who also flips his qubit if he receives the message "tails". The resulting state is ρ. In general, all separable states (and only these) can be prepared from a product states with LOCC operations alone.

4. *Maximally entangled states.* We now know separable states give us zero entanglement. One natural question to ask is whether there is a maximally entangled state. Indeed, at least in bipartite systems consisting of two fixed d dimensional subsystems, such states exist. It turns out that any pure state that is local unitarily equivalent to

$$|\Phi\rangle = \frac{|0,0\rangle + |1,1\rangle + \cdots + |d-1,d-1\rangle}{\sqrt{d}}, \tag{1.122}$$

is maximally entangled, which is well justified because any state ρ can be prepared from such states with certainty using only LOCC operations. One can choose the normalization such that $E(|\Phi\rangle\langle\Phi|) = \log d$.

5. *Continuity.* It is natural to expect the entanglement $E(\rho)$ to change continuously as we vary the state ρ slowly. In other words, the difference of entanglement between two density matrices infinitely close should tend to zero,

$$D(\rho,\sigma) \to 0, \quad \Rightarrow \quad E(\rho) - E(\sigma) \to 0, \tag{1.123}$$

where $D(\rho,\sigma)$ is the distance between states ρ and σ. For example, we can take it to be the trace distance $D(\rho,\sigma) \equiv \mathrm{tr}\,|\rho-\sigma|/2$, where we define $|A| \equiv \sqrt{A^\dagger A}$ to be the positive square root of $A^\dagger A$. To get some feel for this trace distance, one can consider two states $\rho = (I + \vec{r}\cdot\vec{\boldsymbol{\sigma}})/2$ and $\sigma = (I + \vec{s}\cdot\vec{\boldsymbol{\sigma}})/2$. The distance is given by $D(\rho,\sigma) = |\vec{r}-\vec{s}|/2$, which is equal to one half the ordinary Euclidean distance between them on the Bloch sphere. Note that rotations of the Bloch sphere leave the Euclidean distance invariant, which suggests that the trace distance is preserved under unitary transformations in general, $D(U\rho U^\dagger, U\sigma U^\dagger) = D(\rho,\sigma)$.

A function that satisfies the above conditions is known as an *entanglement monotone*. We next introduce different entanglement measures that satisfy the above requirements. For pure states, the von-Neumann entropy is typically employed to quantify the quantum entanglement. In the case of mixed states, we will introduce several different measures of entanglement, which all satisfy the above properties, such as *entanglement of formation*, *entanglement of distillation*, *relative entropy of entanglement*, and *logarithmic negativity*.

1.4.2 Entanglement entropy for pure states

For a bipartite system with Hilbert space $\mathcal{H} = \mathcal{H}_A \otimes \mathcal{H}_B$, one can use the von Neumann entropy to measure the degree of quantum entanglement between A- and B-subsystems when it is in a pure state $\rho = |\psi\rangle \langle\psi|$:

$$E_V(\rho) = -\operatorname{tr} \rho_A \log \rho_A = -\operatorname{tr} \rho_B \log \rho_B, \tag{1.124}$$

where $\rho_A = \operatorname{tr}_B \rho$ (similarly $\rho_B = \operatorname{tr}_A \rho$) is the reduced density matrix for part A after tracing out the degrees of freedom in $\mathcal{H}_B$. We remark that $E_V(\rho)$ can be expressed in terms of the singular values of the Schmidt decomposition of the state (which can be only performed for pure states). To this end, we write the pure state in its unique Schmidt decomposition

$$|\psi\rangle = \sum_{k=1}^{d} \lambda_k |u_k, v_k\rangle , \tag{1.125}$$

where $d \leq \min\{d_A, d_B\}$, $\lambda_k > 0$, $\sum_{k=1}^{d} \lambda_k^2 = 1$, and $\{|u_k\rangle\} \in \mathcal{H}_A$ and $\{|v_k\rangle\} \in \mathcal{H}_B$ are local bases, known as the Schmidt bases. Then we can see that $\rho_A = \sum_k \lambda_k^2 |u_k\rangle \langle u_k|$ and $\rho_B = \sum_k \lambda_k^2 |v_k\rangle \langle v_k|$. The von Neumann entropy is given by

$$E_V(\psi) = -\sum_k \lambda_k^2 \log \lambda_k^2. \tag{1.126}$$

We point out that $d = 1$ corresponds to product states (unentangled). In other words, for an entangled state, we always have $d > 1$, which can be easily seen from the above expression.

One can show that this measure satisfies all requirements we discussed in previous subsection. For example, from Eq. (1.126), it is clear that its value is independent of the basis

we choose. The most tricky one is to prove entanglement cannot be created by LOCC only. We can formulate this question as follows [68]. Considering a state $|\psi\rangle \in \mathcal{H}$, after performing local measurements on A and B and classical communication, we can obtain state $|\phi_i\rangle$ with probability p_i. Then $E_V(|\psi\rangle) \geq \sum_i p_i E_V(|\phi_i\rangle)$. We point out that entanglement cannot increase on average. But nothing prevents, for a given k, that $E_V(|\phi\rangle_k) > E_V(|\psi\rangle)$. In fact, the concept of *entanglement distillation* is based on the fact that one can increase entanglement by LOCC with a probability p_k. Besides satisfying properties we discussed before, von-Neumann entropy has some other nice properties. For example, E_V is additive: $E_V(|\psi_{AB}\rangle \otimes |\phi_{AB}\rangle) = E_V(|\psi_{AB}\rangle) + E_V(|\phi_{AB}\rangle)$.

1.4.3 Quantifying entanglement for mixed states

For a general mixed state ρ, this von-Neumann entropy is no longer a good measure since the classical mixture in ρ will also contribute to the von Neumann entropy. It is also easy to check $\operatorname{tr}\rho_A \log \rho_A \neq \operatorname{tr}\rho_B \log \rho_B$ in general in the definition of the von Neumann entropy Eq. (1.124). One important feature of mixed states is that one can decompose a mixed state into a combination of pure states in infinite many different ways $\rho = \sum_k p_k |\psi_k\rangle \langle\psi_k|$. For example,

$$\rho = \frac{|\text{singlet}\rangle \langle\text{singlet}| + |\text{triplet}\rangle \langle\text{triplet}|}{2} = \frac{|\uparrow\downarrow\rangle \langle\uparrow\downarrow| + |\downarrow\uparrow\rangle \langle\downarrow\uparrow|}{2}. \tag{1.127}$$

If we naively define the entanglement to be $E(\rho) = \sum_k p_k E_V(|\psi_k\rangle)$, we would obtain different results for different decompositions. We remark that every decomposition stands for a way to prepare the state ρ. For example, we can collect N copies ($N \gg 1$) of the system, prepare Np_k of them in the state $|\psi_k\rangle$, and pick a random system. Thus infinitely many decompositions implies infinitely many ways to prepare a given mixed state. As long as there exists one decomposition $\rho = \sum_k p_k \rho_A \otimes \rho_B$, we can prepare such a mixed state via LOCC without any quantum correlations. This can be used as a criterion to tell whether a mixed state is separable or not. However, it is impractical since we need to check all the infinitely

many decompositions. Now we introduce several commonly used entanglement measures, some of which are easy to evaluate.

1. Entanglement of formation. Instead of define the entanglement to be $E(\rho) = \sum_k p_k E_V(|\psi_k\rangle)$ for some particular decomposition of a mixed state, entanglement of formation is defined as

$$E_F(\rho) = \min_{\{p_k, |\psi_k\rangle\}} \sum_k E_V(|\psi_k\rangle), \tag{1.128}$$

where we take the minimum over all possible decompositions. It represents the minimal quantum correlations we need to prepare such a mixed state, thus known as entanglement of formation. While this quantity is again difficult to evaluate, an explicit solution for such nontrivial optimization problem is avaible for two qubits [71], for highly symmetric states [72, 73, 74] like Werner states and isotropic states in arbitrary dimension, and for symmetric two-mode Gaussian states [75]. Here we would focus on the explicit formula of entanglement formation for two qubits, which we will use a lot in later chapters. The exact formula is based on the often used two-qubit **concurrence**, which is defined as [71]

$$\mathcal{C}(\rho) = \max\{0, \lambda_1 - \lambda_2 - \lambda_3 - \lambda_4\}, \tag{1.129}$$

where λ_i's are, in decreasing order, the square roots of the eigenvalues of the matrix $\rho(\sigma_y \otimes \sigma_y)\rho^*(\sigma_y \otimes \sigma_y)$, where ρ^* is the complex conjugate of ρ. The entanglement of formation is then given by

$$\begin{aligned} E_F(\rho) &= h\Big(\frac{1+\sqrt{1-\mathcal{C}^2}}{2}\Big), & (1.130)\\ h(x) &= -x\log_2 x - (1-x)\log_2(1-x). & (1.131) \end{aligned}$$

$E_F(\rho)$ is monotonically increasing and ranges from 0 to 1 as $\mathcal{C}(\rho)$ goes from 0 to 1, so that one can take the concurrence as a measure of entanglement in its own right.

Let us first try out the concurrence for a two-qubit system. Assuming the density matrix is given by:

$$\rho = (1-p)\,|\uparrow\uparrow\rangle\langle\uparrow\uparrow| + p\,|\text{singlet}\rangle\langle\text{singlet}|\,, \tag{1.132}$$

with probability $1-p$ in state $|\uparrow\uparrow\rangle$ and p in state $|\text{singlet}\rangle \equiv (|\uparrow\downarrow\rangle - |\downarrow\uparrow\rangle)/\sqrt{2}$. In the basis of $|\uparrow\uparrow\rangle, |\uparrow\downarrow\rangle, |\downarrow\uparrow\rangle, |\downarrow\downarrow\rangle$,

$$\rho = \begin{bmatrix} 1-p & 0 & 0 & 0 \\ 0 & p/2 & -p/2 & 0 \\ 0 & -p/2 & p/2 & 0 \\ 0 & 0 & 0 & 0 \end{bmatrix}. \tag{1.133}$$

We would expect the concurrence will increase as we increase p since $|\uparrow\uparrow\rangle$ is not entangled but $|\text{singlet}\rangle$ is entangled. We can compute the square roots of the eigenvalues of the matrix $\rho(\sigma_y \otimes \sigma_y)\rho^*(\sigma_y \otimes \sigma_y)$ exactly and we have $\lambda_1 = p, \lambda_2 = 0, \lambda_3 = 0, \lambda_4 = 0$, thus

$$\mathcal{C}(\rho) = \max\{0, p\} = p, \tag{1.134}$$

which is exactly what one might expect.

For a N-qubit system, whose dynamics is governed by a Hamiltonian H, assuming the system is in a thermal equilibrium, we can calculate the entanglement between two arbitrary qubits i and j. The reduced density matrix of those two qubits is obtained by tracing out other degrees of freedom and given by

$$\rho_{ij} = \frac{1}{4}\sum_{\alpha,\beta} p_{\alpha\beta}\sigma_i^\alpha \otimes \sigma_j^\beta, \tag{1.135}$$

where $\sigma^\alpha = \{I, \sigma^x, \sigma^y, \sigma^z\}$ and $p_{\alpha\beta} = \langle \sigma_i^\alpha \otimes \sigma_j^\beta \rangle = \text{tr}\Big(e^{-\beta H}\sigma_i^\alpha \otimes \sigma_j^\beta\Big)/Z$ is real. Z is the partition function and $\beta = 1/k_B T$. In the same basis as Eq. (1.133), the explicit form of ρ_{ij} is given by [76]

$$\rho_{ij} = \begin{bmatrix} \langle k_i^+ k_j^+ \rangle & \langle \sigma_i^- k_j^+ \rangle & \langle k_i^+ \sigma_j^- \rangle & \langle \sigma_i^- \sigma_j^- \rangle \\ \langle \sigma_i^+ k_j^+ \rangle & \langle k_i^- k_j^+ \rangle & \langle \sigma_i^+ \sigma_j^- \rangle & \langle k_i^- \sigma_j^- \rangle \\ \langle k_i^+ \sigma_j^+ \rangle & \langle \sigma_i^- \sigma_j^+ \rangle & \langle k_i^+ k_j^- \rangle & \langle \sigma_i^- k_j^- \rangle \\ \langle \sigma_i^+ \sigma_j^+ \rangle & \langle k_i^- \sigma_j^+ \rangle & \langle \sigma_i^+ k_j^- \rangle & \langle k_i^- k_j^- \rangle \end{bmatrix}, \tag{1.136}$$

where $k^\pm = (1 \pm \sigma_z)/2$, $\sigma^\pm = (\sigma^x \pm i\sigma^y)/2$ and we have dropped the tensor product symbol. We are now ready to evaluate the concurrence once the Hamiltonian is specified. Some of the

elements in the reduced density matrix are typically zero due to symmetry considerations. In particular, if our density matrix is in the form of

$$\rho = \begin{bmatrix} \rho_{00} & 0 & 0 & \rho_{03} \\ 0 & \rho_{11} & \rho_{12} & 0 \\ 0 & \rho_{21} & \rho_{22} & 0 \\ \rho_{30} & 0 & 0 & \rho_{33} \end{bmatrix}, \tag{1.137}$$

the expression of concurrence can be reduced to

$$\mathcal{C}(\rho) = 2\max\{0, |\rho_{12}| - \sqrt{\rho_{00}\rho_{33}}, |\rho_{03}| - \sqrt{\rho_{11}\rho_{22}}\}. \tag{1.138}$$

2. Entanglement cost. The entanglement cost quantifies how much Bell pairs $|\Phi\rangle = (|00\rangle + |11\rangle)/2$ that one needs to create the mixed state ρ via LOCC [77]. It is defined as the asymptotic ratio between the minimum number M of used Bell pairs, and the number N of output copies of ρ:

$$E_C(\rho) = \min_{\text{LOCC}} \lim_{N\to\infty} \frac{M^{\text{in}}}{N^{\text{out}}}, \tag{1.139}$$

which in practice is again very difficult to compute. We should point out that entanglement cost is closely related to the entanglement of formation, which provides some hope to evaluate $E_C(\rho)$. It has been rigorously proved that the asymptotic version of the entanglement of formation, which is defined as

$$E_F^{\infty}(\rho) = \lim_{N\to\infty} \frac{\rho^{\otimes N}}{N}, \tag{1.140}$$

is equal to the entanglement of cost [78]

$$E_F^{\infty}(\rho) = E_C(\rho). \tag{1.141}$$

There are indications, though no general proof, that the entanglement of formation is additive [79],

$$E_F(\rho \otimes \sigma) = E_F(\rho) + E_F(\sigma), \tag{1.142}$$

which implies that $E_F(\rho) = E_F^{\infty}(\rho) = E_C(\rho)$.

3. Distillable entanglement. Distillable entanglement is the converse of the entanglement cost [77]. Namely, it is the asymptotic fraction M/N of Bell pairs which can be extracted from N copies of the state ρ by using the optimal LOCC distiilation protocol,

$$E_D(\rho) = \max_{\text{LOCC}} \lim_{N\to\infty} \frac{M^{\text{out}}}{N^{\text{in}}}, \tag{1.143}$$

which is generally smaller than $E_C(\rho)$. We remark that this measure fails to satisfy the converse of *Nullification*: namely, $E_D(\rho) = 0$ for all disentangled states, but the converse is not true. There exists states which are entangled but for which no entanglement can be distilled from them, and for this reason, they are called *bound entangled states*, which can be quantified by $E_C(\rho) - E_D(\rho)$. It is again difficult to calculate $E_D(\rho)$ for a general state ρ. Therefore, it is important to be able to provide bounds on its value. The *upper bounds* can be provided by, for instance, entanglement of cost, entanglement of formation, relative entropy of entanglement, and logarithmic negativity (which we will introduce shortly). The *lower bound* is more tricky, which typically requires the construction of explicit entanglement purification procedure. Instead, the notion of *conditional entropy* is usually introduced, $C(A|B) = S(\rho_{AB}) - S(\rho_B)$ for a bipartite state ρ_{AB}, where $S(\rho) = -\operatorname{tr}\rho\log\rho$. It was shown that $-C(A|B)$ provides the lower bound for the one way distillable entanglement (known as *Hashing Inequality*):

$$E_D(\rho_{AB}) \geq D_{A\to B}(\rho_{AB}) \geq \max\{S(\rho_B) - S(\rho_{AB}), 0\}, \tag{1.144}$$

where $D_{A\to B}$ is the distillable entanglement under the restriction that the classical communication may only go one way from A to B [80]. This provide a computable nontrivial lower bound to $E_D(\rho)$ (thus also other entanglement measures).

4. Relative entropy of entanglement. It is intuitive to measure the entanglement by considering the minimum "distance" between the state ρ and the convex set $\mathcal{D} \subset \mathcal{H}$ of separable states [81]:

$$E_R(\rho) = \min_{\sigma\in\mathcal{D}} S(\rho||\sigma), \tag{1.145}$$

where $S(\rho||\sigma) = \mathrm{tr}[\rho(\log\rho - \log\sigma)]$ is the entropic distance (i.e. the quantum relative entropy) between ρ and σ. Therefore, the more entangled a state is, the more distinguishable it is from a disentangled state.

So far, we have introduced four types of entanglement measures for a generic mixed state. They all are asymptotically continuous, which means that for a sequence of bipartite Hilbert spaces $H_1, H_2, \cdots$ (typically with increasing dimension) we can have a sequence of quantum states $\rho_1, \rho_2, \cdots$ which converges to $\rho^{\otimes n_1}, \rho^{\otimes n_2}, \ldots$ (typically with increasing n_i) in the trace distance, and the sequence $E(\rho_1)/n_1, E(\rho_2)/n_2, \ldots$ also converges to $E(\rho)$. Thus all these measures reduce to the von Neumann entropy of entanglement for pure states: $E_F(|\psi\rangle) = E_C(|\psi\rangle) = E_R(|\psi\rangle) = E_D(|\psi\rangle) = E_V(|\psi\rangle)$. We have the following chain of nice analytic inequalities [82, 83]:

$$E_F(|\psi\rangle) \geq E_C(|\psi\rangle) \geq E_R(|\psi\rangle) \geq E_D(|\psi\rangle). \tag{1.146}$$

5. Logarithmic negativity. We now introduce a measure which is continuous but not asymptotically continuous, and hence does not reduce to the von Neumann entropy for pure states. Nevertheless, logarithmic negativity is a very useful measure since it can be evaluated very easily, besides its various operational interpretations as an upper bound to $E_D(\rho)$, a bound on teleportation capacity, and an asymptotic entanglement cost for exact preparation under the set of positive partial transpose preserving operations [67].

First, it is helpful to introduce the **Peres-Horodecki** criterion, which is based on the operation of partial transposition of the density matrix [84, 85]. As we mentioned before, given a density matrix ρ, it is basically impossible to go through all possible decompositions of ρ to see whether it is separable or not. The Peres-Horodecki criterion provides a necessary condition for separability, which is very easy to check. It states that, if a state ρ is separable, then its partial transpose ρ^{T_B} is a valid density matrix, in particular positive semidefinite, $\rho^{T_B} \geq 0$. The same holds for ρ^{T_A}. The converse (*i.e.* $\rho^{T_B} \geq 0$ implies ρ is separable) is false in general. However, we should point out that, for low-dimensional systems, specifically

bipartite systems of dimensionality 2×2 and 2×3, the Peres-Horodecki criterion is equivalent to separability. For higher dimensional systems, entangled states with $\rho^{T_B} \geq 0$ have been shown to exist, which are known as *bound entangled*, since their entanglement cannot be distilled to obtain maxiamlly entangled states. Note the partial transposition of a density matrix $\rho = \sum \rho_{ij,kl} \left|i\right\rangle \left\langle j\right| \otimes \left|k\right\rangle \left\langle l\right|$ (expanded in a given local orthonormal basis) is defined as

$$\rho^{T_B} = \sum \rho_{ij,kl} \left|i\right\rangle \left\langle j\right| \otimes \left|l\right\rangle \left\langle k\right|. \tag{1.147}$$

We can try a maximally entangled state $\left|00\right\rangle + \left|11\right\rangle$, whose density matrix is

$$\rho = \frac{\left|00\right\rangle \left\langle 00\right| + \left|11\right\rangle \left\langle 00\right| + \left|00\right\rangle \left\langle 11\right| + \left|11\right\rangle \left\langle 11\right|}{2}. \tag{1.148}$$

Its partial transposition is given by

$$\rho^{T_B} = \frac{\left|00\right\rangle \left\langle 00\right| + \left|10\right\rangle \left\langle 01\right| + \left|01\right\rangle \left\langle 10\right| + \left|11\right\rangle \left\langle 11\right|}{2}, \tag{1.149}$$

having eigenvalues $1/2, 1/2, 1/2, -1/2$ (so ρ^{T_B} is not positive), which implies that ρ is entangled.

Negativity is an entanglement monotone, which attempts to quantify the negativity in the spectrum of the partial transpose (how much the partial transposition of ρ fails to be positive). It is defined as

$$N(\rho) = \frac{||\rho^{T_B}|| - 1}{2} = \max\{0, -\sum_k \lambda_k^-\}, \tag{1.150}$$

where $||X|| = \operatorname{tr}\sqrt{X^\dagger X}$ is the trace norm and $\{\lambda_k^-\}$ are the negative eigenvalues of the partial transpose. A related measure that is more often used is the *logarithmic negativity*:

$$E_N(\rho) = \log||\rho^{T_B}|| = \log[1 + 2N(\rho)]. \tag{1.151}$$

In the case of a maximally entangled state $\left|00\right\rangle + \left|11\right\rangle$, we have $E_N(\rho) = \log 2$. We remark that $E_N(\rho)$ can be zero even if the state is entangled, and it is also additive on tensor products $E_N(\rho \otimes \sigma) = E_N(\rho) + E_N(\sigma)$ (note the negativity $N(\rho)$ is not additive).

1.5 Open quantum system

In this section, we will introduce some basic concepts in open quantum systems. One may wonder why should we care about open systems. There are many reasons in general [86, 87]. Here are several reasons why I think it is interesting, apart from the fact that all systems are generally open (Schrodinger equation which is for closed system only holds over sometime scale rigorously).

First it is important for quantum technologies which are largely based on quantum entanglement. The decoherence induced by the environment is our main enemy and we hope to reduce it. The study of open quantum system may help us to understand the decoherence processes better and may even give us ways to establish robust entanglement. For example, one big topic in open quantum systems is quantum reservoir engineering and control [88]. To date, experiments investigating quantum superpositions and entanglement are hampered by decoherence. However, it was recognized [89] that the engineered interaction with a reservoir can drive the system into a desired steady state. In particular, some dissipation can drive the system of interest into an entangled state [90, 91, 92]. The idea of using and engineering dissipation rather than relying on coherent evolutions represents a paradigm shift with potentially significant practical advantages. Contrary to other methods, entanglement generation by dissipation does not require the preparation of a system in a particular input state and exists, in principle, for an arbitrary long time, which is expected to play an important role in quantum information protocols. These features make dissipative methods inherently stable against weak random perturbations, with the dissipative dynamics stabilizing the entanglement.

Moreover, the study of open quantum system may provide us with new quantum probes [93]. We can use a small controllable quantum system (could be an atom) to interact with a many body complex system for certain amount of time. Our aim is to understand the properties of many body system, which are imprinted in the dynamics of the probes. We hope to build

the map from properties of many body system to the decoherent dynamics of the probe, which would allow us to read off the properties of the many body system of interest.

We will first discuss a general description of nonunitary evolutions in terms of quantum maps and its *Kraus Operator Sum Representations* (OSR), which is crucial for the derivation of Lindblad master equation and for the understanding of the general theory of measurements. Then, by making the Markovian approximation, we drive the Lindlad master equation both from the Kraus OSR formally and from the first principle. We finally provide a different perspective on the Lindblad master equation from the view of quantum measurement, known as *quantum trajectory theory* or *quantum Monte Carlo wavefunction method*.

1.5.1 General description for nonunitary evolution

We consider a closed quantum system (governed by a Hamiltonian H) consisting of a system S and an environment E [94, 86, 95, 96]. Assuming the initial joint state is $\rho_{\mathrm{SE}}(0)$, we have

$$\rho_{\mathrm{SE}}(t) = U(t)\rho_{\mathrm{SE}}U^{\dagger}(t), \tag{1.152}$$

where $U(t) = e^{-iHt}$ is the joint unitary evolution. We hope to track the dynamics of the system S of interest without following the environment E. In fact, the whole point of treating certain degrees of freedom as environment is that they are uncontrolled and too complex to follow in detail. The goal is to develop a formalism to describe the evolution of the system S, given some overall evolution of the joint system environment:

$$\rho_S(t) = \mathrm{tr}_E[U(t)\rho_{\mathrm{SE}}(0)U^{\dagger}(t)]. \tag{1.153}$$

An important special case is where initially the system and environment are uncorrelated: $\rho_{\mathrm{SE}}(0) = \rho_S(0) \otimes \rho_E(0)$. We write $\rho_E(0) = \sum_\nu \lambda_\nu |\nu\rangle \langle\nu|$, a spectral decomposition in an orthonormal basis $\{|\nu\rangle\} \in \mathcal{H}_E$ with non-negative eigenvalues λ_ν. Then we have

$$\rho_S(t) = \sum_{\mu\nu} \sqrt{\lambda_\nu} \langle\nu| U(t) |\nu\rangle \ \rho_S(0) \sqrt{\lambda_\nu} \langle\nu| U^{\dagger}(t) |\mu\rangle = \sum_{\mu\nu} K_{\mu\nu}(t)\rho_S(0)K^{\dagger}_{\mu\nu}(t), \tag{1.154}$$

where $K_{\mu\nu}(t) = \sqrt{\lambda_\nu}\,\langle\mu|\,U(t)\,|\nu\rangle$ are known as **Kraus operators**, only acting on $\mathcal{H}_S$. This equation defines the evolution of the system in terms of Kraus operator, which is known as the **Kraus Operator Sum Representation** (OSR). We remark that the Kraus decomposition is not unique. One can obtain another Kraus decomposition by changing to another basis $\{|\tilde{\nu}\rangle\} \in \mathcal{H}_E$. Different Kraus operators of different decompositions are related to each other by an unitary transformation (the same one that relates the basis). It is useful to regard the above result as a **quantum map** on the density operator:

$$\rho_S(t) = \Phi_t[\rho_S(0)], \tag{1.155}$$

where $\Phi_t[X] = \sum_\alpha K_\alpha(t) X K_\alpha^\dagger(t)$. Here we have collected the indices $\mu\nu$ into a single index $\alpha = (\mu\nu)$. $X \in \mathcal{B}(\mathcal{H}_S)$ lives in the space of linear operators acting on the system Hilbert space. Note that Φ maps operators to operators, hence Φ is called a *superoperator*. To understand the nature of this map better, let us consider the case that the initial state of the system is pure $\rho_S(0) = |\psi_S(0)\rangle\langle\psi_S(0)|$. Then, according to the map, we have

$$\rho_S(t) = \sum_\alpha K_\alpha(t)\,|\psi_S(0)\rangle\,\langle\psi_S(0)|\,K_\alpha^\dagger(t), \tag{1.156}$$

where we can set $K_\alpha(t)\,|\psi_S(0)\rangle = \sqrt{p_\alpha(t)}\,|\psi_\alpha(t)\rangle$ with $p_\alpha(t) = \langle\psi_S(0)|\,K_\alpha^\dagger(t)K_\alpha(t)\,|\psi_S(0)\rangle$ and $\langle\psi_\alpha|\psi_\alpha\rangle = 1$. Thus we have

$$\rho_S(t) = \sum_\alpha p_\alpha(t)\,|\psi_\alpha(t)\rangle\,\langle\psi_\alpha(t)|\,, \tag{1.157}$$

which implies that, in general, the map takes a pure state to a mixed state, since the system becomes entangled with the environment through the interaction.

Let us now discuss the general properties of the quantum map.

1. *Trace preserving.* Under the quantum map Φ, a density matrix is mapped onto another physical density matrix whose trace is also one:

$$\mathrm{tr}[\Phi(\rho)] = \mathrm{tr}(\rho), \tag{1.158}$$

which can be proved by noting that $\sum_\alpha K_\alpha^\dagger K_\alpha = I$ (one can prove this by using the definition of Kraus operators).

2. *Linearity.* One can directly show that the quantum map is linear:

$$\Phi(a\rho_1 + b\rho_2) = a\Phi(\rho_1) + b\Phi(\rho_2), \tag{1.159}$$

where a, b are arbitrary scalars.

3. *Complete Positivity.* Since we are mapping a density matrix to a physical density matrix, the final state must be positive $\Phi(\rho) \geq 0$ (non-negative eigenvalues), which can be easily shown. It is clear that the Kraus representation satisfies these three properties, but it turns out that there are maps that satisfy these properties do not have Kraus representation. In fact, we need to modify and strengthen the positivity property into *complete positivity*. One can show that the quantum map is not only positive, but also a completely positive map. This means that $\Phi \otimes I_R^{(k)}$ is positive for all k, where k is the dimension of an ancillary Hilbert space $\mathcal{H}_R$, and I_R denotes the identity (super-)operator on $\mathcal{H}_R$. Then, it is true that a map Φ has a Kraus OSR if and only if it is trace preserving, linear, and completely positive.

Another representation of quantum map. We have seen that the quantum map can be represented by a Kraus operator sum. Let us go one step further, expanding the Kraus operators in a basis:

$$K_\alpha(t) = \sum_{i=0}^{d_S^2-1} b_{i\alpha}(t) F_i, \tag{1.160}$$

where $\{F_i\}$ are the (time-independent) operator basis for $\mathcal{B}(\mathcal{H}_S)$ ($d_S = \dim(\mathcal{H}_S)$), $b_{i\alpha}$ are the time-dependent elements of a rectangular $d_S^2 \times d_E^2$-dimensional matrix b ($d_E = \dim(\mathcal{H}_E)$), and we choose the basis such that $F_0 = I$. Then we have

$$\rho(t) = \sum_{ij} \chi_{ij}(t) F_i \rho(0) F_j^\dagger, \tag{1.161}$$

where $\chi_{ij}(t) = \sum_\alpha b_{i\alpha}(t) b^*_{j\alpha}(t)$ is a $d_S^2 \times d_S^2$ square matrix. It follows immediately that χ is hermitian and also positive semidefinite. Let us further write the density matrix into the form of

$$\rho(t) = \chi_{00}(t)\rho(0) + \sum_{i>0} \left[\chi_{0i}(t)\rho(0)F_i^\dagger + \chi_{i0}F_i\,\rho(0)\right] + \sum_{i,j>0} \chi_{i,j}(t)F_i\rho(0)F_j^\dagger. \tag{1.162}$$

We can simplify this expression by noting that

$$I = \sum_\alpha K_\alpha^\dagger(t)K_\alpha(t) = \chi_{00}(t)I + \sum_{i>0} \left[\chi_{0i}(t)F_i^\dagger + \chi_{i0}F_i\,\right] + \sum_{i,j>0} \chi_{ij}(t)F_j^\dagger F_i. \tag{1.163}$$

Let us multiply the above equation first from the right by $\rho(0)/2$, then from the left, and add the resulting two equations, which yields:

$$\rho(0) = \chi_{00}(t)\rho(0) + \frac{1}{2}\sum_{i>0} \left[\chi_{0i}(t)\{F_i^\dagger, \rho(0)\} + \chi_{i0}(t)\{F_i, \rho(0)\}\right] + \frac{1}{2}\sum_{i,j>0} \chi_{ij}(t)\{F_j^\dagger F_i, \rho(0)\}. \tag{1.164}$$

We now subtract this equation from Eq. (1.162) to eliminate the $\chi_{00}\rho(0)$ term, yielding

$$\rho(t) - \rho(0) = -i[Q(t), \rho(0)] + \sum_{i,j>0} \chi_{ij}(t)\Big(F_i\rho(0)F_j^\dagger - \frac{1}{2}\{F_j^\dagger F_i, \rho(0)\}\Big), \tag{1.165}$$

where

$$Q(t) \equiv \frac{i}{2}\sum_{j>0}[\chi_{j0}(t)F_j - \chi_{0j}(t)F_j^\dagger], \tag{1.166}$$

is hermitian. We can diagonalize the χ_{ij} matrix via some unitary matrix u: $\Gamma = u\chi u^\dagger$, where Γ is diagonal and positive semidefinite (with eigenvalues $\gamma_k \geq 0$). We define $L_k = \sum_{j>0} u^*_{kj}F_j$, and thus we have $F_i = \sum_{k>0} u_{ki}L_k$, where we note the sum is over $k > 0$ (excluding $L_0 = I$). Then we can write the Eq. (1.165) as

$$\rho(t) - \rho(0) = -i[Q(t), \rho(0)] + \sum_{k>0} \gamma_k(t)\Big(L_k\rho(0)L_k^\dagger - \frac{1}{2}\{L_k^\dagger L_k, \rho(0)\}\Big). \tag{1.167}$$

We should emphasize that we did not make any approximation in the discussion of this subsection. The only assumption we have made is that the initial state can be written as $\rho_S(0) \otimes \rho_E(0)$. In the following subsection, we will make a Markovian approximation to obtain the Lindblad master equation.

1.5.2 Lindblad master equation

In the above subsection, we have studied abstract maps of open quantum systems. While this gives us a general framework for describing the quantum map, it does not directly describe the physics of the dynamics. For that, we need to consider a differential equation and the generator of the dynamics [96]. As we will see, after applying the Markovian approximation, we can find a differential equation for the density matrix of the system of our interest, known as the *Lindblad master equation.* Here we will derive it formally by exploiting the Kraus OSR.

To derive a differential equation for $\rho(t)$, let us consider the infinitesimal time interval dt (we will discuss how small it is shortly), and write

$$\rho(t+dt) = \rho(t) + \mathcal{O}(dt). \tag{1.168}$$

Note here an assumption is made: we assume that the evolution of the quantum system is Markovian, in a sense that $\rho(t+dt)$ is completely determined by $\rho(t)$. This is not generally guaranteed, as the environment, though inaccessible, may have some memory of the system. Nevertheless, in many situations, the Markovian description is a very good approximation.

Based on the Markovian approximation, we now further expand the Kraus operators in terms of dt, where we will have one of the operators K_0 with order one, that we write as

$$K_0(t) = I + [-iH(t) + M(t)]dt, \tag{1.169}$$

where both H, M are chosen to be Hermitian and are zeroth order in dt. And the other Kraus operators K_k with order $\sqrt{dt}$ which has the form

$$K_k(t) = \sqrt{dt}L_k(t), k > 0, \tag{1.170}$$

where L_k are zeroth order in dt. The condition $\sum_k K_k^\dagger K_k = I$ gives

$$M = -\frac{1}{2}\sum_{k>0} L_k^\dagger L_k. \tag{1.171}$$

Upto first order of dt, we have

$$\frac{\mathrm{d}\rho}{\mathrm{d}t} = -i[H(t),\rho] + \sum_{k>0}\big[L_k(t)\rho L_k^\dagger(t) - \frac{1}{2}L_k^\dagger(t)L_k(t)\rho - \frac{1}{2}\rho L_k^\dagger(t)L_k(t)\big]. \tag{1.172}$$

The operators L_k are called Lindblad operators or quantum jump operators (the reason will be clear in the last subsection). The first term is usual Hamiltonian term which generates unitary evolutions. The other terms describe the dissipation of the system due to interaction with the environment. We remark that, in general, we have a time-dependent Markovian process, where $H, L_k^\dagger$ are allowed to change over time, as long as these changes are uncorrelated between different time-segements. We can formally write the Lindblad equation as

$$\frac{\mathrm{d}\rho}{\mathrm{d}t} = \mathcal{L}(t)[\rho(t)], \tag{1.173}$$

where

$$\mathcal{L}(t)[\star] = -i[H(t),\star] + \sum_{k>0}\big[L_k(t)\star L_k^\dagger(t) - \frac{1}{2}L_k^\dagger(t)L_k(t)\star - \frac{1}{2}\star L_k^\dagger(t)L_k(t)\big] \tag{1.174}$$

which is the generator of the dynamics. This Lindblad equation can be solved by $\rho(t) = \Phi_t[\rho(0)]$, where the Markovian evolution operator (it is also a quantum map) is given by

$$\Phi_t = \mathcal{T}e^{\int_0^t ds\,\mathcal{L}(s)}, \tag{1.175}$$

where $\mathcal{T}$ is the time-odering operator. Similar to the procedure in deriving path integral, let us split the time interval $(0,t)$ into n intervals. Then we have $\Phi_t = \mathcal{T}e^{dt\sum_{j=0}^{n-1}\mathcal{L}_j}$, where $dt = t/n$ and $\mathcal{L}_j = \int_{j\,dt}^{(j+1)\,dt} ds\,\mathcal{L}(s)/\tau$ is a "coarse-grained" generator. In the Markovian limit, it is reasonable to assume that the generators of different time intervals commute $[\mathcal{L}_j,\mathcal{L}_k] = 0$ (no memory of the evolution from one interval to the next), while it is still an open question to derive rigorous conditions for this to hold. In fact, we usually assume $\mathcal{L}_j = \mathcal{L}_0$ in the Markovian approximation. Then the quantum map can be written as

$$\Phi_t = e^{\mathcal{L}t}. \tag{1.176}$$

One can show that this is a completely positive map, since we derive the Lindblad master equation from the Kraus OSR (combined with the the Markovian approximation). This forces all the eigenvalues of $\mathcal{L}$, which physically correspond to decay rates, to be non-positive. Given $\rho_j = \rho(j\,dt)$, we can generate $\rho_{j+1} = e^{dt\,\mathcal{L}}\rho_j$. After Taylor expansion, we have

$$\rho_{j+1} = \Big[1 + dt\mathcal{L} + \frac{(dt\mathcal{L})^2}{2} + \cdots\Big]\rho_j, \tag{1.177}$$

In the limit of $dt||\mathcal{L}|| \ll 1$, we get $\dot{\rho} = \mathcal{L}[\rho]$. This implies that the coarse graining time dt should be much smaller compared to the timescale over which ρ changes τ_D. From the discussion below, we will see there is also a lower bound for the coarse graining time.

1.5.3 Lindblad master equation from first principles

The Lindblad form of the master equation that we derived above follows by the fundamental properties of quantum maps under the Markovian approximation. To explicitly derive the Lindblad operators, we must turn to the underlying physics. The basic model is the coupling of the system to the environment. Taken together, they form a "closed system" undergoing unitary evolution, governed by Hamiltonian:

$$H = H_S + H_E + H_{\rm SE}, \tag{1.178}$$

where H_S, H_E are Hamiltonians of the system and the environment, respectively. $H_{\rm SE}$ is the interaction between them. We start with the uncorrelated state $\rho_{\rm SE}(0) = \rho_S(0) \otimes \rho_E(0)$. Typically, the environment is taken to be in thermal equilibrium at some temperature T, $\rho_E(0) = \rho_E^{\rm eq} = e^{-\beta H_E}/\mathcal{Z}_E$ where $\mathcal{Z}_E = \mathrm{tr}\, e^{-\beta H_E}$ with $\beta = 1/k_B T$. The effect of the environment is to cause irreversible decay of the system.

As in standard time-dependent perturbation theory, it is convenient to work in the interaction picture. We have

$$\frac{\mathrm{d}\hat{\rho}_{\rm SE}}{\mathrm{d}t} = -i[\hat{H}_{\rm SE}(t), \hat{\rho}_{\rm SE}(t)], \tag{1.179}$$

where

$$\hat{H}_{\rm SE} = U_0^\dagger(t) H_{\rm SE} U_0(t), \quad \text{with} \quad U_0(t) = e^{-iH_S\,t} \otimes e^{-iH_B\,t}. \tag{1.180}$$

$\hat{\rho}_{\rm SE}(t) = U_0^\dagger(t)\rho_{\rm SE}(t)U_0(t)$ is also in the interaction picture. By tracing out the degrees of freedom of the environment, we obtain (drop the subscript S for $\hat{\rho}_S$)

$$\dot{\hat{\rho}}(t) = -i\,\mathrm{tr}_E[\hat{H}_{\rm SE}(t), \hat{\rho}_{\rm SE}(t)]. \tag{1.181}$$

Let us integrate for a short time interval, giving us:

$$\hat{\rho}(t+\Delta t) = \hat{\rho}(t) + \mathrm{tr}_E\Big\{ -i\int_t^{t+\Delta t} dt'\,[\hat{H}_{\rm SE}(t'), \hat{\rho}_{\rm SE}(t')]\Big\}. \tag{1.182}$$

We should note that this is not in the Markovian form: $\hat{\rho}(t+\Delta t) \neq \hat{\rho}(t) + \mathcal{O}(\Delta t)$.

Before introducing the **Markovian approximation**, let us develop some understanding. Assuming there is some characteristic time scale τ_B (environment correlation time), information from the environment is very unlikely to go back to the system after this time scale. By neglecting (coarse graining) the dynamics within this correlation time scale, the dynamics becomes irreversible. In general, the form of the evolution is given an integral-differential equation: $\dot{\hat{\rho}} = \int K(t-t')[\hat{\rho}(t')]$, where $K(t-t')$ is the *memory kernal*. In the extremely limit of no memory (the bath correlation time is zero $\tau_B \to 0$), we have $K(t-t') \propto \delta(t-t')$, thus $\dot{\hat{\rho}} = \mathcal{L}(t)[\hat{\rho}(t)]$. This is known as the Markovian approximation. Let us understand this by thinking about a classical example. Suppose we put a hot penny into a lake at temperature T. It is clear that there are two important timescales. The first timescale is τ_B during which the "excited water molecules" rethermalize due to many collisions with other molecules in the lake. Another timescale is τ_D, the time it takes for the penny to come to thermal equilibrium. It is clear that the rethermalization of water molecules happens much faster than τ_D. For us, we are interested in how the penny reaches the thermal equilibrium. Therefore, when we construct a theory for it, it is natural to coarse grain over a time scale Δt:

$$\tau_B \ll \Delta t \ll \tau_D. \tag{1.183}$$

Let us return to the formal integration of the Schrodinger equation:

$$\begin{aligned}\hat{\rho}_{\rm SE}(t+\Delta t) &= \hat{\rho}_{\rm SE}(t) - i\int_t^{t+\Delta t} dt'\ [\hat{H}_{\rm SE}(t'), \hat{\rho}_{\rm SE}(t')] \\ &= \hat{\rho}_{\rm SE}(t) + (-i)\int_t^{t+\Delta t} dt'\ [\hat{H}_{\rm SE}(t'), \hat{\rho}_{\rm SE}(t)] \\ &\quad + (-i)^2\int_t^{t+\Delta t} dt' \int_t^{t'} dt''\big[\hat{H}_{\rm SE}(t'), [\hat{H}_{\rm SE}(t''), \hat{\rho}_{\rm SE}(t)]\big] + \cdots\end{aligned} \quad , \tag{1.184}$$

and it is clear how this continues. The sufficient convergence condition is $||\hat{H}_{\rm SE}||\Delta t \ll 1$, which can be satisfied if the coupling between the environment and the system is weak enough. We will only keep the terms we write down above, which is known as the *Born approximation*. For a sufficiently large bath that is in particular much larger than the system, it is reasonable to assume that while the system undergoes non-trivial evolution, the bath remains unaffected, and hence that the state of the composite system at time t is

$$\hat{\rho}_{\rm SE} = \hat{\rho}_S(t)\otimes\hat{\rho}_E(t) + \delta\hat{\rho}(t) \approx \hat{\rho}_S(t)\otimes\hat{\rho}_E(t). \tag{1.185}$$

In the Markovian approximation, we can replace $\hat{\rho}_E(t)$ with $\hat{\rho}_E(0) = \rho_E^{\rm eq}$, since the environment returns to equilibrium after the coarse graining timescale Δt. One can always redefine the Hamiltonian such that the first order term (after performing the trace over the environment tr_E) in Eq. (1.184) vanishes [96]. Then we have:

$$\hat{\rho}(t+\Delta t) - \hat{\rho}(t) = -\int_t^{t+\Delta t} dt' \int_t^{t'} dt''\,\mathrm{tr}_E\big[\hat{H}_{\rm SE}(t'), [\hat{H}_{\rm SE}(t''), \hat{\rho}_{\rm SE}(t)]\big]. \tag{1.186}$$

To proceed, we make a change of variables: $\tau = t' - t''$, $\xi = t' - t$. Then we get:

$$\hat{\rho}(t+\Delta t) - \hat{\rho}(t) = -\int_0^{\Delta t} d\tau \int_\tau^{\Delta t} d\xi\ \mathrm{tr}_E\big[\hat{H}_{\rm SE}(\xi+t), [\hat{H}_{\rm SE}(\xi+t-\tau), \hat{\rho}_{\rm SE}(t)]\big]. \tag{1.187}$$

In the Markovian approximation, the integration over τ is basically nonzero only over the interval $\tau \in (0, \tau_B)$ (since there is a factor $e^{-\tau/\tau_B}$ from the bath correlation). Thus we can safely extend the integration range of τ to $(0, +\infty)$. Besides, for the same reason, we can replace the lower bound of ξ with τ_B, which can be set to zero in the Markovian limit. Thus

we have

$$\begin{aligned}\frac{\mathrm{d}\hat{\rho}}{\mathrm{d}t} &= -\lim_{\Delta t\to 0}\frac{1}{\Delta t}\int_0^\infty d\tau\int_0^{\Delta t} d\xi\ \mathrm{tr}_E\left[\hat{H}_{\mathrm{SE}}(\xi+t),[\hat{H}_{\mathrm{SE}}(\xi+t-\tau),\hat{\rho}_{\mathrm{SE}}(t)]\right]\\ &= -\int_0^\infty d\tau\ \mathrm{tr}_E\left[\hat{H}_{\mathrm{SE}}(t),[\hat{H}_{\mathrm{SE}}(t-\tau),\hat{\rho}_{\mathrm{SE}}(t)]\right].\end{aligned} \tag{1.188}$$

We can go back to the Schrodinger picture by invoking $\hat{\rho}(t) = U_0^\dagger(t)\rho(t)U_0(t)$ and $\hat{H}(t) = U_0^\dagger(t)HU_0(t)$, which gives us:

$$\frac{\mathrm{d}\rho(t)}{\mathrm{d}t} = -i[H_S,\rho(t)] - \int_0^\infty d\tau\,\mathrm{tr}_E\left[H_{\mathrm{SE}},[\hat{H}_{\mathrm{SE}}(-\tau)],\rho(t)\otimes\rho_E^{\mathrm{eq}}\right], \tag{1.189}$$

where $\hat{H}_{\mathrm{SE}}(-\tau)$ is in the interaction picture and we have set $\hbar = 1$ through the all discussion for simplicity. This expression is valid for a general interaction $H_{\mathrm{SE}} = \sum_\alpha S_\alpha\otimes B_\alpha$, with $\langle B_\alpha\rangle_{\mathrm{eq}} = 0$. Here, S_α and B_α are operators acting on Hilbert spaces of the system and the environment, respectively. For $\langle B_\alpha\rangle_{\mathrm{eq}} \neq 0$, we can always redefine $B \to B - \langle B\rangle_{\mathrm{eq}}$. The second term in Eq. (1.189) can be written as

$$\mathrm{tr}_E\left\{\left[H_{\mathrm{SE}},[\hat{H}_{\mathrm{SE}}(-\tau),\rho(t)\otimes\rho_B^{\mathrm{eq}}]\right]\right\} = \langle H_{\mathrm{SE}}\hat{H}_{\mathrm{SE}}(-\tau)\rangle_{\mathrm{eq}}\rho - \langle\hat{H}_{\mathrm{SE}}(-\tau)\rho H_{\mathrm{SE}}\rangle_{\mathrm{eq}} + \mathrm{H.c.}. \tag{1.190}$$

It is straightforward to work out the master equation for $\rho(t)$ once the interaction is specified, which will yields the Lindblad form. We use the following example to illustrate this. One can also formally show that the above master equation can be brought into the Lindblad form [96].

Example. Here we derive the well-known relaxation time T_1 and decoherence time T_2, which characterize the local relaxation of a single qubit, by considering the dynamics of a spin-1/2 system $H_S = -\Delta\sigma^z/2$ coupled to a bath H_E. A general form of the interaction can be in the first order of the Pauli matrices σ^z and $\sigma^\pm = (\sigma^x \pm i\sigma^y)/2$ for the spin-1/2, $H_{\mathrm{SE}} = \sigma^z\otimes X + \sigma^+\otimes Y + \sigma^-\otimes Y^\dagger$, with operators X and Y acting on the bath. We assume $X = X^\dagger$, and $\langle X\rangle = \langle Y\rangle = 0$, where the average denotes the thermal average taken within the bath. In the interaction picture,

$$\hat{H}_{\mathrm{SE}}(-\tau) = \sigma^z\otimes X(-\tau) + \sigma^+\otimes Y(-\tau)e^{i\Delta\tau} + \sigma^-\otimes Y^\dagger(-\tau)e^{-i\Delta\tau}, \tag{1.191}$$

and Eq. (1.190) then becomes

$$\begin{aligned}&\langle XX(-\tau)\rangle(\sigma^z\sigma^z\rho-\sigma^z\rho\sigma^z)+\langle YY^\dagger(-\tau)\rangle e^{-i\Delta\tau}(\sigma^+\sigma^-\rho-\sigma^-\rho\sigma^+)\\&+\langle Y^\dagger Y(-\tau)\rangle e^{i\Delta\tau}(\sigma^-\sigma^+\rho-\sigma^+\rho\sigma^-)+\text{H.c.}\end{aligned}\tag{1.192}$$

where we have assumed certain symmetry properties of the bath such that only $\langle XX\rangle, \langle YY^\dagger\rangle$, and $\langle Y^\dagger Y\rangle$ are nonzero. For example, taking $X = S^z$ and $Y = S^-$ to be spin operators in the bath, the $U(1)$ symmetry in the spin space of the bath is assumed. We therefore obtain the master equation:

$$\dot\rho = -i\big[H_S + H_{\text{Lamb}}, \rho\big] - \mathcal{L}[\rho],\tag{1.193}$$

where the Lamb shift is

$$H_{\text{Lamb}} = \frac{\text{Im}\int_0^\infty d\tau\langle\{Y(\tau), Y^\dagger\}\rangle e^{-i\Delta\tau}}{2}\sigma^z,\tag{1.194}$$

and the Lindbladian superoperator is given by:

$$\begin{aligned}\mathcal{L}[\rho] = &\frac{1}{2}\int_{-\infty}^{\infty} d\tau\langle X(\tau)X\rangle(2\rho-2\sigma^z\rho\sigma^z)\\&+\frac{1}{2}\int_{-\infty}^{\infty} d\tau\langle Y(\tau)Y^\dagger\rangle e^{-i\Delta\tau}\left(\sigma^+\sigma^-\rho+\rho\sigma^+\sigma^- - 2\sigma^-\rho\sigma^+\right)\\&+\frac{1}{2}\int_{-\infty}^{\infty} d\tau\langle Y^\dagger Y(\tau)\rangle e^{-i\Delta\tau}\left(\sigma^-\sigma^+\rho+\rho\sigma^-\sigma^+ - 2\sigma^+\rho\sigma^-\right).\end{aligned}\tag{1.195}$$

For notational convenience, let us introduce the following parameters to denote the coefficients in the Lindbladian:

$$\begin{aligned}2D &\equiv \int_{-\infty}^{\infty} d\tau\langle X(\tau)X\rangle = iG^>_{XX}(\omega=0) = iG^<_{XX}(0) = \frac{iG^>_{XX}(0)+iG^<_{XX}(0)}{2} = \frac{S_X(0)}{2},\\2B^< &\equiv \int_{-\infty}^{\infty} d\tau\langle Y(\tau)Y^\dagger\rangle e^{-i\Delta\tau} = iG^<_{Y^\dagger Y}(\Delta),\\2B^> &\equiv \int_{-\infty}^{\infty} d\tau\langle Y^\dagger Y(\tau)\rangle e^{-i\Delta\tau} = iG^>_{Y^\dagger Y}(\Delta),\\2\bar B &\equiv B^> + B^< = \frac{iG^>_{Y^\dagger Y}(\Delta)+iG^<_{Y^\dagger Y}(\Delta)}{2} = \frac{S_{Y^\dagger}(\Delta)}{2},\end{aligned}\tag{1.196}$$

where *greater* and *lesser* Green's functions follow the conventional definition:

$$G^>_{X,Y}(t) \equiv -i\langle X(t)Y\rangle, \quad G^<_{X,Y}(t) = -i\langle YX(t)\rangle.\tag{1.197}$$

We have also introduce the equilibrium symmetrized fluctuations

$$iG^{>}_{X,Y}(\omega) + iG^{<}_{X,Y}(\omega) = \int dt \langle\{X(t), Y\}\rangle e^{i\omega t}, \tag{1.198}$$

specifically, we have the power spectrum

$$S_X(\omega) = \int dt \langle\{X(t), X^\dagger\}\rangle e^{i\omega t}. \tag{1.199}$$

Here, all parameters $D, B^{>}, B^{<}, \bar{B}$ are real-valued by their definitions. Furthermore, being the physical decay rates, they must be non-negative, which is ensured by the thermodynamic stability of the bath, as will be detailed later.

According to the master equation (1.193), we obtain the equation of motion for $s^z = \langle\sigma^z\rangle/2 = (\rho_{11} - \rho_{22})/2$:

$$\frac{\mathrm{d}}{\mathrm{d}t} s^z = -4\bar{B}\big(s^z - \bar{s}^z\big), \tag{1.200}$$

from which we extract the relaxation time T_1:

$$T_1^{-1} = 4\bar{B} = S_{Y^\dagger}(\Delta), \tag{1.201}$$

where $\bar{s}^z \equiv (B^{>} - B^{<})/4\bar{B}$ is the equilibrium value of the spin-z component. This value can be made sense of by writing down the equation for the diagonal elements of the density matrix:

$$\dot{\rho}_{11} = -2B^{<}\rho_{11} + 2B^{>}\rho_{22}, \quad \text{and} \quad \dot{\rho}_{22} = 2B^{<}\rho_{11} - 2B^{>}\rho_{22}, \tag{1.202}$$

which implies that the transition rate of flipping the spin from up to down is $2B^{<}$ and that of the reverse process is $2B^{>}$. In equilibrium,

$$\frac{\rho_{11}}{\rho_{22}} = \frac{B^{>}}{B^{<}}, \tag{1.203}$$

from which we conclude that the probability of measuring σ^z to be 1 is $B^{>}/2\bar{B}$ and -1 is $B^{<}/2\bar{B}$, which satisfies $\rho_{11}+\rho_{22} = 1$. We next look into the time evolution of the off-diagonal elements:

$$\frac{\mathrm{d}}{\mathrm{d}t}\rho_{12} = i\Delta\rho_{12} - (4D + 2\bar{B})\rho_{12}, \quad \text{and} \quad \frac{\mathrm{d}}{\mathrm{d}t}\rho_{21} = -i\Delta\rho_{21} - (4D + 2\bar{B})\rho_{21}. \tag{1.204}$$

Since $s^x = \langle \sigma^x \rangle = (\rho_{12} + \rho_{21})/2$ and $s^y = \langle \sigma^y \rangle = i(\rho_{12} - \rho_{21})/2$,

$$\frac{\mathrm{d}}{\mathrm{d}t} s^x = \Delta s^y - (4D + 2\bar{B}) s^x \quad \text{and} \quad \frac{\mathrm{d}}{\mathrm{d}t} s^y = -\Delta s^x - (4D + 2\bar{B}) s^y. \tag{1.205}$$

We thus identify the decoherence rate:

$$T_2^{-1} = 4D + 2\bar{B} = S_X(0) + \frac{S_{Y^\dagger}(\Delta)}{2}. \tag{1.206}$$

Note that $S_X(0)$ contributes to the dephasing effect only. This is rooted in the fact that $\sigma^z \otimes X$ commutes with the single NV center Hamiltonian $\Delta\sigma^z/2$. As a result, this type of interaction does not lead to energy flow between the system and the bath, but information flow only, i.e. a relative phase damping between NV center levels.

Combining Eq. (1.202) and Eq. (1.204), the equations of motion for the density matrix can be put into the following form:

$$\frac{\mathrm{d}}{\mathrm{d}t} \hat{\rho} = \begin{pmatrix} -2B^< \rho_{11} + 2B^> \rho_{22} & i\Delta\rho_{12} - T_2^{-1}\rho_{12} \\ -i\Delta\rho_{21} - T_2^{-1}\rho_{21} & 2B^< \rho_{11} - 2B^> \rho_{22} \end{pmatrix}. \tag{1.207}$$

We remark that Eq. (1.200) and Eq. (1.205) are nothing but the Bloch equations:

$$\begin{aligned} \frac{\mathrm{d}s^x}{\mathrm{d}t} &= \left(\vec{s} \times \vec{B}\right)_x - \frac{s^x}{T_2}, \\ \frac{\mathrm{d}s^y}{\mathrm{d}t} &= \left(\vec{s} \times \vec{B}\right)_y - \frac{s^y}{T_2}, \\ \frac{\mathrm{d}s^z}{\mathrm{d}t} &= \left(\vec{s} \times \vec{B}\right)_z - \frac{s^z - \bar{s}^z}{T_1}, \end{aligned} \tag{1.208}$$

with the magnetic field $\vec{B} = \Delta\hat{z}$.

1.5.4 Quantum trajectories and unravelling the Lindblad equation

Quantum measurement. We first introduce the quantum (generalized) measurement, which is crucial to understand the quantum trajectories [96, 86]. It is also generally important when one studies open quantum systems, since many concepts that appear to be different can be related by thinking about measurements. For example, we have introduced

the density matrix in two different cases. First we can prepare the state statistically according to a classical probability distribution of different pure states: $\rho = \sum_i p_i |\psi_i\rangle \langle\psi_i|$. Second, when we consider a state of a subsystem of a larger set of degrees of freedom: $\rho = \mathrm{tr}_E |\psi_{\mathrm{SE}}\rangle \langle\psi_{\mathrm{SE}}|$. These two look unrelated. However, if we think of the environment as performing a measurement of the system but not telling us the result, these two cases are basically equivalent (the environment is basically preparing our density matrix in the second case). Measurements of a quantum system causes collapse of the state with associated randomness. Thus a continuously measured quantum state will evolve stochastically, which is known as a *quantum trajectory*.

Let us make the measurement process we described above more precise. Suppose a quantum meter is coupled to a quantum system. The meter's degrees of freedom get displaced according to the value of the observable A_S (of the system) we want to measure. Suppose the interaction part is $H_{SM} = gA_S P_M$, where P_M is the generator of displacement of the meter position X_M and g is a real coupling constant. Suppose the system is in a quantum state $|\psi_S\rangle = \sum_a c_a |a_S\rangle$, where $\{|a_S\rangle\}$ are eigenstates of A_S, and the meter is at the origin $|0_M\rangle$. The effect of this interaction is to entangle the system with the meter: $e^{-igA_S P_M} \sum_a c_a |a_S\rangle \otimes |0_M\rangle = \sum_a c_a |a_S\rangle \otimes |X_M = ga_S\rangle$. Then if we measure the position of the meter (with fine resolution) $X_M = ga_S$, the system is in $|a_S\rangle$, which occurs with probability $P_{a_s} = |c_a|^2$. This is the von Neumann theory of measurement (a projective measurement), where we assume the meter states are perfectly distinguishable $\langle X'_M | X_M\rangle = \delta(X_M - X'_M)$. For such a projective measurement, we have two rules. First, the probability of measurement outcome is

$$p_a = \langle\psi_S| \hat{P}_a |\psi_S\rangle = |\langle a|\psi_S\rangle|^2. \tag{1.209}$$

Second, the post-measurement state is conditioned on measurement result:

$$|\psi_S\rangle \Rightarrow \frac{\hat{P}_a |\psi_S\rangle}{|| |\psi_S\rangle ||} = |a\rangle, \tag{1.210}$$

where $\hat{P}_a = |a\rangle \langle a|$ are projectors on eigen-space, which form a resolution of the identity

$\sum_a \hat{P}_a = I$.

General theory of measurement. Generally speaking, the meter states are not necessarily perfectly distinguishable. So we need to generalize the concept of measurement that we described before. We know that the system state evolves according to a completely positive map, described by Kraus decomposition. For simplicity, let us take the case that the system is initially in a pure state $\rho^{\text{in}} = |\psi_S\rangle \langle\psi_S|$. Then the state out can be always written as $\rho^{\text{out}} = \sum_i K_i |\psi_S\rangle \langle\psi_S| K_i^\dagger$, where K_i's are Kraus operators, satisfying $\sum_i K_i^\dagger K_i = I$. We have a way to interpret this quantum map—we have a probability

$$p_i = ||K_i |\psi_S\rangle ||^2 = \langle\psi_S| K_i^\dagger K_i |\psi_S\rangle , \tag{1.211}$$

to find the system in

$$|\psi_i\rangle = \frac{K_i |\psi_S\rangle}{||K_i |\psi_S\rangle ||} = \frac{K_i |\psi_S\rangle}{\sqrt{p_i}}. \tag{1.212}$$

The output state is generally mixed because we have thrown out the measurement record stored in the meter, and thus ρ^{out} is a statistical mixture wighted by the probability of different outcomes i. We remark that the Kraus operators are generally not projectors, indicating that this is generally not a projective measurement. The set of operators $\{E_i = K_i^\dagger K_i\}$ are said to form a **POVM** (positive operator-valued measure). A POVM is a set of postive operators that form a resolution of the identity $\sum_i E_i = I$. Projectors form a POVM, but $\{E_i\}$ are generally not projectors. One can generalize to the case that the input state is mixed:

$$\rho^{\text{out}} = \frac{K_i \rho^{\text{in}} K_i^\dagger}{p_i}, \quad \text{with probability} \quad p_i = \text{tr}\big(K_i \rho^{\text{in}}\big). \tag{1.213}$$

Lindblad master equation and continuous measurement. We know that Lindblad master equation describes a completely positive map. It indicates that we can view the Lindblad equation from the point of measurement, which would give us the so called quantum trajectory theory. Consider the following Lindblad equation:

$$\frac{\mathrm{d}\rho}{\mathrm{d}t} = -i[H, \rho] + \sum_i \big[L_i \rho L_i^\dagger - \frac{1}{2}\{L_i^\dagger L_i, \rho\}\big], \tag{1.214}$$

which can be regarded as a differential map (that we have discussed before):

$$\rho(t+dt) = K_0(dt)\rho(t)K_0(dt) + \sum_{i>0} K_i(dt)\rho(t)K_i^\dagger(dt), \tag{1.215}$$

where $K_i(dt) = \sqrt{dt}L_i$, and $K_0(dt) = I - iH_{\text{eff}}dt$. Here we have written

$$H_{\text{eff}} = H - \frac{i}{2}\sum_i L_i^\dagger L_i, \tag{1.216}$$

which is non-Hermitian. The real part is the Hamiltonian and the imaginary part accounts for the decay as we will see. Suppose that at time t the state is pure, $|\psi(t)\rangle$. Then, at time $t+dt$, the state is

$$\rho(t+dt) = (1 - iH_{\text{eff}}dt)\,|\psi(t)\rangle\,\langle\psi(t)|\,(1 + iH_{\text{eff}}^\dagger dt) + dt\sum_i L_i\,|\psi(t)\rangle\,\langle\psi(t)|\,L_i^\dagger. \tag{1.217}$$

Based on the discussion of a completely positive map as the environment performing a measurement of the system and then throwing away the record, we have the following interpretation of the differential map:

- With probability $p_i = \langle\psi(t)|\,K_i^\dagger(dt)K_i(dt)\,|\psi(t)\rangle = dt\,\langle\psi(t)|\,L_i^\dagger L_i\,|\psi(t)\rangle$, the state jumps:

$$|\psi(t)\rangle \Rightarrow \frac{L_i\,|\psi(t)\rangle}{||L_i\,|\psi(t)\rangle\,||}. \tag{1.218}$$

  L_i's are also known as jump operators.

- With probability

$$\begin{aligned} p_0 &= \langle\psi(t)|\,L_0^\dagger(dt)L_0(dt)\,|\psi(t)\rangle \\ &= \langle\psi(t)|\,(1 + iH_{\text{eff}}^\dagger dt)(1 - iH_{\text{eff}}dt)\,|\psi(t)\rangle \\ &= \langle\psi(t)|\,[1 + i(H_{\text{eff}} + H_{\text{eff}}^\dagger)]dt\,|\psi(t)\rangle \\ &= 1 - dt\,\langle\psi(t)|\sum_i L_i^\dagger L_i\,|\psi(t)\rangle \\ &= 1 - \sum_i p_i, \end{aligned} \tag{1.219}$$

there is no jump. In this case, the evolution of the state is governed by the effective non-Hermitian Hamiltonian:

$$|\psi(t)\rangle \Rightarrow \frac{K_0(dt)\,|\psi(t)\rangle}{||K_0(dt)\,|\psi(t)\rangle\,||} = \frac{e^{-iH_{\text{eff}}dt}\,|\psi(t)\rangle}{||e^{-iH_{\text{eff}}dt}\,|\psi(t)\rangle\,||}, \tag{1.220}$$

where we have used $e^{-iH_{\text{eff}}dt} \approx 1 - iH_{\text{eff}}dt$.

In fact, this provides an algorithm for calculating the time-evolution of $\rho(t)$ through a stochastic (Monte Carlo) algorithm. Suppose $\rho(0) = |\psi(0)\rangle\langle\psi(0)|$, the density matrix is a statistical mixture of pure states $|\psi(t)\rangle$. Each pure state evolves stochastically and in a time interval dt, we update the state according to the rule and probability we discussed above. One can simulate the probability distribution by sampling with the statistics above over many realizations of the stochastic evolution of $|\psi(t)\rangle$:

$$\rho(t) = \lim_{N\to\infty} \frac{1}{N} \sum_{i^{\text{th}}\text{ realization}} |\psi_i(t)\rangle\langle\psi_i(t)|\,. \tag{1.221}$$

Therefore, this procedure is also known as the *quantum Monte Carlo Wave function* simulations of the master equation.

CHAPTER 2

Hydrodynamics of vorticity

"I consider that I understand an equation when I can predict the properties of its solutions, without actually solving it."

Paul A. M. Dirac

In this chapter, we study the transport of vorticity in both (semi)classical and quantum regime. We first explore a robust topological transport carried by vortices in a thin film of an easy-plane magnetic insulator between two metal contacts. An electric current in one of the magnetized metal contacts can pump vortices into the insulating bulk. Diffusion and two-dimensional nonlocal Coulomb-like interaction between these vortices will establish a steadystate vortex flow. Vortices leaving the bulk produce an electromotive force at another contact, which is related to the current-induced vorticity pumping by the Onsager reciprocity. The voltage signal decays algebraically with the separation between two contacts, similarly to a superfluid spin transport.

We then formulate an experimentally feasible energy-storage concept based on vorticity (hydro)dynamics within an easy-plane insulating magnet. The free energy, associated with the magnetic winding texture, is built up in a circular easy-plane magnetic structure by injecting a vorticity flow in the radial direction. The latter is accomplished by electrically induced spin-transfer torque, which pumps energy into the magnetic system in proportion to the vortex flux. The resultant magnetic metastable state with a finite winding number

can be maintained for a long time because the process of its relaxation via phase slips is exponentially suppressed when the temperature is well below the Curie temperature.

Finally a quantum theory of vorticity (hydro)dynamics on a general two-dimensional bosonic lattice is developed. In the classical limit of a bosonic condensate, it reduces to conserved plasma-like vortex-antivortex dynamics. The nonlocal topological character of the vorticity flows is reflected in the bulk-edge correspondence dictated by the Stokes theorem. This is exploited to establish physical boundary conditions that realize, in the coarse-grained thermodynamic limit, an effective chemical-potential bias of vorticity. A Kubo formula is derived for the vorticity conductivity—which could be measured in a suggested practical device—in terms of quantum vorticity-flux correlators of the original lattice model. As an illustrative example, we discuss the superfluidity of vorticity, exploiting the particle-vortex duality at a bosonic superfluid-insulator transition.

2.1 Topological Transport of Vorticity in Heisenberg Magnets

2.1.1 Background

Topology and geometry play an important role in modern condensed matter physics [97, 5, 6]. Topological excitations, which are nonlinear order-parameter textures, are interesting physical objects both theoretically and experimentally [98, 99, 100]. Dynamics of these excitations can result in conservation laws that do not result from any symmetries of the system, but rather, derive directly from their topology, rooted in the homotopic properties of the associated fields. A magnetic insulator is a rich platform to study various classes of topological excitations and their (hydro)dynamics. On the practical flip side, we can exploit these excitations to deliver information through charge insulators more effectively than using decaying quasiparticles, such as phonons or magnons [101, 102]. Chiral domain walls in quasi-one-dimensional easy-plane (anti)ferromagnets [55, 56], skyrmions in quasi-two-dimensional magnets [103], and the winding of three-dimensional spin-glass textures [104] have already

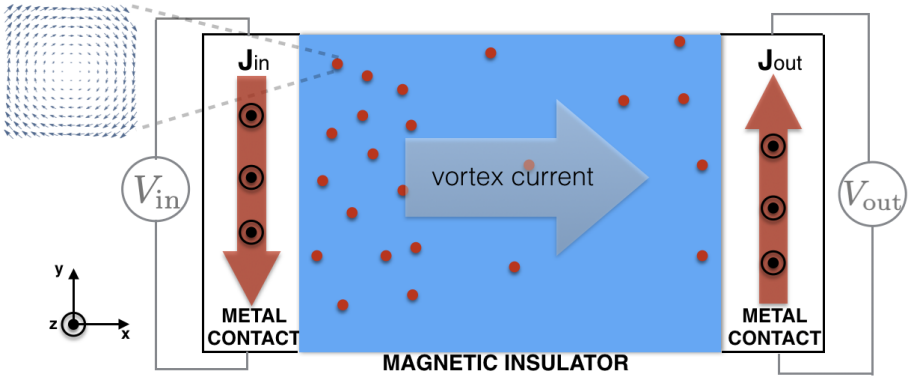

Figure 2.1: A schematic for the proposed injection and detection of vortices. The electric current in the left magnetized contact pumps vortices into the insulating bulk. The applied voltage is $V_{\rm in}$. The vortices leaving the system through the right magnetized contact sustain the output voltage $V_{\rm out}$. The drag coefficient $\mathcal{C}_d \equiv V_{\rm out}/V_{\rm in}$ quantifies the efficiency of the topological vorticity transport.

been investigated extensively, in this context.

Easy-plane magnets support topological excitations referred to as vortices. They are characterized by the U(1) winding number, similar to superconducting vortices, and thus are nonlocal, being immune to arbitrary local perturbations (or "surgeries," in the jargon of topologists). This makes them more robust for long-ranged transport than the previously considered topological defects. In addition, their nonlocal nature engenders the Coulomb-like interaction (logarithmic potential), giving rise to a finite-temperature Kosterlitz-Thouless transition. Also, vortices are promising candidates for information and energy storage [105]. In this section, we will develop the hydrodynamic picture of vortices and realize a superfluid-like transport, based on nonsingular textures in easy-plane magnetic materials.

2.1.2 Main results and discussion

To illustrate our key findings, we focus on the two-terminal geometry of Fig. 2.1. An electric current in the left magnetic metal contact with magnetization $\mathbf{M}$ exerts an adiabatic torque

on the spins of the film at the left boundary. For an appropriate choice of $\mathbf{M}$ (polarized out of the plane), the work done by the torque will energetically bias the vortex injection into the bulk. By regarding these vortices as classical objects, diffusion and nonlocal Coulomb interactions will establish a steady-state distribution of vortex density and its flow. This pumped vorticity will leave the system and induce an electromotive force at the right contact, according to the Onsager-reciprocal process [106]. Using the drag coefficient $\mathcal{C}_d \equiv V_{\rm out}/V_{\rm in}$ to measure the efficiency of this topological transport, we find

$$\mathcal{C}_d = (\pi\eta M)^2 \sigma_c \sigma \mathcal{A}/L\,, \tag{2.1}$$

in the linear-response regime, when $L \to \infty$ (so the magnetic-insulator bulk dominates the impedance for the vorticity flow). σ_c and σ here are the conductivity of electrons in the metal contacts and the effective conductivity of vortices in the insulating bulk, respectively. η is a phenomenological parameter measuring the contact efficiency of the charge-vorticity interconversion. L is the length of the magnetic insulator in the x direction, and $\mathcal{A}$ is the cross section of the metal contacts in the xz plane.

A vortex, being a nonlocal spin texture, shows some beneficial features as compared to chiral domain walls and skyrmions. For instance, the total charge of vorticity is robust to local surgery, such as caused by thermal spin fluctuations. We have the same total vorticity charge even if we arbitrarily deform the spin configuration, as long as the changes are local and not emanating to the boundary. In contrast, local fluctuations could be detrimental to domain-wall chirality [58] and skyrmion number.

At low temperatures, we can generate a vortex lattice in a magnet by utilizing an adiabatic torque on the boundary to control the effective chemical potential associated with the vorticity. This can serve as a platform to explore fundamental physics of emergent solitonic structures, beyond the Abrikosov vortex lattice in superconductors or the skyrmion lattice in chiral magnets. Maintaining skyrmionic crystals out of equilibrium, furthermore, can be more challenging, due to their local character (and the associated finite lifetime,

when they are metastable). Another important aspect is the long-ranged Coulombic interactions between the vortices. We may exploit the associated nonlinear effects to realize semiconductor-inspired transport phenomena like junctions. It is also interesting to explore the natural plasma analogies in the ac response.

2.1.3 Continuity equation and stability

Let us consider a two-dimensional magnetic insulator at low temperatures, such that the coarse-grained local spin-density field $\mathbf{m}(t,x,y) = (m^x, m^y, m^z)$ captures its low-energy dynamics. The vortex density ρ and flux $\mathbf{j}$ constitute the three-current $j^\mu = (\rho, \mathbf{j})$ [107]:

$$j^\mu = \epsilon^{\mu\nu\rho}\epsilon_{zbc}\partial_\nu m^b \partial_\rho m^c/2\pi\,, \tag{2.2}$$

where a, b, c run over three spin-space projections x, y, z and μ, ν, ρ run over three time-space coordinates t, x, y. It is easy to verify that the density defined in Eq. (2.2) is conserved: $\partial_\mu j^\mu = 0$, so long as the vector field $\mathbf{m}(t,x,y)$ is smooth such that $\partial_{\mu\nu}\mathbf{m} = \partial_{\nu\mu}\mathbf{m}$. This is just the continuity equation: $\partial_t\rho + \boldsymbol{\nabla}\cdot\mathbf{j} = 0$.

To see that we can geometrically interpret the current in Eq. (2.2) as a vortex flow, let us integrate the conserved quantity:

$$\mathcal{Q} = \int_\Omega \rho\; dxdy = \frac{1}{2\pi}\int_{\partial\Omega} \mathbf{m}_\parallel^2\, \boldsymbol{\nabla}\phi\cdot d\mathbf{l}\,. \tag{2.3}$$

where we use the Stokes theorem and the fact that ρ is a curl of a vector field. Here, $\mathbf{m}_\parallel \equiv (m_x, m_y)$ is the planar projection of the vector field, ϕ is its polar angle relative to the x axis, and Ω, $\partial\Omega$ denote the bulk and boundary regions. To ensure that ϕ is well defined, we should require $m_\parallel \neq 0$. In the case of an easy-plane anisotropy, $m_\parallel = 1$ on the boundary away from the vortex core (normalizing the vector field so that $\mathbf{m} \to 1$ away from strong textures). Since the polar angle ϕ changes by $2\pi\mathcal{Q}$ in one complete anticlockwise passage around the core, we indeed see that Eq. (2.2) ia a proper expression for the vortex density and current. $\mathcal{Q}$ is simply a S^1 winding number.

In the easy-plane limit, the topological robustness is rooted in the map $\mathbf{m} : S^1 \to S^1$, which can be classified by the fundamental group [27] $\pi_1(S^1) = \mathbb{Z}$. The base manifold is $\partial\Omega \simeq S^1$ and $\mathbf{m}_\parallel$ serves as the XY order parameter (hence S^1 target manifold, in the easy-plane case). We can thus see that magnetic textures with different $\mathcal{Q}$ are not smoothly connected to each other, and the total charge, which is completely determined by the boundary configuration, is robust to local surgery. Physically, a vortex is stable because it is a nonlocal object, which must be moved across the entire system (or towards an antivortex) in order to be eliminated. According to Eq. (2.2), these topological properties extend to general three-component vector field in two spatial dimensions, even in the absence of quantized vortices.

2.1.4 Vortex charge pumping

We illustrate the injection of vorticity in Fig. 2.1, where the linear electric current density (per unit thickness) $\mathbf{J}_{\text{in}} = -J_{\text{in}}\hat{\mathbf{y}}$ in the left contact exerts the local (adiabatic) torque (per unit area in the yz plane) of the form

$$\boldsymbol{\tau} = \eta \mathbf{M} \cdot \mathbf{m} (\mathbf{J}_{\text{in}} \cdot \nabla) \mathbf{m} \,. \tag{2.4}$$

$\mathbf{M} = M\hat{\mathbf{z}}$ here is the (uniform) out-of-plane magnetization of the metallic contact, η is a phenomenological parameter quantifying the strength of the torque, and $\mathbf{m}$ stands for the (3D) magnetization unit vector along the interface. The work done by this torque on the magnetic texture dynamics is then proportional to the vorticity inflow:

$$W = \int dt dy dz \, \boldsymbol{\tau} \cdot (\mathbf{m} \times \partial_t \mathbf{m}) = \pi \eta M I_{\text{in}} \mathcal{Q} \,, \tag{2.5}$$

where $I_{\text{in}} = J_{\text{in}} l$ with l being the thickness of the system in the z direction and we use the fact $\partial_y \mathbf{m} \times \partial_t \mathbf{m}$ is parallel to $\mathbf{m}$ above. Importantly, the torque discriminates between the topological charges $\mathcal{Q}$ of opposite sign. We denote the work for $\mathcal{Q} = 1$ as $W^+ \equiv \pi \eta M I_{\text{in}}$. Note that this work is invariant under the xz-plane reflection, which leaves the vortex charge unchanged [see Fig. 2.2(a)].

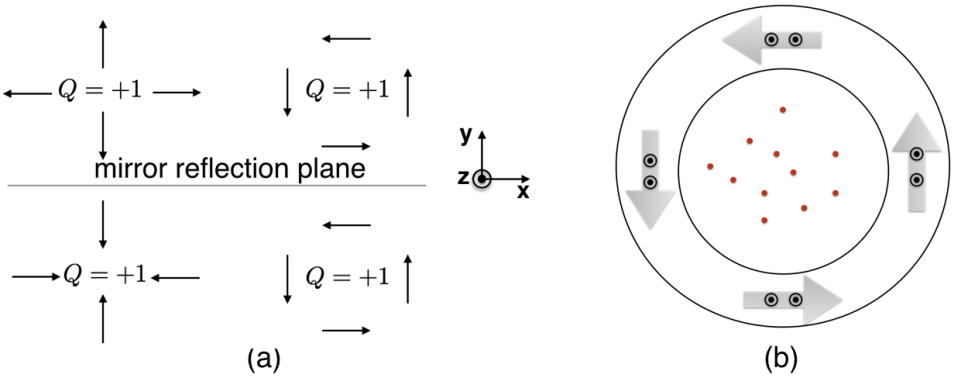

Figure 2.2: Structural symmetries of the vortices and the applied torque setup: (a) Vortex charge $\mathcal{Q}$ is invariant under the xz reflection. (b) A nonequilibrium vortex density can be controlled by the electric current circulating around the magnetic region. Red points represent vortex cores. Arrows represent electric current $\mathbf{I} = I\hat{\mathbf{t}}$, where the unit vector $\hat{\mathbf{t}}$ curls anticlockwise in the metal contact that is magnetized out of the xy plane.

At low temperatures, we can generate a vortex lattice in a magnet by utilizing the torque derived above as follows. In this part, we assume the geometry of the sample is circular [see Fig. 2.2(b)]. For easy-xy-plane magnets, now in two spatial dimensions, the energy is given by

$$\begin{aligned} U =& \frac{1}{2}\int_{\Omega} dxdy \left[A(\boldsymbol{\nabla}\mathbf{m})^2 + Km_z^2\right] \\ & - \frac{1}{2}\int_{\partial\Omega} dl\, \eta M\, \hat{\mathbf{z}} \cdot \left[\mathbf{m} \times (\mathbf{I}\cdot\boldsymbol{\nabla})\mathbf{m}\right], \end{aligned} \tag{2.6}$$

where the first term is the bulk energy composed of the exchange energy $\propto A$ and the anisotropy energy $\propto K$, both positive. The second term is the interface energy (integrated over the boundary of the magnet), due to the torque, which is proportional to the net topological charge within the magnet. The current is assumed to flow around the magnetic insulator, tangentially to the boundary: $\mathbf{I} = I\hat{\mathbf{t}}$, with $\hat{\mathbf{t}}$ [see Fig. 2.2(b)] defined as the anticlockwise unit vector. If the magnetization lies in the xy plane, in a large K approximation,

the energy can be written in terms of the azimuthal angle ϕ:

$$U = \frac{A}{2}\int_\Omega dxdy\,(\boldsymbol{\nabla}\phi)^2 - \frac{\eta MI}{2}\oint_{\partial\Omega} d\mathbf{l}\cdot\boldsymbol{\nabla}\phi\,. \tag{2.7}$$

The second term is quantized as $-\pi\eta MI\mathcal{Q}$ where $\mathcal{Q}$ is the total topological charge. We can minimize the energy

$$U(\mathcal{Q}) = \pi A\mathcal{Q}^2/4 - 2\pi\eta MI\mathcal{Q} \tag{2.8}$$

with respect to $\mathcal{Q}$, by considering a configuration $\boldsymbol{\nabla}\phi = \frac{\mathcal{Q}}{R^2}\hat{\mathbf{z}}\times\mathbf{r}$ (corresponding to a uniform distribution of vortices), where R is the radius of the sample. The first term $\propto \mathcal{Q}^2$ is the Coulomb interaction energy (which depends on the detailed vortices' distribution) and the second, linear term is the torque-induced energy (which controls the effective "chemical potential" of the vorticity). The equilibrium winding number for a given current I is thus found to be $\mathcal{Q}\sim\eta MI/A$. For a fixed $\mathcal{Q}$, the vortices could be expected to form a triangular lattice when R is sufficiently small (depending on the vortex core size $a = \sqrt{A/K}$), in analogy to the Wigner crystal [108]. In the opposite regime, as there is no neutralizing background of opposite charge, the vortices should pile up on the edge, which would modify the above electrostatic consideration.

At finite temperatures, similarly to superfluid films, we expect also a Kosterlitz-Thouless transition, with the critical temperature of $T_{\rm KT}\sim A/k_B$. When $T > T_{\rm KT}$, vortex entropy wins over their energetic cost, resulting in the proliferation of vortex pairs. We do not expect the torque-controlled vortex chemical potential to affect the Kosterlitz-Thouless transition in the thermodynamic limit, due to the long-range repulsion of vortices that prevents an extensive build-up of vorticity.

2.1.5 Topological spin drag

In this section, we assume the geometry of the sample is a strip [See Fig. 2.1]. Below the temperature $T_{\rm KT}$, the vortices are bound into neutral pairs, in thermodynamic equilibrium, and the vorticity flow should, therefore, vanish in linear response. Above $T_{\rm KT}$, the free

vortices proliferate, which should result in a finite conductivity σ. We then expect the constitutive relation $j_x = -\sigma\partial_x\mu$, in terms of the effective electrochemical potential $\mu = \mu_c + V$. $\mu_c \propto \rho$ here is the chemical potential determined by the local vortex density ρ and V is the electrostatic potential due to the nonlocal Coulomb interaction. The current in the bulk is thus given by

$$j_x = -\sigma\partial_x\mu = -D\partial_x\rho + \sigma E_x\,, \tag{2.9}$$

where D is diffusion coefficient and $\mathbf{E} = -\boldsymbol{\nabla}V$ is the fictitious electric field determined by $\boldsymbol{\nabla}\cdot\mathbf{E} = 4\pi^2 A\rho(x)$, with the (open) exchange boundary conditions (i.e., $E_y = 0$ at boundaries). The coefficient $4\pi^2 A$ is particular for the logarithmic interaction for vortices. In a steady state, $\partial_x j_x = 0$, we obtain charge distribution $\rho(x) \sim \rho_L e^{-x/\xi} + \rho_R e^{(x-L)/\xi}$ in the bulk, where $\xi \equiv \sqrt{D/4\pi^2 A\sigma}$, when $L \gg \xi$. Vortices accumulate near the two ends on a characteristic lengthscale of ξ. The magnetic bulk thus acts like a parallel-plate capacitor [see Fig. 2.3(a)]. We can estimate the screening length ξ at high temperatures, $T \gg T_{\rm KT}$, by treating the vortex plasma as nearly ideal and collisionless. To this end, we invoke the Einstein relation [109]: $D/\sigma = k_B T/\rho_0$, where ρ_0 is the equilibrium density of the vortices (irrespective of their charge). This gives $\xi = \sqrt{k_B T/4\pi^2\rho_0 A} \sim \sqrt{T/T_{\rm KT}\rho_0}$, which can be interpreted as the Debye-Hückel length of our two-dimensional two-component plasma.

From the reaction-rate theory [110], the vortex inflow at the left boundary is given by

$$\begin{aligned} j_x^L &= \gamma_L^+(T,I) - \gamma_L^-(T,I) \\ &= \gamma_L(T)\left[e^{(W^+-\mu_L)/k_BT} - e^{-(W^+-\mu_L)/k_BT}\right] \\ &\approx 2\gamma_L(T)(W^+-\mu_L)/k_BT\,, \end{aligned} \tag{2.10}$$

in linear response. Here, $\gamma_L^{\pm}(T,I)$ is the nucleation rate of the vortices with $\mathcal{Q} = \pm 1$, in the presence of an applied electric current I [see Fig. 2.3(b)]. $\gamma_L(T) \sim \nu_L(T)e^{-E_0/k_BT}$ can be thought of as the equilibrium injection rate of vortices, in terms of the attempt frequency $\nu_L(T)$ and an effective energy barrier E_0. Similarly, the vortex outflow at the right boundary

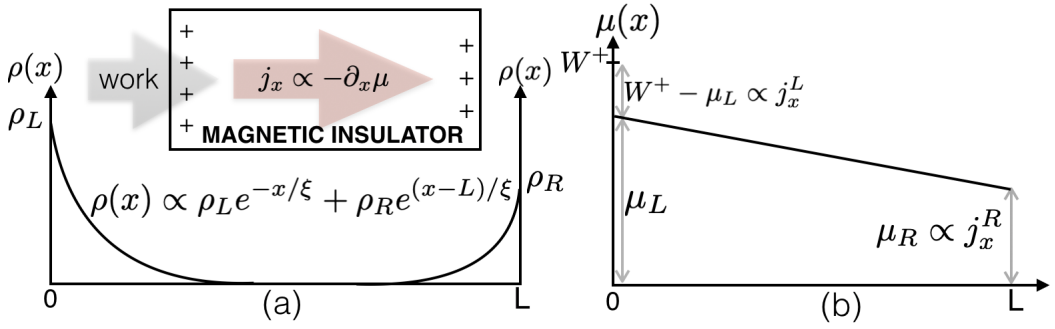

Figure 2.3: (a) Vortex charge density distribution as a function of position x, for a two-dimensional strip extended in the transverse direction. The vorticity accumulates near the two ends with the screening length ξ. The electric-current induced work W^+ (per vortex) at the left end injects vortices into the magnetic bulk. The vortex current is driven by the electrochemical potential μ. (b) Electrochemical potential μ as a function of position x, in linear response. At the left boundary, the vortex inflow is given by $j_x^L \propto W^+ - \mu_L$, while its outflow at the right is $j_x^R \propto \mu_R$. The respective edge electrochemical potentials $\mu_{L,R}$ parametrize the (adiabatic) work required to add an additional vortex there.

is given by

$$j_x^R \approx 2\gamma_R(T)\mu_R/k_BT\,, \tag{2.11}$$

which is driven by the electrochemical potential μ_R that builds up in response to the build up and flow of the vortices from the left contact.

Combining Eqs. (2.9)-(2.11) and imposing $j_x^L = j_x^R = \frac{\sigma}{L}(\mu_L - \mu_R)$, we find for the steady-state current along the x direction:

$$j_x = \frac{W^+}{\frac{L}{\sigma} + \frac{k_BT}{2}\left(\frac{1}{\gamma_L} + \frac{1}{\gamma_R}\right)}\,. \tag{2.12}$$

The dynamics of the order parameter at the right terminal induces an electromotive force [111] $\boldsymbol{\varepsilon} = \pi\eta\mathbf{j}\times\mathbf{M}$, according to the Onsager reciprocal relation [106], where $\mathbf{j}$ is the vorticity outflow normal to the interface and, as before, we are assuming $\mathbf{M} \propto \hat{\mathbf{z}}$. This translates into

the induced normalized voltage

$$\frac{V_{\rm out}}{V_{\rm in}} = \frac{(\pi\eta M)^2\sigma_c\mathcal{A}}{\frac{L}{\sigma}+\frac{k_BT}{2}\left(\frac{1}{\gamma_L}+\frac{1}{\gamma_R}\right)}\,, \tag{2.13}$$

where σ_c is the (Ohmic) conductivity of the metal contacts and $\mathcal{A}$ their cross section in the xz plane. This (negative) drag coefficient between the two metal contacts, which is mediated by the vorticity flow in the magnetic insulator, scales algebraically $\propto L^{-1}$ when $L\to\infty$, which is a generic feature of topological hydrodynamics.

In the limit of narrow metal contacts (in the x direction) and a strong magnetic proximity effect due to the magnetic insulator, we can estimate $\eta M\sim\hbar/e$ (in analogy to the adiabatic torques that were invoked in Ref. [103] for the generation of skyrmion hydrodynamics). Note, however, that for wider contacts, η will scale inversely with their thickness, according to the definition (2.4), so the drag (2.13) will ultimately vanish as $\mathcal{A}^{-1}$. The vorticity hydrodynamics is also expected to get suppressed as the system is scaled up along the z axis. In this limit, as the vortices become larger, $T_{\rm KT}$ increases, the vortex mobility diminishes, while their pinning tendency increases.

2.1.6 Generalization to higher dimensions

Let us consider a σ model with symmetry $\mathrm{O}(n+1)$, denoting the order parameter field by $\mathbf{m}=(m^1,\cdots,m^{n+1})$, in d spatial dimensions. There are two types of topological excitations, in general. The first type is similar to skyrmions, where we collect the infinity at one point, such that the base manifold becomes S^d. The order parameter lives in the coset $\mathrm{O}(n+1)/\mathrm{O}(n)\simeq S^n$ since a vectorial order parameter breaks the symmetry $\mathrm{O}(n+1)$ down to $\mathrm{O}(n)$ when the direction of $\mathbf{m}$ is specified. Topologically-distinct textures are then classified by $\pi_d(S^n)$. When $d=n$, we get skyrmionic textures, according to $\pi_n(S^n)=\mathbb{Z}$. The associated skyrmion current is given by [27]

$$J^\mu=\epsilon^{\mu\nu_1\cdots\nu_n}\epsilon_{a_1\cdots a_{n+1}}m^{a_1}\partial_{\nu_1}m^{a_2}\partial_{\nu_2}m^{a_3}\cdots\partial_{\nu_n}m^{a_{n+1}}\,, \tag{2.14}$$

where we use the Greek letters for space-time indices and the Roman letters for field indices.

Leaving the boundaries free, in the $d = n$ case, however, results in another type of excitation. It is analogous to the two-dimensional vorticity and thus more robust than skyrmions due to its nonlocality. To understand this, let us switch to the boundary of a region in $\mathbb{R}^d$ as the base manifold. We can also effectively reduce the dimensionality of the order-parameter space by introducing a hard-axis anisotropy: This gives $\mathbf{m}_\parallel = (m^1, \cdots, m^d)$. Therefore, the order-parameter manifold is now S^{d-1}. The possible topological textures are classified according to $\pi_{d-1}(S^{d-1}) = \mathbb{Z}$ on the boundary. Such vorticity-type excitations can always be introduced by adding hard axes, as long as $n + 1 \geq d$. To make this physically meaningful, we need $m_\parallel \neq 0$ on the boundary.

Let us now explicitly construct the generalization of vorticity hydrodynamics, for $d = n > 1$, as suggested by $\pi_{d-1}(S^{d-1}) = \mathbb{Z}$. The higher-dimensional vorticity current, which obeys the continuity equation $\partial_\mu j^\mu_a \; \forall a$, is given by

$$j^\mu_a = \epsilon^{\mu\nu_1\cdots\nu_n}\epsilon_{aa_1\cdots a_n}\partial_{\nu_1}m^{a_1}\partial_{\nu_2}m^{a_2}\cdots\partial_{\nu_n}m^{a_n}\,. \tag{2.15}$$

To reproduce our preceding discussion of the two-dimensional vorticity flow, we take $d = n = 2$ and $a = z$. We can, therefore, regard the vorticity density (3.13) as the z component of a vector $\vec{\rho} = (j^0_x, j^0_y, j^0_z)$, which is a conserved *three-dimensional* quantity (corresponding physically to different projections of the order-parameter field). This vectorial vorticity $\vec{\rho}$ is an axial vector, which is invariant under spatial inversion and time reversal. Note the vorticity (2.15) and skyrmion current J^μ are related via $J^\mu = j^\mu_a m_a$, in arbitrary dimensions.

The $d = n = 1$ case is special. The corresponding order-parameter field is two-dimensional: $\mathbf{m} = (m^x, m^y)$. The vorticity density and current are given by

$$j^\mu_a = \epsilon^{\mu\nu}\epsilon_{ab}\partial_\nu m^b\,, \tag{2.16}$$

where μ, ν can be t, x and a, b can be x, y. For example, if we choose $a = x$, then $\rho = \partial_x m^y$

and $j^x = -\partial_t m^y$. Note that the total vorticity charge is bounded:

$$|\mathcal{Q}| = \Big| \int_L^R \partial_x m^y dx \Big| = |m^y(R) - m^y(L)| \leq 2\,, \tag{2.17}$$

which is due to $\pi_0(S^0) = \mathbb{Z}_2$.

2.1.7 Summary and discussion

—It is important to note that we avoid the singular treatment [112] of vortex density by allowing the order parameter to come out of plane in the core. As a result, we have a smooth expression for the vortex density (3.13) in terms of the order-parameter field. This density is a conserved quantity obeying a continuity equation, which can thus exhibit a hydrodynamic behavior. We construct the torque (2.4) that is able to inject vortices and show the vortices can mediate algebraically-decaying transconductances in electrical circuits. In contrast to winding or skyrmions, vortices are "charged" spin textures, which endows them with some beneficial features. For example, vortices are robust against any local perturbation resulted from thermal fluctuation [58], as different topological sectors are distinct globally. Furthermore, vortices provide a possibility to realize *pn* junctions or diodes for spintronic systems, due to their Coulombic interactions, and may offer opportunities for information and energy storage [105]. Another important point is that we do not require the magnitude of the order parameter to be fixed to have a conserved density. This is again in contrast to winding and skyrmions, where the hydrodynamic picture breaks down when there are strong fluctuations in the order-parameter magnitude. In this sense, the vortex transport is more stable than other types of spin and topological flows.

Finally, we remark that our phenomenology of two-dimensional vortex hydrodynamics applies equally well to the antiferromagnetic as well as ferromagnetic films. This is understood from the fact that all the pertinent expressions for the vorticity current, torque, work, etc., are even in the magnetic order parameter $\mathbf{m}$. In a collinear bipartite antiferromagnet, the corresponding contributions from the two sublattices can thus effectively add up,

resulting in the same phenomenology.

2.2 Energy storage in magnetic textures driven by vorticity flow

2.2.1 Background

The centerpiece of the global energy challenge today is a viable method for energy storage, whose key is to convert captured energy into forms that are convenient or economic for long-term storage. Commonly used forms of energy storage are based on chemical energy (lithium-ion batteries), gravitational energy (hydroelectric dam), thermal energy (molten salt), etc. Recent progress in the field of spintronics enables us to manipulate magnetic textures in numerous ways [113, 14, 1], which inspires the possibility of storing energy in the exchange energy associated with topological magnetic textures [105].

Here, we propose a feasible scheme for energy storage in the topological magnetic winding texture of a magnetic insulator. The physical mechanism for charging or discharging is through the control of radial vorticity flows in a Corbino geometry. A "phase slip" in a spin superfluid [57, 58] is known to reduce the phase winding of a one-dimensional system with XY order by 2π, by sending a vortex across it. Vice versa, driving a vortex flow in the opposite direction will naturally build up the winding number, and hence the magnetic exchange energy. Different from Ref. [105], where a locally-induced spin Hall torque is used to produce spin winding of a one-dimensional magnetic loop, the present proposal is based on a quasi-two-dimensional annulus, where a spin-transfer torque is applied over the entire area of the magnetic film, in order to inject an isotropic radial vortex current. This vorticity flow is accomplished at elevated temperatures, where the magnetic system may be disordered with no XY order present, even locally. The topological protection of the induced winding is recovered when, after texturing the magnet by the vortex flow, we cool the system in order to prevent any parasitic phase slips.

Although our structure is limited in terms of energy density compared with the prevalent

lithium-ion battery technology, our approach does have a few advantages. First, magnetic systems are highly nonvolatile and endurable. Magnetic textures protected by nontrivial topological numbers, such as domain walls, vortices, and skyrmions, have already been employed in memory and logic devices [114, 3, 99, 115]. Energy can be stored over an extremely long time scale, with essentially no degradation in charging and discharging cycles. Second, magnetic batteries can be naturally incorporated into spintronic circuits [114, 12, 116, 117], neuromorphic platforms [118, 119, 120, 121], and quantum-information processing tasks based on insulating magnets [122, 23, 123], rendering coherent and low-dissipation operations based purely on spin dynamics. Third, common magnetic materials are environmentally friendly and the development of magnetic batteries is another possible avenue leading to the goal of clean energy.

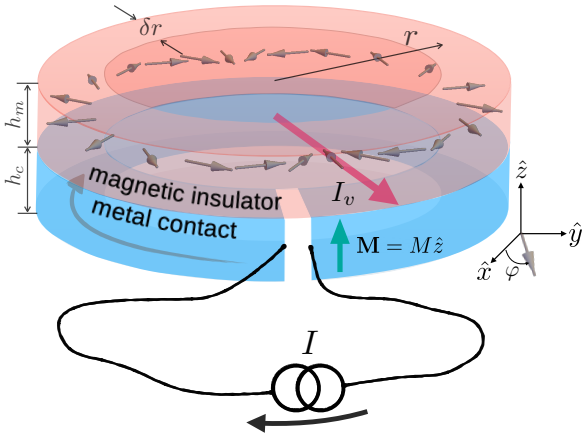

Figure 2.4: The ring-shaped bilayer with a radius r, width δr, and heights h_m for the magnetic insulator and h_c for the metal contact. The order parameter of this magnetic insulator with easy-xy-plane anisotropy is parametrized by the spin space azimuthal angle φ. The (ferromagnetic) metal layer has a uniform magnetization $\mathbf{M} = M\hat{\mathbf{z}}$ and an azimuthal current I. The electric current induces a vortex flow I_v in the radial direction, which builds up an azimuthal winding density $\partial_l \varphi$ of the magnetic order parameter, where $l(= r\theta$ in polar coordinates) is the polar position in the plane of the annulus.

2.2.2 Central concept

To illustrate our concept, we consider the annulus structure depicted in Fig. 2.4. A thin-film easy-plane magnetic insulator is placed on top of a metal contact. The magnetic insulator can be ferro– or antiferromagnetic, with a vectorial order parameter $\mathbf{n}(\mathbf{r}, t)$ which fluctuates in both direction and magnitude. The in-plane texture is described by the spin space azimuthal angle $\varphi(l, t)$, where l is the polar position. The metal annulus has a uniform magnetic order $\mathbf{M} = M\hat{\mathbf{z}}$.

We define the vorticity 3-current in $(2 + 1)$ dimensions within the thin-film magnetic insulator as

$$\mathcal{J}^{\mu} = \epsilon^{\mu\nu\rho}\hat{\mathbf{z}} \cdot (\partial_{\nu}\mathbf{n} \times \partial_{\rho}\mathbf{n})/2\pi, \tag{2.18}$$

which is carried by the magnetic texture [15]. Here $\epsilon^{\mu\nu\rho}$ is the Levi-Civita symbol (with the Einstein summation implied over the Greek indices $\mu = 0, 1, 2 \leftrightarrow t, x, y$). The current obeys a topological conservation law, $\partial_{\mu}\mathcal{J}^{\mu} = 0$. The total vortex number in the bulk Ω,

$$\mathcal{N} = \int_{\Omega} dxdy\ \mathcal{J}^{0} = \frac{1}{2\pi}\int_{\partial\Omega} d\vec{l}\ \mathbf{n}_{\parallel}^{2}\,\vec{\nabla}\varphi, \tag{2.19}$$

by Stokes theorem, is also the total winding number at the boundary $\partial\Omega$. Here $\mathbf{n}_{\parallel}$ is the easy-plane projection of the order parameter $\mathbf{n}$. We remark that this construction is true not only at the low-temperature regime, where $\mathcal{N}$ is integer-valued, but also applicable at high temperatures and the paramagnetic regime (even in the lattice limit [16]), where the vortex number is not quantized.

To load the free energy associated with the magnetic winding texture, we operate the magnetic system near the Curie temperature (paramagnet regime) so that vortices and anti-vortices deconfine to form a two-dimensional, two-component plasma with finite vortex conductivity σ_v [15]. A constant electric current I circulating in the magnetic metal contact (see Fig. 2.4) energetically biases a radial vortex flow I_v [15] based on symmetry analysis. The electric current and vortex current are Magnus cross-coupled as shown in Fig. 2.5(a). We articulate the detailed mechanism in a later section.

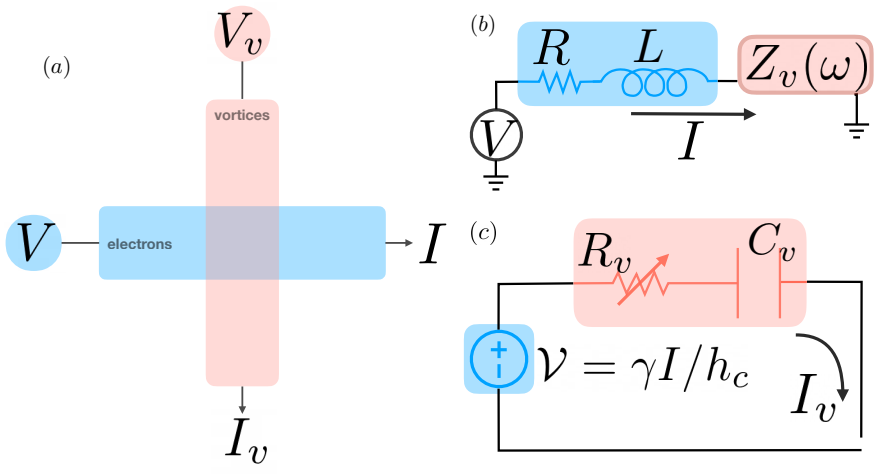

Figure 2.5: (a) Schematic in Fig. 2.4 shows two viscously coupled hydrodynamic entities: one is electron flow I and the other is vortex flow I_v. (b) The electrical circuit, with a current I, resistance R, self-inductance L (due to geometry), and effective impedance $Z_v(\omega)$ arising from the vortex-flow back-action on the electric circuit. (c) Within the vortex circuit, the electric current I acts as a bias $\mathcal{V} = \gamma I/h_c$ for the vortex flow, where γ/h_c parametrizes the Magnus force between the electron and vortex degrees of freedom. Vortex flow through the magnetic bulk experiences resistance R_v which is temperature dependent. The accumulated magnetic texture stores energy according to the capacitance C_v.

Using this externally driven vortex flow, we are able to reverse the typical "phase-slip" process in superfluids [57, 58, 30, 124] and build up a finite order-parameter winding density $\partial_l \varphi$ in the magnetic insulator. The rate of change of the magnetic winding number and the intensity of the vorticity flow are related by the conservation law for the vortex 3-current (2.18):

$$\mathrm{d}\mathcal{N}/\mathrm{d}t = I_v. \tag{2.20}$$

As the winding number accumulates, the magnetic configuration builds up a finite free-energy and exerts a restoring force on the vortex flow, which decays exponentially and eventually vanishes when the restoring force balances the external drive. This type of process is analo-

gous to the experimental proposal by Pearl [125], in which a magnetic screw rotating inside a superconducting cylinder is used to propagate vortices radially in order to increase the azimuthal superflow. In this system, the mechanical energy of the rotating magnetic screw is converted into the energy associated with the increased winding of the order parameter. Similarly, our system converts electrical energy into the exchange energy of the magnetic texture.

Tuning the temperature for our magnetic system well below the Curie temperature T_c keeps the winding texture within plane, due to the easy-plane anisotropy, thus endowing it with topological protection. In this regime, the conductivity of vortices and hence the unwinding process is exponentially suppressed. As a result, the energy associated with the magnetic texture can be stored indefinitely in the absence of an external drive. To release the energy stored in the magnetic winding texture, we can simply raise the temperature near T_c and make use of the natural vortex flow in the "phase-slip" regime. The electromotive force from the vortex flow becomes the output voltage of the magnetic battery.

2.2.3 Main results

As we explain below, the dynamics of the system in Figs. 2.4, 2.5 can be understood by mapping to two coupled circuits, one for electron flow and the other for topological charge (vortex) flow. For the topological charge circuit [see Fig. 2.5(c)], the electric current I in the metal contact plays the role of a bias, which applies the vortex-motive force $\gamma I/h_c$, triggering a vortex current I_v. Here γ/h_c is an interfacial spin-transfer torque parameter to be defined below. The magnetic insulator itself behaves like a vortex capacitor (C_v) and resistor (R_v) in series.

For the electric circuit, a reciprocal electromotive force $\mathcal{E}_{\rm EMF} = \gamma I_v/h_c$ arises from the coupling between electron and vortex dynamics [126, 127], in series with the resistance R and the geometric inductance L of the metal contact. The Onsager reciprocity [106] between

the two circuits can be expressed in the compact form $\mathbf{V} = \hat{\mathcal{R}}\mathbf{I}$,

$$\begin{pmatrix} V \\ V_v \end{pmatrix} = \begin{pmatrix} R + L\frac{\mathrm{d}}{\mathrm{d}t} & \gamma/h_c \\ -\gamma/h_c & R_v \end{pmatrix} \begin{pmatrix} I \\ I_v \end{pmatrix}, \tag{2.21}$$

where V is the electric voltage drop across the metallic contact and $V_v = -\mathcal{Q}/C_v$ is the effective chemical potential associated with the accumulated topological charge $\mathcal{Q} \equiv \mathcal{N}$ [1]. We will see that the electromotive force results in an impedance in the electric circuit, interpolating between a resistance (in the high-frequency response, compared with the characteristic $R_v C_v$ time) and an inductance (at low frequencies). As we discuss below, this inductance can be comparable with the geometrical inductance within the electric circuit, and, therefore, we propose to characterize the vorticity-current interaction through its contribution to the electrical rf inductance.

Lastly, by neglecting the geometric inductance L, we estimate the charging efficiency, defined to be the ratio of the total energy stored to the total energy input, as

$$\eta = \frac{1/2}{RR_v h_c^2/\gamma^2 + 1}, \tag{2.22}$$

from which we see explicitly that the efficiency benefits from a thinner metal contact h_c. The three parameters (R, R_v, and γ/h_c) correspond to three dissipation channels: electrical resistance of the metal, resistance of the vortex current in the magnetic insulator, and their mutual resistance, respectively.

2.2.4 Biased vortex flow

A motive bias for vortex flow is established by a circulating electric current I (see Fig. 2.4) in a magnetically polarized metal contact ($\mathbf{M} = M\hat{\mathbf{z}}$). This current exerts a long-wavelength torque (per unit area) on the magnetic texture [15],

$$\boldsymbol{\tau} = \gamma\, n_z(\vec{j} \cdot \vec{\nabla})\mathbf{n}, \tag{2.23}$$

[1] Note that the resistance matrix $\hat{\mathcal{R}}$ is antisymmetric since the metallic magnetization flips sign under time reversal (when one invokes Onsager reciprocity). One can also easily check the positive-definiteness of the dissipation $\mathbf{I}^T \cdot \mathbf{V} \geq 0$.

where $j = I/h_c\delta r$ is the azimuthal electric current density and n_z is the z component of the magnetic order parameter. $\gamma \equiv \mathrm{sign}(M)\,\pi\hbar h_{\mathrm{eff}}/e$, where the lengthscale h_{eff} can be loosely interpreted as the spatial extent of the torque, as a proximity effect at the interface, within the insulator. The torque does work upon magnetic dynamics at the rate

$$\dot{W} = \int dxdy\ \boldsymbol{\tau} \cdot (\mathbf{n} \times \dot{\mathbf{n}}) = \gamma \int dxdy\ (\vec{\mathcal{J}} \times \vec{j}) \cdot \hat{z}, \tag{2.24}$$

where the integration is performed over the interface. Here, we have taken, for simplicity, the magnitude of the order parameter to be fixed, $\mathbf{n} = 1$. In the high-temperature regime, where $\mathbf{n}$ is fluctuating strongly, a similar result is expected, albeit with a renormalized prefactor. Eq. (2.24) indicates that the coupling between electron and vortex dynamics is Magnus cross-like (see Fig. 2.5(a)). In other words, the electric current tangential to a magnetic interface produces a Magnus force on vortices, resulting in a transverse vortex flow, and vice versa. This underlies the mechanism for building up and relaxing the winding texture in the magnetic insulator.

2.2.5 Mapping onto two coupled circuits

We first consider the vortex dynamics in the magnetic insulator, by exploiting the duality between the XY magnet and electrostatics in two dimensions [128, 129]. In the low-temperature regime (for simplicity) $\mathbf{n}$ is in plane and has a fixed magnitude (though, the results we obtain also generalize to the high-temperature regime where the magnitude of $\mathbf{n}$ is allowed to fluctuate). The duality is accomplished by identifying the total winding of the magnetic order parameter with the electric charge $\mathcal{Q} = \mathcal{N}$, and the spatial gradients of the order-parameter angle with the electric field $\vec{E} = \mathcal{A}\vec{\nabla}\varphi \times \hat{z}$, where $\mathcal{A}$ is the order-parameter stiffness. We can now recast the definition of the winding number (2.19) as Gauss's law for the electric charge $\int d\vec{s} \cdot \vec{E} = \mathcal{Q}/\epsilon$, where $d\vec{s} = d\vec{l} \times \hat{z}$ is the line element in the radial direction and $\epsilon = 1/\mathcal{A}$ is the permittivity (note that making this identification requires the topological charge to be $Q = 2\pi N$, where N is the winding number). Mapping the energy

expression for the insulating magnet to electrostatic notation, gives

$$\mathcal{E} = h_m \frac{\mathcal{A}}{2} \int dxdy \ (\vec{\nabla}\varphi)^2 = h_m \int dxdy \ \frac{\epsilon \vec{E}^2}{2}, \tag{2.25}$$

where h_m is the height of the magnetic insulator.

Therefore, driving topological charges (vortices) from the inner edge to the outer edge can be interpreted as a charging-capacitor process, which is triggered by a charge transfer (that is linked to the winding number) across the annulus. Noting that the power (2.24) can be rewritten as $\dot{W} = \gamma I I_v / h_c$, we can view the metallic contact as a battery with voltage $\mathcal{V} = \gamma I / h_c$ acting on a vortex $R_v C_v$ circuit, as illustrated in Fig. 2.5. The effective capacitance can be extracted by simply equating the energy (2.25) with $\mathcal{E} = \mathcal{Q}^2 / 2C_v$, whereas Ohm's law [130] $\vec{\mathcal{J}} = -\sigma_v \vec{\nabla}\mu$ gives the resistance $R_v = \Delta\mu / I_v$, where $I_v = 2\pi r \mathcal{J}$ is the vortex current and $\Delta\mu$ is the motive force on the vortex flow. Thus, we arrive at the effective vortex capacitance and resistance

$$C_v = \frac{1}{\mathcal{A}} \frac{2\pi r}{h_m \delta r}, \quad R_v = \frac{1}{\sigma_v} \frac{\delta r}{2\pi r}. \tag{2.26}$$

Here σ_v^{-1} is the vortex resistivity whose main contributions arise from vortex collisions (such as umklapp scattering, disorder, etc) and Gilbert damping.

The vortex current acts reciprocally on the electric circuit, as summarized in Eq. (2.21), from which we wish to determine its effective impedance in the electric current. After Fourier transforming and solving for the electric response, we arrive at the total impedance:

$$Z(\omega) \equiv \frac{V(\omega)}{I(\omega)} = R + i\omega L + \frac{i\omega C_v \gamma^2 / h_c^2}{1 + i\omega R_v C_v}, \tag{2.27}$$

where the last term [henceforth denoted $Z_v(\omega)$] is the vorticity impedance, arising from the coupling between electron and vortex dynamics. In the high frequency regime ($\omega \gg 1/\tau$) where $\tau = R_v C_v$ is the time scale of the vortex charging (or discharging) process, one obtains $Z_v(\omega) = \gamma^2 / h_c^2 R_v$, indicating that the magnetic insulator, generating an electromotive force against the input electric current, behaves like a resistor in the electric circuit. In the opposite regime where $\omega \ll 1/\tau$, we have $Z_v(\omega) = i\omega C_v \gamma^2 / h_c^2$, suggesting that the magnetic insulator plays the role of an inductor with $L_v = C_v \gamma^2 / h_c^2$.

2.2.6 Battery efficiency and quantitative estimates

The dc electric current I flowing in the metal contact [Fig. 2.4] eventually results in a steady-state magnetic texture with winding density $\partial_l \varphi = \gamma I/\mathcal{A} h_c h_m \delta r$, and an associated free energy

$$\mathcal{E} = \frac{1}{2} C_v \mathcal{V}^2 = \frac{1}{\mathcal{A}} \frac{\pi r}{h_m \delta r} \Big(\frac{\gamma I}{h_c}\Big)^2, \tag{2.28}$$

at time $t \gg \tau = R_v C_v = 1/\mathcal{A}\sigma_v h_m$. Here, the vortex conductivity $\sigma_v = \rho_v \mu = \rho_v D/k_B T$ depends on the temperature through the free-vortex density ρ_v and vortex mobility μ (via the Einstein relation). In the extreme limit $T \ll T_c$, where $\rho_v \sim 0$, we have zero vortex conductivity leading to $\tau \to \infty$. In the opposite regime (above the Curie temperature $T_c \sim J/k_B$), the order parameter varies on the atomic scale, $\rho_v \sim 1/a^2$ and $D \sim Ja^2/\hbar$, giving the lower bound of the charging time $\tau \sim \hbar/J$. Thus, the vortex conductivity σ_v and τ are highly tunable by temperature.

To estimate the efficiency η of the charging process, we neglect the geometrical inductance of the metal contact and allow the device to charge for a time τ. The charging will be accomplished by using a single square-wave pulse of current I. The total external energy input during the charging process is

$$\mathcal{W} = \int_0^\tau dt\ I\, V(t) = I^2 R\tau + \tau \frac{\mathcal{V}^2}{R_v}(1 - e^{-1}), \tag{2.29}$$

where $V(t)$ is the electric voltage drop across the metal contact that can be obtained by solving Eq. (2.21). These terms take into account the energy loss due to Joule heating and vortex motion as well as the stored energy within the magnetic texture. The numerical factor of the second term is of order unity, replacing this factor with one leads to the efficiency defined in Eq. (2.22) of the charging-process. Considering the regime where $\tau \sim \hbar/J$, we have $\frac{R R_v h_c^2}{\gamma^2} \sim \frac{h_m h_c}{h_{\rm eff}^2} \frac{1/k_F^2}{a\, d}$, where d and k_F are the mean free path and Fermi wave number of electrons within the metal, respectively. It is clear that the efficiency benefits from improving the conducting quality of the metal and decreasing thicknesses of both insulating magnet and metallic contact, which makes sense intuitively. When taking the geometrical inductance L

into account we can improve the efficiency further. In the limiting case of $L \to \infty$, where the charging process is adiabatic, the efficiency can, in principle, approach 1.

The maximal energy-storage capacity, another quantity of interest, is dictated by the Landau criterion for energetic stability [55], where the magnetic texture is maximally wound. It is achieved when the winding texture energy [$\sim \mathcal{A}(\partial_l \varphi)^2$] is comparable to the easy-plane anisotropy energy ($\sim \mathcal{K}$) that fixes the winding within the easy-plane. Let us take the bulk stiffness to be $\mathcal{A} = 5 \times 10^{-12}$ J/m, an easy-plane anisotropy strength of $\mathcal{K} = 5 \times 10^5$ J/m^3, and mass density 5.11 g/cm^3 (yttrium iron garnet), which yields for the winding density $1/\partial_l \varphi = \sqrt{\mathcal{A}/\mathcal{K}} \sim 3\,\text{nm}$ and a specific energy density of 0.1 J/g. Such an energy can be loaded by applying an electric current density of 10^{12}A/m^2 within a thin metal contact, which is feasible experimentally [99]. We can further increase the specific energy density by enhancing the easy-plane anisotropy. For example, in the extreme limit where the order parameter can vary on the atomic scale, $1/\partial_l \varphi \sim a$, we have the specific energy density 10^4 J/kg, which is about an order of magnitude below the capacity of lithium-ion batteries.

To characterize the vorticity-current interaction, which underlies the mechanism of our proposal, we suggest measuring its contribution to the electric inductance in the rf response. To this end, we note that L_v can be manufactured to be comparable with the geometrical inductance L: $\frac{L_v}{L} \sim \frac{1}{\alpha^2} \frac{e^2/a}{J} \frac{a^2}{h_m \delta r} \sim 1$, where α is the fine structure constant and we have used $\delta r h_m \sim 100\,\text{nm}^2$. Alternatively, one can measure the (transient) vortex discharging process, where the electric voltage of the metal is $V(t) = V_{\max} e^{-t/\tau}$, by solving Eq. (2.21) with an open electric circuit. For a thin contact ($h_c \sim h_{\text{eff}}$), one obtains that $V_{\max}\tau \sim \frac{\hbar}{e} \frac{r}{\sqrt{\mathcal{A}/\mathcal{K}}}$. Assuming $r \sim 1$ μm and $\tau \sim$ 10 ns which should be easily accessed experimentally, we get a measurable voltage drop of $V_{\max} \sim 10^{-4}$ V.

2.2.7 Summary and outlook

We have proposed an experimentally feasible energy storage concept in insulating magnets based on the collective transport of vortices, emerging out of the topologically nontrivial real-

space order-parameter textures. This allows to utilize the current-magnet interaction with a focus on the dynamics of topological textures rather than the conventional spin currents. The energy associated with the winding texture can be loaded by electric means which biases vortex flow within the magnet [15, 16]. The system is mapped onto two coupled circuits, where we interpret the energy-loading process as a capacitor-charging action. This energy storage is attractive due its potential longevity [131, 132], endowed by the topological nature of vorticity, and its compatibility with integrated spintronic circuits [114, 12, 116, 117] and quantum-information processes based on insulating magnets [122, 23, 123].

Note that the heating/cooling in the vicinity of T_c (which may be a natural consequence of the Joule heating by the applied current) is invoked in our proposal only to change the vorticity transport parameters, which effectively undergo a transition between diffusive (above T_c) and insulating (below T_c) behaviors. The associated dissipation of energy (by Joule heating) is accounted for in our analysis and would not be of much concern otherwise if the vortex conductivity changes significantly over a small temperature range. Other ways to modulate the impedance of vorticity may in principle be developed in the future.

One could envision a variety of generalizations of our proposal by exploiting different topological hydrodynamics. An immediate example is the magnetic hedgehog in three dimensions. When a hedgehog passes through a chiral magnet [133], a finite skyrmion density is built up which is associated with finite energy and can be devised to store energy. The resultant skyrmion density is protected by Dzyaloshinskii-Moriya interaction which plays a role of easy-plane anisotropy for winding texture. We remark that this is the generic property of n-dimensional nonlocal topological defects, which would establish $(n-1)$-dimensional nonlinear textures when they flow through a medium, dictated by the generalized Stokes' theorem. Other types of topologically conserved local defects, such as skyrmions in two-dimensional magnetic films [103] and three-dimensional skyrmionic textures in frustrated magnets [134], can also be quite valuable potentially for energy-storage purposes. These systems provide ample opportunities to explore energy storage concepts based on spin degrees

of freedom and deserve further investigation.

2.3 Quantum hydrodynamics of vorticity

2.3.1 Background

It is now well appreciated that electrically insulating materials may exhibit a wealth of neutral transport phenomena. The underlying conserved quantities may emerge out of certain symmetries associated with the microscopic spin [9, 113] or pseudospin (e.g., valley [135]) degrees of freedom or, alternatively, topology of the collective dynamics [14]. The former scenario, which has been most thoroughly exploited in the field of spintronics [9, 113], concerns the spin angular momentum along a high symmetry axis of the pertinent heterostructure. As the full axial symmetry is inevitably broken in spin space, at some level, the resultant spin hydrodynamics is always approximate, being useful only on some finite time and/or length scales. The topological hydrodynamics, on the other hand, is potentially more robust, as it is rooted in the topological structure of the dynamical variables rather than any specific structural symmetries [14]. At the heart of this are conservation laws constructed out of a topological invariant of the dynamical field configurations, such as the winding number of a one dimensional XY model [56, 17] or a superfluid [124] or the skyrmion number of a two-dimensional Heisenberg model [103]. These topological invariants are endowed by the homotopic properties of the smooth field configurations of the bulk, following, for example, the $\pi_n(S^n) = \mathbb{Z}$ group-theoretic structure of the n-th homotopy on d-sphere, when $n = d$ [27]. The integer on the right-hand side here counts the conserved topological "charge" that can be associated with the dynamical fields. Being conserved in the bulk, this effective charge can, nonetheless, flow in and out of the medium through its boundaries, which hints at a possibility of its control: The (nonequilibrium) boundary conditions could be devised to bias injection of the topological charge of certain sign and, reciprocally, detect its outflow elsewhere [14]. This points to a conceptual possibility of assigning a bulk conductivity to

the topological charge fluctuations in the material, which could potentially extend many of the useful and intuitive notions associated with the charge conductivity to broad classes of insulating materials. Both device possibilities and novel transport probes of fundamental material properties could then be expected to arise hand in hand. The outlook may, however, be hindered by one key approximation underlying such hydrodynamic constructions: The overarching topological invariant is a property of a low-energy sector of the theory, with pathological excursions between different topological sectors possible in principle. In the case of the winding dynamics, such excursions are known as phase slips, which are central to understanding low-dimensional superfluidity and superconductivity [124]. Skyrmions, likewise, can be created and annihilated by local fluctuations [136, 137]. Such detrimental phase-slip-like events, which ultimately relax any topological configuration towards the global equilibrium, can originate either at the atomistic level, where the coarse-grained treatment of the smooth field theory breaks down, or more macroscopically, where the dynamical variables deviate significantly from their presumed low-energy manifold. Even when such processes are rare, in the limit when they are exponentially suppressed by a large energy barrier, their existence poses a technical challenge in formulating a transport theory. After all, there is no strict continuity equation for the topological charge at the microscopic quantum level, unless we formally separate and eliminate the phase-slip events. Depending on the exact model, parameters, and ambient temperature, furthermore, there may be a plethora of scenarios for the phase-slip dynamics [124], which could diminish the utility of the topological conservation law. In this section, we formulate a topological hydrodynamics that is based on a robust continuity equation immune to all these issues. Its formal distinguishing feature is in the conserved quantity that is related to the field homotopy defined on the boundary rather than the bulk, which, nevertheless, determines a conserved bulk quantity according to a Stokes theorem [15]. We demonstrate this general idea by the ground-up construction of a quantum vorticity hydrodynamics in 2+1 dimensions, offering links to quantum spintronics [14], particle-vortex dualities in many-body systems [138, 139, 140], and quantum

turbulence [141].

2.3.2 Classical vorticity dynamics

A conventional superfluid condensate can be described by a complex-valued order parameter ϕ. The corresponding scalar field $\phi = \sqrt{n}e^{i\varphi} \in \mathbb{C}$ (where $n \geq 0$ is the condensate density and $\varphi \in \mathbb{R}$ is its phase) residing in $2 + 1$ dimensions, $\phi(\mathbf{r}, t)$, realizes an $\mathbb{R}^2 \to \mathbb{C}$ mapping, at any given time t. These field textures are devoid of point defects, as the fundamental homotopy group of the complex plane is trivial, $\pi_1(\mathbb{C}) = 1$. Such two-dimensional textures are, furthermore, all topologically equivalent, having fixed the boundary profile of ϕ on a simply connected patch of $\mathbb{R}^2$, which is reflected in the fact that $\pi_2(\mathbb{C}) = 1$. Despite this, a smooth vector field defines a topological hydrodynamics [14] governed by the continuity equation $\partial_\mu j^\mu = 0$ (with the Einstein summation implied over the Greek letters: $\mu = 0, 1, 2 \leftrightarrow t, x, y$), where

$$j^\mu = \frac{\epsilon^{\mu\nu\xi}\partial_\nu\phi^*\partial_\xi\phi}{2\pi i}. \tag{2.30}$$

Here, $\epsilon^{\mu\nu\xi}$ is the Levi-Civita symbol. For a rigid texture sliding at a velocity $\mathbf{v}$, $\mathbf{j} = \rho\mathbf{v}$, where $\rho \equiv j^0$ and $\mathbf{j} = (j^x, j^y)$. For a sharp vortex in an ordered medium with the free energy minimized by a finite n, $\rho \approx n\delta(\mathbf{r} = \mathbf{r}_0)$, where $\mathbf{r}_0$ is the vortex-core position where n vanishes. Fixing a finite magnitude of the scalar field, the homotopy group would in this case become $\pi_1(S^1) = \mathbb{Z}$, counting essentially the number of vortices in the system. The conserved quantity can be recast as a fictitious flux ($\mathbf{z}$ is the z axis unit vector):

$$\rho = \frac{\mathbf{z}\cdot\nabla\phi^*\times\nabla\phi}{2\pi i} = \frac{\mathbf{z}\cdot\nabla\times\mathbf{A}}{2\pi}, \tag{2.31}$$

associated with the gauge field

$$A = -i\phi^*\nabla\phi. \tag{2.32}$$

Applying Green's theorem, we then see that the conserved topological charge within a patch $\mathcal{S}$,

$$Q \equiv \int_{\mathcal{S}} d^2r\ \rho = \oint_{\partial\mathcal{S}} \frac{d\mathbf{r}\cdot\mathbf{A}}{2\pi} = \oint_{\partial\mathcal{S}} \frac{d\varphi}{2\pi}n, \tag{2.33}$$

is associated with the phase winding around its boundary $\partial\mathcal{S}$. This reveals the geometrical meaning of the conservation law: The charge Q in the bulk can change only in response to a vorticity flow through the boundary.

As an alternative to Eq. (2.30), it might be tempting to write the current density associated with field dynamics as

$$\mathbf{j} = \frac{\mathbf{z} \times \partial_t \mathbf{A}}{2\pi}, \tag{2.34}$$

from which $\partial_t \rho + \nabla \cdot \mathbf{j} = 0$ immediately follows. This current, however, differs from the more physical definition (2.30) by a nonlocal (divergenceless) shift, which would spoil our energetic and Kubo considerations below.

Note that a similar conservation law, with the current (2.34), applies to any other density ρ that can be written as Eq. (2.31) in terms of some field $\mathbf{A}(\phi)$. Our choice of Eq. (2.32) for this field merely results in the physical interpretation of the conservation law in terms of the vorticity (2.33) dynamics. This is particularly relevant for ordered condensates, where the vortices become quantized in terms of the elementary charges $Q = \pm 1$, interacting via a two-dimensional (longrange) electrostatic coupling.

Let us consider some other simple examples of conserved hydrodynamics associated with different choices for the field $\mathbf{A}(\phi)$, which defines the topological charge (2.31). First, we note that there is a gauge freedom in defining $\mathbf{A} : \mathbf{A} \to \mathbf{A} + \nabla f(\phi)$, in terms of an arbitrary function $f(\phi)$, which leaves ρ unchanged. This is why the first-order (derivative) fields like $\mathbf{A} = \nabla n$ are physically inconsequential. Indeed, the corresponding conserved quantity $Q = \oint dn = 0$, for a smooth field $\phi(\mathbf{r})$. Perhaps the simplest nontrivial example is given by $\mathbf{A} = 2pi(\mathrm{Re}\{\phi\}, \mathrm{Im}\{\phi\})$, which results in $Q = \oint d\mathbf{r} \cdot \mathbf{A}/2\pi$. The largest possible charge Q within a given simply connected region (of radius $\sim R$), for a fixed n, corresponds to placing a single vortex in the interior, which gives $Q/\sqrt{n} \to 2\pi R$, the circumference of the region. The corresponding density $\rho/\sqrt{n} \sim 2/R$ vanishes in the thermodynamic limit of $R \to \infty$. We, therefore, conclude that the vorticity density generated by the gauge field (2.32) gives the simplest topological charge that can result in a physically meaningful

extensive hydrodynamics.

2.3.3 Quantum vorticity dynamics

To construct a simple quantum theory, which reproduces the above classical hydrodynamics of vorticity in the limit of $\hbar \to 0$, let us consider a square lattice model sketched in Fig. 2.6. We label each vertex of the lattice by two integer indices: $\imath$ (along the x axis) and $\jmath$ (along the y axis). The same indices are used to label the square plaquettes, according to their lower left corner, as well as the vertical links going upward and the horizontal links to the right of the site $\imath\jmath$. Each site contains a bosonic field Φ obeying the standard commutation algebra $[\Phi, \Phi^\dagger] = 1$ (different sites commute).

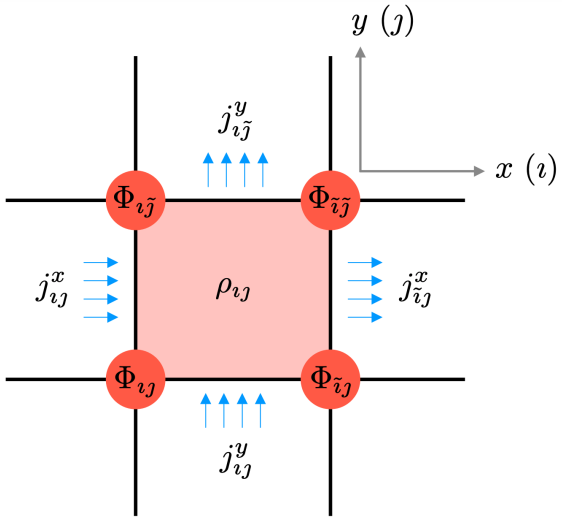

Figure 2.6: A quantum bosonic lattice described by an arbitrary Hamiltonian H. $\Phi_{\imath\jmath}$ is the bosonic field operator at site $\imath, \jmath$, with index $\imath, \jmath$ running along the x, y axis. $\tilde{\imath} = \imath + 1$ and $\tilde{\jmath} = \jmath + 1$. $\rho_{\imath\jmath}$ is the conserved topological charge per plaquette $\imath\jmath$, $j^x_{\imath\jmath}(j^y_{\imath\jmath})$ is the flux per vertical (horizontal) link $\imath\jmath$, which togehter satisfay the quantum continuity equation.

We associate a charge density

$$\rho_{\imath\jmath} \equiv \frac{A^x_{\imath\jmath} - A^x_{\imath\tilde{\jmath}} + A^y_{\jmath} - A^y_{\imath\jmath}}{2\pi a}, \tag{2.35}$$

to each plaquette, where a is the lattice spacing. Here $\tilde{\imath} = \imath + 1$ and $\tilde{\jmath} = \jmath + 1$, and

$$A^x_{\imath\jmath} = \frac{\Phi^\dagger_{\imath\jmath}\Phi_{\tilde{\imath}\jmath}}{2\pi i} + \text{H.c.}, \qquad A^y_{\imath\jmath} = \frac{\Phi^\dagger_{\imath\jmath}\Phi_{\imath\tilde{\jmath}}}{2\pi i} + \text{H.c.}, \tag{2.36}$$

which we assign formally to the corresponding horizontal and vertical sides of the plaquette, respectively. These definitions mimic Eqs. (2.31) and (2.32), respectively, and should reproduce them by coarse graining the field configurations in the classical limit.

According to these conventions,

$$\rho_{\imath\jmath} = \frac{(\Phi^\dagger_{\tilde{\imath}\jmath} - \Phi^\dagger_{\imath\tilde{\jmath}})(\Phi_{\tilde{\imath}\tilde{\jmath}} - \Phi_{\imath\jmath})}{4\pi a^2 i} + \text{H.c.}. \tag{2.37}$$

We also see, from Eq. (2.35), that

$$Q = \sum_{\imath\jmath} \rho_{\imath\jmath}, \tag{2.38}$$

vanishes in the bulk and reduces to the boundary terms, which we can interpret as the quantum version of the net vorticity (2.33). This suggests a conservation law with the boundary fluxes corresponding to the vorticity flow. Indeed, according to the Heisenberg equation of motion (for Hamiltonian H),

$$\partial_t \rho_{\imath\jmath} = \frac{i}{\hbar}[H, \rho_{\imath\jmath}] \tag{2.39}$$

can be seen to satisfy the continuity equation:

$$\partial_t \rho_{\imath\jmath} + \frac{j^x_{\tilde{\imath}\jmath} - j^x_{\imath\jmath} + j^y_{\imath\tilde{\jmath}} - j^y_{\imath\jmath}}{a} = 0. \tag{2.40}$$

Here, the fluxes are obtained by discretizing and quantizing the definition (2.30):

$$j^x_{\imath\jmath} = \frac{(\Phi^\dagger_{\imath\tilde{\jmath}} - \Phi^\dagger_{\imath\jmath})\partial_t(\Phi_{\imath\tilde{\jmath}} + \Phi_{\imath\jmath})}{4\pi a i} + \text{H.c.}, \tag{2.41}$$

and similarly for the other components. The time derivative should always be understood to denote the Heisenberg commutator:

$$\partial_t \mathcal{O} \equiv \frac{i}{\hbar}[H, \mathcal{O}], \tag{2.42}$$

for any (time-independent) operator $\mathcal{O}$. It is useful to emphasize that this conservation law is not rooted in any specific symmetry of the system. Indeed, the form of the Hamiltonian H still remains arbitrary. The continuity is rather dictated by the topology associated with the vorticity (hydro)dynamics in the interior of the system. Specifically, for a fixed field profile on the boundary, an arbitrary smooth field in the bulk yields the same net vorticity, irrespective of the details of the dynamics.

While the definitions (2.36) for the quantum field $\mathbf{A}(\Phi)$ are motivated by the classical limit (2.32), which describes vorticity, any field $\mathbf{A}(\Phi)$ entering Eq. (2.35) would in principle define a conserved dynamics. This is fully analogous to the arbitrary gauge field $\mathbf{A}(\Phi)$ parametrizing classical hydrodynamics associated with Eqs. (2.31) and (2.34), as discussed above. The specific choice (2.36) is motivated by the classical correspondence to a physically meaningful extensive hydrodynamics in bosonic condensates.

Boundary conditions.—The boundary conditions for a nonequilibrium injection of vorticity can be constructed based on energetics and general symmetry principles. In essence, the boundary-induced work can shift the energy barrier for a spontaneous injection of vorticity, in proportion to the applied bias. This bias can be established, for example, by a current applied in a metal contact tangentially to the interface or a driven spin dynamics in an adjacent magnetic insulator. Let us follow the latter scenario, supposing the magnetic order $\mathbf{n}$ in the insulator couples to vorticity dynamics near the interface via a spin-orbit interaction. The relevant coarse-grained work δW associated with a vorticity transfer δQ across the interface then has an adiabatic contribution (at low frequencies) of the form:

$$\delta W = g\mathbf{z} \cdot \mathbf{n} \times \dot{\mathbf{n}} \delta Q. \tag{2.43}$$

g here is a phenomenological interfacial parameter for the coupling, $\mathbf{z}$ is the normal to the (xy) plane of our bosonic film, and $\mathbf{n}$ is taken to be the directional (unitvector) order parameter of a ferromagnetic insulator. For $\mathbf{n}$ steadily precessing around the $\mathbf{z}$ axis, the effective bias

becomes:

$$\mu \equiv \frac{\delta W}{\delta Q} = g\nu\Omega, \tag{2.44}$$

where Ω is the solid angle subtended by $\mathbf{n}$.

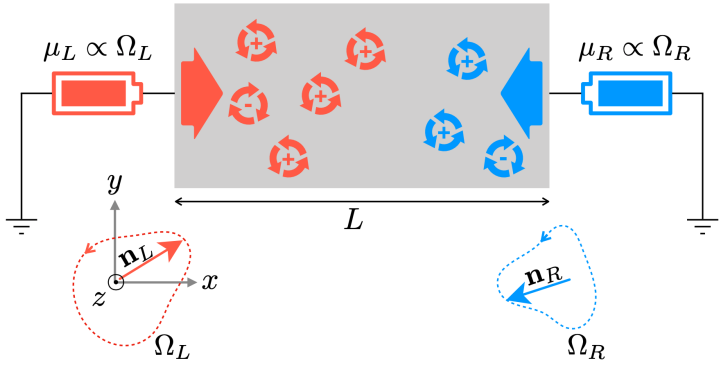

Figure 2.7: Vorticity injection into a bosonic film. Coherently precessing magnetic dynamics $\mathbf{n}_L$ ($\mathbf{n}_R$) at the left (right) side realizes a vorticity reservoir with a conjugate chemical potential μ_L (μ_R). This effectively acts as a battery for the injection of the topological charge Q. A positive chemical potential leads to a build-up of a positive vorticity charge at the interface. If $\mu_L = \mu_R = \mu$ (which could be accomplished by attaching the same magnet symmetrically to both sides), an equilibrium state with the vortex chemical potential μ is established in the steady state, which has a vanishing vortex flux. If $\mu_L \neq \mu_R$, a dc vortex flux (driven by thermal and/or quantum fluctuations) is expected towards the lower chemical-potential side.

This μ can be interpreted as establishing a local chemical potential for the vorticity, supposing that the effective impedance for the vorticity transport is dominated by the bulk region. Physically, Eq. (2.43) describes the interfacial conversion of a pumped spin current (along the $\mathbf{z}$ axis), $\propto \mathbf{z} \cdot \mathbf{n} \times \dot{\mathbf{n}}$ into the vorticity. We have explicitly derived the form of g, for a model of a ferromagnet/superconductor interface, in Ref. [142]. The spin-tovorticity interconversion described by Eq. (2.43), however, can be expected to be general, as the z component of spin and local vorticity transform similarly under the relevant structural (as

well as time-reversal) symmetries.

The natural chemical potential of vorticity in an equilibrium system (i.e., in the absence of magnetic dynamics $\dot{\mathbf{n}}$) is $\mu \to 0$, as the topological charge can freely go in and out of the vacuum. A circuit describing the out-of-equilibrium injection of vorticity into the bosonic medium by magnetic dynamics is sketched in Fig. 2.7. Particularly noteworthy is the case of $\mu_L = \mu_R = \mu$ in the figure, which corresponds to lifting the equilibrium chemical potential for the topological charge by the amount of μ. This geometry is analogous to a rotating superfluid (where the precessing order parameter is replaced by the rotating container) and the frequency glitches in neutronstar pulsars (which have superfluid interiors surrounded by a rotating crust) [143].

Kubo formula.—We are now ready to define the bulk impedance for the topological flow, as an intrinsic property of the bosonic system. Starting with a continuity equation for the coarse-grained quantum dynamics in the bulk, we have

$$\partial_t \rho + \nabla \cdot \mathbf{j} = 0, \tag{2.45}$$

where the conserved density and current are obtained from Eqs. (2.37) and (2.41). We recall that the time derivatives are obtained in the Heisenberg picture. If we perturb the system by a scalar potential $\phi(\mathbf{r}, t)$ that couples to the topological charge, the Hamiltonian becomes

$$H \to H + \int d^2r \; \phi(\mathbf{r}, t)\rho(\mathbf{r}). \tag{2.46}$$

Note that the topological density (2.37) is even under time reversal, while the flux (2.41) is odd, so it vanishes in equilibrium, when $\phi \equiv 0$. For a finite time-dependent potential ϕ, on the other hand, the linear response is given by

$$j_i(\mathbf{r}, t) = \int d^2r' dt' \; \chi_i(\mathbf{r} - \mathbf{r}', t - t')\phi(\mathbf{r}', t'), \tag{2.47}$$

where

$$\chi_i(\mathbf{r} - \mathbf{r}', t - t') \equiv -i\theta(t - t')[j_i(\mathbf{r}, t), \rho(\mathbf{r}', t')], \tag{2.48}$$

according to the Kubo formula (with the equilibrium expectation value implicit on the right-hand side).

To invoke the continuity equation, we differentiate the response function in time:

$$\begin{aligned}\partial_t \chi_i(\mathbf{r}-\mathbf{r}', t-t') &= i\theta(t-t')[j_i(\mathbf{r},t), \partial_{t'}\rho(\mathbf{r}',t')] - i\delta(t-t')[j_i(\mathbf{r},\rho(\mathbf{r}'))] \\ &= -i\theta(t-t')[j_i(\mathbf{r},t), \nabla'\cdot\mathbf{j}(\mathbf{r}',t')] + \delta(t-t')\nabla'\cdot\mathbf{p}_i(\mathbf{r}-\mathbf{r}')\end{aligned}, \tag{2.49}$$

where the auxiliary curl-free function $\mathbf{p}_i$ is formally defined by inverting:

$$\nabla'\cdot\mathbf{p}_i(\mathbf{r}-\mathbf{r}') = -i[j_i(\mathbf{r},\rho(\mathbf{r}'))]. \tag{2.50}$$

We will see that it describes the response that is analogous to the paramagnetic component $\propto i\varrho/m\omega$ of the electrical conductivity (for electrons of mass m and density ϱ). Fourier transforming in time, $\mathbf{j}(\omega) = \int dt e^{i\omega t}\mathbf{j}(t)$ etc., we finally get (summing over repeated indices)

$$j_i(\mathbf{r},\omega) = \frac{i}{\omega}\int d^2r'\ \chi_{ij}(\mathbf{r}-\mathbf{r}',\omega)\varepsilon_j(\mathbf{r}',\omega). \tag{2.51}$$

Here,

$$\chi_{ij}(\mathbf{r}-\mathbf{r}',\omega) \equiv -i\theta(t-t')[j_i(\mathbf{r},t), j_j(\mathbf{r}',t')] + \delta(t-t')p_{ij}(\mathbf{r}-\mathbf{r}') \tag{2.52}$$

is the current-current correlator and

$$\boldsymbol{\varepsilon} \equiv -\nabla\phi \tag{2.53}$$

is the effective electric field. This gives for the conductivity tensor relating $\mathbf{j}(\mathbf{k},\omega)$ to $\boldsymbol{\varepsilon}(\mathbf{k},\omega)$:

$$\sigma_{ij}(\mathbf{k},\omega) = \frac{i}{\omega}\chi_{ij}(\mathbf{k},\omega), \tag{2.54}$$

having also Fourier transformed in real space, $\int d^2r\, e^{-i\mathbf{k}\cdot\mathbf{r}}$.

For the geometry sketched in Fig. 2.7,

$$\varepsilon = g\nu\frac{\Omega_L - \Omega_R}{L}\mathbf{x}, \tag{2.55}$$

supposing that the length of the topological transport channel L is long enough, so that the bulk dominates over the interfacial impedances [14]. We take g and ν to be the same at

the two interfaces. Note that the conductivity should generally depend on the topological chemical potential μ, which can be controlled by the average dynamic bias, $\Omega_L + \Omega_R$ We thus conclude that the sum $\Omega_L + \Omega_R$ effectively gates the bosonic vorticity conduit, while the difference $\Omega_L - \Omega_R$ establishes a topological flux through it. As the conductivity tensor $\hat{\sigma}$ can be exponentially sensitive to μ at low temperatures, this suggests a potential transistor functionality.

Electrical transconductance.—Having established the vorticity response to the magnetic dynamics in the structure like that sketched in Fig. 2.7, we can now consider its nonlocal feedback on the magnetic dynamics. To that end, we invoke the Onsager reciprocity, in order to establish the torque induced by the vorticity flow through the interfaces [142]:

$$\boldsymbol{\tau} = g\mathbf{n} \times \mathbf{z} \times \mathbf{n}j = \theta \mathbf{n} \times \mathbf{z} \times \mathbf{n}, \tag{2.56}$$

where j is the vorticity flux impinging on the magnetic insulator. This is known as the (anti)damping-like torque, which plays an important role in spin-torque-induced magnetic dynamics. In particular, at a critical value of its magnitude θ, the ferromagnet can undergo an instability driving it into coherent self-oscillations. The magnitude of such a torque acting on the right magnet due to a coherent resonant dynamics (at frequency ν) induced in the left magnet is given by

$$\theta = gj = \frac{g^2 \nu \Omega}{L} \sigma_{xx}. \tag{2.57}$$

We recall that g is a phenomenological parameter of the interface, whose existence is dictated by structural symmetries and whose magnitude depends on the details of the interfacial coupling (including corrections due to quantum fluctuations). The longitudinal conductivity σ_{xx} reflects the intrinsic vorticity transport across the bosonic lattice.

In the particle-superfluid limit, when the vorticity is carried by the plasma of solitonic defects with quantized topological charge ± 1 and mobility M, the corresponding conductivity is simply $\sigma_{xx} = 2\rho M$, where ρ is the density of the unbound vortex-antivortex pairs (well above the Kosterlitz-Thouless transition). The associated diffusion coefficient is given by

$D = k_B T M$, according to the Einstein-Smoluchowski relation. For large vortices, the mobility may be limited by the dissipation associated with the normal-fluid component (which is perturbed by the vortex motion). Reference [142] offers some quantitative estimates of the torques induced by vortex motion in high-temperature superconducting films, suggesting its practical relevance.

Superfluidity of vorticity.—Exploiting the particle-vortex duality, we consider a situation when a strong interparticle repulsion prevents the ordinary mass flow. In this case, an insulating state for the particle dynamics may exhibit superfluidity for the topological charge (i.e., vorticity). To this end, we pursue an effective description with the Hamiltonian density:

$$H = \frac{\rho^2}{2\chi} + \frac{\mathcal{A}(\nabla\psi)^2}{2}, \tag{2.58}$$

expressed in terms of the coarse-grained (condensed) vorticity density ρ and its condensate phase ψ. χ is the thermodynamic compressibility of vorticity and $\mathcal{A}$ is the phase stiffness. This form of the Hamiltonian, along with the conjugacy relation $[\psi(\mathbf{r}), \rho(\mathbf{r}')] = i\delta(\mathbf{r} - \mathbf{r}')$, reflects an emergent gauge structure associated with the global conservation of vorticity.

The associated flux can be read out from the Hamilton equation for the density dynamics:

$$\hbar\partial_t\rho = -\partial_\psi H = \mathcal{A}\nabla^2\psi \Rightarrow \mathbf{j} = -\mathcal{A}\nabla\psi/\hbar. \tag{2.59}$$

Phase dynamics is described by the Josephson relation:

$$\hbar\partial_t\psi = \partial_\rho H = \rho/\chi. \tag{2.60}$$

The mean-field current self-correlator can be found as the current response to perturbation $H \to H + \mathbf{s}\cdot\mathbf{j}$, which modifies the equation of motion as:

$$\hbar\partial_t\rho = \mathcal{A}\nabla^2\psi - \mathcal{A}\nabla\cdot\mathbf{s}/\hbar. \tag{2.61}$$

The long-wavelength response thus vanishes, as $\nabla\cdot\mathbf{s} = 0$.

We are therefore left with evaluating the "paramagnetic" contribution, which follows from Eq. (2.50). The associated current-density correlator

$$[\mathbf{j}(\mathbf{r}), \rho(\mathbf{r}')] = -i\mathcal{A}\nabla\delta(\mathbf{r}-\mathbf{r}')/\hbar \tag{2.62}$$

gives

$$p_{ij} = \mathcal{A}\delta(\mathbf{r}-\mathbf{r}')\delta_{ij}/\hbar, \tag{2.63}$$

resulting in the diagonal dynamic (long-wavelength) conductivity

$$\sigma(\omega) = \frac{i\mathcal{A}}{\hbar\omega}. \tag{2.64}$$

Regularizing this result at zero frequency, $\omega \to \omega + i0^+$, we get $\mathrm{Re}\{\sigma\} = (\pi\mathcal{A}/\hbar)\delta(\omega)$. As expected, the static conductivity diverges in the low-frequency limit. In this case, the superfluid bulk has no impedance and the vorticity conductance of the entire structure needs to be determined by carefully considering the interfacial injection physics, which is akin to the Andreev conductance of normal/superconducting interfaces.

2.3.4 Summary and outlook

Motivated by the conceptual attraction of solid-state transport phenomena emerging out of real-space topological invariants [14], we set out to construct a field-theoretic Kubo formalism for evaluating the associated transport coefficients. Two basic issues arise in this regard: (1) The underlying topological invariants typically appear at the level of a coarse-grained classical description that is, furthermore, projected onto a low-energy manifold, in the spirit of the Landau order-parameter formulation; and (2) related to this, there are generally dynamical processes that allow for rapid transitions ("phase slips") between different topological sectors of the theory, which may be driven by classical and/or quantum fluctuations. In this section, we showed that a topological conservation law may also arise at the most microscopic quantum level, without a need for any higher-level Landau-type coarse graining. The conservation law here is distinct from the more conventional examples of the topological hydrodynamics [14], due to the existence of the bulkedge correspondence (such as the bulk vorticity vs

edge winding) rooted in a variant of a Stokes theorem. The nonlocal topological character of the ensuing extensive bulk hydrodynamics engenders a robust continuity equation that is immune to any local fluctuations. Arbitrary global (thermal and quantum) fluctuations, furthermore, are fully accounted for by the topological charge fluxes across the boundaries, which, in turn, offer means for injecting and detecting the bulk hydrodynamics. A general approach for constructing a practical device, in which the transport coefficients associated with this topological hydrodynamics may be measured, can be implemented based on the energetics and thermodynamic reciprocities of the nonequilibrium response. This allows us to formulate a Kubo linear-response approach both for calculating and for measuring the topological charge conductivity. As has been recently illustrated by measuring the electrical transconductance induced by winding dynamics of a hidden magnetic Néel order [144], these ideas may broaden the scope of transport-based investigations of fundamental correlations and ordering in quantum materials. We propose, in particular, to utilize a topological transport probe to test the purported particle-vortex duality of the vortex-superfluid (i.e., particle-insulator) side of the superfluid-insulator quantum phase transition.

CHAPTER 3

Topological transport of deconfined magnetic hedgehogs

"*The people who do make big discoveries are the ones who somehow manage to free themselves from conventional ways of thinking and to see the subject from a new perspective.*"

Anthony James Leggett

In this chapter, we investigate the dynamics of magnetic hedgehogs, which are three-dimensional topological spin textures that exist in common magnets, focusing on their transport properties and connections to spintronics. We show that fictitious magnetic monopoles carried by hedgehog textures obey a topological conservation law, based on which a hydrodynamic theory is developed. We propose a nonlocal transport measurement in the disordered phase, where the conservation of the hedgehog flow results in a nonlocal signal decaying inversely proportional to the distance. The bulk-edge correspondence between hedgehog number and skyrmion number, the fictitious electric charges arising from magnetic dynamics, and the analogy between bound states of hedgehogs in ordered phase and the quark confinement in quantum chromodynamics are also discussed.

3.1 Background

A main theme of spintronics is the utilization of spin degrees of freedom for information transmission and processing [145, 9], either using spin-polarized electric currents, or relying on spins alone to free the transport from Joule heating. Magnons, the quanta of spin wave, have been proposed to be promising data carriers in new computing technologies [10, 24, 12, 116, 25]. A detectable diffusive spin transport can be achieved via magnons in ordered magnetic insulators [146] or even spin-conserving fluctuations in paramagnets [147]. However, such spin currents typically decay exponentially, once the propagation distance exceeds the spin-relaxation length [9]. In alternative transport regimes, where signals are expected to decay algebraically, topology plays a crucial role [14, 7, 1]. Topological spin textures, such as chiral domain walls [56], vortices [148, 149, 15, 16], skyrmions [150, 2, 103], hopfions [45, 46], and hedgehogs [151, 152, 153, 154] are defined homotopically and are topologically protected [14, 7, 1]. Consequently, they are promising to sustain long-distance transport, even in the absence of local spin conservation.

While extensive studies have been devoted to spin textures in low dimensions, three-dimensional (3D) textures such as hedgehogs and hopfions are recently attracting more attention for their rich physics in topological phases [151, 152, 153, 154, 155] and dynamic properties [45, 46, 156, 157]. Hedgehogs exist inherently in 3D Heisenberg magnets. In contrast to 3D skyrmions [134] and hopfions [45, 46], which can be annihilated by shrinking them down to the size of the atomic spacing without affecting spins far away, hedgehogs cannot be removed via local surgeries. The hedgehog flow can therefore be more stable against thermal fluctuations, and has potential applications in memory, logic devices, and energy storage [114, 3, 99, 115, 105, 158].

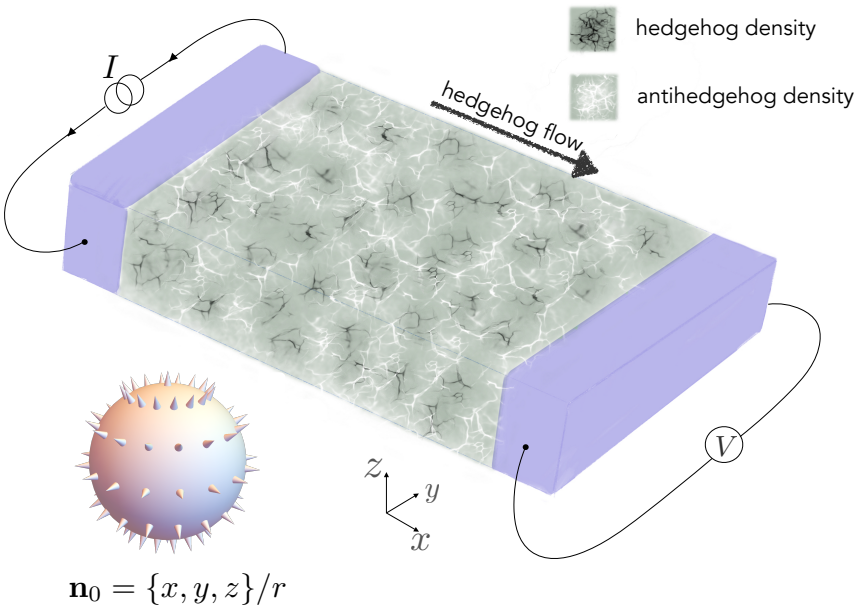

Figure 3.1: A schematic for nonlocal transport measurement of hedgehog currents in a three-dimensional insulating magnet. Two metallic contacts are bridged by a magnetic insulator with hedgehog excitations. In the paramagnetic phase, hedgehogs are free to diffuse, where black and white ripples stand respectively for delocalized hedgehog and antihedgehog densities. An applied electric current I along y within the left metal transfers spin flow into the magnetic texture, which biases a hedgehog flow along x. Reciprocally, the hedgehog flow reaching the right terminal builds up a detectable electric voltage V. The nonlocal drag resistivity, $\varrho \propto V/I$, quantifies the efficiency of the topological hedgehog transport as well as their interfacial exchange coupling with conducting electrons. We also show a familiar example of a hedgehog $\mathbf{n}_0 = \{x, y, z\}/r$.

In this chapter, we explore both topological and energetic properties of magnetic hedgehogs in 3D Heisenberg ferromagnets to investigate their long-distance transport, the viability of which is considered from the following three aspects. A topological conservation law, which is valid in both the magnetically ordered and disordered phase, defines the framework of a hydrodynamic description of hedgehog currents. While (anti)hedgehogs are bound by a lin-

ear potential energy in the magnetically ordered phase, they become deconfined and hence mobile in the paramagnetic phase. We propose a nonlocal transport measurement in the setup as shown in Fig. 3.1. A conserved hedgehog flow can be driven by a transverse electric current applied at an adjacent metal contact, resulting in a nonlocal signal decaying inversely proportional to the system length in the flow direction.

3.2 Topological conservation law

Let us first consider a 3D insulating ferromagnet without accounting for its detailed energetics, but focusing on topological aspects of its vectorial order parameter $\mathbf{n}(\vec{r},t)$, where the bold face is used for axial vectors and the vector arrow marks polar vectors. In the ordered phase, the collinear magnetic order can be described by the directions of $\mathbf{n}$ assuming $|\mathbf{n}|=1$. This would render a sphere order-parameter space S^2, with a nontrivial second homotopy group $\pi_2(S^2)=\mathbb{Z}$ [159]. A point defect, named hedgehog, with an integer-valued topological charge can correspondingly be identified in $\mathbf{n}(\vec{r},t)$. A familiar example for a hedgehog placed at the origin is $\mathbf{n}_0=\{x,y,z\}/|\vec{r}|$.

In the paramagnetic phase, the corresponding (coarse-grained) vector field $\mathbf{n}(\vec{r},t)\in\mathbb{R}^3$ realizes an $\mathbb{R}^3\to\mathbb{R}^3$ mapping at any given time t. This field texture is devoid of defects characterized by the aforementioned quantized charges, since the homotopy group $\pi_2(\mathbb{R}^3)$ is trivial [159]. Nevertheless, the smooth field $\mathbf{n}(\vec{r},t)$ exhibits a topological hydrodynamics governed by the *topological conservation law* $\partial_\mu j^\mu=0$ (with the Einstein summation implied over the Greek indices: $\mu=0,1,2,3\leftrightarrow t,x,y,z$), where

$$j^\mu=\epsilon^{\mu\nu\alpha\beta}\partial_\nu\mathbf{n}\cdot(\partial_\alpha\mathbf{n}\times\partial_\beta\mathbf{n})/8\pi. \tag{3.1}$$

Here, $\epsilon^{\mu\nu\alpha\beta}$ is the Levi-Civita symbol with convention $\epsilon^{0123}=1$. The conserved (topological) charge within a bulk Ω is

$$\mathcal{Q}\equiv\int_\Omega dxdydz\, j^0=\frac{1}{8\pi}\int_{\partial\Omega}dx^j\wedge dx^k\,\mathbf{n}\cdot(\partial_j\mathbf{n}\times\partial_k\mathbf{n}), \tag{3.2}$$

which equals the skyrmion number at boundary $\partial\Omega$, according to the generalized Stokes' theorem [159]. We recognize that charge $\mathcal{Q}$ is precisely the hedgehog number (thus j^μ is the hedgehog current) in the ordered phase, with the last equality in Eq. (3.2) defining the degree of the $S^2 \to S^2$ mapping on the boundary. Our simple example $\mathbf{n}_0$ yields $j^0 \to \delta(\vec{r})$ and thus $\mathcal{Q} = 1$. Here, we remark that the core should be regularized. There is no true singularity in our treatment. In the paramagnetic phase, $\mathcal{Q}$ is no longer quantized due to fluctuations in the magnitude of $\mathbf{n}$. Regardless, the hedgehog current (3.1) is conserved, which sets the stage for the topological hydrodynamics of hedgehogs at an arbitrary temperature. The conservation law also holds in the lattice limit, with proper discretized definitions as we will discuss later. Hereafter, we refer to $j^\mu = (j^0, \mathbf{j})$ as hedgehog density (and flux), irrespective of the temperature.

We stress that, in contrast to two-dimensional skyrmions [150, 2, 103] or three-dimensional Shankar skyrmions [134], which can be created and annihilated locally, the conservation law of hedgehogs is immune to local fluctuations and therefore applicable also in the paramagnetic phase. This robustness of hedgehog flow underpins the hedgehog hydrodynamics. We prove the hedgehog current j^μ is conserved at arbitrary temperatures, which is the underpinning of the hedgehog hydrodynamics. For a general smooth texture $\mathbf{n}$, we can show,

$$\partial_\mu j^\mu = \epsilon^{\mu\nu\alpha\beta}\big[\partial_\mu\partial_\nu\mathbf{n}\cdot(\partial_\alpha\mathbf{n}\times\partial_\beta\mathbf{n}) + \partial_\nu\mathbf{n}\cdot(\partial_\mu\partial_\alpha\mathbf{n}\times\partial_\beta\mathbf{n}) + \partial_\nu\mathbf{n}\cdot(\partial_\alpha\mathbf{n}\times\partial_\mu\partial_\beta\mathbf{n})\big]/8\pi = 0. \quad (3.3)$$

Here, all three terms vanish individually since $\epsilon^{\mu\nu}\partial_\mu\partial_\nu = \epsilon^{\mu\nu}\partial_\nu\partial_\mu = \epsilon^{\nu\mu}\partial_\mu\partial_\nu = -\epsilon^{\mu\nu}\partial_\mu\partial_\nu = 0$, where we change the order of partial derivatives in the first equal sign and we exchange dummy indices μ, ν in the second equal sign. We remark that we did not use the condition $|\mathbf{n}| = 1$, meaning that the conservation of hedgehog currents $\partial_\mu j^\mu = 0$ holds at arbitrary temperatures, irrespective of the magnitude fluctuations of $\mathbf{n}$. This is in contrast to skyrmions and hopfions, whose conservation laws are only true when the magnitude fluctuations of $\mathbf{n}$ are neglectable.

Equation (3.2) establishes a bulk-edge correspondence, indicating that the total hedgehog

number in a bulk interior can fluctuate only by flowing in and out through its boundary. This, in turn, is associated with a corresponding change in the skyrmion number on the boundary, acting as a fingerprint of the hedgehog flow. A close analog in lower dimensions has been thoroughly studied in the context of superfluid phase slips, where the winding number associated with one-dimensional XY textures can be changed by a transverse passage of planar vortices. The 3D bulk-edge correspondence (3.2) manifests when a skyrmion density unwinds or reversely builds up as a thread of a hedgehog current passes through, which has been verified experimentally [133].

3.3 Topological Maxwell equations

We provide, in this section, another formulation of the conservation law as topological Maxwell equations, making connections to the well-known emergent electromagnetic fields associated with generic spin textures [126, 160, 127, 161, 162, 163, 164]. The divergence-free condition $\partial_\mu j^\mu = 0$ can be automatically satisfied by defining the current j^μ as a curl of a rank-2 antisymmetric Maxwell field-strength tensor

$$\mathcal{F}_{\alpha\beta} \equiv \mathbf{n} \cdot (\partial_\alpha \mathbf{n} \times \partial_\beta \mathbf{n})/4\pi, \tag{3.4}$$

whose components are the familiar electromagnetic fields:

$$E^i = \mathbf{n} \cdot (\partial_t \mathbf{n} \times \partial_i \mathbf{n})/4\pi, \quad \epsilon_{ijk} B^k = \mathbf{n} \cdot (\partial_i \mathbf{n} \times \partial_j \mathbf{n})/4\pi. \tag{3.5}$$

The hedgehog current (3.1) can therefore be recast into the form of the Maxwell equations:

$$\epsilon^{\mu\nu\alpha\beta} \partial_\nu \mathcal{F}_{\alpha\beta}/2 = j^\mu, \ \partial_\mu \mathcal{F}^{\mu\nu} = j_e^\nu. \tag{3.6}$$

The second equation defines the electric 4-current, which is also conserved: $\partial_\mu j_e^\mu = 0$, following from the antisymmetric property of $\mathcal{F}$.

Note that fictitious electric and magnetic charges (as sources for $\vec{E}$ and $\mathbf{B}$) have the same symmetries as the real electric and magnetic charges under both time-reversal and parity

operations. The magnetic hedgehog with a quantized topological charge can be identified as a Dirac monopole. In the ordered phase, the quantization can also be understood from the view of the U(1) gauge structure of magnons. For a Heisenberg magnet, one may regard a fixed spin texture $\mathbf{n}(\vec{r})$ to spontaneously break the SU(2) symmetry of the spin algebra. The excitations thus have a smooth part, which can be viewed as describing regular spin waves, and a (singular) topological part, such as hedgehogs in our case. Therefore, the magnetic charges are quantized on a U(1) kernel [32, 126, 161], reminiscent of the 't Hooft and Polyakov approaches to the non-Abelian Higgs model [165]. For the (fictitious) electric sector, both the electric field and the electric charge density emerge solely out of the dynamics of the field configuration. According to the Gauss law, the total electric charge associated with a general local dynamics vanishes.

Electric charge distribution for global dynamics. For a translational motion, $\mathbf{n}(\vec{r},t) = \mathbf{n}_0(x, y, z - vt)$, which describes a hedgehog sliding along the z axis with speed v, the fictitious electric field is

$$\vec{E} = \frac{v(-y, x, 0)}{4\pi r^3}. \tag{3.7}$$

This is precisely the Ampère law for magnetic monopole, while the electric charge density vanishes: $j_e^0 = \nabla \cdot \vec{E} = 0$. For a rotational motion, we take the example of $\mathbf{n}(\vec{r},t) = \mathbf{n}_0[\hat{\mathcal{R}}(\boldsymbol{\omega}t)\vec{r}]$, which describes a hedgehog rotating with angular velocity $\boldsymbol{\omega} = \omega\hat{z}$ (equivalent to precession in spin space), where $\hat{\mathcal{R}}$ is the appropriate rotational matrix. This configuration yields a charge density with finite dipole moment proportional to the angular velocity:

$$j_e^0 = -\frac{3\omega}{4\pi}\frac{z^3}{r^5}. \tag{3.8}$$

The total electric charge remains zero in this example of an isotropic hedgehog configuration, but can be nonzero for a general rotating configuration, where the dynamic relation, $j_e^0 \propto \omega$, remains. Therefore, if there is no overall rotation on thermal average, only the magnetic part j^μ—hedgehog hydrodynamics—survives.

3.4 Conservation law of hedgehogs on a quantum lattice

To construct a simple quantum theory, which reproduces the classical hydrodynamics of hedgehogs in the classical limit of $\hbar \to 0$, let us consider a tetrahedron which is the elementary building block of any lattice (see Fig. 3.2). Each site contains a quantum spin $\mathbf{S} = (S^x, S^y, S^z)$ of magnitude S (in units of $\hbar$), obeying the standard SU(2) spin algebra $[S^a, S^b] = i\epsilon^{abc}S^c$ (spin operators sitting on different sites commute).

We first note that the hedgehog 4-current can be recast as $j^\mu = \epsilon^{\mu\nu\alpha\beta}\partial_\nu \mathcal{F}_{\alpha\beta}/2$ with $\mathcal{F}_{\alpha\beta} = \mathbf{n}\cdot(\partial_\alpha \mathbf{n} \times \partial_\beta \mathbf{n})/4\pi$. Its temporal and spatial components are given by $\rho = \nabla \cdot \mathbf{B}$ and $\mathbf{j} = -\partial_t \mathbf{B} + \nabla \times \mathbf{E}$ respectively, with the emergent magnetic field $B^i = \epsilon^{ijk}\mathbf{n}\cdot(\partial_j \mathbf{n} \times \partial_k \mathbf{n})/8\pi$ and the electric field $E^i = \mathbf{n}\cdot(\partial_t \mathbf{n} \times \partial_i \mathbf{n})/4\pi$. Every triangular facet $\mathbf{A} = A\mathbf{f}$ (A is the area and $\mathbf{f}$ is the normal vector) formed by sites i, j, k (ordered in the right-hand fashion according to $\mathbf{f}$ in Fig. 3.2) can be associated with a skyrmion density and a hedgehog flux:

$$B_{\mathbf{A}} = \frac{c_{ijk}}{8\pi A}, \qquad j_{\mathbf{A}} = -\partial_t B_{\mathbf{A}} + \frac{\gamma_{ijk}}{A}, \tag{3.9}$$

where

$$c_{ijk} \equiv \frac{\mathbf{S}_i \cdot \mathbf{S}_j \times \mathbf{S}_k}{S^3}, \qquad \gamma_{ijk} \equiv \mathbf{E}(\mathbf{r}_{ij})\cdot \mathbf{r}_{ij} + \mathbf{E}(\mathbf{r}_{jk})\cdot \mathbf{r}_{jk} + \mathbf{E}(\mathbf{r}_{ki})\cdot \mathbf{r}_{ki}, \tag{3.10}$$

are the *scalar chirality* and the *circulation* of $\mathbf{E}$ field along the facet. Here $\mathbf{r}_{ij}$ is the vector pointing from site i to j and $\mathbf{E}(\mathbf{r}_{ij})$ is the electric field on this link. By discretizing the electric field, we have

$$\mathbf{E}(\mathbf{r}_{ij})\cdot \mathbf{r}_{ij} = \frac{\mathbf{S}_i \cdot \partial_t(\mathbf{S}_i + \mathbf{S}_j) \times \mathbf{S}_j}{16\pi S^3} + \text{H.c.}, \tag{3.11}$$

where the time derivative should be understood to denote the Heisenberg commutator (for Hamiltonian H and an arbitrary time-independent operator $\mathcal{O}$)

$$\partial_t \mathcal{O} \equiv \frac{i}{\hbar}[H, \mathcal{O}]. \tag{3.12}$$

We remark that the time derivative of spin does not commute with the bare spin operator, even on different sites, in general.

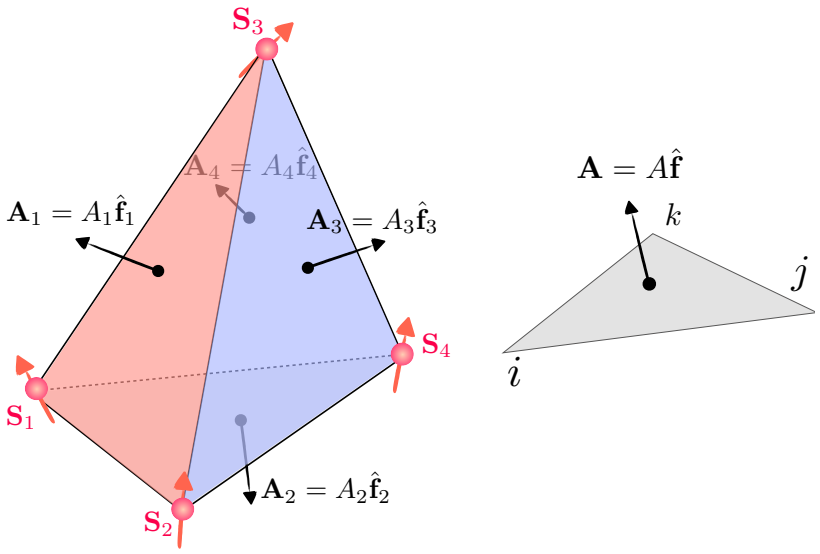

Figure 3.2: A tetrahedron severing as the elementary building block of an arbitrary lattice. $\mathbf{S}_i$ is the spin operator at site i. A skyrmion number and a hedgehog flux (3.9) can be defined for every facet $\mathbf{A} = A\hat{\mathbf{f}}$ with area A and normal vector $\hat{\mathbf{f}}$. A hedgehog density (3.13) can be defined for every tetrahedron, where we choose the normal directions of all facets to be pointing outwards.

By discretizing $\rho = \nabla \cdot \mathbf{B}$ in terms of the skyrmion densities (i.e., emergent $\mathbf{B}$ field) on the four facets, we can associate a hedgehog density

$$\rho = \frac{\sum_{i=1}^{4} B_{\mathbf{A}_i} A_i}{V} = \frac{c_{123} + c_{142} + c_{243} + c_{134}}{8\pi V}, \tag{3.13}$$

to the tetrahedron in Fig. 3.2, where V is its volume. Note definition (3.13) is proportional to the total skyrmion number on all four facets (where we have chosen outwards normal vector as positive direction for defining the orientation). From this, we immediately conclude that the Stokes's theorem also holds at lattice level,

$$\sum_{\text{all cubes}} \rho V = \text{boundary skyrmions}, \tag{3.14}$$

where all the inner facets cancel out and only boundary terms are left. Accordingly, for a

fixed texture on the boundary, an arbitrary smooth field in the bulk yields the same net hedgehog number, irrespective of the details of the dynamics.

With these definitions of ρ and $j_{\mathbf{A}}$, we can verify the hedgehog density and flux satisfy the continuity equation:

$$\partial_t(\rho V) + \sum_{i=i}^{4} j_{\mathbf{A}_i} A_i = 0. \tag{3.15}$$

One notes that there are two different contributions to the hedgehog flux (3.9). The first term, $-\partial_t B_{\mathbf{A}}$, is due to the change of the skyrmion density on the triangular facet. The second term, γ_{ijk}/A, while is inconsequential for the conservation law, is important to ensure that $j_{\mathbf{A}}$ is a local physical current, which is consequential for energetic and Kubo considerations (when one attempts to establish chemical-potential bias of hedgehog and derive its conductivity in linear response).[16]

We emphasize that the conservation law for hedgehogs holds at quantum level (also in the classical limit), irrespective of the form of the Hamiltonian, which indicates that it is topological and is not rooted in any specific symmetry of the system. After coarse-graining process, we obtain $\mathbf{n}$ field out of $\mathbf{S}$ and hedgehog current j^μ in terms of $\mathbf{n}$. It is the conservation of hedgehog current at lattice level that determines the conservation of j^μ at arbitrary temperatures.

3.5 Confinement and deconfinement

We now turn to the energetics and physical dynamics of hedgehogs in Heisenberg magnets. Hedgehogs are confined in the ordered phase, with the potential energy of a hedgehog-antihedgehog pair growing linearly with their separation [166]. One can imagine a string of tension $4\pi\mathcal{A}$ tying them, where $\mathcal{A}$ is the exchange stiffness of the magnetic material [see Eq. (3.16) below]. The confinement is also expected from evaluating the potential energy of a single hedgehog,

$$\mathcal{U} = 4\pi\mathcal{A}R, \tag{3.16}$$

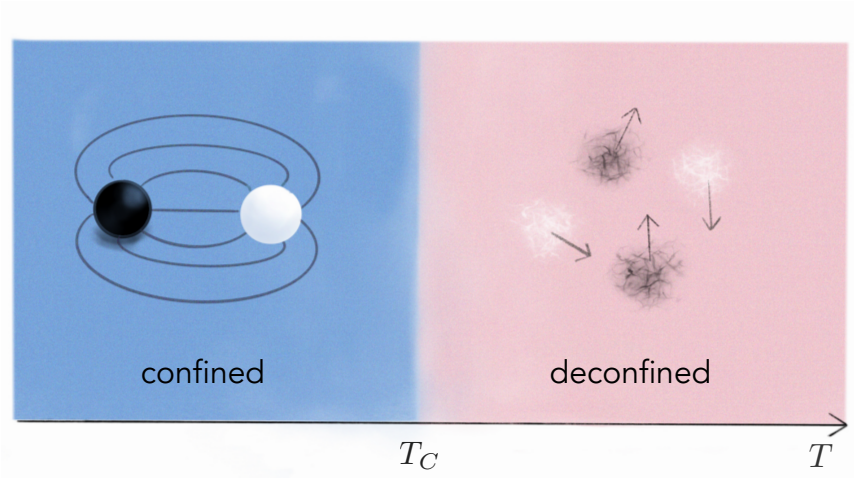

Figure 3.3: Different phases of hedgehogs. At temperatures above the Curie temperature T_C, hedgehogs (black ripples) and antihedgehogs (white ripples) carrying nonquantized topological charges proliferate and become mobile. In the ordered phase, hedgehogs are confined by a linear potential analogous to the quark confinement in QCD. They are singular quantized objects, represented by black and white spheres.

where R is the size of the system. One can directly check this for $\mathbf{n} = \mathbf{n}_0$ placed at the origin of a sphere of radius R. For a hedgehog-antihedgehog pair, all flux from the hedgehog must end at the antihedgehog, forming a flux tube to minimize the energy. Such a system could realize an experimentally accessible analogy to quark confinement in QCD [167, 168].

In the paramagnetic phase, hedgehogs deconfine naturally due to the absence of long-range correlations. Conceptually, the transition to the magnetically disordered phase can be thought of as a result of proliferation of hedgehogs, which form a two-component hedgehog-antihedgehog plasma (while topological charges are no longer quantized) as illustrated in Figs. 3.1 and 3.3. This extends our analogy with the QCD picture: Quarks deconfine and form a so-called quark-gluon plasma at high temperatures where the chiral symmetry is restored and long-range correlation is melted away [169, 170, 171, 172]. The hedgehog system is therefore a promising alternate to study QCD theories in condensed matter systems. Previously considered was the magnetic monopole confinement in superconductors due to

Meissner effect [173, 174, 175, 176, 177], where monopoles enter a deconfined phase as the temperature increases, accompanying the superconductor-insulator transition.

We remark that hedgehogs are not always energy-costly excitations as in Heisenberg magnets. $MnSi_{1-x}Ge_x$ has a stable phase of a hedgehog-antihedgehog lattice [151, 152, 153], where there is evidence that four- and six-spin interactions may play an important role [178, 179, 180]. Here, we formally adopt a nonlocal term, which is particularly compatible with our fictitious electromagnetic formalism, into our Heisenberg Hamiltonian:

$$\mathcal{U} = \int d^3\vec{r} \left[\frac{\mathcal{A}}{2} (\vec{\nabla}\mathbf{n})^2 + \frac{\mathcal{C}}{2} (\partial_i \mathbf{n} \times \partial_j \mathbf{n})^2 \right], \tag{3.17}$$

where Einstein summation is implied over the i, j and $\mathcal{C}$ is a phenomenological parameter. Other quartic terms, such as $(\vec{\nabla}\mathbf{n})^4$, are also present in principle, but the above $\mathcal{C}$ term is of special interest to us. It resembles the Maxwell magnetic field energy $\propto \mathbf{B}^2$ (in the ordered phase, s.t. $|\mathbf{n}| \approx 1$). The total potential energy for a hedgehog is thus $\mathcal{U} \sim \mathcal{A}R - \mathcal{C}/R$, which indicates that hedgehogs are free at a small distance $r \ll \sqrt{\mathcal{C}/\mathcal{A}}$, where the Coulombic term dominates. This phenomena mimics the asymptotic freedom in QCD [167, 168]. Likewise, in a system of small size, the hedgehog confinement becomes insignificant when $\sqrt{\mathcal{C}/\mathcal{A}}$ is comparable to R.

3.6 Biased hedgehog flow

At the heart of the hedgehog transport is the (desired) capability of driving and manipulating the hedgehog current. We focus on the dynamics near the Curie temperature of a ferromagnet, where the hedgehogs get deconfined, while the thermal fluctuations are still not too violent atomistically. The spin dynamics can be described by $\partial_t \mathbf{n} = -\Gamma \mathbf{H}$, where we allow the magnitude $|\mathbf{n}|$ to fluctuate. $\mathbf{H} = \delta F / \delta \mathbf{n}$ is the effective field (with F being the free energy of the ferromagnet) and Γ is a phenomenological dissipative coefficient. As illustrated in Fig. 3.1, we apply an electric current density $\vec{\mathcal{J}} = \mathcal{J}\hat{y}$ in the left metal contact. Given that the mirror-reflection symmetry is broken along the z axis, symmetry considera-

tions [13, 103, 142, 134] suggest that a spin flow can be transferred (per unit volume) into the magnetic texture, in the form:

$$\mathfrak{J} = \frac{3\hbar}{8e\pi}(\vec{\zeta}\cdot\vec{\nabla}\mathbf{n})\times(\vec{\mathcal{J}}\cdot\vec{\nabla}\mathbf{n}), \tag{3.18}$$

where $\vec{\zeta} = \zeta\hat{z}$ is a phenomenologically constructed vector (with the dimension of length), which reflects the mirror-symmetry breaking in the z direction. Note that the spin transfer $\mathfrak{J}$ is isotropic in spin space and thus does not rely microscopically on the presence of a spin-orbit coupling. We also remark that $\mathfrak{J}$ is constructed phenomenologically based on symmetry considerations. Its microscopic origin, magnitude, and direct experimental signatures remain to be explored.

In the presence of this spin transfer, we have $\partial_t\mathbf{n} = -\Gamma\mathbf{H} + \mathfrak{J}/s$, where s is the saturated spin density. The changing rate of the free energy density is thus $P = \partial_t\mathbf{n}\cdot\mathbf{H} = \mathfrak{J}\cdot\partial_t\mathbf{n}/s\Gamma - (\partial_t\mathbf{n})^2/\Gamma$. Here, the second term is the Rayleigh dissipation and the first term yields the total work done by the left contact upon magnetic dynamics:

$$W = \int dxdydzdt\ \frac{\mathfrak{J}\cdot\partial_t\mathbf{n}}{s\Gamma} = \frac{\hbar\lambda\zeta\mathcal{J}}{2es\Gamma}\mathcal{Q}, \tag{3.19}$$

where λ is a length scale, which depends on the effective spatial extent within which the spin transfer, as a proximity effect at the interface, is operative. Note the work is proportional to the topological charge $\mathcal{Q}$. The setup in Fig. 3.1 therefore discriminates between topological charges of opposite sign, biasing a net hedgehog current. We also remark that mirror-symmetry in the z direction is the minimal symmetry we need to break, in order for $\vec{\zeta}$ to effectively realize a polar vector in Eq. (3.18). As a symmetry-allowed process, a hedgehog current can be generated naturally as a channel to release the energy associated with electron dynamics in the left contact (where an electric current is applied, see Fig. 3.1). The electric current in the (left) metal contact provides an effective boundary bias for the hedgehog flow into the bulk, effectively establishing a local chemical potential for hedgehogs:

$$\bar{\mu}_L \equiv \frac{\delta W}{\delta\mathcal{Q}} = \frac{\hbar\lambda\zeta\mathcal{J}}{2es\Gamma}. \tag{3.20}$$

3.7 Nonlocal spin drag

We are now ready to study the transport of hedgehogs in the geometry depicted in Fig. 3.1. To this end, we operate the system in the paramagnetic phase, such that hedgehogs become mobile, rendering a finite effective hedgehog conductivity σ. We employ an Ohmic constitutive relation $j_x = -\sigma\partial_x\mu$ within the magnet. At the left boundary, using an electric current, the chemical potential for hedgehogs is raised by $\bar{\mu}_L$. At the right terminal, which serves as the ground, the natural chemical potential vanishes, as hedgehogs can freely go in and out through the right boundary. The hedgehog flow in y and z directions are nonvanishing in general. Here we assume translational invariance along these two directions and focus on dynamics in x direction. By invoking the reaction-rate theory [181], we obtain the hedgehog inflow and outflow at the left and right boundaries:

$$j_x^L = 2\gamma_L(\bar{\mu}_L - \mu_L)/k_BT, \;\; j_x^R = 2\gamma_R\mu_R/k_BT, \tag{3.21}$$

in linear response. Here, $\mu_{L,R} \equiv \mu(x = 0, L)$ is the chemical potential at two ends of the magnet, where L is its length along the x direction. $\gamma_{L,R} \sim \nu_{L,R}e^{-E_0/k_BT}$ is the equilibrium injection rate of hedgehogs at the respective boundaries, in terms of the attempt frequencies $\nu_{L,R}$ and an effective energy barrier E_0 governed by the core energy. Continuity of the hedgehog flux establishes a steady-state current

$$j_x = \frac{\hbar\mathcal{J}\lambda\zeta/2es\Gamma}{L/\sigma + k_BT/\gamma}, \tag{3.22}$$

where we took $\gamma_L = \gamma_R = \gamma$ for simplicity. k_BT/γ is the boundary impedance. L/σ is the bulk impedance, scaling linearly with the system size, which dominates in the thermodynamic limit $L \to \infty$. This is similar to the ordinary Ohmic impedance for a conserved electric current. The hedgehog conductivity $\sigma = \rho_0 D/k_BT$ is highly tunable via temperature, where ρ_0 and D are the background hedgehog density and the diffusion constant, respectively. In the paramagnetic phase ($T \gtrsim J/k_B$ with J being the exchange energy), let us consider the limiting case where the order parameter varies on the atomic scale. Here, we estimate

$\rho_0 \sim 1/a^3$ and $D \sim Ja^2/\hbar$, with a being the lattice spacing. This yields the optimal conductivity $\sigma \sim 1/a\hbar$ in the paramagnetic phase, while $\rho_0 \propto e^{-E_0/k_BT}$ and thus σ is exponentially small in the ordered phase.

The hedgehog current reaching the right terminal exerts a pumping electromotive force on the metal contact [126, 111, 127], which is determined by invoking the Onsager reciprocity [106]: $\vec{\varepsilon} = \hbar\lambda\, \mathbf{j} \times \vec{\zeta}/2es\Gamma$. This leads to a finite nonlocal drag resistivity (whose sign is opposite to a viscous drag):

$$\varrho \equiv \frac{\varepsilon}{\mathcal{J}} = \frac{(\hbar\lambda\zeta/2es\Gamma)^2}{L/\sigma + k_BT/\gamma}, \tag{3.23}$$

which is defined as the ratio of the detected voltage (per unit length) along y at the right contact to the injected charge current density at the left contact. In the thermodynamic limit, the bulk impedance dominates and thus the resistivity scales algebraically $\varrho \propto L^{-1}$.

In the ordered phase, hedgehog currents vanish in linear response in the thermodynamic limit, while there can be transport in finite-size magnets. The magnet behaves like a hedgehog dielectric, which can be polarized by the hedgehog chemical potential provided by the applied electric current in the contact, like a usual dielectric polarized by an electric field. This may be observed directly with the coherent diffractive imaging [182, 183] or by testing (anti)skyrmion structures on surfaces at two ends [184, 185, 186].

Similar to the work on elastic response of skyrmion crystals [187], one can study the transport feature due to the elasticity of a hedgehog lattice across the hedgehog-lattice melting transition, in the geometry of Fig. 3.1. To this end, the magnet is replaced by a hedgehog lattice, which should be experimentally accessible [151, 152, 153].

Interesting physics emerges when one studies the interplay between electric currents and skyrmion dynamics [162, 188, 189], such as skyrmion Hall effect due to the emergent magnetic flux associated with skyrmions. Similarly, we expect hedgehogs to exhibit rich dynamics under electric currents, due to the possible complexity of emergent 3D magnetic field associated with hedgehogs in general.

3.8 Hedgehog conductivity

Here we deduce the conductivity of hedgehogs, taking the view that they can be treated as point-particles, where collective coordinate approach can be employed.[190, 103] In the diffusion regime, the conductivity is $\hat{\sigma} = \rho_0 \hat{\mu} = \rho_0 \, \hat{D}/k_B T$, where $\hat{\mu}$ is the hedgehog mobility (related to diffusion constant $\hat{D}$ by the Einstein relation) and ρ_0 is the background hedgehog density.[109] The force acting on the hedgehog $\vec{F}$ is related with its velocity via the constitutive relation $\vec{v} = \hat{\mu} \cdot \vec{F}$. To work out the force due to the inherent spin Berry phase effect,[138] we could look at the variation of the spin action:

$$\delta S = s \int d^3\vec{r}dt \; (\mathbf{n} \times \dot{\mathbf{n}}) \cdot \delta \mathbf{n}, \tag{3.24}$$

where $s = \hbar S/a^3$ is the saturated spin density coarse-grained from quantum-mechanical spin operators of length S defined on a microscopic lattice of characteristic constant a. By using the collective variables,

$$\mathbf{n}(\vec{r}, t) = \mathbf{n}(\vec{r} - \vec{R}(t)), \tag{3.25}$$

one obtains

$$\begin{aligned} \delta S &= s\Big[\int d^3\vec{r}dt \; \mathbf{n} \cdot (\partial_x \mathbf{n} \times \partial_y \mathbf{n})\Big] \; (\dot{X}\delta Y - \dot{Y}\delta X) \\ &+ s\Big[\int d^3\vec{r}dt \; \mathbf{n} \cdot (\partial_y \mathbf{n} \times \partial_z \mathbf{n})\Big] \; (\dot{Y}\delta Z - \dot{Z}\delta Y) \\ &+ s\Big[\int d^3\vec{r}dt \; \mathbf{n} \cdot (\partial_z \mathbf{n} \times \partial_x \mathbf{n})\Big] \; (\dot{Z}\delta X - \dot{X}\delta Z), \end{aligned} \tag{3.26}$$

from which we can write down the gyrotropic force acting on a hedgehog:

$$\vec{F} = \boldsymbol{\mathcal{B}} \times \vec{v}. \tag{3.27}$$

Here, we introduce $\boldsymbol{\mathcal{B}} = (\mathcal{B}_x, \mathcal{B}_y, \mathcal{B}_z)$ with $\mathcal{B}_i \equiv 4\pi s \int d^3\vec{r} \, B_i$.

To capture the damping effect, one need to start from Landau-Lifshitz-Gilbert equation and obtains the total force

$$\vec{F} = \boldsymbol{\mathcal{B}} \times \vec{v} + \hat{\eta} \cdot \vec{v} = \big[(\boldsymbol{\mathcal{B}}\times) + \hat{\eta} \cdot \big]\vec{v}. \tag{3.28}$$

Here,

$$[\hat{\eta}]_{ij} = \alpha s \int d^3\vec{r}dt\ \partial_i \mathbf{n} \cdot \partial_j \mathbf{n}, \tag{3.29}$$

is a generalized viscosity tensor, where α is the Gilbert damping. Therefore, the hedgehog conductivity can be formally written as

$$\hat{\sigma} = \rho_0 \hat{\mu} = \rho_0 \big[(\boldsymbol{\mathcal{B}}\times) + \hat{\eta} \cdot \big]^{-1}. \tag{3.30}$$

One can write down the $\hat{\mu}$ (thus $\hat{\sigma}$) explicitly by inverting the matrix equation (3.28).

Three important observations are in order. First, the resistivity tensor $\hat{\rho} = \hat{\sigma}^{-1}$ can be written as a sum of a symmetric tensor and an antisymmetric tensor. The former is damping-related $\hat{\eta}$ which is dissipative while the latter is due to gyrotropic force (rooted in the spin Berry phase), which is nondissipative. Second, when the hedgehog is isotropic (e.g., $\mathbf{n}_0 = \{x, y, z\}/r$), the gyrotropic force vanishes and $[\hat{\eta}]_{ij} = \eta\delta_{ij}$, where $\eta = 4\pi s \int d^3\vec{r}dt\, \partial_x \mathbf{n} \cdot \partial_x \mathbf{n}$. Thus we have conductivity $\hat{\sigma} = \rho_0/\eta\delta_{ij}$. Third, our above derivation is based on collective coordinate approach. This approach breaks down at very high temperatures ($k_B T \geq J$ with J being exchange energy), where we are not able to treat hedgehogs as point particles. In such a case, we expect the conductivity to be saturated and its temperature dependence to be weak. We approximate $\rho_0 \sim 1/a^3$ and $D \sim Ja^2/\hbar$ based on basic dimension analysis. This would give us the optimal hedgehog conductivity $\sigma \sim 1/a\hbar$.

3.9 Discussion and outlook

We note that, though our discussion is based on insulating magnets, it applies equally well to conducting magnets, when the dimension along x is much larger than the other two in Fig. 3.1, so that we can disregard an Ohmic drag between the side contacts. Our symmetry arguments for the hedgehog injection can also be extended to antiferromagnetic systems, with the Néel order parameter, subject to a careful consideration of the magnetic space group.

There are two interesting open questions we did not address beyond phenomenological level: the microscopic origin of the spin transfer (3.18) and a precise description of confinement-deconfinement transition of hedgehogs. We remark that the proposed nonlocal spin drag experiment in Fig. 3.1 also serves as a good testing platform of the deconfinement of hedgehogs in the paramagnetic phase.

The advances in coherent diffractive imaging and vector-field tomography have proven promising for direct observations of 3D magnetic textures, as space and time resolutions are under improvement [182, 183]. This progress makes it possible for our theoretical concepts and proposals to be experimentally investigated for further understanding and future application of 3D topological spin textures.

Our study broadens the scope of 3D spintronics in at least two aspects: Hedgehogs, as commonly existing topological textures in magnets, are promising to support nonlocal transport in magnets and serve as information carriers. The study of the hedgehog current also offers us a handle to manipulate two-dimensional skyrmion textures, with various potential applications in skyrmionics. Transverse skyrmion textures and their associated free energy can be loaded into a chiral magnet by biasing a hedgehog flux through it. If the induced skyrmion density can be preserved at lower temperatures, e.g. by the Dzyaloshinskii-Moriya interaction, this would provide a 3D realization of the energy-storage proposal of Ref. [105]. Being able to change the skyrmion number, the hedgehog flow can also be used to flip the polarity of a vortex core, while maintaining the vorticity.

CHAPTER 4

Squeezing spin entanglement out of magnons

> "*When an old and distinguished person speaks to you, listen to him carefully and with respect — but do not believe him. Never put your trust into anything but your own intellect. Your elder, no matter whether he has gray hair or has lost his hair, no matter whether he is a Nobel laureate — may be wrong. The world progresses, year by year, century by century, as the members of the younger generation find out what was wrong among the things that their elders said. So you must always be skeptical — always think for yourself.*"
>
> *Linus Pauling*

In this chapter, we study the entanglement between two arbitrary spins in a magnetic material, where magnons naturally form a general squeezed coherent state, in the presence of an applied magnetic field and axial anisotropies. Employing concurrence as a measure of entanglement, we demonstrate that spins are generally entangled in thermodynamic equi-

librium, with the amount of entanglement controlled by the external fields and anisotropies. As a result, the magnetic medium can serve as a resource to store and process quantum information. We, furthermore, show that the entanglement can jump discontinuously when decreasing the transverse magnetic field. This tunable entanglement can be potentially used as an efficient switch in quantum-information processing tasks.

4.1 Introduction

Entanglement [66, 67] is a measure of how much quantum information is stored in a quantum state and is one of the most fundamental properties that distinguish a quantum phenomenon from its classical counterpart. It was under a severe skepticism, however, since the discovery of quantum mechanics [191], due to its nonlocality that appeared to violate the local-realism view of causality. Following the derivation of Bell's inequalities, which rendered the nonlocal features of quantum theory accessible to experimental verification, numerous experiments in different systems have been carried out, including photons, neutrinos, electrons, molecules as large as buckyballs, and even small diamonds, unequivocally demonstrating the existence of quantum entanglement [192, 193, 194, 195, 196, 197, 198]. In parallel with these developments, quantum entanglement has come to be recognized as a valuable resource in quantum-information processing [95]. For example, a quantum computer can be much faster and more powerful than a classical one for certain computational tasks, by taking the advantage of the superposition and entanglement in a quantum system [199]. Moreover, we can realize several quantum protocols, such as teleportation, exclusively with the help of entangled states [200]. These merits of entanglement in quantum information science stimulate the research trying to coherently prepare and manipulate it in various systems.

A magnon Bose-Einstein condensate (BEC) [201], where quanta of spin waves condense into a single state, may be taken as a platform to look for controllable entanglement [202], since particles in a condensate are distributed over space in a coherent way. Magnon BEC

is attractive in practice, as it can be driven by microwave [203, 204, 205, 206, 207, 208, 209] or electronic [210, 211] pumping in an insulating ferromagnet through a quasiequilibration process at room temperature. Without magnon pumping, we can also achieve magnon BEC in equilibrium, by introducing an easy-plane anisotropy in the magnetic system [212]. As we show later, magnons condense by forming a general squeezed coherent state, when the system is subjected to external magnetic fields and anisotropies. A squeezed coherent state [213], akin to a coherent state, is a minimum uncertainty state but with uncertainties of conjugate operators being different. This state has been investigated extensively in quantum optics, resulting in many applications. For example, it can be used to improve the precision of atom clocks [214, 215] and quantum-information processing in the continuous-variables regime [216].

In this chapter, we explore the entanglement of arbitrary two spins in a magnetic system (assuming the number of spin sites is N_0), utilizing the concurrence $\mathcal{C}$ [71, 67] as a measure of entanglement, where magnons are condensed into a general squeezed coherent state. The average number of condensed magnons in such a state can be tuned by the external field and magnetic anisotropies [213]. We distinguish between two types of magnons: coherent magnons related to a uniform order-parameter tilting and squeezed magnons related to the anisotropic squeezing effect [see Eq. (4.11) below]. From numerical analysis, we find that the system transits abruptly to a highly entangled state from an unentangled state, when we decrease the number of coherent magnons (denoted by N_c) across a critical value that is determined by the number of squeezed magnons (denoted by N_s):

$$N_c = \sqrt{2N_0N_s}. \tag{4.1}$$

This can be potentially used as a switch in quantum-information processing tasks. Whereas a simple coherent state has no entanglement, a squeezed vacuum state is entangled with concurrence

$$\mathcal{C} = \frac{2}{N_0}\frac{\sqrt{N_s}}{\sqrt{N_s+1}+\sqrt{N_s}}. \tag{4.2}$$

This concurrence will increase as the number of squeezed magnons rises. Resembling squeezed light in quantum optics [216, 217, 218], our squeezed coherent magnetic states can also serve as an essential resource to realize continuous-variables protocols for quantum communication, unconditional quantum teleportation, and one-way quantum computing. Apart from this, we also discuss the entanglement when the condensate is in a Fock state and we match our result with the entanglement of Dicke states [219], which has been well understood in quantum spin squeezing [220, 221, 222]. In contrast to the entanglement between macroscopic building blocks of cavity magnetomechanical systems [223, 224], we are considering the intrinsic spin entanglement within a quantum medium.

4.2 Model

Our model system is a set of localized spins interacting through a nearest-neighbor exchange coupling on a three-dimensional lattice, with axial anisotropies and a tilted magnetic field, according to the following Hamiltonian [225]:

$$H = -J\sum_{\langle i,j\rangle}\mathbf{S}_i\cdot\mathbf{S}_j - \mathbf{B}\cdot\sum_i\mathbf{S}_i + H_1 + H_2, \tag{4.3}$$

$$H_1 = \frac{K}{w}\sum_{\langle i,j\rangle}(S_i^xS_j^x - S_i^yS_j^y), \tag{4.4}$$

$$H_2 = -\mathbf{h}\cdot\sum_i\mathbf{S}_i. \tag{4.5}$$

Here, $\mathbf{S}_i = \boldsymbol{\sigma}_i/2$ is the spin operator on the ith site ($\boldsymbol{\sigma}$ are Pauli matrices and we have set $\hbar = 1$ for simplicity), w is the lattice coordination number (for example, $w = 6$ for a simple cubic lattice), $J > 0$ is the exchange constant of a simple Heisenberg magnet ($J \gg B, |K|$), $|K|$ is the anisotropy strength, $\langle i,j\rangle$ stands for all nearest-neighbor pairs, and $\mathbf{B} = B\,\hat{\mathbf{z}}$, $\mathbf{h} = h\,\hat{\mathbf{x}}$ are the external fields (absorbing all constant factors). We will restrict our discussion to the case $B > |K|$, so that quantum spin fluctuations can be expanded around the z axis.

We will focus on the low-temperature limit, $T \ll J$, where thermal magnons are dilute. It is convenient to switch from the SU(2) spin algebra to the bosonic algebra: $S_i^+ = a_i, S_i^z = 1/2 - a_i^\dagger a_i$, where $a_i^\dagger, a_i$ are the magnon creation and annihilation operators in real space that obey bosonic commutation relations. This transformation is exact, when complemented with the hard-core repulsion for magnons [226]. In the dilute limit, where the average magnon density is small $\langle a_i^\dagger a_i \rangle \ll 1$, as in our case of $J \gg B > |K|$, we can relax the hard-core repulsion constraint and, as a result, the Hamiltonian H can be linearized and rewritten as

$$H = \sum_{\mathbf{k}} (2J\mathbf{k}^2 + B) a_{\mathbf{k}}^\dagger a_{\mathbf{k}} + \frac{K}{2} \sum_{\mathbf{k}} (a_{-\mathbf{k}}^\dagger a_{\mathbf{k}}^\dagger + a_{\mathbf{k}} a_{-\mathbf{k}}) - \frac{h\sqrt{N_0}}{2}(a^\dagger + a) + \cdots . \tag{4.6}$$

Here, $a \equiv a_{q=0}$, the ellipsis represents nonlinear terms, and N_0 is the total number of sites in the system. Note we have set the lattice constant to be 1, which means all quantities with length dimension will be measured in unit of the lattice constant. The above Hamiltonian can be diagonalized by applying Bogoliubov transformations [227, 228] and rewritten as

$$H = \sum_{\mathbf{k} \neq 0} \omega(\mathbf{k}) b_{\mathbf{k}}^\dagger b_{\mathbf{k}} + \omega b^\dagger b, \tag{4.7}$$

where $b^\dagger, b$ and $b_{\mathbf{k}}^\dagger, b_{\mathbf{k}}$ are bosonic operators, $\omega(\mathbf{k}) = \sqrt{(2J\mathbf{k}^2 + B)^2 - K^2}$ and $\omega \equiv \omega(\mathbf{k} = 0)$. The operator b and $b_{\mathbf{k}}$ are related to a and $a_{\mathbf{k}}$ via

$$b = D(\alpha) S(r) a S^\dagger(r) D^\dagger(\alpha); \tag{4.8}$$

$$b_{\mathbf{k}} = S(\phi_{\mathbf{k}}/2) a_{\mathbf{k}} S^\dagger(\phi_{\mathbf{k}}/2),\ \mathbf{k} \neq 0. \tag{4.9}$$

$S(\phi_{\mathbf{k}}/2) = e^{(a_{\mathbf{k}} a_{-\mathbf{k}} - a_{\mathbf{k}}^\dagger a_{-\mathbf{k}}^\dagger)\phi_{\mathbf{k}}/2}$ is a two-mode squeezing operator [229, 230] and $\phi_{\mathbf{k}}$ is determined by $\tanh \phi_{\mathbf{k}} = K/(2J\mathbf{k}^2 + B)$. $S(r) = e^{[a^2 - (a^\dagger)^2]r/2}$ is a squeezing operator [213] with $r = \phi_{\mathbf{k}=0}/2$. $D(\alpha) = e^{\alpha a^\dagger - \alpha^* a}$ is a displacement operator with $\alpha = h\sqrt{N_0} e^{-2r}/2\omega$.

The ground state $|\psi\rangle$ is given by $b|\psi\rangle = 0, b_{\mathbf{k}}|\psi\rangle = 0$ for all $\mathbf{k}$ and thus

$$|\psi\rangle = \big(D(\alpha) S(r) |0\rangle \big) \otimes \left(\prod_{\mathbf{k} \neq 0} S(\phi_{\mathbf{k}}/2) |0\rangle \right), \tag{4.10}$$

where $|0\rangle$ is the Fock vacuum defined by $a_{\mathbf{k}}|0\rangle = 0$ for any wavenumber $\mathbf{k}$. The average number of magnons in the ground state is

$$\langle a_{\mathbf{k}}^{\dagger} a_{\mathbf{k}} \rangle = \delta_{\mathbf{k},0}|\alpha|^2 + \sinh^2 \frac{\phi_{\mathbf{k}}}{2}. \tag{4.11}$$

In the large exchange-coupling limit with the size of the system being finite, the effect of nonzero wavenumber modes is negligible and the ground state reduces to the so called squeezed coherent state $|\psi\rangle = D(\alpha)S(r)|0\rangle$. Under the circumstances, $\langle a_{\mathbf{k}}^{\dagger} a_{\mathbf{k}} \rangle = \delta_{\mathbf{k},0}(|\alpha|^2 + \sinh^2 r)$. We refer to the part related to the coherent parameter α as coherent magnons and the part related to the squeezing parameter r as squeezed magnons, denoted by

$$N_c \equiv |\alpha|^2 \text{ and } N_s \equiv \sinh^2 r, \tag{4.12}$$

respectively.

Staying in the large-J limit, when we turn off both the anisotropy K and the in-plane magnetic field h so that $r = \alpha = 0$, the ground state is the Fock vacuum of operators $a_{\mathbf{k}}$, corresponding to all spins aligned along $\mathbf{B}$. If we turn on the in-plane magnetic field $\mathbf{h}$ and keep the anisotropy off, there are finite number of magnons in the $q = 0$ mode forming a coherent state $|\psi\rangle = D(\alpha)|0\rangle$, where all spins deviate from $\mathbf{B}$ direction uniformly (see Fig. 4.1a). The number of magnons (the degree of the deviation) is determined by the magnitude of $\mathbf{h}$ via $N_c = N_0 h^2/4B^2$, which is much smaller than N_0 in the dilute limit. We emphasize that this is a minimum uncertainty state and equally balanced between S^x and S^y with $\Delta S^x = \Delta S^y = 1/2$ [231]. If we turn on the anisotropy and keep the in-plane magnetic field off, the ground state is a squeezed vacuum state $|\psi\rangle = S(r)|0\rangle$, where spins align along $\mathbf{B}$ on average by noting that $\langle S^x \rangle = \langle S^y \rangle = 0$ but with finite number of condensed magnons $N_s = \sinh^2 r$ (see Fig. 4.1b). The uncertainty is also minimized in this state, but not equally balanced between S^x and S^y. This is also implied from the Hamiltonian H_1 where the in-plane U(1) symmetry is broken explicitly, which is the crucial ingredient for the presence of entanglement. The degree of this squeezing is measured by the squeezing factor r, more explicitly $\Delta S^y/\Delta S^x = e^{2r}$. When both anisotroy and in-plane magnetic field are present, all

spins deviate from **B** on average and the uncertainties in S^x and S^y have the same behavior as the squeezed vacuum state. The average number of condensed magnons is $N = N_s + N_c$, consisting of coherent magnons and squeezed magnons [see Eq. (4.11)]. The entanglement between two arbitrary spins is determined by the interplay between those parts. In other words, we can tune the entanglement by varying the parameters, such as the anisotropy and the in-plane magnetic field which determine N_c and N_s. Note that we refer to this global tilting state as a condensed state, since the number of magnons in the q=0 mode remains to be finite under any spin rotation in the spin space.

In the thermodynamic limit, the contribution to the entanglement due to $q = 0$ mode is negligible and the effective ground state is the squeezed vacuum state $|\psi\rangle = \prod_{\mathbf{k}\neq 0} S(\phi_{\mathbf{k}}/2)\,|0\rangle$. There are only squeezed magnons, because the uniform magnetic field only couples with the $q = 0$ mode. The entanglement in this case is distance dependent, since $|\psi\rangle$ involves finite-wavenumber modes. This will be addressed in Sec. 4.4.5. Before delving into that, let us introduce the entanglement measure we employ in our analysis: the concurrence.

4.3 Entanglement Measures

The problem of measuring entanglement is a vast field of research on its own [66, 67]. Numerous different methods have been proposed to that end. For a pure bipartite state $\rho_{\mathrm{AB}} = |\psi_{\mathrm{AB}}\rangle\langle\psi_{\mathrm{AB}}|$, we usually adopt the von Neumann entropy as the entanglement measure: $S(|\psi_{\mathrm{AB}}\rangle) \equiv -\operatorname{tr}\rho_A \ln\rho_A = -\operatorname{tr}\rho_B \ln\rho_B$. For a general mixed state ρ_{AB}, this von-Neumann entropy is no longer a good measure since the classical mixture in ρ_{AB} will also contribute to the von Neumann entropy. Therefore, many new measures have been introduced, such as entanglement of formation, distillable entanglement, and entanglement cost, which all reduce to the von Neumann entropy when evaluated on pure states. Here we will use the entanglement of formation as the entanglement measure as we can accomplish some analytic results for problems we are interested in. In the next section, we explore the entanglement

between two arbitrary spins for various states we discussed in Section 4.2.

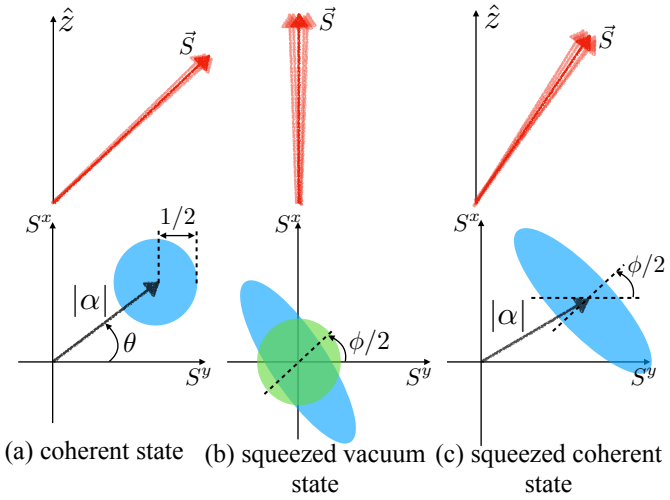

Figure 4.1: (a). A general coherent state $|\alpha\rangle = D(\alpha)\,|0\rangle$, where $D(\alpha) \equiv \exp\{\alpha a^\dagger - \alpha^* a\}$ is a displacement operator with $\alpha = |\alpha|e^{i\theta}$, is the minimum uncertainty state ($\Delta S^x = \Delta S^y = 1/2$). All spins deviate from $\mathbf{B} \propto \hat{\mathbf{z}}$ direction coherently. (b). The general squeezed vacuum state $S(\zeta)\,|0\rangle$, where $S(\zeta) \equiv e^{\left[\zeta^* a^2 - \zeta (a^\dagger)^2\right]/2}$ is the squeezing operator with a squeezing parameter $\zeta = re^{i\phi}$, is also a minimum uncertainty state with uncertainties being squeezed (blue ellipse) compared with the vacuum uncertainties (green disk). The direction of the squeezing (the orientation of the semi-minor axis of the ellipse with respect to the S^x axis) is $\phi/2$. The length of the semi-minor axis is $e^{-r}/2$ and the length of the semi-major axis is $e^r/2$. The average direction of the spin in such state is along $\mathbf{B}$. (c). For the general squeezed coherent state $D(\alpha)S(\zeta)\,|0\rangle$, the degree of the deviation from $\hat{\mathbf{z}}$ is determined by the parameter α and the degree of squeezing of the uncertainty is determined by the squeezing parameter ζ.

4.4 Entanglement Quantification

In the first four subsections, we discuss the entanglement due to the $q = 0$ mode in a finite size sample with large exchange coupling where this mode dominates the quantum fluctuation. In the last subsection, entanglement and its distance dependence are examined

in thermodynamic limit, where finite wavenumber modes must be taken into account.

4.4.1 Fock States

We start with investigating the concurrence between two spins in Fock states $|N\rangle$ where N is the number of magnons in the zero-momentum mode. For the Fock vacuum $|0\rangle$, the concurrence is zero since this is a product state $|\uparrow\uparrow\cdots\uparrow\rangle$. When there is a finite number of magnons, invoking the reduced density matrix (1.136), which is simplified for this specific case, we show the concurrence (Eq. 1.129) between arbitrary two spins is given by

$$\begin{aligned}\mathcal{C}_{\rm Fock} &= 2\max\left\{0, |\langle\sigma_i^+\sigma_j^-\rangle| - \sqrt{\langle k_i^+ k_j^+\rangle\langle k_i^- k_j^-\rangle}\right\} \\ &\approx 2\frac{N}{N_0}\big(1-\sqrt{1-1/N}\,\big). \end{aligned} \tag{4.13}$$

Note that the upper bound of the concurrence is $2/N_0$, which is known as the tight bound for symmetric sharing of entanglement [232]. The concurrence reaches its maximum value when there is only one magnon, corresponding to the state $|\downarrow\uparrow\cdots\uparrow\rangle+|\uparrow\downarrow\cdots\uparrow\rangle+|\uparrow\uparrow\cdots\downarrow\rangle$. This is a generalization of the Bell state $|\Psi^+\rangle\sim|\uparrow\downarrow\rangle+|\downarrow\uparrow\rangle$ and thus maximally entangled. Another feature we should pay attention to is that the concurrence is a decreasing function of N and approaches $1/N_0$ as $N\to\infty$. This is consistent with the analysis of the Dicke state [219] $|N_0/2, M\rangle$ in quantum optics, which describes a system consisting of N_0 two-level systems (spin-1/2 particles) and is a pure symmetric (with respect to permutations) state. $N_0/2-M$ is the number of excited two-level systems (i.e., the flipped spins). The concurrence of such Dicke state is given by [220, 221, 222]

$$\begin{aligned}\mathcal{C}_{\rm Dicke} &= \frac{N_0^2-4M^2-\sqrt{(N_0^2-4M^2)[(N_0-2)^2-4M^2]}}{2N_0(N_0-1)} \\ &\approx \mathcal{C}_{\rm Fock}, \end{aligned} \tag{4.14}$$

where we have identified $N=N_0/2-M$ and specialized to the case $N\ll N_0$ by noting that the number of excited two-level systems is exactly the number of magnons in our context. It should be clear from our discussion above that we must invoke the one-magnon state $|N=1\rangle$

to produce a maximally-entangled configuration.

In Ref. [76], it was found that the entanglement between two spins increases with the number of condensed magnons N, which is contrary to what we discussed above. This discrepancy can be traced to the second term in Eq. (4.13), which, despite being comparable to the first term, was omitted in Ref. [76]. In particular, we see that the entanglement vanishes in the thermodynamic limit, $N_0 \to \infty$, in the Fock state $|N\rangle$ with any N, in agreement with the tight bound for symmetric sharing of entanglement. At a finite temperature T, when two spins sit at a distance smaller than the thermal de Broglie wavelength $\lambda_T \propto \sqrt{J/T}$, we expect the concurrence to be inversely proportional to the total number of sites within the corresponding volume: $\mathcal{C} \propto 1/\lambda_T^3$ (crossing over to $\mathcal{C} \propto 1/N_0$ as $T \to 0$ and λ_T exceeds the system size). Beyond the thermal de Broglie wavelength λ_T, the entanglement should decay exponentially, $\sim e^{-R/\lambda_T}$, with the distance R between two spins, which agrees qualitatively with the analysis of Ref. [76].

4.4.2 Coherent States

Let us turn on the in-plane magnetic field which will lead to a coherent state $|\alpha\rangle \equiv D(\alpha)\,|0\rangle$ as the ground state. We evaluate the elements of density matrix (1.136) in the coherent state and obtain

$$\rho(\sigma_y \otimes \sigma_y)\rho^*(\sigma_y \otimes \sigma_y) \propto 1_{4\times 4}. \tag{4.15}$$

This implies the entanglement between any two spins is zero and there is no quantum correlation stored in spins according to the definition of the concurrence Eq. (1.129). Indeed, this is not surprising and it has been shown any bosonic coherent state is unentangled [202]. It is true as well for spin coherent states since $|\theta,\phi\rangle = \otimes_{l=1}^{N_s}\left[\cos\frac{\theta}{2}\,|\downarrow\rangle_l + e^{i\phi}\sin\frac{\theta}{2}\,|\uparrow\rangle_l\right]$ is a product state where θ and ϕ specify the direction of spins. Coherent states have minimum uncertainty which are equally balanced between S^x and S^y with $\Delta S^x = \Delta S^y = 1/2$. Furthermore, any classical mixture of coherent states, such as $\hat{\rho} = \int d^2\alpha\ P_\alpha\,|\alpha\rangle\,\langle\alpha|$ with $P_\alpha > 0$ being the

probability density in $|\alpha\rangle$, can only increase the uncertainty and also has zero entanglement since classical correlations do not contribute to the entanglement. Such states are known as classical light states in the quantum optics [233]. One typical nonclassical light state is squeezed states and we will examine the entanglement of those states below.

4.4.3 Squeezed Vacuum Magnetic States

By turning on the anisotropy in Hamiltonian H_1 and keeping the in-plane magnetic field off, we can generate the squeezed vacuum state $|\psi\rangle = S(r)\,|0\rangle$ as the ground state, where the uncertainty in S^x is below the vacuum level. There must be quantum correlations in such states since they can never be achieved by mixing coherent states. We show that the concurrence (1.129) between two spins is given by

$$\mathcal{C} = \frac{2}{N_0}\frac{\sqrt{N_s}}{\sqrt{N_s+1}+\sqrt{N_s}}, \tag{4.16}$$

where $N_s = \sinh^2 r$ is the number of magnons in the squeezed vacuum state. In contrast to the Fock state, the concurrence of the squeezed vacuum state increases as we increase the number of magnons. This can be understood by noting that increasing N_s corresponds to squeezing the vacuum more. Namely, the degree of squeezing, $\Delta S^y/\Delta S^x = e^{2r} = (\sqrt{N_s+1}+\sqrt{N_s})^2$, equals unity when $N_s = 0$, which corresponds to zero entanglement. $\Delta S^y/\Delta S^x$ approaches infinity as N_s rises, where the vacuum is infinitely squeezed and has maximum concurrence $1/N_0$, which is half of the tight bound for symmetric sharing of entanglement [232]. We remark that this reduction in the entanglement is due to the odd parity missing in the wave function.

4.4.4 Squeezed Coherent Magnetic States

Now let us turn on both the anisotropy and the in-plane magnetic field, resulting in the squeezed coherent state $|\psi\rangle = D(\alpha)S(r)\,|0\rangle$ as our ground state. We will see that in contrast to the coherent states that retain their (trivial) entanglement character under displacement,

displacing a squeezed state does have a nontrivial effect. Unlike states we discussed above, however, it is difficult to obtain an analytic expression for the concurrence in this case. Therefore, we obtain the concurrence $\mathcal{C}$ numerically by plotting it as a function of r for different values of $|\alpha|$ (see Fig. 4.2a), where we assume the anisotropy $K > 0$ without loss of generality. As increasing the value of $|\alpha|$ from zero, we have zero concurrence under a critical value of $r_c = r_c(|\alpha|)$ (see Fig. 4.2b) and nonzero concurrence above r_c. The maximal concurrence will increase to $2/N_0$ from $1/N_0$ as we increase the number of coherent magnons. Thus we can see that the coherent magnons will unlink the quantum correlations between spins established by a small number of squeezed magnons. This is because the coherent magnons dominate the physics when the number of squeezed magnons is small. However, coherent magnons will be beneficial for information storage when the number of squeezed magnons is large. The upper bound of the concurrence rises since the coherent part involves states with both parities, unlike squeezed vacuum states which only involve even parity states $\{|2k\rangle\}$, and thus increases the upper bound. We remark that, in contrast to the discussion in Sec. 4.4 B where the displacement operation does not yield entanglement since it is acting on a trivial state (Fock vacuum state), the displacement operator here results in nontrivial entanglement behavior as it acts on a squeezed state which is entangled.

To determine this transition, we study the critical value $N_s^{1/4} = \sqrt{\sinh r_c}$ numerically and plot it as a function of $|\alpha|$ which can be fitted well with a linear relation (see Fig. 3.3b). We conclude that there is no entanglement when

$$N_c \geq \sqrt{2N_0N_s}. \tag{4.17}$$

Otherwise we have nonzero entanglement. This transition is discontinuous as implied from Fig. 3.3a. When $|\alpha|$ is large, $N_0\mathcal{C}$ is a step function of r, which can be potentially used as an efficient switch in quantum information processing tasks.

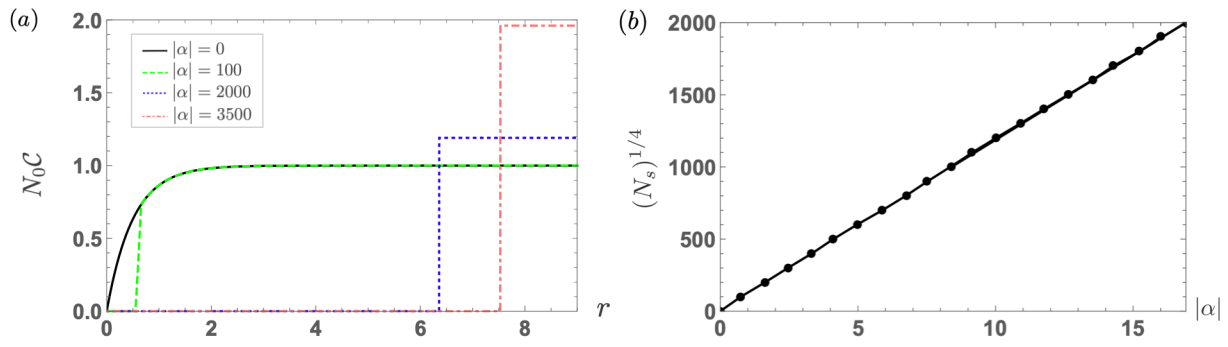

Figure 4.2: (a). Concurrence $\mathcal{C}$ as a function of the number of squeezed magnons $N_s = \sinh^2 r$ for different number of coherent magnons $N_c = |\alpha|^2$. $|\alpha| = 0$ corresponds to the squeezed vacuum state (see Eq. (4.16)), where the maximal concurrence is $1/N_0$. As we increase the number of coherent magnons, the physics is dominated by the coherent part when the number of squeezed magnons is small. As a result, the concurrence is zero. However, the presence of the coherent part can increase the upper bound of the concurrence once the number of squeezed magnons is above some critical value $\sinh^2 r_c$, which depends on the amount of coherent magnons we put into the system. (b). Critical values $(N_s)^{1/4} = \sqrt{\sinh r_c}$ as a function of $|\alpha|$, which can be fitted using a linear relation. When the number of coherent magnons is larger than $\sqrt{2N_0N_s}$, the coherent part dominates the physics and the concurrence is zero. Otherwise, we have a finite concurrence. In the numerical study above, we set $N_0 = 10^8$.

4.4.5 Thermodynamic Limit

In the thermodynamic limit, one can see that the entanglement between two arbitrary spins due to $q = 0$ mode vanishes from our discussion above. Under the circumstances, nonzero wavenumber modes should be taken into account and we can show that the concurrence between a spin at $\mathbf{R}_i$ and a spin at $\mathbf{R}_j$ in d dimension is given by

$$\mathcal{C}_{ij} = \max\left\{0, \mathcal{T}(\gamma, \lambda, \eta)\right\}, \tag{4.18}$$

where

$$\mathcal{T}(\gamma,\lambda,\eta) \approx \frac{1}{(2\pi)^d}\left|\int_{\text{B.Z.}} d^d\mathbf{q}\frac{\eta\cos\left(\gamma\hat{\mathbf{R}}\cdot\mathbf{q}\right)}{\sqrt{(1+2\lambda^2\mathbf{q}^2)^2-\eta^2}}\right| + \frac{1}{(2\pi)^d}\int_{\text{B.Z.}} d^d\mathbf{q}\left[1-\frac{1+2\lambda^2\mathbf{q}^2}{\sqrt{(1+2\lambda^2\mathbf{q}^2)^2-\eta^2}}\right]. \quad (4.19)$$

Here $\gamma = |\mathbf{R}| = |\mathbf{R}_i - \mathbf{R}_j|$ and $\lambda = \sqrt{J/B}$ are the distance between two spins and the exchange length. $\eta = |K|/B < 1$ is a dimensionless parameter and $\hat{\mathbf{R}} = (\mathbf{R}_i - \mathbf{R}_j)/|\mathbf{R}|$. B.Z. represents the Brillouin zone.

Here we sketch the derivation of Eq. (4.18) (Eq. (4.13) and Eq. (4.16) are similar). In state $|\psi\rangle = \prod_{\mathbf{k}\neq 0} S(\phi_{\mathbf{k}}/2)\,|0\rangle$, where $S(\phi_{\mathbf{k}}/2) = e^{(a_{\mathbf{k}}a_{-\mathbf{k}} - a^\dagger_{\mathbf{k}}a^\dagger_{-\mathbf{k}})\phi_{\mathbf{k}}/2}$ is the two-mode squeezing operator and $\phi_{\mathbf{k}}$ is determined by $\tanh\phi_{\mathbf{k}} = K/(2J\mathbf{k}^2 + B)$, we evaluate the reduced density matrix Eq. (1.136) for a spin at $\mathbf{R}_i$ and a spin at $\mathbf{R}_j$ in d dimension and obtain

$$\rho_{ij} = \begin{bmatrix} 1-2\langle a_i^\dagger a_i\rangle + \langle a_i^\dagger a_i a_j^\dagger a_j\rangle & 0 & 0 & \langle a_i^\dagger a_j^\dagger\rangle \\ 0 & \langle a_i^\dagger a_i\rangle - \langle a_i^\dagger a_i a_j^\dagger a_j\rangle & \langle a_j^\dagger a_i\rangle & 0 \\ 0 & \langle a_i^\dagger a_j\rangle & \langle a_j^\dagger a_j\rangle - \langle a_i^\dagger a_i a_j^\dagger a_j\rangle & 0 \\ \langle a_i a_j\rangle & 0 & 0 & \langle a_i^\dagger a_i a_j^\dagger a_j\rangle \end{bmatrix}. \quad (4.20)$$

Here we have used the fact that expectation value of any product of odd number of magnon creation or annihilation operators vanishes (this is true for any squeezed vacuum state), for example $\langle\psi|\, a_i^\dagger a_i a_j\,|\psi\rangle = 0$. Then one can determine the explicit form of $\rho(\sigma_y\otimes\sigma_y)\rho^*(\sigma_y\otimes\sigma_y)$ and show that the concurrence Eq. (1.129) is given by

$$\mathcal{C}(\rho_{ij}) = 2\,\max\left\{0, |\langle a_i^\dagger a_j^\dagger\rangle| - \langle a_i^\dagger a_i\rangle + \langle a_i^\dagger a_i a_j^\dagger a_j\rangle\right\} \quad (4.21)$$

Invoking identities

$$\langle\psi|\, a_{\mathbf{q}}^\dagger a_{\mathbf{k}}^\dagger\,|\psi\rangle = -\delta_{\mathbf{q},-\mathbf{k}}\sinh\frac{\phi_{\mathbf{k}}}{2}\cosh\frac{\phi_{\mathbf{k}}}{2}; \quad (4.22)$$

$$\langle\psi|\, a_{\mathbf{q}}^\dagger a_{\mathbf{k}}\,|\psi\rangle = \delta_{\mathbf{q},\mathbf{k}}\sinh^2\frac{\phi_{\mathbf{k}}}{2}, \quad (4.23)$$

we obtain the explicit expression of the concurrence

$$\mathcal{C}(\rho_{ij}) = \max\{0, \mathcal{T}\}, \tag{4.24}$$

where

$$\mathcal{T} = \frac{1}{(2\pi)^d}\left| \int_{\text{B.Z.}} \sinh\frac{\phi_{\mathbf{q}}}{2}\cosh\frac{\phi_{\mathbf{q}}}{2} e^{i\mathbf{q}\cdot(\mathbf{R_j}-\mathbf{R_i})}\, d^d\mathbf{q}\right| - \frac{1}{(2\pi)^d}\int_{\text{B.Z.}} \sinh^2\frac{\phi_{\mathbf{q}}}{2}\, d^d\mathbf{q}. \tag{4.25}$$

Here B.Z. represents the Brillouin zone. Considering $\tanh\phi_{\mathbf{k}} = K/(2J\mathbf{k}^2 + B)$ and introducing parameters $\gamma = |\mathbf{R}| = |\mathbf{R}_i - \mathbf{R}_j|$, $\lambda = \sqrt{J/B}$, $\eta = |K|/B$ and $\hat{\mathbf{R}} = (\mathbf{R}_i - \mathbf{R}_j)/|\mathbf{R}|$, we can rewrite Eq. (4.25) and obtain Eq. (4.18):

$$\mathcal{T}(\gamma,\lambda,\eta) \approx \frac{1}{(2\pi)^d}\left| \int_{\text{B.Z.}} d^d\mathbf{q} \frac{\eta\cos\left(\gamma\hat{\mathbf{R}}\cdot\mathbf{q}\right)}{\sqrt{(1+2\lambda^2\mathbf{q}^2)^2-\eta^2}}\right| + \frac{1}{(2\pi)^d}\int_{\text{B.Z.}} d^d\mathbf{q}\left[1 - \frac{1+2\lambda^2\mathbf{q}^2}{\sqrt{(1+2\lambda^2\mathbf{q}^2)^2-\eta^2}}\right]. \tag{4.26}$$

Applying Wick's theorem to $\langle a_i^\dagger a_i a_j^\dagger a_j\rangle$ and using $|\langle a_i^\dagger a_j^\dagger\rangle| \sim \mathcal{O}(\eta/\lambda^2)$, $|\langle a_i^\dagger a_j\rangle| < \langle a_i^\dagger a_i\rangle \sim \mathcal{O}\big(\eta^{2+d/2}/\lambda^d\big)$, which are all small, we see that the quartic correlator can be neglected.

Figure 4.3a visualizes the distance γ dependence of concurrence $\mathcal{C}_{ij}$ in dimension $d = 1$, $d = 2$ and $d = 3$, respectively. It suggests that $\mathcal{C}_{ij}$ is smaller when the dimension is higher. From Fig. 4.3b, we can see that, keeping other parameters fixed, $\mathcal{C}_{ij}$ will decrease to zero as we increase the distance γ to a critical value γ_c, which is proportional to the exchange length λ. In other words, spins within the exchange length can communicate and entangle with each other. Note that, in the limit of diverging exchange length $\lambda \to \infty$, the overall value of concurrence will vanish even though spins can entangle with each other over a long distance.

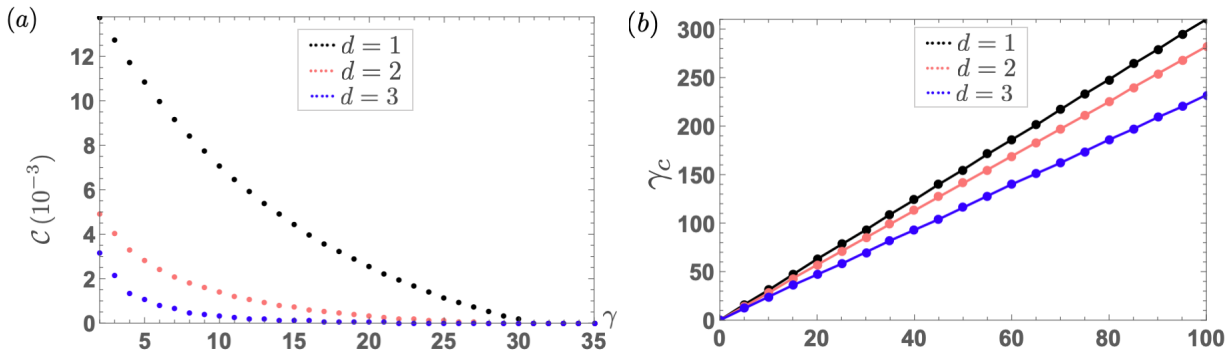

Figure 4.3: (a). Concurrence as a function of the distance γ between two spins in dimension $d = 1$, $d = 2$ and $d = 3$, respectively. The overall value of the concurrence will decrease as we increase the dimension of our system. In a given dimension, the concurrence is finite but will decrease as we increase the distance between these two spins within a critical distance γ_c, beyond which the concurrence vanishes. We have set $\lambda = 10$, $\eta = 0.5$ and $\hat{\mathbf{R}} = \hat{\mathbf{x}}$ in higher dimension. (b). Critical distance γ_c as a function of the correlation length λ, which can be fitted well with a linear relation. We have set $\eta = 0.5$.

4.4.6 Remarks

Let us modify the H_1 and H_2 to allow for more general squeezed coherent states,

$$\begin{aligned} H_1 &= \frac{K}{w}\sum_{\langle ij\rangle}\left[\cos\theta_1(S_i^xS_j^x - S_i^yS_j^y) + 2\sin\theta_1 S_i^xS_j^y\right], \\ H_2 &= -h\cos\theta_2\sum_i S_i^x - h\sin\theta_2\sum_i S_i^y. \end{aligned} \tag{4.27}$$

Compared with the original Hamiltonian (4.3), we have rotated the in-plane magnetic field and anisotropy by θ_2 and $\theta_1/2$, respectively, $H_1 \to U(\theta_1/2)H_1U(\theta_1/2)^\dagger$ and $H_2 \to U(\theta_2)H_2U(\theta_2)^\dagger$ with $U(\theta) = \prod_i e^{-i\theta S_i^z}$ being the rotation operator. Therefore, the entanglement should only depend on the physical angle $\theta_2 - \theta_1/2$. The ground state of this Hamiltonian, in the large exchange-coupling limit (so that we can neglect nonzero wavenumber modes [234]), is given by $|\psi\rangle = D(\alpha)S(\zeta)\,|0\rangle$ with $\zeta = re^{i\theta_1}$ and $\alpha = \sqrt{N_0}h[e^{i\theta_2}\cosh 2r -$

$e^{i(\theta_1-\theta_2)}\sinh 2r]/2\omega$, where $\omega=\sqrt{B^2-K^2}$ and r is determined by $\tanh 2r = K/B$. We recover what we have obtained before [see Eq. (4.10)] when $\theta_1=\theta_2=0$, as expected. We point out that, by taking this angle dependence into account, the behavior of the concurrence does not get modified qualitatively, since its angular variation is much smaller than the absolute value (see Fig. 4.4).

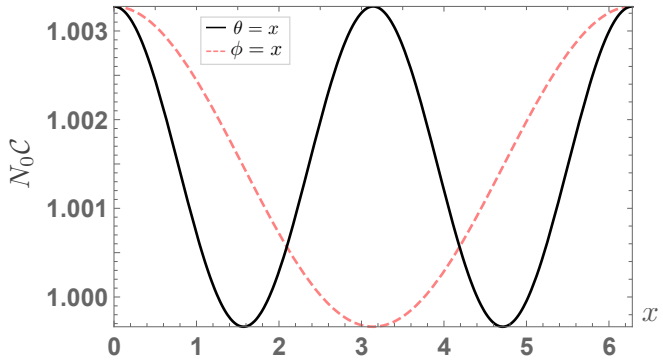

Figure 4.4: Concurrence as a function of one angle (setting the another angle to zero). For the pink dashed curve, we plot the concurrence as a function of the angle ϕ and set $\theta=0$. For the black solid curve, we plot the concurrence as a function of the angle θ and set $\phi=0$. We find that concurrence is periodic with period 2π in ϕ and π in θ. In both cases, we set $N_s=\sinh^2 4, N_c=9\times10^4$ and $N_0=10^8$.

The above Hamiltonian realizes the general squeezed coherent state $D(\alpha)S(\zeta)\left|0\right\rangle$ with $\alpha=|\alpha|e^{i\theta}$ and $\zeta=re^{i\phi}$ being complex-valued, where $D(\alpha)=e^{\alpha a^\dagger-\alpha^* a}$ is the displacement operator and $S(\zeta)=e^{[\zeta^* a^2-\zeta(a^\dagger)^2]/2}$ is the squeezing operator. The entanglement in such states only depends on $|\phi/2-\theta|$ instead of depending on these two angles separately. This is implied from the Fig. 4.1c where the only physical angle is $|\phi/2-\theta|$. More explicitly, we have $D(|\alpha|e^{i\theta})S(re^{i\phi})\left|0\right\rangle \to D(|\alpha|e^{i(\theta-\phi/2)})S(r)\left|0\right\rangle$ under a gauge transformation $a\to ae^{i\phi/2}$ which will not alter any physics of the system. We find numerically the concurrence

is periodic with period 2π in ϕ (the pink curve in Fig. 4.4) and π in θ (the black curve in Fig. 4.4). This is consistent with what we discussed above where $\zeta = re^{i\theta_1}$ and $\alpha = \sqrt{N_0}h[e^{i\theta_2}\cosh 2r - e^{i(\theta_1-\theta_2)}\sinh 2r]/2\omega$. Under the gauge transformation, we have the ground state $D(\alpha e^{-i\theta_1/2})S(r)\,|0\rangle$ where $\alpha e^{-i\theta_1/2} = \sqrt{N_0}h[e^{i(\theta_2-\theta_1/2)}\cosh 2r - e^{-i(\theta_2-\theta_1/2)}\sinh 2r]/2\omega$ and thus the entanglement only depends on the physical angle $\theta_2 - \theta_1/2$.

A few ways have recently been proposed to store and control quantum information in magnetic systems. For example, topological defects can be used as quantum information carriers [235] and two spins can be coupled via the spin-superfluid mode harbored by an antiferromagnetic domain wall [236]. Our discussion can be also applied to entangle two distant spin qubits (see Fig. 4.5). Let us consider the situation where two spin qubits are placed in the vicinity of a ferromagnetic insulator. Then, turn on the coupling $\tilde{J}$ between spin qubits and the insulator strong enough so that the two spins are entangled as if they are part of the magnetic insulator. Upon the sufficiently rapid turnoff of the coupling, we can obtain the isolated system of the two spin qubits that remain entangled.

4.5 Summary and Outlook

We have investigated the entanglement generation and entanglement control in a magnetic system. In the low temperature regime $T \ll J$, magnons form a general squeezed coherent state, which is a minimum uncertainty state with the quantum noise in one observable reduced below its vacuum level with the sacrifice of enhanced uncertainties in the another observable. We showed these squeezed states can be fully controlled by tuning applied external fields and in-plane anisotropies. Utilizing the entanglement of formation, or more specifically the concurrence, as a measure of entanglement, we illustrated that in the large exchange-coupling limit, a general squeezed coherent state, including its special case of a squeezed vacuum state, exhibits a high degree of entanglement between two arbitrary spins, as opposed to a coherent state which is not entangled. Therefore, a magnetic system can

serve as a resource for storing quantum information and processing quantum information, such as quantum teleportation, quantum network and quantum logical encoding.

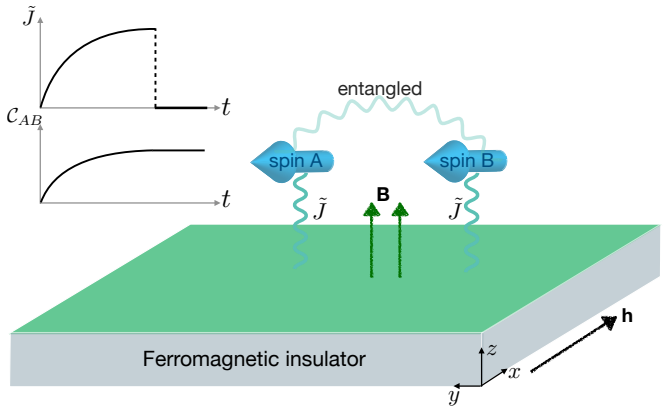

Figure 4.5: Spin A and B are placed above a ferromagnetic insulator subjected to magnetic fields **h**, **B** and anisotropies, which realizes the Hamiltonian that we discussed in Sec. 4.2. Turning on the coupling $\tilde{J}(t)$ between spins and the insulator adiabatically so that these spins behavior like a part of the insulator and thus the concurrence $\mathcal{C}_{AB}$ grows correspondingly. This entanglement remains even after the coupling $\tilde{J}$ is turned off so long as this turnoff process is rapid enough.

As temperature rises, we expect a thermal crossover from squeezing dominated regime to simply Fock-coherent regime discussed in Sec. 4.4A. A more systematic study of the temperature dependence of entanglement is left for a future work. In our analysis, we ignored the dipole-dipole interaction. For the uniform mode, the dipolar interactions would simply contribute a shape-dependent demagnetizing field, which can be absorbed into our anisotropy constants [237]. For the large-**k** modes, the effective anisotropies would become **k**-dependent, which would modify the quantitative details of our analysis. At this point, for simplicity, we are focusing on the materials where dominant anisotropies are crystalline. Two-mode squeezing arises naturally also in Heisenberg antiferromagnets [238], resulting

in a large entanglement between two antiparallel magnetic sublattices even in the absence of magnetic anisotropies. It may be interesting to study the spatial distribution of this entanglement as well as its possible tunability by external parameters.

In the thermodynamic limit, the entanglement attributable to the zero wavenumber mode vanishes due to the existence of the tight bound for symmetric sharing of entanglement $2/N_0$. Thus nonzero wavenumber modes should be taken into account and we studied the distance dependence of the concurrence. The existence of the tight bound is because we are considering the entanglement between two spins. How will the entanglement bound change if we consider the entanglement between two regions (that can contain many spins separately in general) instead of just two spins? This scaling property of the entanglement is well understood when the bipartite system is a gapped ground state of a local Hamiltonian and known as the entanglement area law [239]. Its constant correction is known as the topological entanglement entropy [240] characterizing many-body states that possess topological order. For a mixed state, however, as in our case, the scaling property is far from being well understood. Nevertheless, we would expect the upper bound of the entanglement to increase as we consider the entanglement between two regions in general, since the Hilbert space is larger compared with the two-spin case. Therefore, it can potentially store more quantum information, with the exact scaling behavior remaining to be explored.

CHAPTER 5

Bell-state generation for spin qubits via dissipative coupling

> "*Feynman's cryptic remark, 'no one is that much smarter ...,' to me, implies something Feynman kept emphasizing: that the key to his achievements was not anything magical but the right attitude, the focus on nature's reality, the focus on asking the right questions, the willingness to try (and to discard) unconventional answers, the sensitive ear for phoniness, self-deception, bombast, and conventional but unproven assumptions.*"
>
> *Philip Warren Anderson*

In this chapter, we show that a magnetically-active medium can act as a coupler for distant spin qubits for entanglement generation. While previous studies focus on the competition between coherent coupling and local relaxation, we reveal an effective coupling of dissipative nature in this work. We theoretically investigate the different dynamical regimes of the entanglement evolution in the presence of this dissipative coupling and demonstrate the advantage of its utilization as a route to generate steady entanglement and even Bell

state, insensitive to the initial state. Our work points to a new direction of the application of spintronic schemes in future quantum information technology.

5.1 Background

Entanglement between individually addressable qubits is the key to many quantum-information processes [95, 241]. The realization of qubits has been achieved in several cases, such as trapped atoms [242, 243, 244, 245], quantum dots [246, 247, 248], superconducting qubits [249], and nitrogen-vacancy (NV) centers [250], etc. For example, the NV qubit has a long coherence time and a good performance in the initialization and readout of spin states [251, 252, 253]. However, because the direct dipolar interactions between NVs extend only up to tens of nanometers, the generation of entanglement between distant qubits has been one of the main adversities in building a scalable platform for practical applications. A potential solution to this problem is to exploit hybrid quantum devices [254], where qubits are interfaced with a solid-state system [255, 256, 257, 258, 259, 260]. The latter, being long-range correlated, can act as a medium to induce an effective coherent coupling between the qubits, based on which certain two-qubit gates can be implemented [261, 262]. Meanwhile, the presence of a medium also enhances dissipation effects. To achieve a finite entanglement between qubits, the timescale set by the coherent coupling needs to be shorter than that of the local qubit relaxation. The competition between the two has thus been the focus of recent investigations [261, 262, 263, 93, 236, 264, 265, 266, 267].

Dissipation is not always detrimental to quantum effects. Entanglement generation in an open quantum system by environment engineering was first discussed in the context of quantum optics [268, 269]. It was shown formally that two qubits can be entangled by undergoing Markovian dissipative dynamics [270]. Various proposals have been made to realize this, mainly in quantum optical and electronic systems [271, 272, 273, 274, 275, 276, 277, 88, 278]. In addition, dissipation is intensely investigated as a resource for quantum

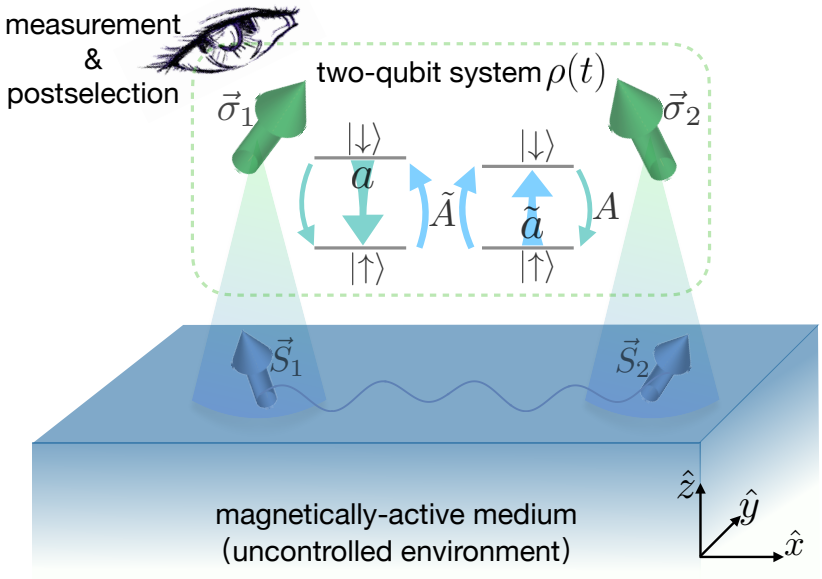

Figure 5.1: A system composed of two spin qubits is coupled with a magnetic environment, which induces local relaxations a, $\tilde{a}$, mediates dissipative couplings A, $\tilde{A}$, as well as coherent couplings between two qubits. The two qubits may achieve a stable entangled state with large enough A and $\tilde{A}$, and even a Bell state with the help of measurement and postselection.

error correction [279, 280, 281, 282, 283, 284] and other quantum information tasks [285, 286, 287, 288]. Non-Hermitian Hamiltonians, frequently invoked to handle dissipative effects in the Hamiltonian form, can exhibit exceptional points [289] that have been shown to be sweet spots to enhance entanglement [290, 291].

In this work, we discuss the dissipative coupling and entanglement generation induced by a generic noisy magnetic medium, in a hybrid quantum system sketched in Fig. 5.1. The qubits can be NVs or other isolated quantum defects and the medium is a generic solid-state system emitting magnetic field noise, which can arise from fluctuations of spin or pseudospin degrees of freedom [292]. Since many magnetic materials with different correlation properties are generally available, artificial design of the environment is not required as a first step, while spintronic engineering and tunability are promising for future studies.

To treat the induced coherent and dissipative couplings in a unified manner, we derive the

full master equation [86, 96] that determines the time evolution of the qubit entanglement. Specifically, two distinct types of dissipation are identified, bearing analogy to the local damping and the spin pumping-mediated viscosity in the classical spin dynamics [293]: One is the local relaxation, which originates in energy and information exchanges between a single qubit and the medium. The other is the dissipative coupling between the qubits induced by the correlated medium they both couple to, which appears to have gone underappreciated so far [261, 262, 93, 236, 264, 265, 266, 267] but manifests naturally in our treatment. While the former is detrimental to quantum entanglement, we show the latter can help to establish a steady entanglement between qubits, even in a pessimistic scenario where the coherent coupling is absent. The long-time behavior of the qubits exhibits a dynamic phase transition. When the dissipative coupling is comparable to the local relaxation, the Lindbladian evolution induced by the medium can result in sizable robust entanglement between the qubits. This can be achieved for qubit separation on a lengthscale dictated by the relevant excitations responsible for dissipation (such as magnons for a magnetically ordered medium). Furthermore, we can stabilize a Bell state in the time evolution governed by a non-Hermitian Hamiltonian when complemented by proper postselections [294, 295, 296, 297], where different dynamic phases are separated by an exceptional point.

5.2 Model

Let us consider an illustrative model consisting of two spin qubits weakly coupled to a magnet, with the following Hamiltonian:

$$H = H_{\rm S} + H_{\rm E} + H_{\rm SE}. \tag{5.1}$$

Here, $H_{\rm S} = -(\Delta_1\sigma_1^z + \Delta_2\sigma_2^z)/2$ is the Hamiltonian for the system with two qubits subjected to magnetic fields Δ_1 and Δ_2, respectively, along the z direction, $H_{\rm E}$ is an unspecified Hamiltonian of the medium as an environment for the system, and $H_{\rm SE} = \lambda(\vec{\sigma}_1 \cdot \vec{S}_1 + \vec{\sigma}_2 \cdot \vec{S}_2)$ describes the system-environment interaction with coupling strength λ, where $\vec{\sigma}_i$ stands

for the Pauli matrice of the ith qubit, and $\vec{S}_i$ for local spin density operators it couples to within the medium. Without loss of generality, we assume $\Delta_1 \geq \Delta_2 \geq 0$. We will consider an axially-symmetric environment $H_{\rm E}$ in spin space, while a generalization would be straightforward. It would also be straightforward to generalize the treatment to the dipolar coupling between the qubit and the medium [93, 236].

The following Lindblad master equation of the density matrix of the two-qubit system can be derived microscopically based on the Born and Markov approximations:

$$\frac{\mathrm{d}}{\mathrm{d}t}\rho = -i\big[H_{\rm S} + H_{\rm eff}, \rho\big] - \mathcal{L}[\rho]. \tag{5.2}$$

Leaving the derivation to the appendix A, we start with a phenomenological understanding of it on symmetry grounds. Here, $H_{\rm eff}$ is the medium-induced effective coherent coupling between qubits, participating in the unitary system evolution, while $\mathcal{L}[\rho]$ is the dissipative Lindbladian expanded in the usual form:

$$\mathcal{L}[\rho] = \sum_{nm} h_{nm}\big(\mathcal{O}_m^\dagger \mathcal{O}_n \rho + \rho \mathcal{O}_m^\dagger \mathcal{O}_n - 2\mathcal{O}_n \rho \mathcal{O}_m^\dagger\big), \tag{5.3}$$

where the coefficient matrix h is Hermitian and positive-semidefinite [86, 96], and $\mathcal{O} = (\sigma_1^-, \sigma_2^-, \sigma_1^+, \sigma_2^+, \sigma_1^z, \sigma_2^z)$ comprises qubit operators.

The most general form of $H_{\rm eff}$, allowed by the axial symmetry, is $H_{\rm eff} = J_z\sigma_1^z\sigma_2^z + J_\perp(\sigma_1^x\sigma_2^x + \sigma_1^y\sigma_2^y) + D\hat{z}\cdot\vec{\sigma}_1\times\vec{\sigma}_2$, summation of an XXZ model and a Dzyaloshinskii-Moriya (DM) interaction term. The DM interaction must vanish if, for example, the structure is invariant under π z-rotation (see Fig. 5.1 for the coordinate frame). These coherent couplings induced by the magnetic medium can build up a finite entanglement within the timescale inversely proportional to the coupling strength, if it is shorter than the timescale set by dissipation. In the limiting case of a full isotropicity in spin space and $\Delta_i = 0$, $H_{\rm eff}$ is further reduced to a Heisenberg form $H_{\rm eff} = J\vec{\sigma}_1\cdot\vec{\sigma}_2$ resembling the RKKY coupling [298]. These effective coupling parameters are all real constants determined by the Green's functions of the medium (see appendix A), as is consistent with previous results from Schrieffer-Wolff

transformation [261, 262, 93, 236, 264, 265, 266, 267]. Direct dipolar interaction between qubits is typically negligible, except for very small spacings.

In the dissipative Lindblad part, h is block diagonal due to the axial symmetry. In general terms, we have

$$h = \begin{pmatrix} \tilde{a} & \tilde{A} \\ \tilde{A}^* & \tilde{a} \end{pmatrix} \oplus \begin{pmatrix} a & A^* \\ A & a \end{pmatrix} \oplus \begin{pmatrix} d & \mathfrak{D} \\ \mathfrak{D}^* & d \end{pmatrix}, \tag{5.4}$$

where $\tilde{a}, a, d$ and $\tilde{A}, A, \mathfrak{D}$ are real and complex phenomenological parameters, respectively. These parameters represent three types of dissipative effects: a and $\tilde{a}$ are associated with local decay and the reverse process. They govern local relaxation of individual qubits, giving rise to the relaxation time T_1 and contribute to the decoherence time T_2 of a single qubit. In contrast, A and $\tilde{A}$ are related to cooperative decay and the reverse process involving both qubits, and are referred to as dissipative couplings, which depend on the distance between the two qubits. They are the focus of this work. d and $\mathfrak{D}$ are pure-dephasing parameters, originating from those terms in $H_{\rm SE}$ that commute with $H_{\rm S}$, namely $\lambda \sum_{i=1,2} \sigma_i^z S_i^z$. They only cause information but not energy exchange between the system and the medium, and in practice can be suppressed by dynamic decoupling [299, 300, 301, 302]. We thus neglect them in the following discussions. The Lindbladian (5.3) can then be brought into a diagonal form with four quantum-jump operators [303, 304]

$$\begin{aligned} J_1 &= \sqrt{\frac{\tilde{a} + |\tilde{A}|}{2}} \left(\sigma_1^- + \sigma_2^-\right), \quad J_2 = \sqrt{\frac{\tilde{a} - |\tilde{A}|}{2}} \left(\sigma_1^- - \sigma_2^-\right), \\ J_3 &= \sqrt{\frac{a + |A|}{2}} \left(\sigma_1^+ + \sigma_2^+\right), \quad J_4 = \sqrt{\frac{a - |A|}{2}} \left(\sigma_1^+ - \sigma_2^+\right), \end{aligned} \tag{5.5}$$

yielding

$$\underline{\mathcal{L}}[\rho] = \sum_{i=1}^{4} \mathcal{D}_{J_i}[\rho], \tag{5.6}$$

where the dissipator is defined as $\mathcal{D}_J[\rho] \equiv J^\dagger J \rho + \rho J^\dagger J - 2 J \rho J^\dagger$.

Microscopically, all parameters are given by the Green's functions of the medium in equilibrium (see appendix A), such that the fluctuation-dissipation theorem dictates that they are not independent: $\tilde{a} = e^{-\beta\Delta}a$ and $\tilde{A} = e^{-\beta\Delta}A$, where $\beta = 1/k_BT$ and $\Delta \equiv (\Delta_1 + \Delta_2)/2$. The zero temperature therefore corresponds to $\tilde{a} = \tilde{A} = 0$, where only the decay processes survive. Also, the thermodynamic stability of the magnetic medium imposes $a \geq |A|$ and $\tilde{a} \geq |\tilde{A}|$ (see appendix A), which ensures the matrix h is positive-semidefinite.

5.3 Dissipative coupling vs local relaxation

Let us now explore the entanglement evolution of two qubits focusing on the dissipative effects, by setting ourselves in a pessimistic situation where the induced coherent dynamics is absent:

$$\frac{\mathrm{d}}{\mathrm{d}t}\rho = -i[H_{\mathrm{S}}, \rho] - \underline{\mathcal{L}}[\rho]. \tag{5.7}$$

Here, we treat the scenario of zero temperature $\tilde{a} = \tilde{A} = 0$ analytically to demonstrate the effects of local relaxation and dissipative couplings. Numerical results for finite temperature are presented in the appendix A, which does not qualitatively change our conclusion below.

The qubits are initialized into a trivial product state, taking the example of $|\uparrow\downarrow\rangle$ for the sake of concreteness. We show the master equation (5.7) can be reduced to an equation for $x \equiv \mathrm{Re}\,\langle\uparrow\downarrow|\,\rho\,|\downarrow\uparrow\rangle$ (see appendix A):

$$\ddot{x} + 4a\dot{x} + 4\left(\delta^2 + a^2 - |A|^2\right)x = 0, \tag{5.8}$$

where $\delta \equiv (\Delta_1 - \Delta_2)/2$ is the local field asymmetry. This equation resembles a damped oscillator with complex characteristic frequencies

$$\omega_\pm = \pm 2\omega_0 - i2a, \tag{5.9}$$

where $\omega_0 \equiv \sqrt{\delta^2 - |A|^2}$. The real part gives the coherent beating of the density matrix elements, while the imaginary part reflects decoherence. The contribution from local relaxation

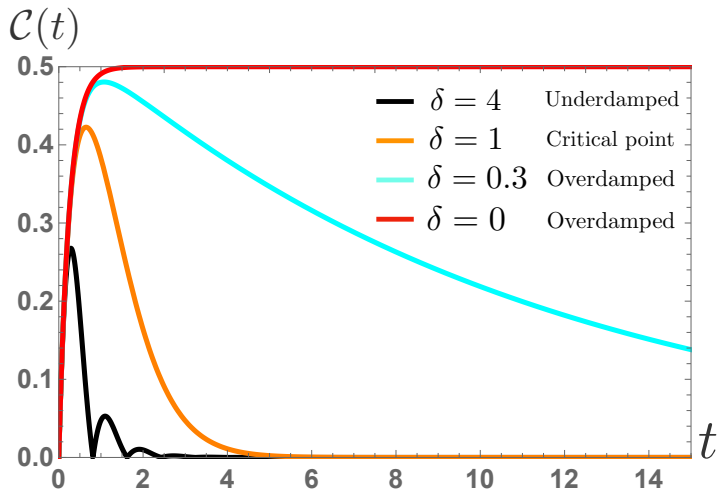

Figure 5.2: Concurrence of two qubits as a function of time, with initial state $|\uparrow\downarrow\rangle$, where we set both local dissipation a and dissipative coupling $|A|$ to be 1. The black curve corresponds to the underdamped quantum regime. The orange curve is at the critical point $\delta = 1$, where entanglement decays as $\mathcal{C}(t) \propto te^{-2at}$. The cyan, $\delta = 0.3$, and the red, $\delta = 0$, curves are in overdamped quantum regime, where the lifetime of entanglement is extended dramatically.

$-i2a$ leads to a decaying envelope factor e^{-2at} in the entanglement between two qubits (as detailed below), indicating its detrimental effect on quantum coherence as expected.

We identify three distinct parameter regimes for the quantum dynamics. In the underdamped regime, $\delta > |A|$, ω_0 is real valued. To quantify the time evolution of the entanglement between the two qubits, we calculate the *concurrence* [71] as a function of time: $\mathcal{C}(t) = 2e^{-2at}|A \sin \omega_0 t| \sqrt{\delta^2 - |A \cos \omega_0 t|^2}/\omega_0^2$. See Fig. 5.2. The entanglement oscillates with frequency $2\omega_0$ as the system decays rapidly to the ground state $|\uparrow\uparrow\rangle$ on the time scale $\tau = 1/2a$. At the critical point $\delta = |A|$, $\omega_0 = 0$, there is no oscillation. The concurrence evolves as $\mathcal{C}(t) \propto te^{-2at}$, where the final steady state is also $|\uparrow\uparrow\rangle$. As shown in Fig. 5.2, we have a larger transient-peak entanglement and the decay process is slowed down moderately compared with the underdamped regime.

In the overdamped regime, $\delta < |A|$, ω_0 becomes purely imaginary and $\omega_\pm = -2i(a \pm \kappa_0)$,

with $\kappa_0 = \sqrt{|A|^2 - \delta^2}$. The time-dependent concurrence is

$$\mathcal{C}(t) = 2e^{-2at}|A| \sinh \kappa_0 t \sqrt{|A \cosh \kappa_0 t|^2 - \delta^2}/\kappa_0^2. \tag{5.10}$$

In addition to a larger transient peak entanglement, the decay process has been slowed down dramatically. On a long time scale $t \gg 1/\kappa_0$, $\mathcal{C}(t) \propto e^{-2(a-\kappa_0)t}$. The entanglement can last for $\tau = 1/2(a - \kappa_0)$, which becomes $\tau = 1/2(a - |A|)$ when the two local fields are the same, $\delta = 0$. See Fig. 5.2. It is clear from this expression of the lifetime τ that the dissipative coupling A and the local relaxation a, though both originating from the qubits-magnet coupling, have opposite effects on the quantum entanglement in the nonunitary evolution. The local dissipation tends to destroy any quantum coherence whereas the dissipative coupling can be exploited to extend the lifetime of entanglement and even realize steady entangled states. With equal local fields $\delta = 0$, a finite entanglement can persist for a long time before eventually decaying to zero in the large dissipative coupling regime $|A| \lesssim a$. Based on their (greater) Green's function expressions [305] $2a = i\lambda^2 G^{>}_{S_1^+ S_1^-}(\Delta) = i\lambda^2 G^{>}_{S_2^+ S_2^-}(\Delta)$, $2A = i\lambda^2 G^{>}_{S_1^+ S_2^-}(\Delta)$, $|A| \lesssim a$ physically corresponds to the scenario with two qubits placed within a lengthscale dictated by the relevant excitations responsible for dissipation. For example, for qubits coupled to a magnetically ordered medium via processes of magnon absorption and emission, this lengthscale is set by the wavelength of the magnon at frequency Δ. Furthermore, the concurrence lifetime extends to infinity $\tau \to \infty$ when $|A|$ reaches its maximal allowed value $|A| = a$, and thus a steady entanglement is achieved, $\mathcal{C}(\infty) = 1/2$ for the final state

$$\rho_\infty = \left(|\uparrow\uparrow\rangle \langle\uparrow\uparrow| + |00\rangle \langle 00|\right)/2. \tag{5.11}$$

Noting that the singlet $|00\rangle$ cannot be evolved to a different state by the operative jump operators or the system Hamiltonian, it is a dark state—the system would stay in this pure state indefinitely. For this reason, a steady-state entanglement can also be reached at finite temperatures when $a = |A|$, $\tilde{a} = |\tilde{A}|$ (see appendix A), though with a smaller concurrence, since the singlet now has a smaller probability amplitude in the final state, with other states, such as $|\downarrow\downarrow\rangle$, mixed in.

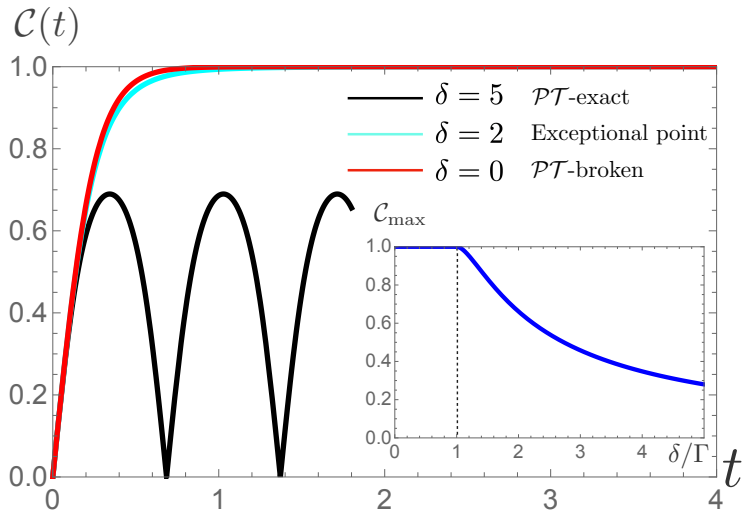

Figure 5.3: Concurrence of qubits as a function of time with initial state $|\uparrow\downarrow\rangle$ under continuous measurements and postselections. We set $\Gamma = 2$. The black curve $\delta = 5$ is in the $\mathcal{PT}$-exact regime, where entanglement oscillates and its maximal value is less than 1. At the exceptional point (cyan curve), there is no oscillation and its maximal value is 1. In $\mathcal{PT}$-broken regime (red curve), entanglement is $\mathcal{C}(t) = \tanh 2\Gamma t$. The inset shows the maximal concurrence as a function of δ/Γ.

We stress that the above critical point and the associated transition from underdamped to overdamped regime result from the dissipative couplings, which are the main focus of this article. We next show how to generate Bell states by exploiting this dissipative coupling, when combined with proper measurements and postselections.

5.4 Non-Hermitian Hamiltonian scheme

Let us turn to the evolution of qubits under measurements (see Fig. 5.1), which is often invoked to perform feedback and conditional control as a valuable resource in controlling open quantum systems [70, 306, 307, 308, 309]. To this end, we rewrite the master equation (5.7)

in the following form:

$$\frac{\mathrm{d}}{\mathrm{d}t}\rho = -i\big[\underline{H}_{\rm eff},\rho\big] + 2\sum_{i=1}^{4} J_i\rho J_i^\dagger, \tag{5.12}$$

where

$$\underline{H}_{\rm eff} = H_S - i\sum_i J_i^\dagger J_i, \tag{5.13}$$

is a non-Hermitian Hamiltonian. Correspondingly, the commutator should now be understood as $\big[\underline{H}_{\rm eff},\rho\big] \equiv \underline{H}_{\rm eff}\rho - \rho\underline{H}_{\rm eff}^\dagger = [H_S,\rho] - i\{\sum_i J_i^\dagger J_i,\rho\}$. By subjecting the two qubits to continuous measurements of the absolute value of their total spin z component $\underline{\sigma}^z = \sigma_1^z + \sigma_2^z$ and subsequently conditioning the postselection on zero outcomes, we can effectively forbid all quantum jump processes (5.5), as $[J_i,\underline{\sigma}^z] \neq 0$. This monitored dynamics of the two-qubit system formally eliminates the last term in Eq. (5.12) and reduces quantum dynamics to a non-Hermitian Hamiltonian form in the $\underline{\sigma}^z = 0$ subspace [289], $d\rho/dt = -i\big[\underline{H}_{\rm eff},\rho\big]$, whose integration is appropriately normalized to give [310]:

$$\rho(t) = \frac{e^{-i\underline{H}_{\rm eff}t}\rho_0 e^{i\underline{H}_{\rm eff}^\dagger t}}{\mathrm{tr}\left(e^{-i\underline{H}_{\rm eff}t}\rho_0 e^{i\underline{H}_{\rm eff}^\dagger t}\right)}, \tag{5.14}$$

in terms of the initial qubits state ρ_0. Since the effective Hamiltonian (5.13) conserves the quantum number $\underline{\sigma}^z$ $[\underline{H}_{\rm eff},\underline{\sigma}^z] = 0$, the subspace $\mathcal{H}$ spanned by $\{|\uparrow\downarrow\rangle, |\downarrow\uparrow\rangle\}$ is closed under time evolution. The eigenkets of $\underline{H}_{\rm eff}$ in $\mathcal{H}$ are

$$\begin{aligned} |s\rangle &= e^{i\varphi}\sin\theta\,|\uparrow\downarrow\rangle + \cos\theta\,|\downarrow\uparrow\rangle\,, \\ |a\rangle &= -\cos\theta\,|\uparrow\downarrow\rangle + e^{i\varphi}\sin\theta\,|\downarrow\uparrow\rangle\,, \end{aligned} \tag{5.15}$$

with associated eigenenergies $E_{s(a)} = \mp\omega - i(a+\tilde{a})$. Here, θ and φ are determined by the sum of dissipative couplings $\Gamma = |A| + |\tilde{A}|$ and the local field asymmetry δ: For $\delta \geq \Gamma$, $\omega = \sqrt{\delta^2-\Gamma^2}$, $\cos\theta \equiv \Gamma/\sqrt{|\omega+\delta|^2+\Gamma^2}$ and $e^{i\varphi}\sin\theta \equiv -i(\omega+\delta)/\sqrt{|\omega+\delta|^2+\Gamma^2}$; for $\delta < \Gamma$, the principal value is taken for $\omega = i\kappa = i\sqrt{\Gamma^2-\delta^2}$.

Bell state generation.—We now show that steady Bell states can be generated based on the monitored dynamics governed by $\underline{H}_{\rm eff}$ (5.13), focusing on the two-qubit dynamics in the

subspace $\mathcal{H}$, which applies to zero and finite temperatures. Similarly to the unmonitored scenario, we can identify three distinct parameter regimes: parity-time ($\mathcal{PT}$) symmetry broken regime, $\delta < \Gamma$, the exceptional point, $\delta = \Gamma$, and $\mathcal{PT}$-exact regime, $\delta > \Gamma$ [311, 312, 313].

In the $\mathcal{PT}$-broken regime, eigenvalues E_a and E_s are purely imaginary with $\mathrm{Im}\, E_a > \mathrm{Im}\, E_s$. Thus the probability in the eigenmode $|a\rangle$ ($|s\rangle$) grows (decays) in time, and all probability eventually flows into the eigenmode $|a\rangle$. For an arbitrary initial state $\rho_0 = \sum_{i,j=\{a,s\}} p_{ij} |i\rangle\langle j|$, one can analytically solve for $\rho(t)$ according to Eq. (5.14):

$$\rho(t)=\frac{p_{aa}e^{2\kappa t}|a\rangle\langle a|+p_{as}\,|a\rangle\langle s|+p_{sa}\,|s\rangle\langle a|+p_{ss}e^{-2\kappa t}\,|s\rangle\langle s|}{p_{aa}e^{2\kappa t}+p_{as}\,\langle s|a\rangle+p_{sa}\,\langle a|s\rangle+p_{ss}e^{-2\kappa t}}, \tag{5.16}$$

which ultimately evolves into $|a\rangle\langle a|$ when $t \gg 1/2\kappa$, irrespective of the initial state as long as $p_{aa} \neq 0$. Since $|a\rangle = \left(|\uparrow\downarrow\rangle + e^{i\tilde{\varphi}}\,|\downarrow\uparrow\rangle\right)/\sqrt{2}$ is a maximally entangled state, where $e^{i\tilde{\varphi}} = (-\kappa + i\delta)/\Gamma$ in the $\mathcal{PT}$-broken regime, the two qubits eventually reach the maximal concurrence. As an illustrative example, we evaluate the time-dependent concurrence, with initial state $|\uparrow\downarrow\rangle$ and equal local fields $\delta = 0$, $\mathcal{C}(t) = \tanh 2\Gamma t$, as shown in Fig. 5.3. In practice, the entanglement-growth rate 2κ needs to be larger than the postselection rate ($\sim$ the rate of leaking out of the subspace $\mathcal{H}$ of our interest) $2(a + \tilde{a} - \kappa)$ for the system to settle into the Bell state. The optimal scenario is when $\delta = 0$, $|A| = a$, and $|\tilde{A}| = \tilde{a}$, the same as that in the overdamped quantum regime without postselection.

At the exceptional point, $\underline{H}_{\mathrm{eff}}$ is nondiagonalizable, since the eigenstates $|a\rangle$ and $|s\rangle$ coalesce into $\left(|\uparrow\downarrow\rangle + i\,|\downarrow\uparrow\rangle\right)/\sqrt{2}$. The two qubits will gradually evolve into this sole state where they are maximally entangled. For example, starting with a trivial state $|\uparrow\downarrow\rangle$, the concurrence $\mathcal{C}(t) = 2\Gamma t\sqrt{1+\Gamma^2t^2}/(1+2\Gamma^2t^2)$, algebraically approaching 1. See Fig. 5.3.

In the $\mathcal{PT}$-exact regime, the eigenenergies E_s and E_a have nonzero real parts. The amplitudes of eigenmodes $|s\rangle$ and $|a\rangle$ keep oscillating without reaching a steady state, hence no steady entanglement. The frequency of entanglement oscillation is 2ω, as shown in Fig. 5.3. The maximal entanglement one can achieve is $\mathcal{C}_{\max}(\eta) = \sqrt{2-1/\eta^2}/\eta$, with $\eta = \delta/\Gamma$, which

is less than 1. Notably, the second derivative of $\mathcal{C}_{\max}$ is discontinuous across the exceptional point ($\eta = 1$), reflecting a dynamic phase transition (see Fig. 5.3).

This discussion, again, highlights the role of the nonlocal dissipative couplings in realizing an exceptional point in the dynamics, further triggering an entanglement transition in the long-time steady state. In the large nonlocal dissipative coupling regime, we achieve steady Bell states.

5.5 Discussion and outlook

We remark that the non-Hermitian Hamiltonian scheme is precise when the rate of measurements is infinite. As this rate approaches zero, we recover the full Lindblad dynamics. It could be intriguing to explore, within our framework, possible dynamic phase transitions or crossovers induced by finite-rate measurements.

In our case, the possible forms of induced coherent interactions and quantum jump operators are determined by the axial symmetry of the generic media. This may render a general guidance in studying the dynamics of hybrid quantum systems in the presence of other classes of symmetries, especially their long-time entanglement behavior.

The theoretical framework developed here provides a good starting point for further studies on the relationship between the entanglement dynamics and thermodynamic properties of the medium. One may be able to manipulate and control entanglement via engineering the magnetic medium [89, 314, 88, 315, 316], enabled by recent progress in the field of spintronics [113, 14, 11]. It is especially interesting to look into media with anisotropies, which have been shown to be good entanglement reservoirs [23, 123, 317]. By extending our equilibrium Green's function treatment to allow for a quasi-equilibrium spin chemical potential, we may be able to study the scenario with a spintronically pumped medium, where local relaxations and dissipative couplings are tunable.

Lastly, NV centers have been demonstrated as good quantum probes of local fields and

noise [318]. Here, we propose to extend this to nonlocal characteristics. For example, one may use it to detect quantum phase transitions and steady exotic phases that are characterized by nonlocal quantum correlations.

APPENDIX A

Appendices to Chapter 5

A.1 Microscopic derivation of the master equation of the two qubits

In this section, we derive the master equation for the two-qubit system interacting with a magnetic medium. The system Hamiltonian is $H_S = -(\Delta_1\sigma_1^z + \Delta_2\sigma_2^z)/2$ and the interaction Hamiltonian is $H_{\rm SE} = \lambda\sum_{\alpha=1,2}\left(\sigma_\alpha^+ S_\alpha^- + \sigma_\alpha^- S_\alpha^+ + \sigma_\alpha^z S_\alpha^z\right)$, where $\sigma^\pm = (\sigma^x \pm i\sigma^y)/2$, $S^\pm = S^x \pm iS^y$, and $\vec{S}_\alpha$ is the local spin density operator within the magnetic medium. To apply the formalism (1.189) directly, we shift the total Hamiltonian by $-\lambda\langle S^z\rangle(\sigma_1^z + \sigma_2^z)$, which is equivalent to making $S_\alpha^z \to \tilde{S}_\alpha^z = S_\alpha^z - \langle S^z\rangle$, such that $\langle\tilde{S}_\alpha^z\rangle = 0$. Here and in what follows, we refer to $\tilde{S}^z$ as S^z for notational convenience. Without loss of generality, we assume $\Delta_1 \geq \Delta_2 \geq 0$. Substituting

$$H_{\rm SE}(-\tau) = \lambda\sum_\alpha\Big[\sigma_\alpha^+ S_\alpha^-(-\tau)e^{i\Delta_\alpha\tau} + \sigma_\alpha^- S_\alpha^+(-\tau)e^{-i\Delta_\alpha\tau} + \sigma_\alpha^z S^z(-\tau)\Big], \tag{A.1}$$

into Eq. (1.190) yields an explicit expression

$$\begin{aligned}&\langle S_\alpha^- S_\beta^+(-\tau)\rangle e^{-i\Delta_\beta\tau}(\sigma_\alpha^+\sigma_\beta^-\rho - \sigma_\beta^-\rho\sigma_\alpha^+) + \langle S_\alpha^+ S_\beta^-(-\tau)\rangle e^{i\Delta_\beta\tau}(\sigma_\alpha^-\sigma_\beta^+\rho - \sigma_\beta^+\rho\sigma_\alpha^-)\\ &\quad + \langle S_\alpha^z S_\beta^z(-\tau)(\sigma_\alpha^z\sigma_\beta^z\rho - \sigma_\beta^z\rho\sigma_\alpha^z) + \text{H.c.},\end{aligned} \tag{A.2}$$

where Einstein summation is implied over $\alpha, \beta = 1, 2$. The effect of the above terms on the evolution of the density matrix can be grouped under two operators, an effective Hamiltonian and a Lindbladian, in the master equation (1.189):

$$\dot{\rho} = -i[H_S + H_{\rm eff}, \rho] - \mathcal{L}[\rho]. \tag{A.3}$$

The medium-induced effective qubit-qubit interaction is

$$H_{\text{eff}} = J_1^{\alpha\beta}\sigma_\alpha^+\sigma_\beta^- + J_2^{\alpha\beta}\sigma_\alpha^-\sigma_\beta^+ + J_z^{\alpha\beta}\sigma_\alpha^z\sigma_\beta^z, \tag{A.4}$$

and the Lindbladian superoperator is given by

$$\begin{aligned}\mathcal{L}[\rho] = &\tilde{A}_{\alpha\beta}(\sigma_\alpha^+\sigma_\beta^-\rho + \rho\sigma_\alpha^+\sigma_\beta^- - 2\sigma_\beta^-\rho\sigma_\alpha^+)\\ &+ A_{\alpha\beta}(\sigma_\alpha^-\sigma_\beta^+\rho + \rho\sigma_\alpha^-\sigma_\beta^+ - 2\sigma_\beta^+\rho\sigma_\alpha^-)\\ &+ D_{\alpha\beta}(\sigma_\alpha^z\sigma_\beta^z\rho + \rho\sigma_\alpha^z\sigma_\beta^z - 2\sigma_\beta^z\rho\sigma_\alpha^z).\end{aligned} \tag{A.5}$$

A.1.1 Coherent couplings

The coherent couplings in Eq. (A.4) can all be related to the real part of retarded Green's functions of the magnetic medium. Firstly,

$$J_z^{\alpha\beta} = -\frac{i\lambda^2}{2}\int_0^\infty \left[\langle S_\alpha^z S_\beta^z(-\tau)\rangle - \langle S_\alpha^z(-\tau)S_\beta^z\rangle\right]d\tau = -\frac{i\lambda^2}{2}\int_0^\infty \langle[S_\alpha^z(\tau), S_\beta^z]\rangle d\tau = \lambda^2\frac{G^R_{S_\alpha^z S_\beta^z}(0)}{2} \tag{A.6}$$

is real valued by definition. Here we have adopted the standard definition for the retarded Green's function $G^R_{AB}(\omega) = -i\int_0^\infty\langle[A(\tau), B]\rangle e^{i\omega\tau}d\tau$. Secondly,

$$\begin{aligned}J_1^{\alpha\beta} &= \frac{-i}{2}\int_0^\infty \left[\langle S_\alpha^- S_\beta^+(-\tau)\rangle e^{-i\Delta_\beta\tau} - \langle S_\alpha^-(-\tau)S_\beta^+\rangle e^{i\Delta_\alpha\tau}\right]d\tau,\\ J_2^{\alpha\beta} &= \frac{-i}{2}\int_0^\infty \left[\langle S_\alpha^+ S_\beta^-(-\tau)\rangle e^{i\Delta_\beta\tau} - \langle S_\alpha^+(-\tau)S_\beta^-\rangle e^{-i\Delta_\alpha\tau}\right]d\tau.\end{aligned} \tag{A.7}$$

Therefore,

$$
\begin{aligned}
J_1^{\alpha\beta}\sigma_\alpha^+\sigma_\beta^- + J_2^{\alpha\beta}\sigma_\alpha^-\sigma_\beta^+ =& \sum_{\alpha\neq\beta}(J_1^{\alpha\beta}+J_2^{\beta\alpha})\sigma_\alpha^+\sigma_\beta^- + \sum_\alpha \left(J_1^{\alpha\alpha}\sigma_\alpha^+\sigma_\alpha^- + J_2^{\alpha\alpha}\sigma_\alpha^-\sigma_\alpha^+\right) \\
=& \sum_{\alpha\neq\beta}(J_1^{\alpha\beta}+J_2^{\beta\alpha})\sigma_\alpha^+\sigma_\beta^- + \sum_\alpha \frac{J_1^{\alpha\alpha}-J_2^{\alpha\alpha}}{2}[\sigma_\alpha^+,\sigma_\alpha^-] \\
&+ \sum_\alpha \frac{J_1^{\alpha\alpha}+J_2^{\alpha\alpha}}{2}(\sigma_\alpha^+\sigma_\alpha^- + \sigma_\alpha^-\sigma_\alpha^+) \\
=& \lambda^2 \frac{G^R_{S_2^+S_1^-}(\Delta_1)+G^A_{S_2^+S_1^-}(\Delta_2)}{2}\sigma_1^+\sigma_2^- + \text{H.c.} \\
&+ \sum_\alpha \left[\lambda^2 \text{Im}\int_0^\infty \langle\{S_\alpha^-(\tau),S_\alpha^+\}\rangle e^{-i\Delta_\alpha\tau}d\tau\right]\frac{\sigma_\alpha^z}{2} \\
&+ \lambda^2\sum_\alpha \frac{G^R_{S_\alpha^+S_\alpha^-}(\Delta_\alpha)+G^A_{S_\alpha^+S_\alpha^-}(\Delta_\alpha)}{4} \\
\approx& \left[\lambda^2 \mathfrak{Re} G^R_{S_2^+S_1^-}(\Delta)\sigma_1^+\sigma_2^- + \text{H.c.}\right] + H_{\text{Lamb}} + \text{const.}
\end{aligned}
\tag{A.8}
$$

is Hermitian. In the last step, we have approximated $\Delta_1 \approx \Delta_2 \approx \Delta \equiv (\Delta_1+\Delta_2)/2$. This is sufficient for the discussion of medium-induced dynamics (both coherent and dissipative), since we are primarily interested in the scenario with $\Delta_1 \approx \Delta_2$, on the scale set by induced interqubit coupling $\propto \lambda^2$. The expansion with respect to $\Delta_1 - \Delta_2$ would thus induce higher-order corrections. Here, we have denoted $\mathfrak{Re}\, G^R_{A,B}(t,t') \equiv \left[G^R_{A,B}(t,t') + G^A_{A,B}(t,t')\right]/2$, noting this "real" part becomes the ordinary real part $\mathfrak{Re} \to \text{Re}$ when $A = B^\dagger$. The Lamb shift $H_{\text{Lamb}} \propto \sigma^z$, which we have already encountered at the level of single-spin dynamics Eq. (1.194), can be absorbed into the bare system Hamiltonian H_S, and we drop the real constant term in later discussions. We therefore obtain the total induced effective interaction Hamiltonian (A.4):

$$
H_{\text{eff}}/\lambda^2 = \left[\mathfrak{Re} G^R_{S_2^+S_1^-}(\Delta)\,\sigma_1^+\sigma_2^- + \text{H.c.}\right] + \frac{G^R_{S_1^zS_2^z}(0)+G^R_{S_2^zS_1^z}(0)}{2}\,\sigma_1^z\sigma_2^z, \tag{A.9}
$$

which is a close analogy to the RKKY interactions induced by itinerant electrons between magnetic moments in a metal.

A.1.2 Lindbladian

We now derive Eq. (4-6) in the main text to identify the two types of dissipation—local relaxation and dissipative couplings—expressed in terms of greater or less Green's functions of the magnet. They are related to the imaginary part of retarded Green's functions via *the fluctuation-dissipation theorem*. The coefficients in the Lindbladian operator (A.5) are given by

$$\begin{aligned}
\tilde{A}_{\alpha\beta} &= \frac{\lambda^2}{2}\int_0^\infty \left[\langle S_\alpha^- S_\beta^+(-\tau)\rangle e^{-i\Delta_\beta\tau} + \langle S_\alpha^-(-\tau)S_\beta^+\rangle e^{i\Delta_\alpha\tau}\right]d\tau \\
&\approx \frac{\lambda^2}{2}\int_{-\infty}^\infty \langle S_\alpha^- S_\beta^+(\tau)\rangle e^{i\Delta\tau}d\tau \equiv \frac{i\lambda^2 G^<_{S_\beta^+ S_\alpha^-}(\Delta)}{2}, \\
A_{\alpha\beta} &= \frac{\lambda^2}{2}\int_0^\infty \left[\langle S_\alpha^+ S_\beta^-(-\tau)\rangle e^{i\Delta_\beta\tau} + \langle S_\alpha^+(-\tau)S_\beta^-\rangle e^{-i\Delta_\alpha\tau}\right]d\tau \\
&\approx \frac{\lambda^2}{2}\int_{-\infty}^\infty \langle S_\alpha^+(\tau) S_\beta^-\rangle e^{i\Delta\tau}d\tau \equiv \frac{i\lambda^2 G^>_{S_\alpha^+ S_\beta^-}(\Delta)}{2}, \\
D_{\alpha\beta} &= \frac{\lambda^2}{2}\int_0^\infty \left[\langle S_\alpha^z S_\beta^z(-\tau)\rangle + \langle S_\alpha^z(-\tau)S_\beta^z\rangle\right]d\tau \\
&= \frac{\lambda^2}{2}\int_{-\infty}^\infty \langle S_\alpha^z(\tau) S_\beta^z\rangle d\tau \equiv \frac{i\lambda^2 G^>_{S_\alpha^z S_\beta^z}(0)}{2} = \frac{i\lambda^2 G^<_{S_\beta^z S_\alpha^z}(0)}{2},
\end{aligned} \tag{A.10}$$

where the approximation $\Delta_1 \approx \Delta_2 \approx \Delta$ is again taken in the first two equations. It can be directly observed that $A_{\alpha\alpha}, \tilde{A}_{\alpha\alpha}, D_{\alpha\alpha}$ are real valued, and $A_{12}^* = A_{21}, \tilde{A}_{12}^* = \tilde{A}_{21}, D_{12}^* = D_{21}$. We introduce the following parameters to clean up the notation: $a \equiv A_{11} = A_{22}$, $\tilde{a} \equiv \tilde{A}_{11} = \tilde{A}_{22}$, $d \equiv D_{11} = D_{22}$, assuming the medium is homogeneous, and $A \equiv A_{12}$, $\tilde{A} \equiv \tilde{A}_{21}$, and $\mathfrak{D} \equiv D_{12}$. We then can write the Lindbladian (A.5) into the form of

$$\mathcal{L}[\rho] = \sum_{nm} h_{nm}\left(\mathcal{O}_m^\dagger \mathcal{O}_n \rho + \rho \mathcal{O}_m^\dagger \mathcal{O}_n - 2\mathcal{O}_n \rho \mathcal{O}_m^\dagger\right), \tag{A.11}$$

with the column vector $\mathcal{O}$=$(\sigma_1^-, \sigma_2^-, \sigma_1^+, \sigma_2^+, \sigma_1^z, \sigma_2^z)^T$ and

$$h = \begin{pmatrix} \tilde{a} & \tilde{A} \\ \tilde{A}^* & \tilde{a} \end{pmatrix} \oplus \begin{pmatrix} a & A^* \\ A & a \end{pmatrix} \oplus \begin{pmatrix} d & \mathfrak{D} \\ \mathfrak{D}^* & d \end{pmatrix}, \tag{A.12}$$

where $\oplus$ denotes the direct sum of matrices. Originated from those terms in $H_{\rm SE}$ that commute with $H_{\rm S}$, namely $\lambda\sum_{i=1,2}\sigma_i^z S_i^z$, the terms in Eq. (A.11) with parameters d and

$\mathfrak{D}$ are pure dephasing. They only cause information but not energy exchange between the system and the medium, and can be suppressed by dynamic decoupling in practice.

In the following discussion, we focus on the four remaining dissipative parameters: a, $\tilde{a}$, A, and $\tilde{A}$. For one qubit, for example, by setting $\alpha, \beta = 1$, we reproduce the results of the single qubit scenario, where the local relaxation of individual qubits is governed by the parameters a and $\tilde{a}$. They correspond to $B^<$ and $B^>$ in Eq. (1.196) associated with local decay and the reverse process. The parameters A and $\tilde{A}$ apply to a system with multiple qubits and are related to cooperative decay and the reverse process, which we refer to as dissipative couplings. These parameters are not independent of each other: $\tilde{a} = e^{-\beta\Delta}a$ and $\tilde{A} = e^{-\beta\Delta}A$, in thermal equilibrium, where $\beta = 1/k_BT$. In particular at $T = 0$, the decay processes $\tilde{a} = \tilde{A} = 0$.

The coefficient matrix h is diagonalizable in general and Eq. (A.11) can take the form of

$$\underline{\mathcal{L}}[\rho] = \sum_{i=1}^{4} \mathcal{D}_{J_i}[\rho], \tag{A.13}$$

with the dissipator $\mathcal{D}_J[\rho] \equiv J^\dagger J\rho + \rho J^\dagger J - 2J\rho J^\dagger$. There are four quantum-jump operators (as we have neglected the dephasing effects):

$$\begin{aligned} J_1 &= \sqrt{\frac{\tilde{a} + |\tilde{A}|}{2}} \left(\sigma_1^- + \sigma_2^-\right), J_2 = \sqrt{\frac{\tilde{a} - |\tilde{A}|}{2}} \left(\sigma_1^- - \sigma_2^-\right), \\ J_3 &= \sqrt{\frac{a + |A|}{2}} \left(\sigma_1^+ + \sigma_2^+\right), J_4 = \sqrt{\frac{a - |A|}{2}} \left(\sigma_1^+ - \sigma_2^+\right). \end{aligned} \tag{A.14}$$

A.2 Symmetry-dictated possible forms of the induced effective Hamiltonian

For a two-qubit system with the axial symmetry around z axis in spin space, the interaction between the two qubits in general takes the form of

$$H_{\text{eff}} = J_z\sigma_1^z\sigma_2^z + J_\perp(\sigma_1^x\sigma_2^x + \sigma_1^y\sigma_2^y) + D\hat{z} \cdot \vec{\sigma}_1 \times \vec{\sigma}_2, \tag{A.15}$$

which is an XXZ model allowing a Dzyaloshinskii-Moriya (DM) interaction. Further, adding a mirror symmetry with respect to the xz-plane (containing both qubit sites) dictates a vanishing D. In the fully isotropic limit, the interaction becomes Heisenberg $H_{\text{eff}} \propto \vec{\sigma}_1 \cdot \vec{\sigma}_2$.

Denoting $\mathfrak{Re}G^R_{S_2^+S_1^-}(\Delta) = g_1 + ig_2$,

$$\mathfrak{Re}G^R_{S_2^+S_1^-}(\Delta)\,\sigma_1^+\sigma_2^- + \text{H.c.} = \frac{g_1}{2}(\sigma_1^x\sigma_2^x + \sigma_1^y\sigma_2^y) + \frac{g_2}{2}\hat{z}\cdot\vec{\sigma}_1\times\vec{\sigma}_2. \tag{A.16}$$

We precisely obtain the effective two-qubit Hamiltonian (A.9) in the general form (A.15), where we identify $J_z = [G^R_{S_1^zS_2^z}(0) + G^R_{S_2^zS_1^z}(0)]/2$, $J_\perp = g_1/2$, and $D = g_2/2$, setting the irrelevant overall factor $\lambda = 1$. For the explicit expressions:

$$\begin{aligned} g_1 &= \frac{G^R_{S_2^+S_1^-}(\Delta) + G^R_{S_1^+S_2^-}(\Delta) + G^A_{S_2^+S_1^-}(\Delta) + G^A_{S_1^+S_2^-}(\Delta)}{4}, \\ g_2 &= \frac{G^R_{S_2^+S_1^-}(\Delta) - G^R_{S_1^+S_2^-}(\Delta) + G^A_{S_2^+S_1^-}(\Delta) - G^A_{S_1^+S_2^-}(\Delta)}{4i}. \end{aligned} \tag{A.17}$$

Both g_1 and g_2 are real, g_1 is nonzero in general, and g_2 is finite only when the xz-reflection symmetry as well as the π x- or z-rotation symmetries are broken in the system. The DM interaction, similar to other coherent couplings, can build up finite entanglement between the two qubits. For example, taking $H_{\text{DM}} = D\hat{z}\cdot\vec{\sigma}_1\times\vec{\sigma}_2$ and initial state $|\uparrow\downarrow\rangle$, we obtain for the state of the two qubits: $|\psi(t)\rangle = \cos(2Dt)\,|\uparrow\downarrow\rangle - \sin(2Dt)\,|\downarrow\uparrow\rangle$, which has concurrence $\mathcal{C}_{\text{DM}}(t) = |\sin(4Dt)|$. Therefore, we can conclude that the entanglement would oscillate between 0 and 1 with frequency $8D$. We typically require the timescale $1/D$ to be shorter than the timescale set by the dissipation such that we can make use of the entanglement before it decays to zero.

In the SU(2)-symmetric limit and setting $\Delta \to 0$, the effective Hamiltonian (A.9) simplifies into the Heisenberg form, as expected:

$$\begin{aligned} H_{\text{eff}} &= \frac{G^R_{S_2^xS_1^x}(0) + G^R_{S_1^xS_2^x}(0)}{2}\,(\sigma_1^x\sigma_2^x + \sigma_1^y\sigma_2^y) + \frac{G^R_{S_2^zS_1^z}(0) + G^R_{S_1^zS_2^z}(0)}{2}\,\sigma_1^z\sigma_2^z \\ &= \frac{G^R_{S_2^xS_1^x}(0) + G^R_{S_1^xS_2^x}(0)}{2}\,\vec{\sigma}_1\cdot\vec{\sigma}_2. \end{aligned} \tag{A.18}$$

If, furthermore, the qubit sites can be exchanged under a spatial symmetry, then $H_{\text{eff}} = G^R_{S_1^xS_2^x}(0)\,\vec{\sigma}_1\cdot\vec{\sigma}_2$.

A.3 Thermodynamic stability of the magnetic medium

The positive semidefinite evolution governed by Eq. (2) in the main text requires the constraints:

$$a \geq |A|, \qquad \tilde{a} \geq |\tilde{A}|. \tag{A.19}$$

In this section, we show that they are naturally guaranteed by the thermodynamic stability of the magnetic medium. In the following, we show $\tilde{a} \geq |\tilde{A}|$, namely $iG^<_{S^+S^-}(\omega) \geq \left|iG^<_{S_2^+S_1^-}(\omega)\right|$, and $a \geq |A|$ can be proved in the same spirit. Let us consider the response in the magnetic medium to the following perturbation:

$$H'(t) = \sum_{\alpha=1,2} \left(\lambda_\alpha e^{-i\omega t} S_\alpha^- + \text{H.c.}\right) = \lambda_1 e^{-i\omega t} S_1^- + \lambda_1^* e^{i\omega t} S_1^+ + \lambda_2 e^{-i\omega t} S_2^- + \lambda_2^* e^{i\omega t} S_2^+. \tag{A.20}$$

The corresponding linear-response dissipation power can be calculated via

$$\begin{aligned}
P \equiv & \frac{\mathrm{d}}{\mathrm{d}t}\langle H(t)\rangle = \langle \partial_t H'(t)\rangle = -i\omega e^{-i\omega t} \sum_{\alpha=1,2} \lambda_\alpha \langle S_\alpha^-\rangle + i\omega e^{i\omega t} \sum_{\alpha=1,2} \lambda_\alpha^* \langle S_\alpha^+\rangle \\
= & -i\omega \sum_{\alpha,\beta} \lambda_\alpha \frac{\lambda_\beta^*}{\hbar} G^A_{S_\beta^+ S_\alpha^-}(\omega) + i\omega \sum_{\alpha,\beta} \lambda_\alpha^* \frac{\lambda_\beta}{\hbar} G^R_{S_\alpha^+ S_\beta^-}(\omega) \\
= & i\omega \frac{|\lambda_1|^2}{\hbar}\left[G^R_{S_1^+S_1^-}(\omega) - G^A_{S_1^+S_1^-}(\omega)\right] + i\omega \frac{|\lambda_2|^2}{\hbar}\left[G^R_{S_2^+S_2^-}(\omega) - G^A_{S_2^+S_2^-}(\omega)\right] \\
& + i\omega \frac{\lambda_1\lambda_2^*}{\hbar}\left[G^R_{S_2^+S_1^-}(\omega) - G^A_{S_2^+S_1^-}(\omega)\right] + i\omega \frac{\lambda_1^*\lambda_2}{\hbar}\left[G^R_{S_1^+S_2^-}(\omega) - G^A_{S_1^+S_2^-}(\omega)\right] \\
= & i\omega \frac{|\lambda_1|^2}{\hbar} 2i\,\mathrm{Im}\, G^R_{S_1^+S_1^-}(\omega) + i\omega \frac{|\lambda_2|^2}{\hbar} 2i\,\mathrm{Im}\, G^R_{S_2^+S_2^-}(\omega) + i\omega \frac{\lambda_1\lambda_2^*}{\hbar} 2i\,\mathfrak{Im}\, G^R_{S_2^+S_1^-}(\omega) \\
& + i\omega \frac{\lambda_1^*\lambda_2}{\hbar} 2i\,\mathfrak{Im}\, G^R_{S_1^+S_2^-}(\omega) \\
= & \frac{\omega|\lambda_1|^2}{\hbar} A_{S_1^+S_1^-}(\omega) + \frac{\omega|\lambda_2|^2}{\hbar} A_{S_2^+S_2^-}(\omega) + \frac{\omega\lambda_1\lambda_2^*}{\hbar} A_{S_2^+S_1^-}(\omega) + \frac{\omega\lambda_1^*\lambda_2}{\hbar} A_{S_1^+S_2^-}(\omega),
\end{aligned} \tag{A.21}$$

where we have used the Kubo formula in

$$\langle S_\alpha^+\rangle = \sum_\beta \frac{\lambda_\beta}{\hbar} e^{-i\omega t} G^R_{S_\alpha^+ S_\beta^-}(\omega), \quad \text{and} \quad \langle S_\alpha^-\rangle = \langle S_\alpha^+\rangle^* = \sum_{\beta=1,2} \frac{\lambda_\beta^*}{\hbar} e^{i\omega t} G^A_{S_\beta^+ S_\alpha^-}(\omega), \tag{A.22}$$

Here, $\mathfrak{Im} G^R_{AB}(\omega) = \left[G^R_{AB}(\omega) - G^A_{AB}(\omega)\right]/2i$ is the "imaginary" part of the retarded Green's function, which is reduced to the ordinary imaginary part for $A = B^\dagger$, and $A_{A,B}(\omega) \equiv$

$-2\mathfrak{Im}G^R_{A,B}(\omega) = 2\mathfrak{Im}G^A_{A,B}(\omega)$ is the *spectral density*. Invoking the fluctuation-dissipation theorem $G^<_{A,B}(\omega) = iA_{A,B}(\omega)/(1-e^{\beta\hbar\omega})$, the requirement of the equilibrium stability $P \geq 0$ imposes

$$|\lambda_1|^2\tilde{a} + |\lambda_2|^2\tilde{a} + \lambda_1\lambda_2^*\tilde{A} + \lambda_1^*\lambda_2\tilde{A}^* \geq 0 \Longleftrightarrow \tilde{a} \geq \frac{-\lambda_1\lambda_2^*\tilde{A} + \text{c.c.}}{|\lambda_1|^2 + |\lambda_2|^2} \tag{A.23}$$

for all frequency ω and arbitrary values of λ_1 and λ_2. We therefore obtain

$$\tilde{a} \geq \text{Max}\left\{\frac{-\lambda_1\lambda_2^*A_{12} + \text{c.c.}}{|\lambda_1|^2 + |\lambda_2|^2}\right\} = |\tilde{A}|. \tag{A.24}$$

A.4 Full entanglement dynamics

In this section, we study the full entanglement dynamics governed by the master equation:

$$\frac{\mathrm{d}}{\mathrm{d}t}\rho = -i[H_S, \rho] - \underline{\mathcal{L}}[\rho]. \tag{A.25}$$

Taking a trivial product state $|\uparrow\downarrow\rangle$ as the initial state, the time evolution of all the relevant elements of $\rho(t)$ is given by

$$\begin{aligned}
\dot{\rho}_{00} &= -4\tilde{a}\rho_{00} + 2a(\rho_{11}+\rho_{22}) + 2|A|(\rho_{12}+\rho_{21}),\\
\dot{\rho}_{11} &= -2(a+\tilde{a})\rho_{11} + 2\tilde{a}\rho_{00} + 2a\rho_{33} - \Gamma(\rho_{12}+\rho_{21}),\\
\dot{\rho}_{22} &= -2(a+\tilde{a})\rho_{22} + 2\tilde{a}\rho_{00} + 2a\rho_{33} - \Gamma(\rho_{12}+\rho_{21}),\\
\dot{\rho}_{33} &= -4a\rho_{33} + 2\tilde{a}(\rho_{11}+\rho_{22}) + 2|\tilde{A}|(\rho_{12}+\rho_{21}),\\
\dot{\rho}_{12} &= 2\big[i\delta - (a+\tilde{a})\big]\rho_{12} - \Gamma(\rho_{11}+\rho_{22}) + 2|\tilde{A}|\rho_{00} + 2|A|\rho_{33}\\
\dot{\rho}_{21} &= 2\big[-i\delta - (a+\tilde{a})\big]\rho_{21} - \Gamma(\rho_{11}+\rho_{22}) + 2|\tilde{A}|\rho_{00} + 2|A|\rho_{33},
\end{aligned} \tag{A.26}$$

with net dissipative coupling $\Gamma \equiv |A| + |\tilde{A}|$ and local field asymmetry $\delta \equiv (\Delta_1 - \Delta_2)/2$. In general, we need to solve the above six coupled differential equations with the constraint $\mathrm{tr}\,\rho(t) = 1$.

A.4.0.1 Derivation of Eq. (8) in the main text

At zero temperature, $\tilde{a} = |\tilde{A}| = 0$, the coupled differential equations above reduce to a single equation for $x \equiv \mathrm{Re}\,\langle\uparrow\downarrow|\,\rho\,|\downarrow\uparrow\rangle$:

$$\ddot{x} + 4a\dot{x} + 4(\delta^2 + a^2 - |A|^2)x = 0, \tag{A.27}$$

with the initial condition $\rho(t=0) = |\uparrow\downarrow\rangle\,\langle\uparrow\downarrow|$. We first note that, in our situation, $\rho_{33}(t) = 0$ since $\rho_{33}(0) = 0$ and the differential equation for ρ_{33} is reduced to $\dot{\rho}_{33} = -4a\rho_{33}$. We also have

$$\dot{\rho}_{11} - \dot{\rho}_{22} = -2a(\rho_{11} - \rho_{22}) \longrightarrow \rho_{11}(t) = \rho_{22}(t) + e^{-2at}. \tag{A.28}$$

Invoking $\mathrm{tr}\,\rho = 1$, we obtain

$$\rho_{00}(t) = 1 - 2\rho_{22}(t) - e^{-2at}. \tag{A.29}$$

Choosing the free parameters to be ρ_{22}, ρ_{12} and ρ_{21} we denote $\rho_{22} = h(t)$ and $\rho_{12} = x(t) + iy(t)$. We can reduce Eq. (A.26) to three coupled differential equations:

$$\begin{aligned} \dot{h} &= -2ah - 2|A|x \\ \dot{x} &= -2\delta y - 2ax - 2|A|h - |A|e^{-2at}, \\ \dot{y} &= 2\delta x - 2ay, \end{aligned} \tag{A.30}$$

and equivalently,

$$\begin{aligned} \frac{\mathrm{d}(he^{2at})}{\mathrm{d}t} &= -2|A|xe^{2at}, \\ \frac{\mathrm{d}(ye^{2at})}{\mathrm{d}t} &= 2\delta xe^{2at}, \\ \frac{\mathrm{d}(xe^{2at})}{\mathrm{d}t} &= -2\delta(ye^{2at}) - 2|A|(he^{2at}) - |A|, \end{aligned} \tag{A.31}$$

from which we obtain

$$\ddot{x} + 4a\dot{x} + 4(\delta^2 + a^2 - |A|^2)x = 0. \tag{A.32}$$

Starting from this equation, one can solve for the density matrix $\rho(t)$ and thus the

concurrence $\mathcal{C}(t)$ between the two qubits. For example, in the overdamped regime,

$$x(t) = -\frac{|A|}{2\kappa_0}\sinh 2\kappa_0 t\, e^{-2at},\;\; y(t) = -\frac{|A|\delta e^{-2at}}{\kappa_0^2}\sinh^2\kappa_0 t,\;\; h(t) = \frac{|A|^2 e^{-2at}}{\kappa_0^2}\sinh^2\kappa_0 t. \tag{A.33}$$

where $\kappa_0 = \sqrt{|A|^2 - \delta^2}$. In this case, the full density matrix reads

$$\rho(t) = \begin{bmatrix} 1 - \frac{|A|^2\cosh 2\kappa_0 t - \delta^2}{\kappa_0^2}e^{-2at} & 0 & 0 & 0 \\ 0 & \frac{|A|^2\cosh^2\kappa_0 t - \delta^2}{\kappa_0^2}e^{-2at} & x(t)+iy(t) & 0 \\ 0 & x(t)-iy(t) & \frac{|A|^2}{\kappa_0^2}e^{-2at}\sinh^2\kappa_0 t & 0 \\ 0 & 0 & 0 & 0 \end{bmatrix}. \tag{A.34}$$

The concurrence is thus given by

$$\mathcal{C}(t) = 2|x(t)+y(t)| = 2|A|\sinh\kappa_0 t e^{-2at}\sqrt{|A\cosh\kappa_0 t|^2 - \delta^2}/\kappa_0^2. \tag{A.35}$$

A time scale for the decay of the entanglement can be extracted:

$$1/\tau = 2a - 2\kappa_0 = 2\big(a - \sqrt{|A|^2 - \delta^2}\big) \geq 0. \tag{A.36}$$

Therefore, to extend the lifetime of the entanglement, one can reduce the local field asymmetry δ or increase the dissipative coupling $|A|$. As one particular interesting scenario, equal local fields $\delta = 0$ yields the lifetime of entanglement $\tau = 1/(a - |A|)$, indicating that local relaxation a and the dissipative coupling $|A|$ have perfectly opposite effects on entanglement. The maximal allowed value of $|A| = a$ can be reached when the spatial separation of the two qubits are short enough. This length scale is set by the relevant excitations responsible for dissipation, such as magnons in a magnetic medium. When $|A| = a$, we can achieve a steady entanglement with concurrence $\mathcal{C}(\infty) = 1/2$, with the final steady state being

$$\rho(\infty) = \frac{|00\rangle\langle 00| + |\uparrow\uparrow\rangle\langle\uparrow\uparrow|}{2}, \tag{A.37}$$

where $|00\rangle$ is the singlet state and also a dark state in this situation. This can be seen from the effects of jump operators acting on the state: out of the four quantum-jump operators (A.14), only J_3 is operative and $J_3|00\rangle = 0$.

A.4.0.2 Dynamics of entanglement at finite temperature

At finite temperatures, both local relaxations a, $\tilde{a}$ and dissipative couplings $|A|$, $|\tilde{A}|$ are non-vanishing. There is no analytic solution to the master equation (A.26). Instead, numerical solutions are studied. Similar to the conclusion we have drawn in the main text, we find that increasing the dissipative couplings $|A|$ and $|\tilde{A}|$ could extend the lifetime of entanglement dramatically and steady entanglement can be obtained when $|A|$ and $|\tilde{A}|$ reach their allowed maximal values $|A| = a$ and $|\tilde{A}| = \tilde{a}$. Recall that these four parameters are not independent: $a/\tilde{a} = |A|/|\tilde{A}| = e^{\beta\Delta}$, where $\beta = 1/k_B T$.

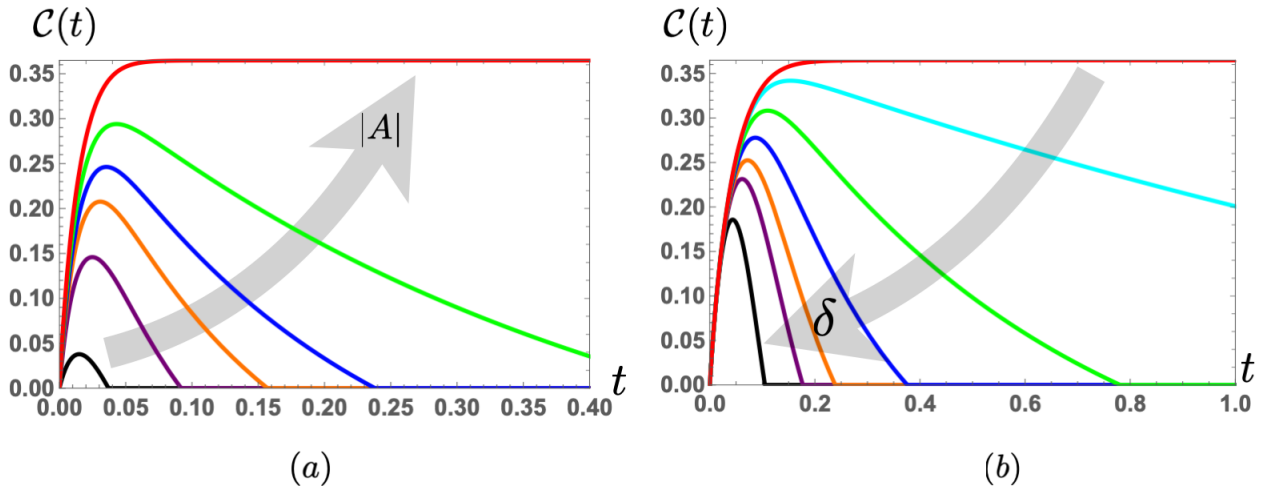

Figure A.1: Concurrence as a function of time for the initial state $|\uparrow\downarrow\rangle$ at a finite temperature. (a). The local relaxations are set to $a = 30$, $\tilde{a} = 3$, and the local fields are equal $\delta = 0$. Curves of different colors are plotted with an increasing dissipative coupling $|A| \to \{20, 25, 27, 28, 29, 30\}$ along the direction of the gray arrow. The two dissipative couplings are related by $|A|/|\tilde{A}| = a/\tilde{a} = 10$. When $|A|$ reaches its maximal values 30 (and $|\tilde{A}| = |A|/10$ reaches its maximal allowed value 3), we achieve steady entanglement (red curve). (b). The concurrence for $a = |A| = 10, \tilde{a} = |\tilde{A}| = 1$ and varying $\delta \to \{0, 2, 4, 6, 8, 10, 16\}$.

As shown in Fig. A.1 (a), with the local relaxations fixed $a = 30$, $\tilde{a} = 3$ and the local fields set to be equal $\delta = 0$, the lifetime of entanglement increases as we increase the dissi-

pative coupling $|A|$ (and also $|\tilde{A}|$ accordingly). A steady entanglement with the concurrence being around 0.35 is achieved when the dissipative couplings $|A|$ and $|\tilde{A}|$ reach their allowed maximal values $|A| = a = 30$ and $|\tilde{A}| = \tilde{a} = 3$. In Fig. A.1 (b), we fix all dissipation parameters and vary δ. The lifetime of entanglement decreases as δ increases, which is also consistent with the trend at zero temperature [see Eq. (A.36)].

In Fig. A.2, we show that a finite steady-state entanglement can always be achieved when the dissipative couplings reach their allowed maximal values $|A| = a$ and $|\tilde{A}| = \tilde{a}$, with $\delta = 0$. When $|A| = |\tilde{A}|$, the final steady entanglement is zero and the final density matrix is $\rho_\infty = \mathbb{I}_{4\times4}/4$. This corresponds to infinite temperature. The entire x axis with $|\tilde{A}| = 0$ shows the zero-temperature case, where the steady concurrence is $1/2$ as we have discussed before. A steady entanglement smaller than $1/2$ persists for finite temperatures, in the regime $|\tilde{A}|/|A| = e^{-\beta\Delta} < 1$, while $|\tilde{A}| > |A|$ is unphysical. At finite temperatures, the density matrix of the steady state is also partly made of the singlet state, which remains a dark state as $J_1 |00\rangle = J_3 |00\rangle = 0$ (only these two jump operators are operative).

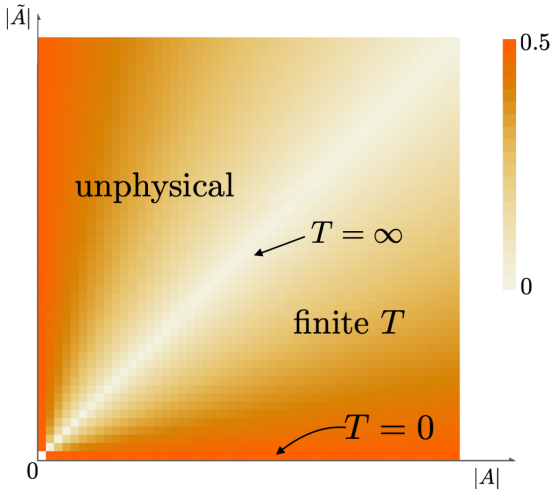

Figure A.2: Final steady-state concurrence as a function of dissipative couplings $|A|$ and $|\tilde{A}|$, assuming they are at their maximal values $|A| = a$ and $|\tilde{A}| = \tilde{a}$, and $\delta = 0$. The initial state is $|\uparrow\downarrow\rangle$.

REFERENCES

[1] Hector Ochoa and Yaroslav Tserkovnyak. Quantum skyrmionics. *Int. J. Mod. Phys. B*, 33(21):1930005, 2020/02/04 2019.

[2] Wanjun Jiang, Pramey Upadhyaya, Wei Zhang, Guoqiang Yu, M. Benjamin Jungfleisch, Frank Y. Fradin, John E. Pearson, Yaroslav Tserkovnyak, Kang L. Wang, Olle Heinonen, Suzanne G. E. te Velthuis, and Axel Hoffmann. Blowing magnetic skyrmion bubbles. *Science*, 349(6245):283–286, 2015.

[3] Albert Fert, Vincent Cros, and João Sampaio. Skyrmions on the track. *Nature Nanotechnology*, 8(3):152–156, 2013.

[4] Joel E. Moore. The birth of topological insulators. *Nature*, 464:194 EP –, 03 2010.

[5] Xiao-Liang Qi and Shou-Cheng Zhang. Topological insulators and superconductors. *Rev. Mod. Phys.*, 83:1057–1110, Oct 2011.

[6] M. Z. Hasan and C. L. Kane. Colloquium: Topological insulators. *Rev. Mod. Phys.*, 82:3045–3067, Nov 2010.

[7] Jiadong Zang, Vincent Cros, and Axel Hoffmann, editors. *Topology in Magnetism*. Springer International Publishing, 2018.

[8] Jung Hoon Han. *Skyrmions in Condensed Matter*. Springer International Publishing, 2017.

[9] Igor Žutić, Jaroslav Fabian, and S. Das Sarma. Spintronics: Fundamentals and applications. *Rev. Mod. Phys.*, 76:323–410, Apr 2004.

[10] V. Baltz, A. Manchon, M. Tsoi, T. Moriyama, T. Ono, and Y. Tserkovnyak. Antiferromagnetic spintronics. *Rev. Mod. Phys.*, 90:015005, Feb 2018.

[11] A. Avsar, H. Ochoa, F. Guinea, B. Özyilmaz, B. J. van Wees, and I. J. Vera-Marun. Colloquium: Spintronics in graphene and other two-dimensional materials. *Rev. Mod. Phys.*, 92:021003, Jun 2020.

[12] A. V. Chumak, V. I. Vasyuchka, A. A. Serga, and B. Hillebrands. Magnon spintronics. *Nature Physics*, 11(6):453–461, 2015.

[13] So Takei and Yaroslav Tserkovnyak. Superfluid spin transport through easy-plane ferromagnetic insulators. *Phys. Rev. Lett.*, 112:227201, Jun 2014.

[14] Yaroslav Tserkovnyak. Perspective: (beyond) spin transport in insulators. *Journal of Applied Physics*, 124(19):190901, 2018.

[15] Ji Zou, Se Kwon Kim, and Yaroslav Tserkovnyak. Topological transport of vorticity in heisenberg magnets. *Phys. Rev. B*, 99:180402, May 2019.

[16] Yaroslav Tserkovnyak and Ji Zou. Quantum hydrodynamics of vorticity. *Phys. Rev. Research*, 1:033071, Nov 2019.

[17] Yaroslav Tserkovnyak, Ji Zou, Se Kwon Kim, and So Takei. Quantum hydrodynamics of spin winding. *Phys. Rev. B*, 102:224433, Dec 2020.

[18] Dalton Jones, Ji Zou, Shu Zhang, and Yaroslav Tserkovnyak. Energy storage in magnetic textures driven by vorticity flow. *Phys. Rev. B*, 102:140411, Oct 2020.

[19] Ji Zou, Shu Zhang, and Yaroslav Tserkovnyak. Topological transport of deconfined hedgehogs in magnets. *Phys. Rev. Lett.*, 125:267201, Dec 2020.

[20] Mostafa Tanhayi Ahari, Shu Zhang, Ji Zou, and Yaroslav Tserkovnyak. Biasing topological charge injection in topological matter. *Phys. Rev. B*, 104:L201401, Nov 2021.

[21] Bei Zeng, Xie Chen, Duan-Lu Zhou, and Xiao-Gang Wen. *Quantum Information Meets Quantum Matter: From Quantum Entanglement to Topological Phases of Many-Body Systems*. Springer, March 29, 2019.

[22] H.Y. Yuan, Yunshan Cao, Akashdeep Kamra, Rembert A. Duine, and Peng Yan. Quantum magnonics: When magnon spintronics meets quantum information science. *Physics Reports*, 965:1–74, 2022.

[23] Ji Zou, Se Kwon Kim, and Yaroslav Tserkovnyak. Tuning entanglement by squeezing magnons in anisotropic magnets. *Phys. Rev. B*, 101:014416, Jan 2020.

[24] Andrii V. Chumak, Alexander A. Serga, and Burkard Hillebrands. Magnon transistor for all-magnon data processing. *Nature Communications*, 5(1):4700, 2014.

[25] K. Vogt, F. Y. Fradin, J. E. Pearson, T. Sebastian, S. D. Bader, B. Hillebrands, A. Hoffmann, and H. Schultheiss. Realization of a spin-wave multiplexer. *Nature Communications*, 5(1):3727, 2014.

[26] Ji Zou, Shu Zhang, and Yaroslav Tserkovnyak. Bell-state generation for spin qubits via dissipative coupling. page arXiv:2108.07365, August 2021.

[27] Mikio Nakahara. *Geometry, Topology and Physics*. CRC Press, 2 edition edition, June 6, 2003.

[28] Kenji Ueno, Koji Shiga, Shigeyuki Morita, and Toshikazu Sunada. *A Mathematical Gift, I: The Interplay Between Topology, Functions, Geometry, and Algebra*. American Mathematical Society, 2005.

[29] Steven Weinberg. *Gravitation and Cosmology: Principles and Applications of the General Theory of Relativity*. Wiley, 1972.

[30] Steven M. Girvin and Kun Yang. *Modern Condensed Matter Physics*. Cambridge University Press, 1st edition edition, 2019.

[31] Claudio Chamon, Mark O. Goerbig, Roderich Moessner, and Leticia F. Cugliandolo, editors. *Topological Aspects of Condensed Matter Physics: Lecture Notes of the Les Houches Summer School*. Oxford University Press, 2017.

[32] Sidney Coleman. *Aspects of Symmetry: Selected Erice Lectures*. Cambridge University Press, 1988.

[33] A. A. Belavin and A. M. Polyakov. Metastable states of two-dimensional isotropic ferromagnets. *Soviet Journal of Experimental and Theoretical Physics Letters*, 22:245, November 1975.

[34] Michael Stone and Paul Goldbart. *Mathematics for Physics: A Guided Tour for Graduate Students*. Cambridge University Press, 2009.

[35] M. Shifman. *Advanced Topics in Quantum Field Theory: A Lecture Course*. Cambridge University Press, February 20, 2012.

[36] Horatiu Nastase. *Classical Field Theory*. Cambridge, 2019.

[37] L. D. Faddeev. Some comments on the many-dimensional solitons. *Letters in Mathematical Physics*, 1(4):289–293, 1976.

[38] T. H. R. Skyrme and Basil Ferdinand Jamieson Schonland. A non-linear field theory. *Proceedings of the Royal Society of London. Series A. Mathematical and Physical Sciences*, 260(1300):127–138, 1961.

[39] Egor Babaev, Ludvig D. Faddeev, and Antti J. Niemi. Hidden symmetry and knot solitons in a charged two-condensate bose system. *Phys. Rev. B*, 65:100512, Feb 2002.

[40] Tin-Lun Ho. Spinor bose condensates in optical traps. *Phys. Rev. Lett.*, 81:742–745, Jul 1998.

[41] Yuki Kawaguchi, Muneto Nitta, and Masahito Ueda. Knots in a spinor bose-einstein condensate. *Phys. Rev. Lett.*, 100:180403, May 2008.

[42] Bryan Gin-ge Chen, Paul J. Ackerman, Gareth P. Alexander, Randall D. Kamien, and Ivan I. Smalyukh. Generating the hopf fibration experimentally in nematic liquid crystals. *Phys. Rev. Lett.*, 110:237801, Jun 2013.

[43] Paul Sutcliffe. Skyrmion knots in frustrated magnets. *Phys. Rev. Lett.*, 118:247203, Jun 2017.

[44] Yizhou Liu, Roger K. Lake, and Jiadong Zang. Binding a hopfion in a chiral magnet nanodisk. *Physical Review B*, 98(17):174437–, 11 2018.

[45] X. S. Wang, A. Qaiumzadeh, and A. Brataas. Current-driven dynamics of magnetic hopfions. *Phys. Rev. Lett.*, 123:147203, Sep 2019.

[46] Yizhou Liu, Wentao Hou, Xiufeng Han, and Jiadong Zang. Three-dimensional dynamics of a magnetic hopfion driven by spin transfer torque. *Phys. Rev. Lett.*, 124:127204, Mar 2020.

[47] Noah Kent, Neal Reynolds, David Raftrey, Ian T. G. Campbell, Selven Virasawmy, Scott Dhuey, Rajesh V. Chopdekar, Aurelio Hierro-Rodriguez, Andrea Sorrentino, Eva Pereiro, Salvador Ferrer, Frances Hellman, Paul Sutcliffe, and Peter Fischer. Creation and observation of hopfions in magnetic multilayer systems. *Nature Communications*, 12(1):1562, 2021.

[48] J H C Whitehead. An expression of hopf's invariant as an integral. *Proceedings of the National Academy of Sciences of the United States of America*, 33(5):117–123, 05 1947.

[49] Frank Wilczek and A. Zee. Linking numbers, spin, and statistics of solitons. *Physical Review Letters*, 51(25):2250–2252, 12 1983.

[50] Yong-Shi Wu and A. Zee. Comments on the hopf lagrangian and fractional statistics of solitons. *Physics Letters B*, 147(4):325–329, 1984.

[51] Alexander Altland and Ben D. Simons. *Condensed matter field theory*. Cambridge University Press, 2nd edition, 2010.

[52] Eduardo Fradkin. *Field Theories of Condensed Matter Physics*. Cambridge University Press, 2 edition edition, 2013.

[53] Ramamurti Shankar. *Quantum Field Theory and Condensed Matter*. Cambridge, 2017.

[54] Alexander G. Abanov. Topology, geometry and quantum interference in condensed matter physics. *arXiv e-prints*, page arXiv:1708.07192, August 2017.

[55] E. B. Sonin. Spin currents and spin superfluidity. *Advances in Physics*, 59(3):181–255, 05 2010.

[56] Se Kwon Kim, So Takei, and Yaroslav Tserkovnyak. Topological spin transport by brownian diffusion of domain walls. *Phys. Rev. B*, 92:220409, Dec 2015.

[57] Se Kwon Kim and Yaroslav Tserkovnyak. Topological effects on quantum phase slips in superfluid spin transport. *Phys. Rev. Lett.*, 116:127201, Mar 2016.

[58] Se Kwon Kim, So Takei, and Yaroslav Tserkovnyak. Thermally activated phase slips in superfluid spin transport in magnetic wires. *Phys. Rev. B*, 93:020402, Jan 2016.

[59] Tom Banks. *Modern Quantum Field Theory: A Concise Introduction*. Cambridge University Press, 2008.

[60] A. Zee. *Quantum Field Theory in a Nutshell*. Princeton University Press, 2 edition, 2010.

[61] Sayak Dasgupta and Ji Zou. Zeeman term for the néel vector in a two sublattice antiferromagnet. *Phys. Rev. B*, 104:064415, Aug 2021.

[62] I Affleck. Quantum spin chains and the haldane gap. *Journal of Physics: Condensed Matter*, 1(19):3047–3072, may 1989.

[63] F.D.M. Haldane. Continuum dynamics of the 1-d heisenberg antiferromagnet: Identification with the o(3) nonlinear sigma model. *Physics Letters A*, 93(9):464–468, 1983.

[64] F. D. M. Haldane. Nonlinear field theory of large-spin heisenberg antiferromagnets: Semiclassically quantized solitons of the one-dimensional easy-axis néel state. *Phys. Rev. Lett.*, 50:1153–1156, Apr 1983.

[65] F. D. M. Haldane. O(3) nonlinear σ model and the topological distinction between integer- and half-integer-spin antiferromagnets in two dimensions. *Phys. Rev. Lett.*, 61:1029–1032, Aug 1988.

[66] Luigi Amico, Rosario Fazio, Andreas Osterloh, and Vlatko Vedral. Entanglement in many-body systems. *Rev. Mod. Phys.*, 80:517–576, May 2008.

[67] Martin B. Plbnio and Shashank Virmani. An introduction to entanglement measures. *Quantum Info. Comput.*, 7(1):1–51, January 2007.

[68] Vlatko Vedral. *Introduction to Quantum Information Science*. Oxford University Pres, 2013.

[69] Gerardo Adesso. Entanglement of Gaussian states. *arXiv e-prints*, pages quant–ph/0702069, February 2007.

[70] Howard M. Wiseman. *Quantum Measurement and Control*. Cambridge University Press, 2009.

[71] William K. Wootters. Entanglement of formation of an arbitrary state of two qubits. *Phys. Rev. Lett.*, 80:2245–2248, Mar 1998.

[72] Barbara M. Terhal and Karl Gerd H. Vollbrecht. Entanglement of formation for isotropic states. *Phys. Rev. Lett.*, 85:2625–2628, Sep 2000.

[73] K. G. H. Vollbrecht and R. F. Werner. Entanglement measures under symmetry. *Phys. Rev. A*, 64:062307, Nov 2001.

[74] J. Eisert, T. Felbinger, P. Papadopoulos, M. B. Plenio, and M. Wilkens. Classical information and distillable entanglement. *Phys. Rev. Lett.*, 84:1611–1614, Feb 2000.

[75] G. Giedke, M. M. Wolf, O. Krüger, R. F. Werner, and J. I. Cirac. Entanglement of formation for symmetric gaussian states. *Phys. Rev. Lett.*, 91:107901, Sep 2003.

[76] H. Y. Yuan and Man-Hong Yung. Thermodynamic entanglement of magnonic condensates. *Phys. Rev. B*, 97:060405, Feb 2018.

[77] Charles H. Bennett, David P. DiVincenzo, John A. Smolin, and William K. Wootters. Mixed-state entanglement and quantum error correction. *Phys. Rev. A*, 54:3824–3851, Nov 1996.

[78] Patrick M Hayden, Michal Horodecki, and Barbara M Terhal. The asymptotic entanglement cost of preparing a quantum state. *Journal of Physics A: Mathematical and General*, 34(35):6891–6898, aug 2001.

[79] Michał Horodecki, Aditi Sen(De), and Ujjwal Sen. Rates of asymptotic entanglement transformations for bipartite mixed states: Maximally entangled states are not special. *Phys. Rev. A*, 67:062314, Jun 2003.

[80] Igor Devetak and Andreas Winter. Distillation of secret key and entanglement from quantum states. *Proceedings of the Royal Society A: Mathematical, Physical and Engineering Sciences*, 461(2053):207–235, 2005.

[81] V. Vedral, M. B. Plenio, K. Jacobs, and P. L. Knight. Statistical inference, distinguishability of quantum states, and quantum entanglement. *Phys. Rev. A*, 56:4452–4455, Dec 1997.

[82] Michał Horodecki, Paweł Horodecki, and Ryszard Horodecki. Limits for entanglement measures. *Phys. Rev. Lett.*, 84:2014–2017, Feb 2000.

[83] Matthew J. Donald, Michał Horodecki, and Oliver Rudolph. The uniqueness theorem for entanglement measures. *Journal of Mathematical Physics*, 43(9):4252–4272, 2002.

[84] Asher Peres. Separability criterion for density matrices. *Phys. Rev. Lett.*, 77:1413–1415, Aug 1996.

[85] Michał Horodecki, Paweł Horodecki, and Ryszard Horodecki. Separability of mixed states: necessary and sufficient conditions. *Physics Letters A*, 223(1):1–8, 1996.

[86] Heinz-Peter Breuer and Francesco Petruccione. *The Theory of Open Quantum Systems*. Oxford University Press, 2007.

[87] L M Sieberer, M Buchhold, and S Diehl. Keldysh field theory for driven open quantum systems. *Reports on Progress in Physics*, 79(9):096001, aug 2016.

[88] Hanna Krauter, Christine A. Muschik, Kasper Jensen, Wojciech Wasilewski, Jonas M. Petersen, J. Ignacio Cirac, and Eugene S. Polzik. Entanglement generated by dissipation and steady state entanglement of two macroscopic objects. *Phys. Rev. Lett.*, 107:080503, Aug 2011.

[89] J. F. Poyatos, J. I. Cirac, and P. Zoller. Quantum reservoir engineering with laser cooled trapped ions. *Phys. Rev. Lett.*, 77:4728–4731, Dec 1996.

[90] M. B. Plenio and S. F. Huelga. Entangled light from white noise. *Phys. Rev. Lett.*, 88:197901, Apr 2002.

[91] Frank Verstraete, Michael M. Wolf, and J. Ignacio Cirac. Quantum computation and quantum-state engineering driven by dissipation. *Nature Physics*, 5(9):633–636, 2009.

[92] A. S. Parkins, E. Solano, and J. I. Cirac. Unconditional two-mode squeezing of separated atomic ensembles. *Phys. Rev. Lett.*, 96:053602, Feb 2006.

[93] B. Flebus and Y. Tserkovnyak. Quantum-impurity relaxometry of magnetization dynamics. *Phys. Rev. Lett.*, 121:187204, Nov 2018.

[94] Bei Zeng, Xie Chen, Duan-Lu Zhou, and Xiao-Gang Wen. *Quantum information meets quantum matter: From quantum entanglement to topological phases of many-body systems*. Springer, 2019.

[95] Michael A. Nielsen and Isaac L. Chuang. *Quantum Computation and Quantum Information*. Cambridge University Press, 10th anniversary edition edition, January 31, 2011.

[96] Daniel A. Lidar. Lecture Notes on the Theory of Open Quantum Systems. *arXiv e-prints*, page arXiv:1902.00967, February 2019.

[97] N. D. Mermin. The topological theory of defects in ordered media. *Rev. Mod. Phys.*, 51:591–648, Jul 1979.

[98] Hans-Benjamin Braun. Topological effects in nanomagnetism: from superparamagnetism to chiral quantum solitons. *Advances in Physics*, 61(1):1–116, 2012.

[99] Stuart S. P. Parkin, Masamitsu Hayashi, and Luc Thomas. Magnetic domain-wall racetrack memory. *Science*, 320(5873):190–194, 2008.

[100] S. Mühlbauer, B. Binz, F. Jonietz, C. Pfleiderer, A. Rosch, A. Neubauer, R. Georgii, and P. Böni. Skyrmion lattice in a chiral magnet. *Science*, 323(5916):915–919, 2009.

[101] Steven S.-L. Zhang and Shufeng Zhang. Magnon mediated electric current drag across a ferromagnetic insulator layer. *Phys. Rev. Lett.*, 109:096603, Aug 2012.

[102] Y. Kajiwara, K. Harii, S. Takahashi, J. Ohe, K. Uchida, M. Mizuguchi, H. Umezawa, H. Kawai, K. Ando, K. Takanashi, S. Maekawa, and E. Saitoh. Transmission of electrical signals by spin-wave interconversion in a magnetic insulator. *Nature*, 464(7286):262–266, 2010.

[103] Héctor Ochoa, Se Kwon Kim, and Yaroslav Tserkovnyak. Topological spin-transfer drag driven by skyrmion diffusion. *Phys. Rev. B*, 94:024431, Jul 2016.

[104] Héctor Ochoa, Ricardo Zarzuela, and Yaroslav Tserkovnyak. Spin hydrodynamics in amorphous magnets. *Phys. Rev. B*, 98:054424, Aug 2018.

[105] Yaroslav Tserkovnyak and Jiang Xiao. Energy storage via topological spin textures. *Phys. Rev. Lett.*, 121:127701, Sep 2018.

[106] Lars Onsager. Reciprocal relations in irreversible processes. i. *Phys. Rev.*, 37:405–426, Feb 1931.

[107] We use bold face $\mathbf{A}$ to indicate it is a pseudovector and vector arrow $\vec{A}$ to imply it is a vector.

[108] E. Wigner. On the interaction of electrons in metals. *Physical Review*, 46(11):1002–1011, 12 1934.

[109] A. Einstein. Über die von der molekularkinetischen Theorie der Wärme geforderte Bewegung von in ruhenden Flüssigkeiten suspendierten Teilchen. *Annalen der Physik*, 322(8):549–560, January 1905.

[110] Peter Hänggi, Peter Talkner, and Michal Borkovec. Reaction-rate theory: fifty years after kramers. *Rev. Mod. Phys.*, 62:251–341, Apr 1990.

[111] Yaroslav Tserkovnyak and Matthew Mecklenburg. Electron transport driven by nonequilibrium magnetic textures. *Phys. Rev. B*, 77:134407, Apr 2008.

[112] Petter Minnhagen. The two-dimensional coulomb gas, vortex unbinding, and superfluid-superconducting films. *Rev. Mod. Phys.*, 59:1001–1066, Oct 1987.

[113] Sadamichi Maekawa, Sergio O. Valenzuela, Eiji Saitoh, and Takashi Kimura, editors. *Spin Current*. Series on Semiconductor Science and Technology. Oxford University Press, 2015.

[114] D. A. Allwood, G. Xiong, C. C. Faulkner, D. Atkinson, D. Petit, and R. P. Cowburn. Magnetic domain-wall logic. *Science*, 309(5741):1688–1692, 2005.

[115] Albert Fert. Nobel lecture: Origin, development, and future of spintronics. *Rev. Mod. Phys.*, 80:1517–1530, Dec 2008.

[116] Alexander Khitun, Mingqiang Bao, and Kang L Wang. Magnonic logic circuits. *Journal of Physics D: Applied Physics*, 43(26):264005, jun 2010.

[117] Jin Lan, Weichao Yu, Ruqian Wu, and Jiang Xiao. Spin-wave diode. *Phys. Rev. X*, 5:041049, Dec 2015.

[118] J. Grollier, D. Querlioz, and M. D. Stiles. Spintronic nanodevices for bioinspired computing. *Proceedings of the IEEE*, 104(10):2024–2039, Oct 2016.

[119] Kun Yue, Yizhou Liu, Roger K. Lake, and Alice C. Parker. A brain-plausible neuromorphic on-the-fly learning system implemented with magnetic domain wall analog memristors. *Science Advances*, 5(4), 2019.

[120] Jacob Torrejon, Mathieu Riou, Flavio Abreu Araujo, Sumito Tsunegi, Guru Khalsa, Damien Querlioz, Paolo Bortolotti, Vincent Cros, Kay Yakushiji, Akio Fukushima, Hitoshi Kubota, Shinji Yuasa, Mark D. Stiles, and Julie Grollier. Neuromorphic computing with nanoscale spintronic oscillators. *Nature*, 547(7664):428–431, 2017.

[121] Abhronil Sengupta and Kaushik Roy. Neuromorphic computing enabled by physics of electron spins: Prospects and perspectives. *Applied Physics Express*, 11(3):030101, feb 2018.

[122] So Takei, Yaroslav Tserkovnyak, and Masoud Mohseni. Spin superfluid josephson quantum devices. *Phys. Rev. B*, 95:144402, Apr 2017.

[123] Akashdeep Kamra, Even Thingstad, Gianluca Rastelli, Rembert A. Duine, Arne Brataas, Wolfgang Belzig, and Asle Sudbø. Antiferromagnetic magnons as highly squeezed fock states underlying quantum correlations. *Phys. Rev. B*, 100:174407, Nov 2019.

[124] Bertrand I. Halperin, Gil Refael, and Eugene Demler. Resistance in superconductors. *International Journal of Modern Physics B*, 24(20n21):4039–4080, 2010.

[125] J. Pearl. Vortexes are creating a stir in the superconducting field. *Electronics*, 1966.

[126] G E Volovik. Linear momentum in ferromagnets. *J. Phys. C: Solid State Phys.*, 20(7), 1987.

[127] Clement H. Wong and Yaroslav Tserkovnyak. Hydrodynamic theory of coupled current and magnetization dynamics in spin-textured ferromagnets. *Phys. Rev. B*, 80:184411, Nov 2009.

[128] J M Kosterlitz. The critical properties of the two-dimensional xy model. *Journal of Physics C: Solid State Physics*, 7(6):1046–1060, mar 1974.

[129] Sayak Dasgupta, Shu Zhang, Ibrahima Bah, and Oleg Tchernyshyov. Quantum statistics of vortices from a dual theory of the XY ferromagnet. *arXiv e-prints*, page arXiv:1909.05248, 2019.

[130] L. P. Pitaevskii and E.M. Lifshitz. *Physical Kinetics*, volume 10 of *Course of Theoretical Physics S*. Butterworth-Heinemann, 1981.

[131] A. J. Smith, J. C. Burns, S. Trussler, and J. R. Dahn. Precision measurements of the coulombic efficiency of lithium-ion batteries and of electrode materials for lithium-ion batteries. *Journal of The Electrochemical Society*, 157(2):A196, 2010.

[132] D. Apalkov, B. Dieny, and J. M. Slaughter. Magnetoresistive random access memory. *Proceedings of the IEEE*, 104(10):1796–1830, Oct 2016.

[133] P. Milde, D. Köhler, J. Seidel, L. M. Eng, A. Bauer, A. Chacon, J. Kindervater, S. Mühlbauer, C. Pfleiderer, S. Buhrandt, C. Schütte, and A. Rosch. Unwinding of a skyrmion lattice by magnetic monopoles. *Science*, 340(6136):1076–1080, 2013.

[134] Ricardo Zarzuela, Héctor Ochoa, and Yaroslav Tserkovnyak. Hydrodynamics of three-dimensional skyrmions in frustrated magnets. *Phys. Rev. B*, 100:054426, Aug 2019.

[135] A. H. Castro Neto, F. Guinea, N. M. R. Peres, K. S. Novoselov, and A. K. Geim. The electronic properties of graphene. *Rev. Mod. Phys.*, 81:109–162, Jan 2009.

[136] Sebastian A. Diaz and Daniel P. Arovas. Quantum Nucleation of Skyrmions in Magnetic Films by Inhomogeneous Fields. *arXiv e-prints*, page arXiv:1604.04010, April 2016.

[137] Amel Derras-Chouk, Eugene M. Chudnovsky, and Dmitry A. Garanin. Quantum collapse of a magnetic skyrmion. *Phys. Rev. B*, 98:024423, Jul 2018.

[138] Xiao-Gang Wen. *Quantum Field Theory of Many-body Systems: From the Origin of Sound to an Origin of Light and Electrons*. Oxford University Press, 2007.

[139] Nathan Seiberg, T. Senthil, Chong Wang, and Edward Witten. A duality web in 2+1 dimensions and condensed matter physics. *Annals of Physics*, 374:395–433, 2016.

[140] T. Senthil, Dam Thanh Son, Chong Wang, and Cenke Xu. Duality between (2+1)d quantum critical points. *Physics Reports*, 827:1–48, 2019. Duality between (2+1)d quantum critical points.

[141] Matthew S. Paoletti and Daniel P. Lathrop. Quantum turbulence. *Annual Review of Condensed Matter Physics*, 2(1):213–234, 2011.

[142] Se Kwon Kim, Roberto Myers, and Yaroslav Tserkovnyak. Nonlocal spin transport mediated by a vortex liquid in superconductors. *Phys. Rev. Lett.*, 121:187203, Oct 2018.

[143] Brynmor Haskell and Andrew Melatos. Models of pulsar glitches. *International Journal of Modern Physics D*, 24(03):1530008, 2015.

[144] So Takei, Amir Yacoby, Bertrand I. Halperin, and Yaroslav Tserkovnyak. Spin superfluidity in the $\nu = 0$ quantum hall state of graphene. *Phys. Rev. Lett.*, 116:216801, May 2016.

[145] S. A. Wolf, D. D. Awschalom, R. A. Buhrman, J. M. Daughton, S. von Molnár, M. L. Roukes, A. Y. Chtchelkanova, and D. M. Treger. Spintronics: A spin-based electronics vision for the future. *Science*, 294(5546):1488–1495, 2001.

[146] L. J. Cornelissen, J. Liu, R. A. Duine, J. Ben Youssef, and B. J. van Wees. Long-distance transport of magnon spin information in a magnetic insulator at room temperature. *Nature Physics*, 11(12):1022–1026, 2015.

[147] Koichi Oyanagi, Saburo Takahashi, Ludo J. Cornelissen, Juan Shan, Shunsuke Daimon, Takashi Kikkawa, Gerrit E. W. Bauer, Bart J. van Wees, and Eiji Saitoh. Spin transport in insulators without exchange stiffness. *Nature Communications*, 10(1):4740, 2019.

[148] S. C. Chae, N. Lee, Y. Horibe, M. Tanimura, S. Mori, B. Gao, S. Carr, and S.-W. Cheong. Direct observation of the proliferation of ferroelectric loop domains and vortex-antivortex pairs. *Phys. Rev. Lett.*, 108:167603, Apr 2012.

[149] F. P. Chmiel, N. Waterfield Price, R. D. Johnson, A. D. Lamirand, J. Schad, G. van der Laan, D. T. Harris, J. Irwin, M. S. Rzchowski, C. B. Eom, and P. G. Radaelli. Observation of magnetic vortex pairs at room temperature in a planar α-fe2o3/co heterostructure. *Nature Materials*, 17(7):581–585, 2018.

[150] K. Everschor-Sitte, J. Masell, R. M. Reeve, and M. Kläui. Perspective: Magnetic skyrmions—overview of recent progress in an active research field. *Journal of Applied Physics*, 124(24):240901, 2018.

[151] Y. Fujishiro, N. Kanazawa, T. Nakajima, X. Z. Yu, K. Ohishi, Y. Kawamura, K. Kakurai, T. Arima, H. Mitamura, A. Miyake, K. Akiba, M. Tokunaga, A. Matsuo, K. Kindo, T. Koretsune, R. Arita, and Y. Tokura. Topological transitions among skyrmion- and hedgehog-lattice states in cubic chiral magnets. *Nature Communications*, 10(1):1059, 2019.

[152] Toshiaki Tanigaki, Kiyou Shibata, Naoya Kanazawa, Xiuzhen Yu, Yoshinori Onose, Hyun Soon Park, Daisuke Shindo, and Yoshinori Tokura. Real-space observation of short-period cubic lattice of skyrmions in mnge. *Nano Letters*, 15(8):5438–5442, 08 2015.

[153] Naoya Kanazawa, Shinichiro Seki, and Yoshinori Tokura. Noncentrosymmetric magnets hosting magnetic skyrmions. *Advanced Materials*, 29(25):1603227, 2017.

[154] Predrag Nikolic. Topological orders of monopoles and hedgehogs: From electronic and magnetic spin-orbit coupling to quarks. *Phys. Rev. B*, 101:115144, Mar 2020.

[155] Arjun Rana, Chen-Ting Liao, Ezio Iacocca, Ji Zou, Minh Pham, Emma-Elizabeth Cating Subramanian, Yuan Hung Lo, Sinéad A. Ryan, Xingyuan Lu, Charles S. Bevis, Jr Karl, Robert M., Andrew J. Glaid, Young-Sang Yu, Pratibha Mahale, David A. Shapiro, Sadegh Yazdi, Thomas E. Mallouk, Stanley J. Osher, Henry C. Kapteyn, Vincent H. Crespi, John V. Badding, Yaroslav Tserkovnyak, Margaret M. Murnane, and Jianwei Miao. Direct observation of 3D topological spin textures and their interactions using soft x-ray vector ptychography. *arXiv e-prints*, page arXiv:2104.12933, April 2021.

[156] Xiao-Xiao Zhang, Andrey S. Mishchenko, Giulio De Filippis, and Naoto Nagaosa. Electric transport in three-dimensional skyrmion/monopole crystal. *Phys. Rev. B*, 94:174428, Nov 2016.

[157] N. Kanazawa, Y. Nii, X. X. Zhang, A. S. Mishchenko, G. De Filippis, F. Kagawa, Y. Iwasa, N. Nagaosa, and Y. Tokura. Critical phenomena of emergent magnetic monopoles in a chiral magnet. *Nature Communications*, 7(1):11622, 2016.

[158] Dalton Jones, Ji Zou, Shu Zhang, and Yaroslav Tserkovnyak. Energy storage in magnetic textures driven by vorticity flow. *arXiv e-prints*, page arXiv:2003.12121, March 2020.

[159] Mikio Nakahara. *Geometry, Topology and Physics*. CRC Press, 2 edition edition, 2003.

[160] Naoto Nagaosa and Yoshinori Tokura. Emergent electromagnetism in solids. *Physica Scripta*, T146:014020, jan 2012.

[161] Gen Tatara. Effective gauge field theory of spintronics. *Physica E: Low-dimensional Systems and Nanostructures*, 106:208 – 238, 2019.

[162] T. Schulz, R. Ritz, A. Bauer, M. Halder, M. Wagner, C. Franz, C. Pfleiderer, K. Everschor, M. Garst, and A. Rosch. Emergent electrodynamics of skyrmions in a chiral magnet. *Nature Physics*, 8(4):301–304, 2012.

[163] Sebastián A. Díaz, Jelena Klinovaja, and Daniel Loss. Topological magnons and edge states in antiferromagnetic skyrmion crystals. *Phys. Rev. Lett.*, 122:187203, May 2019.

[164] Kevin A. van Hoogdalem, Yaroslav Tserkovnyak, and Daniel Loss. Magnetic texture-induced thermal hall effects. *Phys. Rev. B*, 87:024402, Jan 2013.

[165] Alexander Markovich Polyakov. *Gauge fields and strings*. CRC Press, September 14, 1987.

[166] Haï"m Brezis, Jean-Michel Coron, and Elliott H Lieb. Harmonic maps with defects. *Comm. Math. Phys.*, 107(4):649–705, 1986.

[167] John B. Kogut. The lattice gauge theory approach to quantum chromodynamics. *Rev. Mod. Phys.*, 55:775–836, Jul 1983.

[168] Leo P. Kadanoff. The application of renormalization group techniques to quarks and strings. *Rev. Mod. Phys.*, 49:267–296, Apr 1977.

[169] Larry McLerran. The physics of the quark-gluon plasma. *Rev. Mod. Phys.*, 58:1021–1064, Oct 1986.

[170] Henrik Bohr and H.B. Nielsen. Hadron production from a boiling quark soup: A thermodynamical quark model predicting particle ratios in hadronic collisions. *Nuclear Physics B*, 128(2):275 – 293, 1977.

[171] W. Cassing and E. L. Bratkovskaya. Parton transport and hadronization from the dynamical quasiparticle point of view. *Phys. Rev. C*, 78:034919, Sep 2008.

[172] A. Peshier and W. Cassing. The hot nonperturbative gluon plasma is an almost ideal colored liquid. *Phys. Rev. Lett.*, 94:172301, May 2005.

[173] Holger Bech Nielsen and P. Olesen. Vortex Line Models for Dual Strings. *Nucl. Phys.*, B61:45–61, 1973. [,302(1973)].

[174] Y. Nambu. Strings, monopoles, and gauge fields. *Phys. Rev. D*, 10:4262–4268, Dec 1974.

[175] G.'t Hooft. Magnetic monopoles in unified gauge theories. *Nuclear Physics B*, 79(2):276 – 284, 1974.

[176] James S. Ball and Ariel Caticha. Superconductivity: A testing ground for models of confinement. *Phys. Rev. D*, 37:524–535, Jan 1988.

[177] Marco Cardoso, Pedro Bicudo, and Pedro D. Sacramento. Confinement of monopole field lines in a superconductor at t$\neq$0. *Annals of Physics*, 323(2):337 – 355, 2008.

[178] Yutaka Akagi, Masafumi Udagawa, and Yukitoshi Motome. Hidden multiple-spin interactions as an origin of spin scalar chiral order in frustrated kondo lattice models. *Phys. Rev. Lett.*, 108:096401, Feb 2012.

[179] Shun Okumura, Satoru Hayami, Yasuyuki Kato, and Yukitoshi Motome. Magnetic hedgehog lattices in noncentrosymmetric metals. *Phys. Rev. B*, 101:144416, Apr 2020.

[180] Christoph Schütte and Achim Rosch. Dynamics and energetics of emergent magnetic monopoles in chiral magnets. *Phys. Rev. B*, 90:174432, Nov 2014.

[181] Peter Hänggi, Peter Talkner, and Michal Borkovec. Reaction-rate theory: fifty years after kramers. *Rev. Mod. Phys.*, 62:251–341, Apr 1990.

[182] Claire Donnelly, Manuel Guizar-Sicairos, Valerio Scagnoli, Sebastian Gliga, Mirko Holler, Jörg Raabe, and Laura J. Heyderman. Three-dimensional magnetization structures revealed with x-ray vector nanotomography. *Nature*, 547(7663):328–331, 2017.

[183] Claire Donnelly, Simone Finizio, Sebastian Gliga, Mirko Holler, Aleš Hrabec, Michal Odstrčil, Sina Mayr, Valerio Scagnoli, Laura J. Heyderman, Manuel Guizar-Sicairos, and Jörg Raabe. Time-resolved imaging of three-dimensional nanoscale magnetization dynamics. *Nature Nanotechnology*, 15(5):356–360, 2020.

[184] Niklas Romming, Christian Hanneken, Matthias Menzel, Jessica E. Bickel, Boris Wolter, Kirsten von Bergmann, André Kubetzka, and Roland Wiesendanger. Writing and deleting single magnetic skyrmions. *Science*, 341(6146):636–639, 2013.

[185] Gong Chen and Andreas K. Schmid. Imaging and tailoring the chirality of domain walls in magnetic films. *Advanced Materials*, 27(38):5738–5743, 2015.

[186] Nicolas Rougemaille and AK Schmid. Magnetic imaging with spin-polarized low-energy electron microscopy. *The European Physical Journal-Applied Physics*, 50(2), 2010.

[187] Hector Ochoa, Se Kwon Kim, Oleg Tchernyshyov, and Yaroslav Tserkovnyak. Gyrotropic elastic response of skyrmion crystals to current-induced tensions. *Phys. Rev. B*, 96:020410, Jul 2017.

[188] Martin Stier, Wolfgang Häusler, Thore Posske, Gregor Gurski, and Michael Thorwart. Skyrmion–anti-skyrmion pair creation by in-plane currents. *Phys. Rev. Lett.*, 118:267203, Jun 2017.

[189] Karin Everschor-Sitte, Matthias Sitte, Thierry Valet, Artem Abanov, and Jairo Sinova. Skyrmion production on demand by homogeneous DC currents. *New Journal of Physics*, 19(9):092001, sep 2017.

[190] Michael Stone. Magnus force on skyrmions in ferromagnets and quantum hall systems. *Phys. Rev. B*, 53:16573–16578, Jun 1996.

[191] A. Einstein, B. Podolsky, and N. Rosen. Can quantum-mechanical description of physical reality be considered complete? *Phys. Rev.*, 47:777–780, May 1935.

[192] Paul G. Kwiat, Klaus Mattle, Harald Weinfurter, Anton Zeilinger, Alexander V. Sergienko, and Yanhua Shih. New high-intensity source of polarization-entangled photon pairs. *Phys. Rev. Lett.*, 75:4337–4341, Dec 1995.

[193] Zhi Zhao, Yu-Ao Chen, An-Ning Zhang, Tao Yang, Hans J. Briegel, and Jian-Wei Pan. Experimental demonstration of five-photon entanglement and open-destination teleportation. *Nature*, 430(6995):54–58, 2004.

[194] Xing-Can Yao, Tian-Xiong Wang, Ping Xu, He Lu, Ge-Sheng Pan, Xiao-Hui Bao, Cheng-Zhi Peng, Chao-Yang Lu, Yu-Ao Chen, and Jian-Wei Pan. Observation of eight-photon entanglement. *Nature Photonics*, 6:225 EP –, 02 2012.

[195] J. A. Formaggio, D. I. Kaiser, M. M. Murskyj, and T. E. Weiss. Violation of the leggett-garg inequality in neutrino oscillations. *Phys. Rev. Lett.*, 117:050402, Jul 2016.

[196] B. Hensen, H. Bernien, A. E. Dréau, A. Reiserer, N. Kalb, M. S. Blok, J. Ruitenberg, R. F. L. Vermeulen, R. N. Schouten, C. Abellán, W. Amaya, V. Pruneri, M. W. Mitchell, M. Markham, D. J. Twitchen, D. Elkouss, S. Wehner, T. H. Taminiau, and R. Hanson. Loophole-free bell inequality violation using electron spins separated by 1.3 kilometres. *Nature*, 526:682 EP –, 10 2015.

[197] Markus Arndt, Olaf Nairz, Julian Vos-Andreae, Claudia Keller, Gerbrand van der Zouw, and Anton Zeilinger. Wave–particle duality of c60 molecules. *Nature*, 401(6754):680–682, 1999.

[198] K. C. Lee, M. R. Sprague, B. J. Sussman, J. Nunn, N. K. Langford, X.-M. Jin, T. Champion, P. Michelberger, K. F. Reim, D. England, D. Jaksch, and I. A. Walmsley. Entangling macroscopic diamonds at room temperature. *Science*, 334(6060):1253–1256, 2011.

[199] Richard P. Feynman. Simulating physics with computers. *International Journal of Theoretical Physics*, 21(6):467–488, Jun 1982.

[200] Charles H. Bennett, Gilles Brassard, Claude Crépeau, Richard Jozsa, Asher Peres, and William K. Wootters. Teleporting an unknown quantum state via dual classical and einstein-podolsky-rosen channels. *Phys. Rev. Lett.*, 70:1895–1899, Mar 1993.

[201] Yury M. Bunkov and Vladimir L. Safonov. Magnon condensation and spin superfluidity. *Journal of Magnetism and Magnetic Materials*, 452:30–34, 2018.

[202] Christoph Simon. Natural entanglement in bose-einstein condensates. *Phys. Rev. A*, 66:052323, Nov 2002.

[203] S. O. Demokritov, V. E. Demidov, O. Dzyapko, G. A. Melkov, A. A. Serga, B. Hillebrands, and A. N. Slavin. Bose–einstein condensation of quasi-equilibrium magnons at room temperature under pumping. *Nature*, 443(7110):430–433, 2006.

[204] V. E. Demidov, O. Dzyapko, S. O. Demokritov, G. A. Melkov, and A. N. Slavin. Thermalization of a parametrically driven magnon gas leading to bose-einstein condensation. *Phys. Rev. Lett.*, 99:037205, Jul 2007.

[205] V. E. Demidov, O. Dzyapko, S. O. Demokritov, G. A. Melkov, and A. N. Slavin. Observation of spontaneous coherence in bose-einstein condensate of magnons. *Phys. Rev. Lett.*, 100:047205, Jan 2008.

[206] V. E. Demidov, O. Dzyapko, M. Buchmeier, T. Stockhoff, G. Schmitz, G. A. Melkov, and S. O. Demokritov. Magnon kinetics and bose-einstein condensation studied in phase space. *Phys. Rev. Lett.*, 101:257201, Dec 2008.

[207] O. Dzyapko, V. E. Demidov, M. Buchmeier, T. Stockhoff, G. Schmitz, G. A. Melkov, and S. O. Demokritov. Excitation of two spatially separated bose-einstein condensates of magnons. *Phys. Rev. B*, 80:060401, Aug 2009.

[208] Sergio M. Rezende. Theory of coherence in bose-einstein condensation phenomena in a microwave-driven interacting magnon gas. *Phys. Rev. B*, 79:174411, May 2009.

[209] Sergio M. Rezende. Wave function of a microwave-driven bose-einstein magnon condensate. *Physical Review B*, 81(2):020414–, 01 2010.

[210] Scott A. Bender, Rembert A. Duine, and Yaroslav Tserkovnyak. Electronic pumping of quasiequilibrium bose-einstein-condensed magnons. *Phys. Rev. Lett.*, 108:246601, Jun 2012.

[211] Scott A. Bender, Rembert A. Duine, Arne Brataas, and Yaroslav Tserkovnyak. Dynamic phase diagram of dc-pumped magnon condensates. *Phys. Rev. B*, 90:094409, Sep 2014.

[212] B. Flebus, S. A. Bender, Y. Tserkovnyak, and R. A. Duine. Two-fluid theory for spin superfluidity in magnetic insulators. *Phys. Rev. Lett.*, 116:117201, Mar 2016.

[213] Rodney Loudon. *The Quantum Theory of Light*. Oxford University Press, 2000.

[214] Ian D. Leroux, Monika H. Schleier-Smith, and Vladan Vuletić. Orientation-dependent entanglement lifetime in a squeezed atomic clock. *Phys. Rev. Lett.*, 104:250801, Jun 2010.

[215] Anne Louchet-Chauvet, Jürgen Appel, Jelmer J Renema, Daniel Oblak, Niels Kjaergaard, and Eugene S Polzik. Entanglement-assisted atomic clock beyond the projection noise limit. *New Journal of Physics*, 12(6):065032, jun 2010.

[216] Samuel L. Braunstein and Peter van Loock. Quantum information with continuous variables. *Rev. Mod. Phys.*, 77:513–577, Jun 2005.

[217] A. Furusawa, J. L. Sørensen, S. L. Braunstein, C. A. Fuchs, H. J. Kimble, and E. S. Polzik. Unconditional quantum teleportation. *Science*, 282(5389):706–709, 1998.

[218] Nicolas C. Menicucci, Steven T. Flammia, and Olivier Pfister. One-way quantum computing in the optical frequency comb. *Phys. Rev. Lett.*, 101:130501, Sep 2008.

[219] R Friedberg and J T Manassah. Dicke states and bloch states. *Laser Physics Letters*, 4(12):900–911, dec 2007.

[220] Jian Ma, Xiaoguang Wang, C.P. Sun, and Franco Nori. Quantum spin squeezing. *Physics Reports*, 509(2):89 – 165, 2011.

[221] Xiaoguang Wang and Barry C. Sanders. Relations between bosonic quadrature squeezing and atomic spin squeezing. *Phys. Rev. A*, 68:033821, Sep 2003.

[222] X. Wang and K. Mølmer. Pairwise entanglement in symmetric multi-qubit systems. *The European Physical Journal D - Atomic, Molecular, Optical and Plasma Physics*, 18(3):385–391, Mar 2002.

[223] Jie Li and Shi-Yao Zhu. Entangling two magnon modes via magnetostrictive interaction. *New Journal of Physics*, 21(8):085001, aug 2019.

[224] Zhedong Zhang, Marlan O. Scully, and Girish S. Agarwal. Quantum entanglement between two magnon modes via kerr nonlinearity driven far from equilibrium. *Phys. Rev. Research*, 1:023021, Sep 2019.

[225] In general, we can write a symmetric exchange coupling H_1 as $\sum_{\langle i,j\rangle}(K_1 S_i^x S_j^x + K_2 S_i^y S_j^y + K_3 S_i^z S_j^z)$, in the principal-axes coordinate frame. So long as $K_1 \neq K_2$, this will only redefine constants in our discussion but not alter the analysis.

[226] The transformation preserves the Pauli commutation algebra only when we restrict the boson operators $\hat{a}_i$ to the subspace with $\hat{a}_i^\dagger \hat{a}_i \to \{0, 1\}$, i.e., $\hat{a}_i \to a_i \equiv P_i \hat{a}_i P_i$, with $P_i \equiv |0\rangle_{ii}\langle 0| + |1\rangle_{ii}\langle 1|$. The appropriate spin operators, $S_i^+ = a_i$ and $S_i^z = 1/2 - a_i^\dagger a_i$, are then, in fact, expressed in terms of these projected operators. Upon substituting these into the Hamiltonian, however, we can drop the projection operators, at the expense of introducing the hard-core repulsion. In the dilute-magnon limit, furthermore, the latter can be simply disregarded.

[227] N. N. Bogoljubov. On a new method in the theory of superconductivity. *Il Nuovo Cimento (1955-1965)*, 7(6):794–805, 1958.

[228] Akashdeep Kamra and Wolfgang Belzig. Super-poissonian shot noise of squeezed-magnon mediated spin transport. *Physical Review Letters*, 116(14):146601–, 04 2016.

[229] Ping Yun-Xia, Cheng Ze, Zhang Bo, and Cheng Zheng-Ze. Entanglement properties of two-mode squeezed coherent states in radiation field. *Communications in Theoretical Physics*, 49(4):1013–1016, apr 2008.

[230] Tohya Hiroshima. Decoherence and entanglement in two-mode squeezed vacuum states. *Phys. Rev. A*, 63:022305, Jan 2001.

[231] We use the standard notation: $\Delta S^x = \sqrt{\langle (S^x - \langle S^x \rangle)^2 \rangle}$ and the minimum uncertainty relation is given by $\Delta S^x \Delta S^y = |\langle [S^x, S^y] \rangle|/2 = S^z/2 \approx 1/4$ when the average magnon density is small.

[232] Masato Koashi, Vladimír Bužek, and Nobuyuki Imoto. Entangled webs: Tight bound for symmetric sharing of entanglement. *Phys. Rev. A*, 62:050302, Oct 2000.

[233] Barry C Sanders. Review of entangled coherent states. *Journal of Physics A: Mathematical and Theoretical*, 45(24):244002, may 2012.

[234] Similar argument can be made for nonzero wavenumber modes. The parameter in the two-mode squeezing operator will become complex-valued.

[235] So Takei and Masoud Mohseni. Quantum control of topological defects in magnetic systems. *Phys. Rev. B*, 97:064401, Feb 2018.

[236] B. Flebus and Y. Tserkovnyak. Entangling distant spin qubits via a magnetic domain wall. *Phys. Rev. B*, 99:140403, Apr 2019.

[237] Charles Kittel. *Introduction to Solid State Physics*. Wiley, 8 edition edition, 2004.

[238] Akashdeep Kamra, Even Thingstad, Gianluca Rastelli, Rembert A. Duine, Arne Brataas, Wolfgang Belzig, and Asle Sudbø. Antiferromagnetic Magnons as Highly Squeezed Fock States underlying Quantum Correlations. *arXiv e-prints*, page arXiv:1904.04553, Apr 2019.

[239] J. Eisert, M. Cramer, and M. B. Plenio. Colloquium: Area laws for the entanglement entropy. *Rev. Mod. Phys.*, 82:277–306, Feb 2010.

[240] Alexei Kitaev and John Preskill. Topological entanglement entropy. *Phys. Rev. Lett.*, 96:110404, Mar 2006.

[241] Nicolas Brunner, Daniel Cavalcanti, Stefano Pironio, Valerio Scarani, and Stephanie Wehner. Bell nonlocality. *Rev. Mod. Phys.*, 86:419–478, Apr 2014.

[242] B. B. Blinov, D. L. Moehring, L. M. Duan, and C. Monroe. Observation of entanglement between a single trapped atom and a single photon. *Nature*, 428(6979):153–157, 2004.

[243] Jürgen Volz, Markus Weber, Daniel Schlenk, Wenjamin Rosenfeld, Johannes Vrana, Karen Saucke, Christian Kurtsiefer, and Harald Weinfurter. Observation of entanglement of a single photon with a trapped atom. *Phys. Rev. Lett.*, 96:030404, Jan 2006.

[244] Rainer Blatt and David Wineland. Entangled states of trapped atomic ions. *Nature*, 453(7198):1008–1015, 2008.

[245] Colin D. Bruzewicz, John Chiaverini, Robert McConnell, and Jeremy M. Sage. Trapped-ion quantum computing: Progress and challenges. *Applied Physics Reviews*, 6(2):021314, 2021/03/24 2019.

[246] Daniel Loss and David P. DiVincenzo. Quantum computation with quantum dots. *Phys. Rev. A*, 57:120–126, Jan 1998.

[247] F. Basso Basset, M. B. Rota, C. Schimpf, D. Tedeschi, K. D. Zeuner, S. F. Covre da Silva, M. Reindl, V. Zwiller, K. D. Jöns, A. Rastelli, and R. Trotta. Entanglement swapping with photons generated on demand by a quantum dot. *Phys. Rev. Lett.*, 123:160501, Oct 2019.

[248] Haifeng Qiao, Yadav P. Kandel, Sreenath K. Manikandan, Andrew N. Jordan, Saeed Fallahi, Geoffrey C. Gardner, Michael J. Manfra, and John M. Nichol. Conditional teleportation of quantum-dot spin states. *Nature Communications*, 11(1):3022, 2020.

[249] G Wendin. Quantum information processing with superconducting circuits: a review. *Reports on Progress in Physics*, 80(10):106001, sep 2017.

[250] Marcus W. Doherty, Neil B. Manson, Paul Delaney, Fedor Jelezko, Jörg Wrachtrup, and Lloyd C.L. Hollenberg. The nitrogen-vacancy colour centre in diamond. *Physics Reports*, 528(1):1–45, 2013.

[251] Y. Chu, M. Markham, D. J. Twitchen, and M. D. Lukin. All-optical control of a single electron spin in diamond. *Phys. Rev. A*, 91:021801, Feb 2015.

[252] N. Bar-Gill, L. M. Pham, A. Jarmola, D. Budker, and R. L. Walsworth. Solid-state electronic spin coherence time approaching one second. *Nature Communications*, 4(1):1743, 2013.

[253] Gopalakrishnan Balasubramanian, Philipp Neumann, Daniel Twitchen, Matthew Markham, Roman Kolesov, Norikazu Mizuochi, Junichi Isoya, Jocelyn Achard, Johannes Beck, Julia Tissler, Vincent Jacques, Philip R. Hemmer, Fedor Jelezko, and Jörg Wrachtrup. Ultralong spin coherence time in isotopically engineered diamond. *Nature Materials*, 8(5):383–387, 2009.

[254] M Wallquist, K Hammerer, P Rabl, M Lukin, and P Zoller. Hybrid quantum devices and quantum engineering. *Physica Scripta*, T137:014001, dec 2009.

[255] Hailong Wang, Shu Zhang, Nathan J. McLaughlin, Benedetta Flebus, Mengqi Huang, Yuxuan Xiao, Eric E. Fullerton, Yaroslav Tserkovnyak, and Chunhui Rita Du. Quantum Sensing of Spin Transport Properties of an Antiferromagnetic Insulator. *arXiv e-prints*, page arXiv:2011.03905, November 2020.

[256] Chunhui Du, Toeno van der Sar, Tony X. Zhou, Pramey Upadhyaya, Francesco Casola, Huiliang Zhang, Mehmet C. Onbasli, Caroline A. Ross, Ronald L. Walsworth, Yaroslav Tserkovnyak, and Amir Yacoby. Control and local measurement of the spin chemical potential in a magnetic insulator. *Science*, 357(6347):195–198, 2017.

[257] Paolo Andrich, Charles F. de las Casas, Xiaoying Liu, Hope L. Bretscher, Jonson R. Berman, F. Joseph Heremans, Paul F. Nealey, and David D. Awschalom. Long-range spin wave mediated control of defect qubits in nanodiamonds. *npj Quantum Information*, 3(1):28, 2017.

[258] Toeno van der Sar, Francesco Casola, Ronald Walsworth, and Amir Yacoby. Nanometre-scale probing of spin waves using single electron spins. *Nature Communications*, 6(1):7886, 2015.

[259] C. S. Wolfe, V. P. Bhallamudi, H. L. Wang, C. H. Du, S. Manuilov, R. M. Teeling-Smith, A. J. Berger, R. Adur, F. Y. Yang, and P. C. Hammel. Off-resonant manipulation of spins in diamond via precessing magnetization of a proximal ferromagnet. *Phys. Rev. B*, 89:180406, May 2014.

[260] C. S. Wolfe, S. A. Manuilov, C. M. Purser, R. Teeling-Smith, C. Dubs, P. C. Hammel, and V. P. Bhallamudi. Spatially resolved detection of complex ferromagnetic dynamics using optically detected nitrogen-vacancy spins. *Applied Physics Letters*, 108(23):232409, 2016.

[261] Luka Trifunovic, Oliver Dial, Mircea Trif, James R. Wootton, Rediet Abebe, Amir Yacoby, and Daniel Loss. Long-distance spin-spin coupling via floating gates. *Phys. Rev. X*, 2:011006, Jan 2012.

[262] Luka Trifunovic, Fabio L. Pedrocchi, and Daniel Loss. Long-distance entanglement of spin qubits via ferromagnet. *Phys. Rev. X*, 3:041023, Dec 2013.

[263] L. D. Contreras-Pulido and R. Aguado. Entanglement between charge qubits induced by a common dissipative environment. *Phys. Rev. B*, 77:155420, Apr 2008.

[264] Clara Mühlherr, V. O. Shkolnikov, and Guido Burkard. Magnetic resonance in defect spins mediated by spin waves. *Phys. Rev. B*, 99:195413, May 2019.

[265] Denis R Candido, Gregory D Fuchs, Ezekiel Johnston-Halperin, and Michael E Flatté. Predicted strong coupling of solid-state spins via a single magnon mode. *Materials for Quantum Technology*, 1(1):011001, dec 2020.

[266] Tomaifmmode Neuman, Derek S. Wang, and Prineha Narang. Nanomagnonic cavities for strong spin-magnon coupling and magnon-mediated spin-spin interactions. *Phys. Rev. Lett.*, 125:247702, Dec 2020.

[267] Masaya Fukami, Denis R. Candido, David D. Awschalom, and Michael E. Flatté. Opportunities for long-range magnon-mediated entanglement of spin qubits via on- and off-resonant coupling. *arXiv e-prints*, page arXiv:2101.09220, January 2021.

[268] J. F. Poyatos, J. I. Cirac, and P. Zoller. Quantum reservoir engineering with laser cooled trapped ions. *Phys. Rev. Lett.*, 77:4728–4731, Dec 1996.

[269] M. B. Plenio, S. F. Huelga, A. Beige, and P. L. Knight. Cavity-loss-induced generation of entangled atoms. *Phys. Rev. A*, 59:2468–2475, Mar 1999.

[270] Fabio Benatti, Roberto Floreanini, and Marco Piani. Environment induced entanglement in markovian dissipative dynamics. *Phys. Rev. Lett.*, 91:070402, Aug 2003.

[271] S. Diehl, A. Micheli, A. Kantian, B. Kraus, H. P. Büchler, and P. Zoller. Quantum states and phases in driven open quantum systems with cold atoms. *Nature Physics*, 4(11):878–883, 2008.

[272] Y. Lin, J. P. Gaebler, F. Reiter, T. R. Tan, R. Bowler, A. S. Sørensen, D. Leibfried, and D. J. Wineland. Dissipative production of a maximally entangled steady state of two quantum bits. *Nature*, 504(7480):415–418, 2013.

[273] M. E. Kimchi-Schwartz, L. Martin, E. Flurin, C. Aron, M. Kulkarni, H. E. Tureci, and I. Siddiqi. Stabilizing entanglement via symmetry-selective bath engineering in superconducting qubits. *Phys. Rev. Lett.*, 116:240503, Jun 2016.

[274] G. Kordas, S. Wimberger, and D. Witthaut. Dissipation-induced macroscopic entanglement in an open optical lattice. *EPL (Europhysics Letters)*, 100(3):30007, nov 2012.

[275] S. Nicolosi, A. Napoli, A. Messina, and F. Petruccione. Dissipation-induced stationary entanglement in dipole-dipole interacting atomic samples. *Phys. Rev. A*, 70:022511, Aug 2004.

[276] Nobuhiko Yokoshi and Hajime Ishihara. Weak-light nonlinearity using a dark state in coupled quantum dots. *Journal of the Physical Society of Japan*, 86(8):083401, 2017.

[277] D. Kienzler, H.-Y. Lo, B. Keitch, L. de Clercq, F. Leupold, F. Lindenfelser, M. Marinelli, V. Negnevitsky, and J. P. Home. Quantum harmonic oscillator state synthesis by reservoir engineering. *Science*, 347(6217):53–56, 2015.

[278] M. Benito, M. J. A. Schuetz, J. I. Cirac, G. Platero, and G. Giedke. Dissipative long-range entanglement generation between electronic spins. *Phys. Rev. B*, 94:115404, Sep 2016.

[279] F. Reiter, A. S. Sørensen, P. Zoller, and C. A. Muschik. Dissipative quantum error correction and application to quantum sensing with trapped ions. *Nature Communications*, 8(1):1822, 2017.

[280] Eliot Kapit. Hardware-efficient and fully autonomous quantum error correction in superconducting circuits. *Phys. Rev. Lett.*, 116:150501, Apr 2016.

[281] Joachim Cohen and Mazyar Mirrahimi. Dissipation-induced continuous quantum error correction for superconducting circuits. *Phys. Rev. A*, 90:062344, Dec 2014.

[282] C. Daniel Freeman, C. M. Herdman, and K. B. Whaley. Engineering autonomous error correction in stabilizer codes at finite temperature. *Phys. Rev. A*, 96:012311, Jul 2017.

[283] Z. Leghtas, S. Touzard, I. M. Pop, A. Kou, B. Vlastakis, A. Petrenko, K. M. Sliwa, A. Narla, S. Shankar, M. J. Hatridge, M. Reagor, L. Frunzio, R. J. Schoelkopf, M. Mirrahimi, and M. H. Devoret. Confining the state of light to a quantum manifold by engineered two-photon loss. *Science*, 347(6224):853–857, 2015.

[284] S. Shankar, M. Hatridge, Z. Leghtas, K. M. Sliwa, A. Narla, U. Vool, S. M. Girvin, L. Frunzio, M. Mirrahimi, and M. H. Devoret. Autonomously stabilized entanglement between two superconducting quantum bits. *Nature*, 504(7480):419–422, 2013.

[285] Mazyar Mirrahimi, Zaki Leghtas, Victor V Albert, Steven Touzard, Robert J Schoelkopf, Liang Jiang, and Michel H Devoret. Dynamically protected cat-qubits: a new paradigm for universal quantum computation. *New Journal of Physics*, 16(4):045014, apr 2014.

[286] Kavan Modi, Hugo Cable, Mark Williamson, and Vlatko Vedral. Quantum correlations in mixed-state metrology. *Phys. Rev. X*, 1:021022, Dec 2011.

[287] Agnieszka Górecka, Felix A Pollock, Pietro Liuzzo-Scorpo, Rosanna Nichols, Gerardo Adesso, and Kavan Modi. Noisy frequency estimation with noisy probes. *New Journal of Physics*, 20(8):083008, aug 2018.

[288] T. Botzung, S. Diehl, and M. Müller. Engineered dissipation induced entanglement transition in quantum spin chains: From logarithmic growth to area law. *Phys. Rev. B*, 104:184422, Nov 2021.

[289] Carl M Bender. Making sense of non-hermitian hamiltonians. *Reports on Progress in Physics*, 70(6):947–1018, may 2007.

[290] S. Lin, X. Z. Zhang, C. Li, and Z. Song. Long-range entangled zero-mode state in a non-hermitian lattice. *Phys. Rev. A*, 94:042133, Oct 2016.

[291] H. Y. Yuan, Peng Yan, Shasha Zheng, Q. Y. He, Ke Xia, and Man-Hong Yung. Steady bell state generation via magnon-photon coupling. *Phys. Rev. Lett.*, 124:053602, Feb 2020.

[292] Shu Zhang and Yaroslav Tserkovnyak. Flavors of noise in magnetic Weyl semimetals. *arXiv e-prints*, page arXiv:2108.07305, August 2021.

[293] Yaroslav Tserkovnyak. Exceptional points in dissipatively coupled spin dynamics. *Phys. Rev. Research*, 2:013031, Jan 2020.

[294] Michael J. Gullans and David A. Huse. Dynamical purification phase transition induced by quantum measurements. *Phys. Rev. X*, 10:041020, Oct 2020.

[295] Sarang Gopalakrishnan and Michael J. Gullans. Entanglement and purification transitions in non-hermitian quantum mechanics. *Phys. Rev. Lett.*, 126:170503, Apr 2021.

[296] Alberto Biella and Marco Schiró. Many-Body Quantum Zeno Effect and Measurement-Induced Subradiance Transition. *arXiv e-prints*, page arXiv:2011.11620, November 2020.

[297] Shao-Kai Jian, Zhi-Cheng Yang, Zhen Bi, and Xiao Chen. Yang-Lee edge singularity triggered entanglement transition. *arXiv e-prints*, page arXiv:2101.04115, January 2021.

[298] Here the microscopic expression of J is $2J = G^R_{S_1^x S_2^x}(0) + G^R_{S_2^x S_1^x}(0) = G^R_{S_1^y S_2^y}(0) + G^R_{S_2^y S_1^y}(0) = G^R_{S_1^z S_2^z}(0) + G^R_{S_2^z S_1^z}(0)$ when the spin space is isotropic.

[299] Lorenza Viola, Emanuel Knill, and Seth Lloyd. Dynamical decoupling of open quantum systems. *Phys. Rev. Lett.*, 82:2417–2421, Mar 1999.

[300] K. Khodjasteh and D. A. Lidar. Fault-tolerant quantum dynamical decoupling. *Phys. Rev. Lett.*, 95:180501, Oct 2005.

[301] R. Lo Franco, A. D'Arrigo, G. Falci, G. Compagno, and E. Paladino. Preserving entanglement and nonlocality in solid-state qubits by dynamical decoupling. *Phys. Rev. B*, 90:054304, Aug 2014.

[302] Gerardo A Paz-Silva, Seung-Woo Lee, Todd J Green, and Lorenza Viola. Dynamical decoupling sequences for multi-qubit dephasing suppression and long-time quantum memory. *New Journal of Physics*, 18(7):073020, jul 2016.

[303] Jean Dalibard, Yvan Castin, and Klaus Mølmer. Wave-function approach to dissipative processes in quantum optics. *Phys. Rev. Lett.*, 68:580–583, Feb 1992.

[304] We have gauged out the phases of $A, \tilde{A}$ by absorbing them into the definition of $\sigma^{\pm}$.

[305] We use common convention for the greater Green's function: $G^>_{AB}(\omega) = -i\int_{-\infty}^{\infty}\langle A(t)B(0)\rangle e^{i\omega t}dt$.

[306] D. B. Hume, T. Rosenband, and D. J. Wineland. High-fidelity adaptive qubit detection through repetitive quantum nondemolition measurements. *Phys. Rev. Lett.*, 99:120502, Sep 2007.

[307] V. Negnevitsky, M. Marinelli, K. K. Mehta, H. Y. Lo, C. Flühmann, and J. P. Home. Repeated multi-qubit readout and feedback with a mixed-species trapped-ion register. *Nature*, 563(7732):527–531, 2018.

[308] L. Jiang, J. S. Hodges, J. R. Maze, P. Maurer, J. M. Taylor, D. G. Cory, P. R. Hemmer, R. L. Walsworth, A. Yacoby, A. S. Zibrov, and M. D. Lukin. Repetitive readout of a single electronic spin via quantum logic with nuclear spin ancillae. *Science*, 326(5950):267–272, 2009.

[309] Xin H. H. Zhang and Harold U. Baranger. Heralded bell state of dissipative qubits using classical light in a waveguide. *Phys. Rev. Lett.*, 122:140502, Apr 2019.

[310] Dorje C. Brody and Eva-Maria Graefe. Mixed-state evolution in the presence of gain and loss. *Phys. Rev. Lett.*, 109:230405, Dec 2012.

[311] W D Heiss. The physics of exceptional points. *Journal of Physics A: Mathematical and Theoretical*, 45(44):444016, oct 2012.

[312] Alexey Galda and Valerii M. Vinokur. Parity-time symmetry breaking in spin chains. *Phys. Rev. B*, 97:201411, May 2018.

[313] Alexey Galda and Valerii M. Vinokur. Parity-time symmetry breaking in magnetic systems. *Phys. Rev. B*, 94:020408, Jul 2016.

[314] B. Kraus and J. I. Cirac. Discrete entanglement distribution with squeezed light. *Phys. Rev. Lett.*, 92:013602, Jan 2004.

[315] Christine A Muschik, Hanna Krauter, Kasper Jensen, Jonas M Petersen, J Ignacio Cirac, and Eugene S Polzik. Robust entanglement generation by reservoir engineering. *Journal of Physics B: Atomic, Molecular and Optical Physics*, 45(12):124021, jun 2012.

[316] S. McEndoo, P. Haikka, G. De Chiara, G. M. Palma, and S. Maniscalco. Entanglement control via reservoir engineering in ultracold atomic gases. *EPL (Europhysics Letters)*, 101(6):60005, mar 2013.

[317] Akashdeep Kamra, Wolfgang Belzig, and Arne Brataas. Magnon-squeezing as a niche of quantum magnonics. *Applied Physics Letters*, 117(9):090501, 2020.

[318] Francesco Casola, Toeno van der Sar, and Amir Yacoby. Probing condensed matter physics with magnetometry based on nitrogen-vacancy centres in diamond. *Nature Reviews Materials*, 3(1):17088, 2018.